Deconstructing the trypanosome cytoskeleton: from structures to functions via components and complexes.

A thesis submitted for the degree of Doctor of Philosophy in the University of Oxford

Trinity term 2011

Neil Portman
Lincoln College
The Sir William Dunn School of Pathology

Table of Contents

Figures and tables

Chapter 1

Chapter 3

Chapter 4

Chapter 5

Abstract

Trypanosomatid protozoan parasites are the causative agents of a number of diseases responsible for the death of thousands of people in developing countries. There is currently little hope for the development of vaccines and existing treatment regimens are associated with high toxicity. *Trypanosoma brucei* is the etiological agent of devastating parasitic disease in humans and livestock in sub-saharan Africa. The pathogenicity and growth of these parasites are intimately linked to their shape and form which are in turn derived from a highly ordered microtubule-based cytoskeleton. Here I have investigated some of the critical structures of the cytoskeleton in terms of their molecular composition with a view toward interrogating their functions.

I have used a combined reverse genetics/comparative proteomics approach to identify over 20 novel components of the paraflagellar rod, an essential structure for the mammalian infective form of the parasite. I have iterated this approach to define interdependent sub-groups within the cohort which provide clues to the function of the paraflagellar rod.

I next applied the same comparative proteomics techniques to investigate the differences between the protein composition of two life-cycle stages of the parasite. I have identified novel components of a unique mobile transmembrane junction called the flagella connector, and of the flagellum attachment zone, a structure that is essential for cell division. In addition I have defined a pair of paralogous cytoskeletal proteins that show life-cycle stage specificity.

Finally, I have used electron tomography, reverse genetics and in situ protein tagging to define the morphology of the flagellar pocket collar, a critical structure required for parasite viability, and provide new insights into its molecular composition, function and biogenesis.

Acknowledgements

First and foremost I would like to express my unreserved gratitude to my supervisor Professor Keith Gull whose constant support and generosity over the last few years have been humbling.

The Gull lab is an incredible place in which to do science and I would like to thank everybody in the group, past and present, for ideas and support and contributing towards such a stimulating environment. Particular thanks go to Nicole, Steve, Bill, Sue, Eva, and Richard, my fellow long-term inmates. Also thanks to Helen and Andrea for running such a tight ship and Paul McKean and Michael Ginger for advice and support. I have benefitted hugely from the expertise of Mike Shaw and Ben Thomas, who have my gratitude.

Special thanks go to Sylvain for his infectious enthusiasm and being a great friend.

I spent a very productive week in the lab of Professor Dick McIntosh at the University of Colorado, Boulder and my thanks go to him and his lab members for their help, particularly Johanna for putting in the long hours with me.

My thanks also go to the Sir William Dunn School of Pathology and Lincoln College for support both intellectual and financial.

My work in the lab has been supported by the Wellcome Trust and the BBSRC.

Finally, I'd like to thank my family. Mum and Dad for giving me opportunities that they never had and of course my wife Carli whose love and unwavering support make it all worthwhile.

Abbreviations

BLAST: Basic local alignement search tool.

bp: base pair.

CAP: Cytoskeleton associated protein

CMRP: Collar MORN repeat protein

DAPI: 4,6-diamidino-2-phenylinidole.

ddH2O: double-distilled water.

DiGE: Difference gel electrophoresis.

DNA: Deoxiribonucleic acid.

dNTP: Deoxyribonucleoside triphosphate.

EDTA: Ethylenedinitrilo tetraacetic acid (disodium salt).

ESAG: Expression site associated gene

FAZ: Flagellum attachment zone.

FC: Flagella connector

FP: Flagellar pocket

FPC: Flagellar pocket Collar

GFP: Green fluorescent protein.

GPI: Glycosylphosphatidylinositol.

IFT: Intraflagellar transport

iTRAQ: isotope tags for relative and absolute quantitation

K: Kinetoplast

kDa: kiloDalton.

LB: Luria Broth.

MORN: Membrane occupation and recognition nexus

mtq: microtubule quartet

N: Nucleus

ORF: Open reading frame.

PCR: Polymerase chain reaction.

PFC: Paraflagellar rod proteome component.

PFR: Paraflagellar rod.

RNA: ribonucleic acid.

SDS-PAGE: Sodium dodecyl sulphate-polyacrylamide gel electrophoresis

VSG: Variant surface glycoprotein.

WCB: whole cell body

ZPFM: Zimmerman's post fusion medium.

Declaration

No portion of the work referred to in this thesis has been submitted in support of an application for another degree or qualification of this or any other university or other institute of learning.

Chapter 1

Introduction

Sections of this introduction were published as an invited review in The International Journal for Parasitology (Portman and Gull 2010).

1.1. Trypanosomatid protozoa

Trypanosomatid protozoan parasites are the causative agents of a number of diseases responsible for the death of thousands of people in developing countries. There is currently little hope for the development of vaccines and existing treatment regimens are associated with high toxicity. *Trypanosoma brucei* is the etiological agent of devastating parasitic disease in humans and livestock in Africa. Two subspecies are known to infect humans, *T. b. gambiense* in central and western Africa and *T. b. rhodesiense* in southern and eastern Africa. *T. b. gambiense* is associated with chronic African trypanosomiasis, commonly known as African sleeping sickness, whereas *T. b. rhodesiense* is associated with an acute form of the disease. The related parasites *Trypanosoma cruzi* and *Leishmania spp.* cause American trypanosomiasis, also known as Chagas disease, and Leishmaniasis respectively. The pathogenicity and growth of these parasites are intimately linked to their shape and form which are in turn derived from a highly ordered microtubule-based cytoskeleton (Figure 1.1). The life cycle of the parasites cycles between an insect vector (for *T. brucei* the Tsetse fly, *Glossina spp.*) and a mammalian host and is characterised by extreme changes in cellular morphology.

This thesis primarily focuses on the molecular characterisation of cytoskeletal structures that play key roles in the cell cycle, life cycle and pathogenicity of *T. brucei*. In this Introduction, I will first consider the various structures of the cytoskeleton in terms of their interdependency and dynamics through the cell and life cycles. I will then go on to review the current literature on one of the most intriguing cytoskeletal structures, the paraflagellar rod (PFR).

1.1.2. Trypanosomatid morphology

The major categories of trypanosomatid morphologies: trypomastigote, epimastigote, promastigote and amastigote, are defined by the position and morphology of the single flagellum, the nucleus and

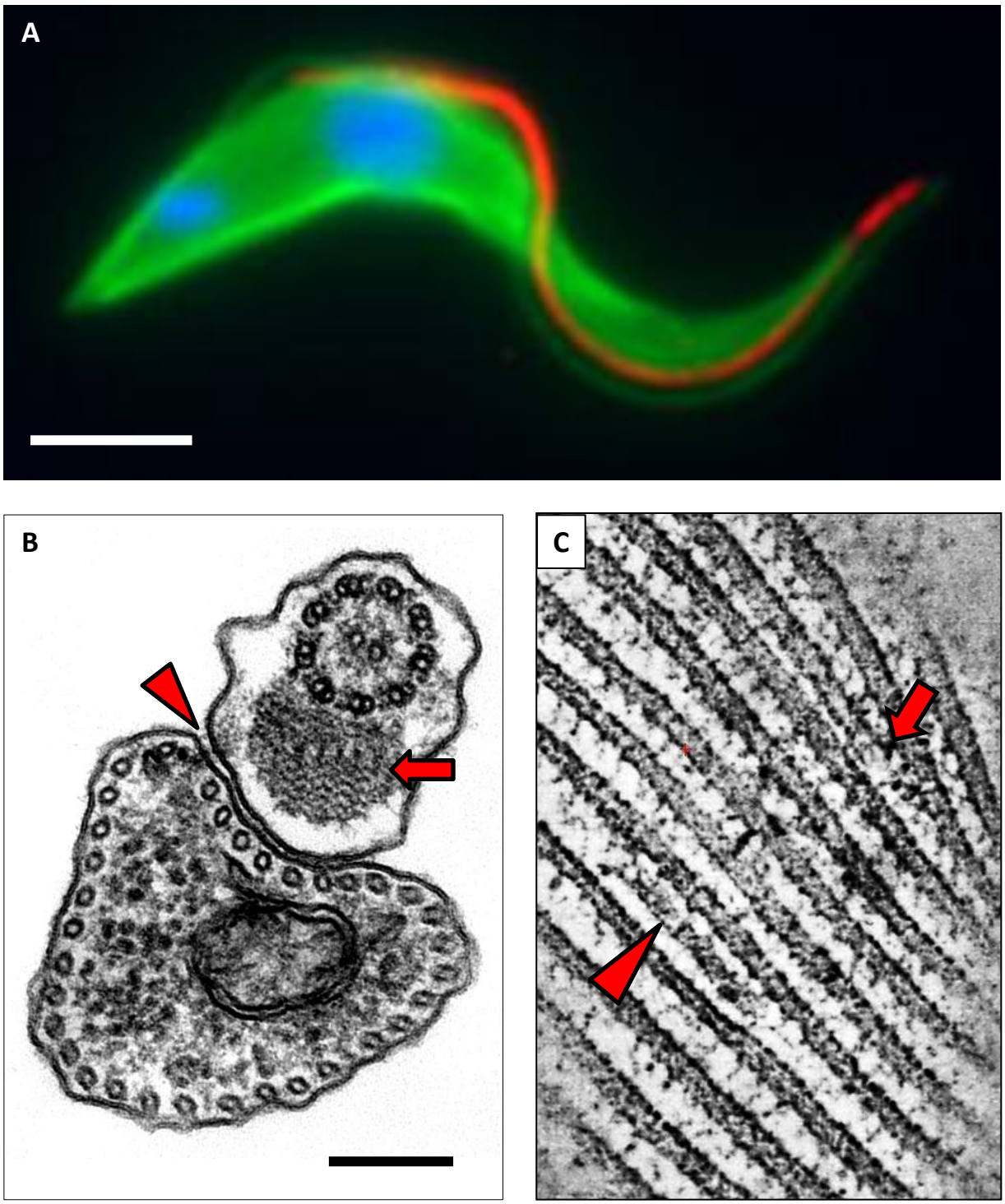

Figure 1.1. The cytoskeleton. A) Immunofluorescence image of procyclic form *T. brucei*. The microtubule array and axoneme are shown in green (tubulin), the paraflagellar rod is in red (ROD1) and the nucleus and kinetoplast in blue (DAPI). Bar = 5 μm. B) TEM of a transverse section through the anterior end of procyclic form showing the microtubule array and the flagellum. Arrow = paraflagellar rod, arrowhead = FAZ, bar = 200 nm. C) Nominal 10 nm thick pseudosection from a tomographic reconstruction of procyclic form. The regular spacing of the microtubules and the intermicrotubule cross bridges can be clearly seen. Arrow, a microtubule ends in the array and the neighbouring microtubules come together to preserve the intermicrotubule spacing. Arrowhead, a short microtubule intercalated into the array.

the kinetoplast (McGhee and Cosgrove 1980). The kinetoplast consists of the densely packed, concatenated DNA of the single mitochondrion and is the defining feature of the order *Kinetoplastida* which includes the trypanosomatids. The flagellum is attached to the kinetoplast via its basal body and hence the position of the base of the flagellum, its course and its point of emergence are intimately associated with the relative position of the kinetoplast in the cell. The anterior and posterior poles of the cell are usually defined in terms of the normal direction of translocation of motile forms. In this way forward motility corresponds to translocation in an anterior direction (Hill 2003). In trypomastigotes the kinetoplast is positioned posterior to the nucleus and the long flagellum extends towards the anterior and is attached to the cell body for most of its length. Epimastigotes and promastigotes are defined by a kinetoplast positioned anterior to the nucleus and a long flagellum that is attached to the cell body in epimastigotes or free in promastigotes. Finally amastigotes are small rounded cells that constitute the intracellular lifecycle stage of *Leishmania spp.* and *T. cruzi*. These cells again have the kinetoplast situated on the anterior side of the nucleus but the flagellum is very short and does not emerge onto the cell surface. This diversity of forms reflects both the cell cycle and life cycle requirements and the very different environmental challenges encountered by cells at each stage.

1.1.2. *T. brucei* life-cycle and differentiation

T. brucei has a complex lifecycle with multiple distinct phases encompassing a passage through the insect vector and mammalian host (Vickerman 1985). Beginning in the midgut of the insect vector, proliferative procyclic form trypomastigotes, in which the kinetoplast is positioned midway between the nucleus and the posterior pole of the cell, migrate through the digestive tract to the proventriculus, arresting in G2 and becoming longer and thinner to form non-proliferative mesocyclic forms. During this elongation process the posterior-kinetoplast distance remains relatively constant whereas the posterior-nucleus distance decreases until the kinetoplast adopts an anterior position relative to the nucleus in the epimastigote morphology (Sharma, Gluenz et al. 2009). These cells then undergo a single extreme asymmetric division to produce long and short daughter epimastigote

cells(Sharma, Peacock et al. 2008). The long daughter cell is then thought to die while the short daughter cell migrates to the salivary gland where a second site of infection is established. In the salivary gland, epimastigotes become attached to the salivary gland epithelium via junctional complexes arising from elaborations of the flagellar membrane that may involve the PFR (Tetley and Vickerman 1985). Attached epimastigotes are proliferative and once established the infection lasts for the lifetime of the fly. In a process that is not currently well-understood, attached epimastigotes give rise to pre-metacyclic and then metacyclic trypomastigotes that are subsequently transferred to the mammalian host when the fly takes a bloodmeal (Sharma, Gluenz et al. 2009). In the host bloodstream, parasites initiate a third proliferative cycle as extracellular long slender bloodstream form trypomastigotes (Vickerman 1985). In the bloodstream, the parasite population bypasses the humoral immune response using an extreme form of antigenic variation (Cross 1977; Ferrante and Allison 1983; McCulloch 2004). The mechanism of immune evasion involves the tightly controlled expression in each individual cell of a single isoform of a variable surface glycoprotein (VSG) (Chaves, Rudenko et al. 1999; Borst 2002) from a genomic repertoire of as many as 1500 antigenically distinct variants (Field and Boothroyd 1996; Berriman, Ghedin et al. 2005; Hutchinson, Picozzi et al. 2007). In any given cell there is a small chance of switching expression to another VSG variant. During the course of an infection the host immune system will mount a successful challenge against the dominant VSG variant but by this time subpopulations of parasites will have switched their antigenic coat and evade this immune response. Subsequent proliferation of these founder cells results in the waves of parasitaemia characteristic of *T. brucei* infections (Barry and McCulloch 2001; Morrison, Majiwa et al. 2005). The pathology of infection exhibits symptoms in two stages. In the first stage, the haemolymphatic stage, parasites are present in the circulatory and lymphatic systems leading to severe headaches, fever and joint pain and can eventually lead to anaemia and cardiac or kidney failure. If left untreated, parasites eventually cross the blood-brain barrier initiating the neurological phase that begins with disruption of the sleep cycle (hence African sleeping sickness) and leads to mental deterioration, coma and death. As parasite load in the circulatory system increases, a quorum

sensing mechanism via the elusive parasite derived factor SIF (stumpy induction factor) (Reuner, Vassella et al. 1997; Vassella, Reuner et al. 1997) induces some cells to become arrested in G0/1 and begin the morphological changes to non-proliferative stumpy form trypomastigotes. This includes an overall reduction in cell length but an increase in cell volume (Tyler, Matthews et al. 2001; Fenn and Matthews 2007; Rotureau, Subota et al. 2011) and is accompanied by pre-adaptations to life in the insect vector, such a switch from glycolysis to the TCA cycle as a carbon source with a concomitant elaboration of the mitochondrion (Matthews 2005). Stumpy forms are then ingested by a fly and travel with the bloodmeal to the midgut where they complete the differentiation back to procyclic forms.

The presence of distinct bloodstream form stages is known as pleomorphism and is in contrast to the situation in commonly used laboratory strains which are morphologically more similar to long slender forms (Matthews, Ellis et al. 2004). These strains, termed monomorphic, proliferate rapidly in the bloodstream of the mammalian host but do not differentiate into stumpy forms. This is likely due to selection over many generations for cell populations that grow rapidly (i.e. without SIF induced growth arrest) without selection for transmissibility through the fly (Fenn and Matthews 2007). There is some debate in the literature regarding the importance of the stumpy form in the process of differentiation from bloodstream to procyclic forms due to the finding that monomorphic bloodstream forms can be induced to differentiate into procyclic forms by various stimuli without passing through an intermediate stumpy form phase (Li, Li et al. 2003).

1.2. The flagellum

The eukaryotic flagellum is a widely conserved organelle and was a feature of the ancestor of all eukaryotes. The flagellum is implicated in an ever growing spectrum of human genetic disease (Gerdes, Davis et al. 2009) and is an attribute of many pathogenic organisms. It has been the subject of a number of recent proteomic characterisations in several model organisms and this analysis of components has also been extended to substructures of the axoneme such as the radial spokes and basal bodies (Yang, Diener et al. 2006; Kilburn, Pearson et al. 2007).

Trypanosomatids produce a single flagellum which is involved in numerous aspects of parasite biology including motility, cytokinesis, environment sensing, attachment to the host (Vickerman 1973; Robinson and Gull 1991; Beattie and Gull 1997; Ogbadoyi, Robinson et al. 2003; Oberholzer, Bregy et al. 2007; Oberholzer, Marti et al. 2007) and in the case of *T. brucei*, flagellar function plays a key role in the survival of the mammalian bloodstream stage (Broadhead, Dawe et al. 2006).

1.2.1. Ultrastructure of the *T. brucei* flagellum

The *T. brucei* flagellum incorporates the canonical 9+2 microtubular eukaryotic axoneme (Figure 1.2) and a structure unique to kinetoplastids termed the paraflagellar rod (PFR – see below) which is required for flagellar motility (Bastin, Sherwin et al. 1998). The flagellum plays important roles in cell motility, pathogenicity and cell division and contains components that strongly suggest roles in sensing and signalling (Broadhead, Dawe et al. 2006; Griffiths, Portman et al. 2007; Oberholzer, Marti et al. 2007; Ginger, Portman et al. 2008).

The flagellum follows the standard eukaryotic model of nucleation from a triplet microtubule basal body with a probasal body located on the anterior side in a perpendicular orientation. In addition to its role in flagellar nucleation, the basal body is also attached to the kinetoplast via a membrane spanning junction known as the tripartite attachment complex (TAC) (Robinson and Gull 1991; Ogbadoyi, Robinson et al. 2003). This intimate association means that duplication of the basal body

and subsequent segregation is responsible for the segregation of the kinetoplast DNA during the cell cycle (Robinson and Gull 1991; Gluenz, Povelones et al. 2011).

The nine outer doublet microtubules of the axoneme consist of a complete microtubule of 13 protofilaments, the a-tubule, and an attached incomplete microtubule of 11 protofilaments with an additional protofilament ribbon, the b-tubule (Figure 1.2.). These nine outer doublet microtubules form a ring with radial symmetry that surrounds a central pair of singlet microtubules, c1 and c2, that nucleate above the basal body in the transition zone. The axoneme is decorated with a number of additional structures such as the outer dynein arms, the inner dynein arms, the radial spokes, the nexin links which connect neighbouring doublets and the central pair projections. These structures repeat along the long axis of the axoneme with a 96 nm periodicity. The motile force of flagella is usually provided by the outer dynein arm complexes which consist of heavy, intermediate and light components. In *T. brucei* four of these decorate the surface of the a-tubule of each outer doublet in each 96 nm repeat. They induce flagellar bending by forming transient interactions with the b-tubule of the neighbouring doublet in an ATP dependent process. This involves a conformational change to the structure of the outer dynein arm that results in neighbouring microtubule doublets sliding in relation to each other (Gibbons and Rowe 1965; Gibbons and Gibbons 1973; Sale and Satir 1977). The inner dynein arm complexes are thought to regulate the mode of flagellar beat and show greater variation in composition than outer dynein arms with at least six distinct species within each 96 nm repeat (Porter and Sale 2000). The central pair microtubules are surrounded by large protein complexes often referred to as central pair projections and these are thought to transduce signals from the central pair to the dynein arms via the radial spoke complexes that project from each a-tubule. Recently several studies have analysed the proteomic composition of flagella from a diverse set of organisms (Ostrowski, Blackburn et al. 2002; Pazour, Agrin et al. 2005; Smith, Northey et al. 2005; Broadhead, Dawe et al. 2006). One of the most striking features of these analyses is the diversity in protein composition of an organelle so well conserved at the ultrastructural level.

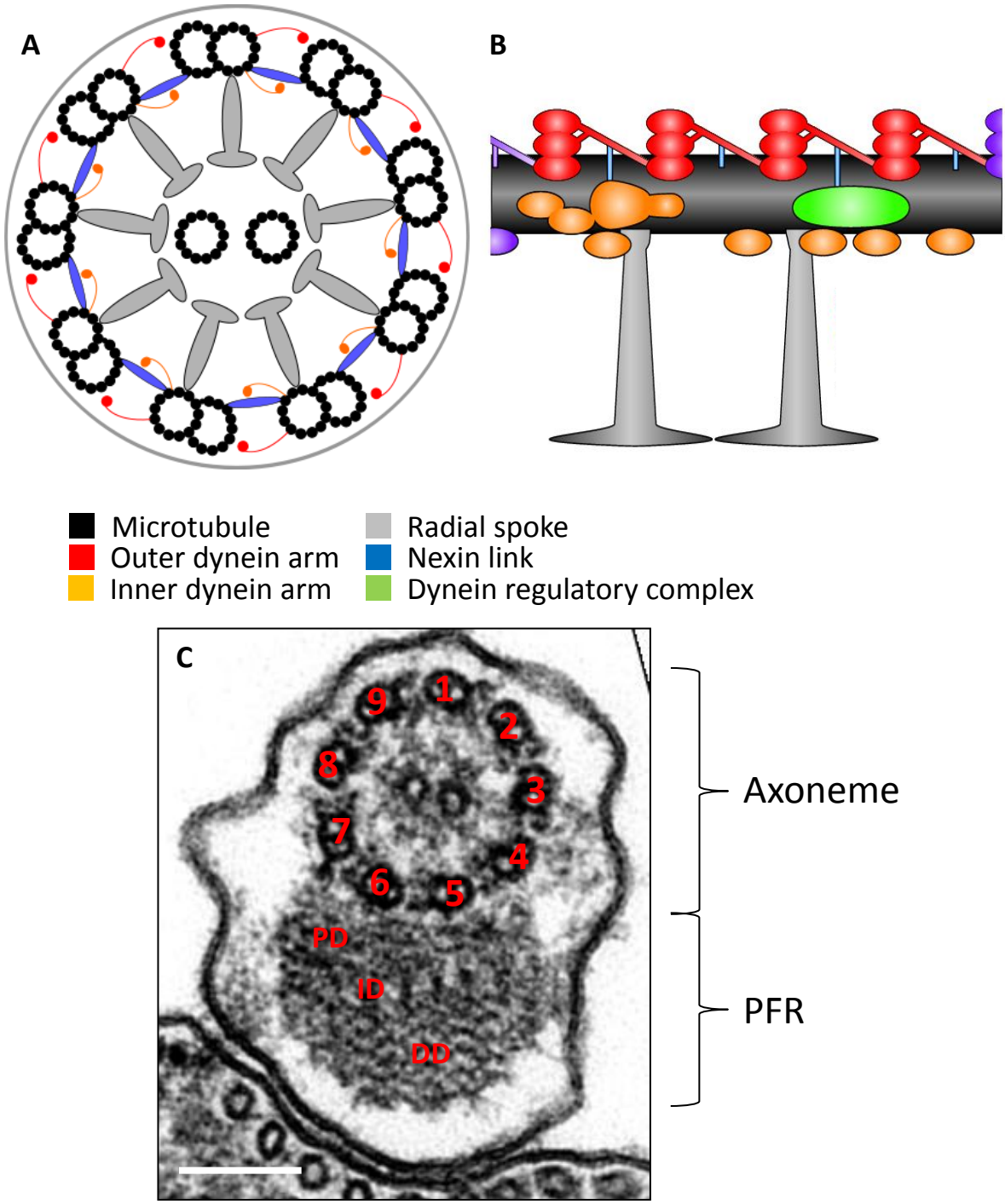

Figure 1.2. The axoneme. Cartoon representation of A) a transverse section and B) a longitudinal section of a typical eukaryotic axoneme. Black = microtubule, red = outer dynein arm, orange = inner dynein arm, grey = radial spoke, blue = nexin link, green = dynein regulatory complex. The cross-sectional diameter of the axoneme is around 200 nm and the longitudnal section represents a single 96 nm repeat unit. C) In *T. brucei* the invariant orientation of the PFR and central pair with the axoneme allows the unambiguous identification of each outer doublet. PD = proximal, ID = intermediate and DD = distal domain of the PFR. Bar = 100 nm

Although the ultrastructure of the flagellum has been studied extensively over many years, the recent identification of ponticuli - intriguing post-assembly modifications to the lumen of b-tubules in the outer doublets of the *T. brucei* axoneme – demonstrates the continuing capacity of this complex organelle to surprise and perplex (Vaughan, Shaw et al. 2006).

1.2.2. Flagellar assembly

Most eukaryotic flagella, including those of the *kinetoplastida*, are assembled by a process known as intraflagellar transport (IFT) (Kozminski, Johnson et al. 1993). This involves two sets of motors: kinesin 2 for anterograde transport and cytoplasmic dynein 1b for retrograde transport; that carry cargo to and from the growing flagellar tip (Scholey 2003). IFT rafts dock at sites at the transitional fibres near the flagellar basal body and track along the outer doublet microtubules. Although IFT is nearly ubiquitous in eukaryotes that assemble a flagellum, there are some well-known examples of IFT-independent flagellar formation, most notably in the apicomplexans and related lineages. For example, the genome of the malaria parasite *Plasmodium* is completely devoid of genes encoding any known IFT component and this correlates with the finding that in the gamete stage this organism assembles its flagellum in the cytoplasm and only then extrudes it to the cell surface (Briggs, Davidge et al. 2004). This particular form of flagellar formation has also been noted in other organisms, such as *Drosophila melanogaster*, which uses intracytoplasmic flagellum formation during spermatogenesis (although other cilia and flagella in this organism are assembled by IFT) (Han, Kwok et al. 2003). It has been postulated that intracytoplasmic flagellum formation reflects a need for very rapid extension of flagella in specific cell types.

1.2.3. The role of flagellar motility in *T. brucei* cytokinesis

Bloodstream form *T. brucei* appear to be exquisitely sensitive to ablation of flagellar components and appear to rely on flagellar function to complete cytokinesis. A number of recent studies have demonstrated the contrast between phenotypes associated with ablation of individual flagellar components in procyclic and bloodstream form *T. brucei* (Branche, Kohl et al. 2006; Broadhead,

Dawe et al. 2006; Ralston and Hill 2006; Ralston, Lerner et al. 2006; Farr and Gull 2009). Flagellar function in procyclic form cells can be disrupted by ablation of individual flagellar components with little or no impact on the growth rate of the cell population. However, when the same proteins are ablated in the bloodstream form, cells become monstrous and contorted with multiple nuclei, kinetoplasts and flagella, indicating a catastrophic failure in cytokinesis. An RNAi target sequencing (RIT-seq) study conducted by Horn and co-workers (Alsford, Turner et al. 2011) assayed the loss of fitness associated with RNAi-mediated knockdown of over 99% of the open reading frames in the *T. brucei* genome. Proteins with Gene Ontology terms associated with the axoneme or flagellar motility were highly enriched in a set of genes that conferred a loss of fitness on bloodstream but not procyclic forms. The underlying molecular mechanisms behind this dichotomy remain unclear although numerous differences between bloodstream form and procyclic form cells could be implicated and indeed, this may be a combinatorial or pleiotropic phenomenon. There are many differences between these cell types: organelle segregation patterns; cleavage point initiation; the presence of the canonical flagella connector in procyclic but not bloodstream forms (see below); that all point to contrasting patterns that could be differentially influenced by flagellar mutants. Also under culture conditions the bloodstream form cell cycle is significantly faster than that of commonly used laboratory strains of procyclic form and it may be that this time difference allows these procyclic form cells greater latitude in the final stages of cell division. An increase in the time taken to complete cytokinesis could therefore have lethal consequences for the proper segregation and positioning of organelles and cleavage furrows in the bloodstream form but not the procyclic form.

Bloodstream form cytokinesis failure has been demonstrated in RNAi mutants with a diverse range of effects on the flagellum. For example, in the procyclic form, ablation of PFR2 results in the loss of most of the PFR structure (Bastin, Sherwin et al. 1998) whilst ablation of the flagellar protein TbPACRGA has very little effect on the morphology of the flagellum due to redundancy with TbPACRGB (Dawe, Farr et al. 2005). However, despite the differences in procyclic form phenotype,

ablation of either PFR2 or TbPACRGA alone is lethal to the bloodstream form trypanosome (Broadhead, Dawe et al. 2006). Ablation of Tbmbo2, DIGIT and Trypanin result in viable cells with qualitatively different motility defects in the procyclic form (Hutchings, Donelson et al. 2002; Broadhead, Dawe et al. 2006) and yet produce equivalent lethal phenotypes in the bloodstream form (Broadhead, Dawe et al. 2006; Ralston and Hill 2006). Finally, a homologue to the trypanosome axonemal protein TAX-1 (Broadhead, Dawe et al. 2006) was shown to be a small component of one of the various inner arm dynein complexes in *Chlamydomonas* (Yamamoto, Yanagisawa et al. 2006). Ablation of this single component in procyclic form *T. brucei* does not interfere with overall axoneme structure (Farr 2007) and does not compromise cell growth (Broadhead, Dawe et al. 2006) yet produces the dramatic lethal phenotype on ablation in bloodstream form trypanosomes (Broadhead, Dawe et al. 2006). A recent report from Hill and co-workers (Ralston, Kisalu et al. 2011) has suggested that it is not flagellar motility per se that is required for viability of the bloodstream form due to the finding that cells with impaired motility as a result of the expression of a non-functional dynein light chain (LC1) are viable. When expressed in procyclic forms, this mutant protein had a limited deleterious effect on cell motility, slowing down cell translocation but preserving the forward motion. This is in contrast to the phenotype observed after RNAi against the same protein in which cells translocate in the reverse direction. In the bloodstream form, RNAi yielded the same phenotype as described above but expression of the mutant protein disrupted cell movement without inducing cytokinesis failure. Whether this result represents a requirement for correct flagellar structure (disrupted by RNAi) rather than correct flagellar function (disrupted in the LC1 mutant) as suggested in the study or whether it demonstrates that preservation of some residual forward motility is sufficient to rescue the cytokinesis defect has yet to be determined.

Productive movement of the cell has been shown to be an essential mechanism in the clearance of the VSG from the cell surface into the flagellar pocket (see below) in bloodstream form trypanosomes (Engstler, Pfohl et al. 2007). It is possible that if the process of VSG clearance is defective, endo- and exocytotic processes internalising VSG and delivering newly synthesised protein

to the cell surface will be impaired, leading to the vastly enlarged flagellar pocket morphology observed in flagellum mutants. These enlarged pockets would provide unassailable physical challenges to the precise morphogenetic patterning required for trypanosome cytokinesis.

There is evidence that aberrant flagellar structure and function can also impair proliferation and morphogenesis in procyclic forms. Simultaneous ablation of the two homologues of PACRG in procyclic form *T. brucei* results in reduced growth rates compared to wild-type populations (Dawe, Farr et al. 2005). These double-knock-down cells exhibit defects in kinetoplast positioning, paralysed flagella and disruptions to the outer doublet microtubular ring of the axoneme. The contribution of each of these defects to the reduction in growth rate is not currently known but a reduction in cell motility is an early manifestation in this phenotype. Some studies have demonstrated the aggregation of *T. brucei* cells after RNAi ablation of flagellar proteins under certain culture conditions (Branche, Kohl et al. 2006; Ralston, Lerner et al. 2006; Baron, Ralston et al. 2007). In these cases, the slow-down in growth observed could be rescued by agitating the cultures, suggesting that cell motility, either as a direct effect or as a secondary effect (e.g. cells becoming locally concentrated due to settling in the culture flask), plays a role in the growth rate of cell populations. However, there are discrepancies in the procyclic form growth phenotypes reported in the literature (Branche, Kohl et al. 2006; Broadhead, Dawe et al. 2006; Ralston, Lerner et al. 2006; Baron, Ralston et al. 2007). Use of different growth media in different laboratories and treatment of the culture are likely variables that would need to be controlled in order to conduct an accurate comparison. As trypanosome cell density follows a classical microbiological growth curve in culture with lag, log and stationary phases, it is important to analyse any studies of population growth with these phases in mind. Rescue of bloodstream form motility mutants by agitation of the culture medium has not yet been demonstrated, however it has been shown that turbulence in the mammalian host bloodstream is not sufficient to rescue the phenotype (Griffiths, Portman et al. 2007). It is possible that it is the specific auger-like twisting motility of *T. brucei* that is necessary for

the completion of cytokinesis and that turbulence in the mammalian bloodstream does not sufficiently provide this.

As well as motility functions, most if not all flagella have sensory/regulatory functions. These translate to an influence for flagella in many cellular processes (Ginger, Portman et al. 2008). There is evidence that cilia and flagella act as part of specific cell cycle check points in a number of organisms with *C. reinhardtii* being the best studied. Recently the role of the flagellum as an instrument of signal transduction, including an involvement in Hedgehog signalling, has excited much interest (for reviews see Scholey and Anderson 2006; Pedersen and Rosenbaum 2008). It may be that loss of flagellar motility in bloodstream form *T. brucei* interferes with critical signalling pathways involved in cell cycle progression. It should be noted that in all of the motility mutants that have so far been shown to cause lethality in the bloodstream form, the flagellum is still built, raising the possibility of some requirement for correct flagellar function in a flagellar-derived signalling pathway. The role of cilia and flagella in cell cycle regulation has also been discussed from the point of view of the sequestration (as the flagellar basal body) of one of the centrioles needed for mitotic spindle formation (Pan and Snell 2007; Ralston, Kabututu et al. 2009). The trypanosome flagellum, however, unlike that of *Chlamydomonas* or the vertebrate primary cilium, is not resorbed during the cell cycle (Sherwin and Gull 1989) and the basal body is not required for mitotic spindle formation, so even if this specific biology of a flagellum or cilium exists in other cells it is unlikely to be a factor in the cytokinesis defects observed in bloodstream form motility mutants.

1.3. The cytoskeleton

1.3.1. The microtubule array

The following descriptions are largely based on analyses of the culture adapted procyclic form of *T. brucei* but the general features are for the most part shared by all lifecycle stages.

The framework of the cytoskeleton consists of 100 or more individual microtubules that are extensively modified and arranged in a helical array orientated to the anterior-posterior axis of the cell beneath the pellicular membrane (Sherwin and Gull 1989; Gull 1999) (Figure 1.1.). Microtubules are formed by the polymerisation of dimers of α- and β-tubulin into protofilaments such that the α-tubulin component of one dimer connects to the β-tubulin component of the next and so on. Each microtubule consists of 13 protofilaments arranged in a helical pattern and each turn of the helix contains 13 tubulin dimers, one from each protofilament. This constant orientation of the tubulin dimers within the microtubule means that there is an intrinsic polarity to the polymer. At one end α-tubulin is exposed and this is termed the minus end, whilst at the other end, termed the plus end, only β-tubulin is exposed. Assembly and disassembly of microtubules occurs predominantly at the plus end. The microtubules of the subpellicular array are connected to one another and to the pellicular membrane and these connections serve to maintain constant intermicrotubule and microtubule-to-membrane distances (Sherwin and Gull 1989) (Figure 1.1.). With only two notable exceptions, all of the microtubules of the cytoskeleton are arranged such that the dynamic plus ends face the posterior end of the cell and the more stable minus ends face the anterior (Robinson, Sherwin et al. 1995). The exceptions to this are the microtubules of the flagellum and a specialised quartet of microtubules (mtq) in which the microtubules are orientated such that the plus ends face the anterior of the cell (Gull 1999). Taking a view through the cell from the posterior end, the cross sectional diameter increases to its maximum size in the vicinity of the nucleus. From this point the diameter of the cell then gradually decreases towards the anterior tip. Throughout the cell the

intermicrotubule distance in the subpellicular corset is maintained and this necessitates the presence of microtubules of different lengths in the array (Figure 1.1.C.). When a microtubule ends in the array the neighbouring microtubules come together and become cross-linked to one another, thus preserving the intermicrotubule distance and the integrity of the subpellicular corset (Gull 1999). In this way the cross-sectional diameter of the cell at any given point is a direct function of the number of microtubules present in the array (Gull 1999) (Figure 1.1.B.).

1.3.2. The flagellum attachment zone (FAZ)

The mtq nucleate in the vicinity of the basal body and extend via their plus ends around a specialised membrane compartment, known as the flagellar pocket (see below), in a left-handed helix before joining the subpellicular array (Lacomble, Vaughan et al. 2009). As part of the subpellicular array the mtq constitute part of a complex membrane spanning junction known as the flagellum attachment zone (FAZ) (Figure 1.1.B.). The FAZ connects the flagellum to the cell body and extends to the anterior tip of the cell (Vickerman 1969; Sherwin and Gull 1989; Woods, Sherwin et al. 1989). In addition to the mtq the FAZ consists of the FAZ filament, regularly spaced electron dense junctional complexes known as the FAZ maculae adherans and filaments that connect through the pellicular and flagellar membranes (Vaughan, Kohl et al. 2008; Lacomble, Vaughan et al. 2009). Flagella length plays a crucial role in the positioning of the ingression point of the cleavage furrow during cytokinesis and there is much evidence to suggest that this is a function of the length of the associated FAZ rather than a direct result of the position of the flagellar tip, although of course the two factors are inextricably linked in these cells. Donelson and co-workers (LaCount, Barrett et al. 2002) showed that expression of the *Trypanosoma cruzi* protein GP72, the orthologue of the *T. brucei* FAZ protein fla1, in procyclic form *T. brucei* resulted in cells with detached flagella that nonetheless were able to undergo cytokinesis and maintain a stable population for a short time before wild-type revertants became dominant. This is in contrast to the phenotype observed on ablation of fla1 which also yielded cells with detached flagella but suffered severe cytokinesis defects. It was proposed that GP72 exerted a dominant negative effect, preventing FAZ formation and resulting in complete

flagellar detachment. However, analysis of the GP72-expressing population reveals a distinct change in cellular morphology with cells appearing to be significantly shortened at the anterior. This fits a model whereby a short FAZ-like structure containing GP72 assembles and defines an intrusion point for the cleavage furrow in a position posterior to that in wildtype. Unfortunately the localisation of GP72 in these cells was not determined and this hypothetical model remains to be tested.

1.3.3. The flagella connector

During the cell cycle of procyclic forms, the tip of the new flagellum is connected to the lateral aspect of the old flagellum by a mobile transmembrane junction known as the flagella connector (FC) (Moreira-Leite, Sherwin et al. 2001) (Figure 1.3.). The FC appears as an asymmetric trilaminar structure. In longitudinal sections, three distinct domains are observed corresponding to structures within the old flagellum, spanning the two flagellar membranes and within the new flagellum (Moreira-Leite, Sherwin et al. 2001). In transverse section, these three domains are further subdivided into three parallel zones with plate-like structures within both the old and new flagellum (Briggs, McKean et al. 2004). The invariant orientation of the axonemal outer doublets with respect to the PFR and central pair (Figure 1.3.) enabled Briggs et al (Briggs, McKean et al. 2004) to determine that the FC is always associated with doublets 7, 8 and 9 of the old flagellum. The FC tracks the tip of the new flagellum throughout the elongation process, disappearing at a variable time during cytokinesis. Although the mechanism of FC motility has not yet been described, the motile force appears to be generated in the portion of the FC associated with the old flagellum. Ablation of new flagellum formation results in tubes of flagellar membrane extending from the flagellar pocket and tracking alongside the old flagellum. The FC is still formed in these cells and it appears to be this that drags the membrane sleeve out onto the cell surface (Davidge, Chambers et al. 2006). The FC is a fascinating structure but is only known at the molecular level by a single monoclonal antibody (AB1) for which the antigen has not been determined. In Chapter 4 of this thesis, I will present evidence of the first FC component to be identified.

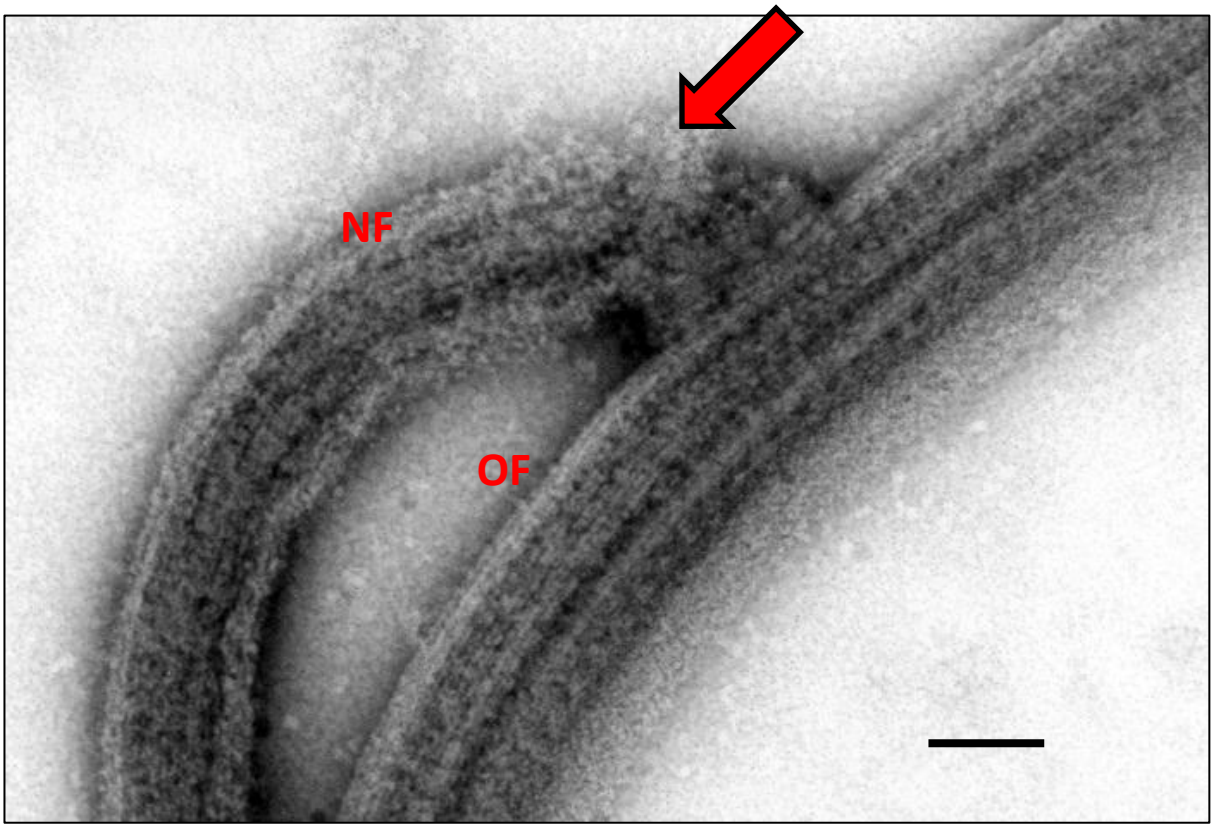

Figure 1.3. The flagella connector. Negatively stained procyclic form whole mount cytoskeleton. The tip of the new flagellum (NF) is connected to the lateral aspect of the old flagellum (OF) by the flagella connector (arrow). Bar = 200 nm.

1.3.4. The flagellar pocket

From its initiation at the basal body, the flagellum emerges into the flagellar pocket (FP), a vase-shaped invagination of the pellicular membrane that is the sole site of endo- and exocytosis for the cell (Landfear and Ignatushchenko 2001) and which houses many receptors involved in host-parasite interactions and nutrient uptake (Steverding 2000; Drain, Bishop et al. 2001; Hung, Qiao et al. 2004; Field, Natesan et al. 2007; Vanhollebeke, De Muylder et al. 2008; Field and Carrington 2009) (Figure 1.4.). Endocytosis occurs via clathrin coated vesicles and rates are around 10-fold higher in the bloodstream form of *T. brucei* than in the procyclic form reflecting the role of the FP in the internalisation and recycling of VSG from the cell surface (Morgan, Hall et al. 2002; Overath and Engstler 2004). The FP is notable for the almost total absence of an underlying microtubule array which is presumably necessitated by the need for access and egress of transport vesicles. However, the mtq are attached to the posterior face of the FP and a recent study on bloodstream form trypanosomes suggests that they may perform a function in the transport of molecules into this compartment as a prelude to internalisation (Gadelha, Rothery et al. 2009). Supporting the view that the presence of a microtubule array is refractory to the ability to internalise molecules, the FP membrane associated with the mtq was found to be devoid of clathrin-coated pits.

The boundaries of the FP are defined by a set of cytoskeletal structures that also serve to delimit at least four distinct membrane domains in the cell (Gadelha, Rothery et al. 2009; Lacomble, Vaughan et al. 2009). At the base of the FP, where flagellum intrusion occurs, an intriguing structure known as the collarette surrounds the external surface of the flagellar membrane (Vickerman 1973; Lacomble, Vaughan et al. 2009). In lateral section the collarette appears as thin fibres that flank the flagellum (Figure 1.4.) and in transverse section the collarette can be seen to be composed of nine regularly spaced tubular doublets connected by plate-like fibrillar structures. The collarette is mirrored on the interior face of the flagellar membrane by a set of recently identified radial fibres (Lacomble, Vaughan et al. 2009). Like the collarette these occur with nine-fold symmetry that reflects the arrangement of the doublet microtubules of the axoneme, suggesting a membrane spanning

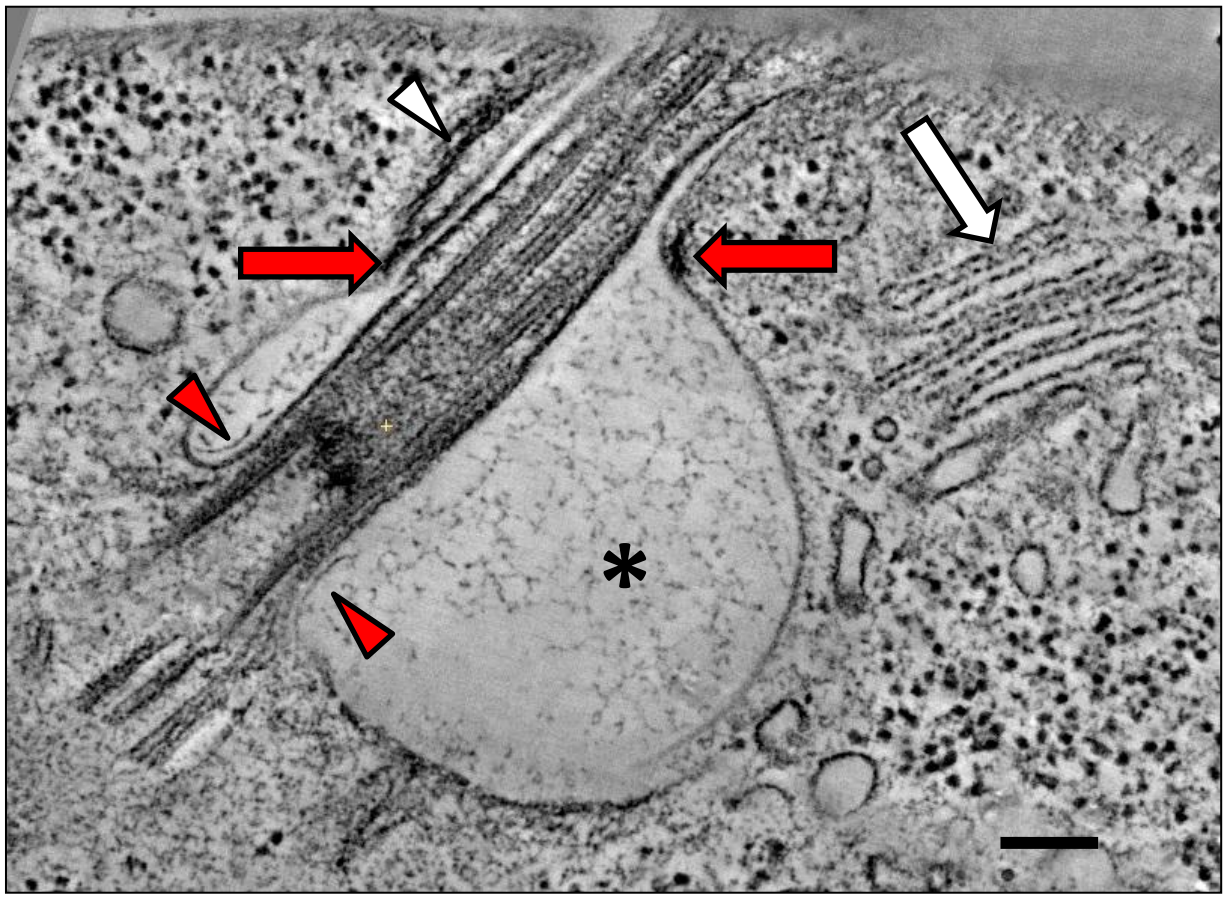

Figure 1.4. The flagellar pocket. Nominal 10 nm thick pseudosection from a tomographic reconstruction of a procyclic form cell. Red arrows show the flagellar pocket collar on either side of the neck region. Red arrowheads show the collarette in longitudinal section. White arrow marks the position of the Golgi and white arrowhead shows the mtq. * = flagellar pocket lumen, bar = 200 nm.

influence from the internal structure of the flagellum. A third set of fibres known as the transitional fibres link the triplet microtubules of the basal body to the interior surface of the flagellar membrane (Lacomble, Vaughan et al. 2009). Little is known of the composition or function of these elements but their location demarks the transition from the membrane domain of the flagellum to that of the FP. The flagellum traverses the FP lumen and emerges onto the exterior of the cell through a constriction of the FP known as the neck region. At this point the cross sectional diameter of the flagellar pocket is only slightly larger than that of the flagellum which it surrounds, presumably restricting communication between the flagellar pocket lumen and the external milieu.

1.3.5. The flagellar pocket collar

At the base of the neck region an electron dense ring of material surrounds and constricts the lumen on the cytoplasmic face of the membrane. This structure is known as the flagellar pocket collar (FPC) (Henley, Lee et al. 1978; Sherwin and Gull 1989) and its location marks the transition point where the flagellar pocket membrane domain becomes the neck membrane domain (Figure 1.4.). In addition to its aspect on the cytoplasmic face of the membrane, the FPC has also been described in several studies in terms of a ring of intramembrane particles (Henley, Lee et al. 1978; Gadelha, Rothery et al. 2009), strongly suggesting a transmembrane element to the structure and reinforcing the view of a major influence of the cytoskeleton on the formation and maintenance of distinct membrane domains. Robinson and co-workers recently published the first identification of a component of the FPC, BILBO1 (Bonhivers, Nowacki et al. 2008). RNAi-mediated ablation of BILBO1 resulted in the failure of FP biogenesis (or perhaps a reduction in FP stability) with flagella emerging directly from the pellicular membrane and not attached to the cell body along their length. With this there is a concomitant loss of FAZ structure and basal body segregation and the accumulation of monstrous cells indicative of cytokinesis failure and/or organelle mispositioning.

A newly identified short microtubule known as the neck microtubule is also located in this neck region (Lacomble, Vaughan et al. 2009). It is positioned adjacent to the mtq and follows their left-

handed helical path around the neck but does not extend below the FPC or into the subpellicular array. The neck microtubule lies outside the circle described by the FPC and so far its function, orientation and biogenesis are unknown. The neck region constitutes the third discreet membrane domain as it differs from the pellicular membrane in being devoid of an underlying microtubule array (with the exception of the mtq) but shows no evidence of the endocytic activity described for the FP membrane domain (Gadelha, Rothery et al. 2009).

1.3.6. The Golgi and bilobe

The mtq traverse the FPC and associate with other components of the FAZ which begin the attachment of the flagellum to the cell body in the neck region. The Golgi is positioned in the cytoplasm adjacent to the neck region and this positioning is also mediated by cytoskeletal components. The Golgi is associated with a particular localisation of TbCentrin2 known as the bilobe structure which also contains TbCentrin4 (He, Pypaert et al. 2005; Shi, Franklin et al. 2008). Prior to duplication, the existing Golgi is associated with the anterior lobe and during the cell cycle the new Golgi assembles at the posterior one. At approximately the same time as kinetoplast segregation occurs, the bilobe itself duplicates in a process that involves the transient localisation of TbPolo-like kinase to the structure (de Graffenried, Ho et al. 2008). Each Golgi becomes associated with one of the bilobe structures which then segregate prior to cytokinesis. Recently the Warren and He groups have reported that two of the novel components identified in the flagellum proteome (Broadhead, Dawe et al. 2006) are associated with the bilobe. Both CMRP (Collar-associated MORN Repeat Protein - also known as TbMORN1) (Morriswood, He et al. 2009) and TbLRRP1 (previously known as HERTS) (Zhou, Gheiratmand et al. 2010) label a hook-shaped structure adjacent to the flagellar exit point. As both of these proteins were identified in the flagellum proteome this demonstrates that they are tightly associated with the detergent insoluble flagellum cytoskeleton. Immunofluorescent analysis of purified flagella using an antibody against TbCentrin4 shows that this component of the bilobe also remains associated with the flagellar cytoskeleton after detergent extraction (Shi, Franklin et al. 2008). The localisation of these proteins is fascinating. The study by Warren and co-workers

and data presented in this thesis show that the posterior hook of CMRP is associated with, and may even be a component of, the FPC. An extension from the hook lies adjacent to the FAZ and partially colocalises with the bilobe as defined by the localisation of TbCentrin2. TbLRRP1 has a similar localisation pattern and taken together these data suggest a role for the bilobe in mediating interactions between the FPC, the FAZ and the Golgi. In Chapter 5 of this thesis I will present data on CMRP that strongly suggests a key role for this protein in the FPC.

1.3.7. The cytoskeleton in the life cycle

The majority of studies of the cytoskeleton in *T. brucei* have been conducted in the two lifecycle stages that are amenable to culture in the laboratory: the procyclic form from the tsetse fly midgut and the long slender bloodstream form which is the proliferative life cycle stage in the mammalian host. These are both trypomastigote forms with the kinetoplast situated posterior to the nucleus and a single long flagellum that extends from a basal body situated in the posterior portion of the cell (Vickerman 1985). At specific points during its passage from the tsetse fly digestive tract, through the salivary glands and into the mammalian host *T. brucei* adopts both trypomastigote and epimastigote forms (the latter being characterised by an anterior position of the kinetoplast and flagellum in relation to the nucleus) (Vickerman 1985). However, even within these general categories numerous morphologically distinct sub forms exist (Sharma, Gluenz et al. 2009). These range from extremely long, slender cells to relatively short, broad cells. Such drastic changes in morphology are accomplished through asymmetric division events (Sharma, Peacock et al. 2008) or through differentiation of growth arrested cells (Matthews 2005) but all must be accomplished within the confines of the highly ordered microtubule cytoskeleton that persists throughout the life and cell cycles. For example, the transition from the trypomastigote procyclic form in the tsetse midgut to the non-proliferative trypomastigote mesocylic form in the proventriculus involves an increase in cell length from 21 to 36 μm (Sharma, Peacock et al. 2008) and is associated with active extension of the microtubules at the posterior end of the cell (Rotureau, Subota et al. 2011). Interestingly, flagellar length also increases in line with the increase in cell body length. This increase in cell length is

followed in the next life-cycle stage by a dramatic decrease in cell length and adoption of an epimastigote morphology with the associated exchange in the relative positions of the nucleus and kinetoplast along the long axis of the cell. This change in cell morphology is a result of an extreme assymetric division event that results in a short epimastigote cell that goes on to establish the salivary gland infection and a long epimastigote that is thought to constitute a terminally differentiated dead end stage (Sharma, Peacock et al. 2008). The mechanism of asymmetric division appears to involve the relative lengths of the old and new flagella. All *T. brucei* life-cycle stages possess a single flagellum and a second new flagellum is built once per cell cycle alongside the existing one (Gull 1999). The new flagellum is always positioned to the posterior of the old flagellum allowing the provenance of each to be distinguished unambiguously. During cytokinesis, the initial site of cleavage furrow ingression is determined by the position of the tip of the new flagellum (Gull 1999). In the procyclic form, ablation of IFT components initially results in the production of short new flagella and in later stages the new flagellum fails to form at all, although length of the old flagellum is not affected (Davidge, Chambers et al. 2006; Absalon, Blisnick et al. 2008). This leads to a mispositioning of the cleavage furrow and the production of short daughter cells inheriting the new flagellum and long daughter cells that inherit the old flagellum. In the asymmetric division of post-mesocyclic epimastigote cells, the new flagellum is significantly shorter than the old flagellum, thus positioning the cleavage furrow such that a very long daughter cell and a very short daughter cell are formed (Sharma, Peacock et al. 2008).

1.3.8. The microtubule array in the cell cycle

The cytoskeleton must also accommodate the production of near identical daughter cells in the proliferative life cycle stages with the concomitant changes in cell morphology and the need to faithfully duplicate and segregate all cellular structures. During the cell cycle, cell volume increases prior to division of daughter cells and this must be accommodated within the confines of the existing microtubule array which persists throughout. This is accomplished by the extension of the posterior end of the cell through the extension of microtubules from their plus ends and intercalation into the

array of very short microtubules which then extend between the existing microtubules (Sherwin, Schneider et al. 1987; Sherwin and Gull 1989) (Figure 1.1.). In order for this to occur the existing intermicrotubule connections must be severed and the identification of a putative calpain-related protease, CAP5.5, associated with the subpellicular corset provides a potential candidate for this role (Hertz-Fowler, Ersfeld et al. 2001; Olego-Fernandez, Vaughan et al. 2009). Although both are morphologically trypomastigotes the long slender bloodstream form cells differ from the procyclic form trypomastigotes in terms of the relative position of the kinetoplast in the cell and the organisation of the nuclei and kinetoplasts during the cell cycle (Vickerman 1965; Vickerman 1985; Sherwin and Gull 1989; Woodward and Gull 1990; Tyler, Matthews et al. 2001). The kinetoplast is positioned much closer to the posterior pole of the cell in the bloodstream form. In cells that have completed both nuclear and kinetoplast S phase (2K2N cells), the nuclei and kinetoplasts are arranged in a `posterior-K-K-N-N-anterior` morphology as opposed to the `posterior-K-N-K-N-anterior` morphology adopted by procyclic form 2K2N cells.

1.3.9. Cytoskeletal events in the procyclic form cell cycle

One of the earliest events in the cell division process is the nucleation of a new mtq adjacent to what will become the basal body of the new flagellum. This probasal body rotates through 90 degrees and docks with the FP membrane to form a new mature basal body (Sherwin and Gull 1989) which then extends a new flagellum into the lumen of the FP. The FC forms whilst the tip of the new flagellum is still within the FP lumen. Interestingly, although the FC is invariably associated with doublets 7, 8 and 9 of the old flagellum once the new flagellum has emerged from the FP (Briggs, McKean et al. 2004), at this early stage it is associated with doublets 5, 6 and 7 (Lacomble, Vaughan et al. 2010). This reflects the initial position of the new basal body on the anterior side of the old flagellum. It has long been puzzling that the new flagellum begins to extend from an anterior position relative to the old flagellum but rapidly adopts a posterior position whilst still fully contained within the lumen of the FP. The recent advances in the ability to reconstruct 3-dimensional representations of cells with high

resolution via electron tomography have provided the opportunity to address questions such as these. We now know that early in the process of new flagellum elongation, the new basal body rotates in an anticlockwise direction around the fulcrum of the old basal body to take up a position on the posterior side of the old flagellum (Lacomble, Vaughan et al. 2010). This necessitates the ability for the FC to not only move along microtubule doublets during extension of the new flagellum but also to move between microtubule doublets during its rotation about the old flagellum. One consequence of the rotation of the new basal body is the folding of the FP membrane over the old mtq, which act as a rib. This results in a partially bifurcated FP with a single lumen beneath the flagellar exit point and two distinct compartments at its base, separated by a ridge of cytoplasm. The old flagellum emerges into the anterior lobe and the new flagellum into the posterior one. At this stage the FP opens onto the cell surface at a single exit point with one FPC and the new flagellum is still completely contained within the FP. The partially bifurcated FP then resolves into two separate FP compartments each with its own FPC and the new flagellum extends out onto the cell surface. There are currently two apparently contradictory models of new FPC formation in the literature. Based on their study of BILBO1, Bonhivers et al (Bonhivers, Nowacki et al. 2008) proposed a model whereby FPC duplication proceeds by a process of elongation of the existing FPC along the long axis of the cell followed by a constriction along the short axis to generate two discreet FPC structures. This invokes a semi-conservative pattern of inheritance with the mother FPC contributing to daughter FPC formation. However, a recent study that used electron tomography to interrogate biogenesis of the new flagellar pocket identified putative FPC material forming around the new neck region following the translocation of the new flagellum (Lacomble, Vaughan et al. 2010). This suggests an apparently de novo manner of new FPC formation.

The semi-conservative model is compelling in its simplicity, avoiding as it does the issue of how two discreetly formed FPCs would resolve to accommodate the fact that the tip of the new flagellum is attached to the old flagellum via the FC. In the semi-conservative model, the tip of the new flagellum would simply extend through a single elongated FPC which would then resolve into two discreet FPCs

behind it. However, the semi-conservative model is based almost entirely on the observation of elongated FPCs by Bonhivers and co-workers and in Chapter 5 of this thesis I will present an alternative interpretation of this phenomenon.

Whilst the new flagellum rotates around the old flagellum, the new mtq continue to extend alongside the existing mtq and join the subpellicular array where they form the new FAZ (Lacomble, Vaughan et al. 2010). Extension of the new FAZ closely follows (Kohl, Sherwin et al. 1999), and is dependent upon, the growth of the new flagellum such that ablation of flagellar extension (by RNAi directed against IFT components) results in a short or absent FAZ (Absalon, Blisnick et al. 2008) whereas ablation of the FAZ yields cells with normal length flagella that are detached from the cell body (LaCount, Barrett et al. 2002; Vaughan, Kohl et al. 2008).

The new flagellum extends alongside the old flagellum until it reaches a stop point at approximately 0.6 of the unit length of the old flagellum (Davidge, Chambers et al. 2006). The mechanism of the stop point is not currently known but it may involve conformational changes to the flagella connector to prevent further translocation along the old flagellum. After this time, the tip of the new flagellum no longer moves in relation to the old flagellum and continuing flagellar extension is associated with a rapid increase in the distance between the old and new basal bodies in which the new basal body moves further into the posterior portion of the cell body (Sherwin and Gull 1989; Robinson and Gull 1991). It has been proposed that this fixing of the position of the new flagellum tip in combination with the attachment of the new flagellum to the cell body via the FAZ and the mechanical force of new flagellum extension provides the mechanism for basal body segregation (Briggs, McKean et al. 2004; Davidge, Chambers et al. 2006). This model fits with the observation by Robinson et al (Robinson, Sherwin et al. 1995) of biphasic basal body segregation. Interestingly, no flagella connector has been detected in long slender bloodstream form *T. brucei*. This correlates with the observation that in the bloodstream form, basal body segregation during cell division occurs to a far lesser extent than in procyclic forms (Briggs, McKean et al. 2004) .

1.3.9. The phenomenon of life-cycle stage specific paralogous proteins

Notwithstanding the differences in morphology between bloodstream and procyclic forms, at the ultrastructural level the organisation and appearance of the microtubules of the subpellicular corset are indistinguishable. However, a number of cytoskeletal proteins have been identified that show life-cycle stage-specific expression in *T. brucei*. The first of these was the calpain-like protein CAP5.5 (Hertz-Fowler, Ersfeld et al. 2001). A polyclonal antibody against CAP5.5, isolated by immunising rabbits with detergent and salt extracted procyclic form cells, showed that the protein was only expressed in procyclic form trypanosomes and appeared relatively late in the course of differentiation, after about 9 hours compared to 2 to 3 hours for the expression of procyclin (a GPI-anchored protein that coats the external face of the pellicular membrane in the procyclic form) and 4 hours for the loss of the VSG coat (Birkett, Parma et al. 1992; Matthews and Gull 1994). By immunofluorescence analysis of detergent extracted cells both the polyclonal antisera and a later monoclonal antiserum generated against the C terminus of the protein decorated the whole cell body with the exception of the flagellum in a pattern consistent with an association with the microtubule cytoskeleton (Hertz-Fowler, Ersfeld et al. 2001). The protein was shown to be both myristoylated and palmitoylated *in vivo* which, coupled with its strong association with the subpellicular microtubules, was suggestive of a role in mediating the close interaction between the subpellicular microtubule corset and the pellicular membrane. More recently sequencing of the *T. brucei* genome (Berriman, Ghedin et al. 2005) allowed the identification of an in-paralogue of CAP5.5 which was named CAP5.5V (Olego-Fernandez, Vaughan et al. 2009). The coding sequence for CAP5.5V is located on a sub-telomeric portion of chromosome 8 that derives from a relatively recent duplication of a 0.5Mb section of chromosome 4 which includes the locus for CAP5.5. The sequences of CAP5.5 and CAP5.5V differ significantly only in the C terminus of the protein and in the 3'UTR, the presumed location of cis-regulatory elements associated with regulation of protein expression, and both N terminal acylation sites are preserved in CAP5.5V. Olega-Fernandez et al used RTPCR to show that CAP5.5V mRNA is present in monomorphic bloodstream forms but not in procyclic forms, in

direct contrast to the expression profile of CAP5.5. Inducible RNAi directed against the C terminal coding sequence of each gene were shown to be highly discriminatory to the target mRNA allowing specific knockdown of each protein individually. In both life-cycle stages, knockdown of the corresponding protein resulted in a slowdown of population growth rate and the accumulation of cells with abnormal numbers of nuclei and/or kinetoplasts, particularly the 1K0N cytoplasts known as zoids. This phenotype is consistent with organelle or cleavage furrow mispositioning and is similar to that observed following ablation of other microtubule associated proteins (Baines and Gull 2008). Cells in both lifecycle stages showed abnormalities in the organisation of microtubules in the subpellicular corset following RNAi directed against the endogenous protein. Bundles of cytoplasmic microtubules were observed and the normally invariable inter-microtubule spacing was disrupted. This is consistent with a model whereby CAP5.5 and CAP5.5V play a role in creating or breaking inter-microtubule connections. Importantly, this study highlights that CAP5.5 and CAP5.5V appear to play analogous roles in the two life-cycle stages studied which raises the intriguing question of why two variants of this protein are needed at all. In Chapter 4 of this thesis I will present an initial description of a novel pair of paralogous cytoskeletal proteins that show life-cycle stage specificity in a similar way to CAP5.5 and CAP5.5V.

Another pair of paralogous microtubule associated proteins have also been shown to display stage-specific expression in *T. brucei*. CAP15 and CAP17 are small (15kDa and 17kDa respectively) proteins that have been shown to stabilise microtubules when expressed in mammalian cells and share around 50% sequence identity distributed across the length of the proteins (Vedrenne, Giroud et al. 2002). CAP17 contains an additional 20 residue hydrophobic domain in the C terminus. These proteins were identified by comparison of bloodstream and procyclic form lysates following separation by SDS-PAGE. Further analysis by Western blot using specific antisera raised against each protein determined that CAP17 is not expressed in the bloodstream form whereas CAP15 is expressed in both life-cycle stages examined but is tenfold more abundant in bloodstream form extracts. Immunolocalisation of both proteins showed a pattern consistent with an association with

the subpellicular microtubule corset but interestingly only in the anterior part of the cell. Overexpression of either protein relocated the signal to an even distribution across the microtubule array. In procyclic forms this resulted in an organelle positioning/cytokinesis defect phenotype qualitatively similar to those discussed above. The authors postulated that these CAPs play a role in the stabilisation of microtubules in the less dynamic anterior portion of the cell and that the redistribution of protein as a result of overexpression over-stabilises the dynamic posterior end of the cell leading to organelle positioning and segregation defects. As with CAP5.5, both proteins have analogous localisations and appear to have similar functions.

The microtubule array is not the only part of the *T. brucei* cytoskeleton for which stage specific paralogous proteins have been identified. The transmembrane domain-containing glycoprotein protein fla1 is an essential component of the FAZ, occupying a position on the external surface of the cell between the pellicular and flagellar membranes. The initial characterisation of fla1 used an antibody raised against the N terminal portion of the protein to demonstrate expression in both bloodstream and procyclic forms (Nozaki, Haynes et al. 1996). However, the recent completion of the *T. brucei* genome sequencing project (Berriman, Ghedin et al. 2005) has revealed that there are three paralogous fla1 family proteins in a repeated region of chromosome 8. These proteins share extensive homology in the N terminus and would likely be indistinguishable by antibodies raised against epitopes in this area. A recent microarray analysis of transcripts from bloodstream and procyclic forms identified fla1 as being significantly up-regulated in the procyclic form (Koumandou, Natesan et al. 2008). Interestingly, the protein recently identified as fla2 (LaCount, Barrett et al. 2002) was significantly up-regulated in the bloodstream form. The third member of the fla family, named here as fla3, is almost indistinguishable in terms of coding and protein sequence from fla2 and is unlikely to be detectable as a separate entity in most proteomics or transcriptomics analyses. fla1 shares 65% identity with fla2/3 at the level of protein sequence and the latter contain a 44 residue proline rich insert at approximately the midpoint of the protein that is not present in fla1. Although the differences between fla1 and fla2 have yet to be fully investigated, it is interesting to

note that these proteins are likely to be exposed on the cell surface and variants may therefore be required as part of the different surface coat environments in the two life cycle stages. The possession of a proline-rich insert in fla2/3 suggests a high level of secondary structure in this region which may serve to generate vertical or horizontal space in the dense VSG coat, facilitating interactions with other external FAZ components.

1.3.10. Summary

The stages of the *T. brucei* lifecycle have for many years been defined by their morphology and it is only relatively recently that molecular markers for the various forms have become available although some stages still lack any definitive molecular identifier. The tectonic changes to cell morphology associated with the processes of cell division and differentiation necessitate a dynamic cytoskeleton that undergoes regular restructuring but must at the same time maintain fidelity of the microtubule array.

1.4. The paraflagellar rod

The paraflagellar rod (PFR) is one of several unique attributes characterising the biology of kinetoplastid protozoa and has served as a focus for speculation since its first identification by Keith Vickerman in 1962 (Vickerman 1962). The PFR runs alongside the canonical 9+2 microtubular axoneme of Kinetoplastida and Euglenida (members of the monophyletic group, Euglenozoa), although here I will largely focus on studies involving the kinetoplastid family, Trypanosomatidae. Several early studies defined the ultrastructure of the PFR in various trypanosomatids (reviewed by Bastin, Matthews et al. 1996; Maga and LeBowitz 1999) including species of *Trypanosoma*, *Phytomonas*, *Leishmania* and *Herpetomonas*. (de Souza and Souto-Padron 1980). Although the defining components of the PFR appear conserved throughout Kinetoplastida and Euglenida, the PFR ultrastructure is variable in size between species and in some cases a significantly reduced PFR is present. The Kinetoplastida PFR is a complex, trilaminar lattice-like structure with proximal, intermediate and distal domains defined (Figure 1.1). Transmission electron microscopy (TEM) reveals the proximal domain as a simple structure whilst the intermediate and distal domains show precise orientations of thick and thin filaments whose arrangement is often characteristic of the species (de Souza and Souto-Padron 1980; Farina, Attias et al. 1986; Sant'Anna, Campanati et al. 2005). The proximal domain of the PFR is linked to the axonemal microtubule doublets 4 to 7 by electron dense filaments (Farina, Attias et al. 1986) that are highly resistant to detergent and salt treatment but do yield to mild treatment with trypsin (Russell, Newsam et al. 1983). In trypomastigote forms, and to some extent in epimastigote forms, the flagellum is attached along the cell body. In such cases, the proximal domain of the PFR is linked via filaments to the inner face of the flagellar membrane and then to the Flagellum Attachment Zone (FAZ). The PFR and axoneme maintain a precise orientation in regard to each other with the central pair microtubules having a consistent position (Gadelha, Wickstead et al. 2006). Mis-orientations or complete absence of the central pair can result from mutations in flagellar and basal body proteins (McKean, Baines et al.

2003; Branche, Kohl et al. 2006; Gadelha, Wickstead et al. 2006; Ralston, Lerner et al. 2006; Dawe, Shaw et al. 2007) and there is some indication that variations can occur in overall position of the flagellum in relation to the cell body (Branche, Kohl et al. 2006). However, evidence is still lacking as to whether there are specific changes to PFR structure or flagellar/cell body orientation in relation to flagellar wave progression.

1.4.1. Protein components of the PFR

A steadily increasing cohort of proteins is implicated as components of the PFR. Early studies identified two highly abundant proteins, PFR1 and PFR2, that are now considered as the classic defining components of the PFR. Since then around 15 additional proteins have been associated with the PFR through biochemical, bioinformatic and immunological techniques. The nature of these components provides increasing evidence for a PFR role in metabolic, regulatory and signalling functions. PFR components fall broadly into four groups: those involved in forming the lattice structure; those involved in adenine nucleotide signalling and metabolism; those involved in calcium signalling; and those for which a function has not yet been proposed.

Comparison between flagella purified from the euglenid *Euglena gracilis* (possessing a PFR) and flagella from *Chlamydomonas reinhardtii* (no PFR), a flagellate green alga used for many years as a model for studying flagellar biology, identified two gel bands as likely highly abundant PFR components on the basis of their absence in the latter (Hyams 1982). These proteins of 80 kDA and 69 kDa apparent molecular weight were named PFR1 and PFR2, respectively, and proof of their association with the PFR was provided by biochemical dissection studies in *Crithidia fasciculata* where flagellar preparations enriched for PFR components were shown to consist predominantly of two proteins of 76 kDa and 68 kDa after separation by SDS-PAGE (Russell, Newsam et al. 1983). PFR1 and PFR2 were also subsequently observed by SDS-PAGE separation of purified flagella of *Herpetomonas megaseliae* (Cunha, De Souza et al. 1984). The first molecular characterisation of these components was made in *Trypanosoma brucei* and suggested that these bands were encoded

by one gene and the diversity resulted from differential protein folding (Schlaeppi, Deflorin et al. 1989). Subsequently, molecular evidence was presented for a simpler multigene explanation (Birkett, Parma et al. 1992) and a second gene was then characterised (Deflorin, Rudolf et al. 1994). The genome sequencing projects for *T. brucei*, *Trypanosoma cruzi* and *Leishmania major* now show that the genes encoding PFR1 and PFR2 are distinct but related and are present in separate tandem arrays (Berriman, Ghedin et al. 2005; El-Sayed, Myler et al. 2005; Ivens, Peacock et al. 2005). Sequence analysis showed that both proteins are the result of a single gene duplication event that predates the divergence of Euglenida and Kinetoplastida and that all known extant instances of these proteins fit into a simplified and consolidated PFR1 and PFR2 nomenclature (Talke and Preisfeld 2002; Gadelha, LeBowitz et al. 2004). As a final confirmation, monoclonal antibodies and epitope tagging linked both proteins to a specific localisation in the PFR (Gallo and Schrevel 1985; Bastin, Bagherzadeh et al. 1996; Kohl, Sherwin et al. 1999; Maga, Sherwin et al. 1999).

The PFR is a feature of all life cycle stages of all Kinetoplastida studied to date with the exception of amastigote stages where the reduced flagellum does not emerge from the flagellar pocket. For many years it was thought that the endosymbiont-bearing Kinetoplastida placed in the *Crithidia*, *Blastocrithidia* and *Herpetomonas* genera did not adhere to this rule and did not possess a PFR (Freymuller and Camargo 1981). However, recent work has shown that *Crithidia deanei* encodes and expresses a divergent PFR1 that is able to partially rescue a *Leishmania mexicana* PFR1 null mutant (Gadelha, Wickstead et al. 2005). Immunofluorescence using an antibody that recognises PFR1 and PFR2 in various Kinetoplastida labelled the proximal portion of the *C. deanei* flagellum. Such endosymbiont-containing kinetoplastids had previously been characterised as lacking a PFR. Furthermore, careful examination of *C. deanei* flagella by TEM revealed the presence of a structure resembling a reduced proximal domain of the canonical tri-laminar PFR of other Kinetoplastida with a location consistent with the immunofluorescence labelling. Thus the PFR, in various guises, appears to be a consistent feature of all Kinetoplastida.

1.4.2. Other protein components

Early studies using monoclonal reagents clearly indicated the presence of components in addition to PFR1 and PFR2. The ROD1 monoclonal antibody, produced by injecting mice with detergent extracted *T. brucei* procyclic form cells as part of an extensive screen for cytoskeletal components, (Woods, Sherwin et al. 1989) labelled the distal domain of the PFR by immunogold labelling and recognised two bands of 180 kDa and 200 kDa apparent molecular weight by Western blot. Cell fractionation, detergent extraction and proteolysis techniques similar to those used to demonstrate the association of PFR1 and PFR2 with the PFR in *C. fasciculata* (Russell, Newsam et al. 1983) were also used to identify a set of putative components between 122 and 147 kDa from the flagellum of *H. megaseliae* (Moreira-Leite, de Souza et al. 1999). Early attempts to identify less abundant PFR components used antisera to known mammalian cytoskeletal components and often found cross-reactivity with the PFR (Schneider, Lutz et al. 1988). Unfortunately, it became clear that the PFR is a highly antigenic structure and often showed reactivity to many pre-immune sera or cross-reactivity with specific polyclonal antibodies even when affinity purified. Although some studies showed similar banding patterns on Western blots, these were not translated into confirmed identities at the sequence level. The high cross-reactivity of the PFR with many antisera impedes experimental interrogation and great stringency in experimental design is required when using such reagents for localisation studies. In trypanosomes, however, some approaches have been able to use complex (polyclonal-polyspecific) antisera and reveal the molecular identity of PFR antigens. Complex antisera against detergent extracted *T. brucei* were used to screen a lambda-phage expression library of *T. brucei* cDNA clones (Woodward, Carden et al. 1994). One clone (5.20) was identified, antisera to which had a very similar labelling pattern to ROD1 by both immunogold TEM and Western blot analysis. Whether this cDNA encodes the antigen for ROD1 is still unknown but the repetitive 5.20 protein is now displayed in the genome project of *T. brucei* as Tb11.01.6740 and is identified in Chapter 3 as part of a PFR2-dependent cohort of flagellar proteins.

A screen of both *T. brucei* whole cell extracts and cytoskeleton preparations with *T. brucei* infected bovine serum identified two candidate PFR proteins (Imboden, Muller et al. 1995). A serum fraction affinity purified against *T. brucei* proteins of > 180 kDa strongly labelled the flagellum and screening of a cDNA expression library identified two high molecular weight repeat proteins named I2 and I17. By immunogold TEM an antibody raised against I2 labelled the whole of the PFR while one raised against I17 specifically labelled the area between the PFR and the axoneme where the linking filaments are located.

The number of identified PFR proteins was increased by a series of antibody and phage expression library screens to identify the proteins PAR3, PAR2, PAR1 and PAR4 in *T. cruzi* (Saborio, Manuel Hernandez et al. 1989; Fouts, Stryker et al. 1998). PAR3 and PAR2 correspond to the known PFR components PFR1 and PFR2, respectively. Antibodies specific to PAR1 and PAR4 both label the flagellum of *T. cruzi* trypomastigotes. Bioinformatic analysis suggested the presence of open reading frames potentially encoding homologues of these proteins in the genomes of *T. brucei* and *L. mexicana* and that PAR1 may be a divergent member of the PFR1/2 family. A proteomic analysis of the *T. brucei* flagellum (Broadhead, Dawe et al. 2006) confirmed the expression and flagellar localisation of these proteins in this organism and in Chapter 3 I show that in *T. brucei* PAR1 has a localisation consistent with the PFR and is not assembled into the flagellum after RNA interference (RNAi – a mechanism that inhibits gene expression) ablation of PFR2.

Analysis of the Tritryp genomes (*T. brucei, T. cruzi* and *L. major*) (Berriman, Ghedin et al. 2005; El-Sayed, Myler et al. 2005; Ivens, Peacock et al. 2005) allowed identification of PFR1/2 related sequences and production of Pfam domains. This process drew attention to two proteins that contain domains in common with PFR1 and PFR2 (Clark, Kovtunovych et al. 2005). These have been named PFR5 and PFR6 and have predicted molecular weights of 87 kDa and 75 kDa, respectively. PFR5 has an additional Src Homology 3 domain that is not present in other members of the PFR protein family. This domain binds proline-rich motifs and is involved in the formation of protein

complexes although whether PFR5 has a role in the organisation of the PFR structure remains to be determined. The authors showed that transcripts for both PFR5 and PFR6 are significantly more abundant in *T. cruzi* trypomastigote and epimastigote life cycle stages than in the amastigote stage, although in all stages the abundance of transcript was significantly lower than that observed for PFR1 or PFR2. As with PAR1, PFR5 was identified in a proteomic analysis of the *T. brucei* flagellum (Broadhead, Dawe et al. 2006).

All of these proteins apart from I17, which appears to be absent from the Leishmanial lineage, are represented by predicted open reading frames in the genome projects for *T. brucei*, *T. cruzi* and *L. major* (Berriman, Ghedin et al. 2005; El-Sayed, Myler et al. 2005; Ivens, Peacock et al. 2005) reflecting a likely core composition for the PFR.

Intriguingly gamma tubulin was added to the growing list of potential PFR proteins with localisation to the flagellum of *Leishmania tropica* shown with monoclonal antibodies raised to peptides (Libusova, Sulimenko et al. 2004). Gamma tubulin is normally associated with microtubule organising centres where it is involved in the nucleation of cytoplasmic and mitotic microtubules (reviewed by Raynaud-Messina and Merdes 2007). It also localises to the basal body of the flagellum in *T. brucei* where it plays an essential role in the nucleation of the central pair microtubules (McKean, Baines et al. 2003). The possible role for gamma tubulin in the PFR remains cryptic. In the absence of functional data for a role for gamma tubulin in the PFR, this study exemplifies the difficulties encountered interpreting specificity of localisations when using even excellent monoclonal reagents. My examination of the peptides used to raise the monoclonal antibodies in the context of recent *Leishmania* genome information (Ivens, Peacock et al. 2005) reveals some level of possible cross-reactivity with other proteins.

Finally, recent work has shown that a novel myosin isoform, myosin XXI, that is restricted to kinetoplastids and down-regulated in the amastigote life cycle stage localises to the flagellum of *Leishmania donovani* (Katta, Sahasrabuddhe et al. 2009). Immunofluorescence analysis using a

polyclonal antibody raised against recombinant MYO21 protein revealed a very strong signal at the proximal end of the flagellum with punctate staining throughout the cell body and along the length of the flagellum. Immunofluorescence double labelling with axonemal and PFR markers showed that the strong MYO21 signal at the base of the flagellum partially colocalised with the PFR suggesting a localisation in the extreme proximal domain of the PFR or in the area between the axoneme and the PFR. This proximal PFR localisation was also observed by immunogold thin section TEM and immunofluorescence analyses of GFP-tagged MYO21 domains showed that the tail region is necessary and sufficient for the observed localisation. As with many other identified PFR components, a function for MYO21 has yet to be determined although recently a role for actin dynamics in the formation of the kinetoplastid flagellum, and in particular the PFR, has been proposed (Tammana, Sahasrabuddhe et al. 2008) and is discussed later.

1.4.3. Adenine homeostasis

Adenine nucleotides are involved or implicated in many aspects of flagellar function in diverse organisms. The major motor proteins of the flagellum, the outer dynein arm axonemal dyneins, contain AAA-ATPase domains and conformational changes to these proteins induced by the hydrolysis of ATP drive the microtubule sliding that generates the flagellar beat. Inner dynein arms are stimulated by low levels of ADP, suggesting that adenine nucleotide homeostasis is an important part of flagellar function (Yagi 2000). Evidence from studies in many organisms suggests a pivotal role for the second messenger cAMP in the motility of spermatozoa (Kinukawa, Oda et al. 2006). It is thought that cAMP signalling is modulated by protein kinase A or via the Epac/Rap pathway and is proposed to be involved in the conversion of microtubule sliding to flagellar beat (Kinukawa, Oda et al. 2006 and references therein).

snl2 (Bastin, Ellis et al. 2000) is an inducible mutant cell line of *T. brucei* with RNAi targeted against PFR2. Ablation of PFR2 leads to a failure of the cell to fully assemble a PFR. Pullen et al (Pullen, Ginger et al. 2004) hypothesised that minor components of the PFR could be identified by

comparing flagella extracted from wild-type (PFR+) and *snl2*-induced (PFR-) cells due to these components entering the soluble phase in the absence of the PFR structure. By comparing samples after separation by two-dimensional electrophoresis a number of spots were identified that were reduced after RNAi ablation of PFR2. Proteins from two of the spots were identified by tandem mass spectrometry as adenylate kinases (AKs) which were given the names TbADKA and TbADKB. Adenylate kinases are important enzymes in adenine nucleotide homeostasis and function to maintain the balance between the mono-, di- and tri-phosphate states. An epitope tagged copy of TbADKA was shown to localise along the whole length of the PFR. Both purified flagella and detergent extracted cytoskeletons were shown to have AK activity which was lost in preparations of *snl2* after RNAi induction, suggesting that AK activity in the insoluble fractions of the cell is restricted to the flagellum and in particular to the PFR. Importantly, although the residues involved in the structure and function of adenylate kinases in other organisms are conserved, both of these PFR adenylate kinases have 55 amino acid N-terminal extensions that show some sequence conservation between them. Peptides derived from these extensions were detected by tandem mass spectrometry showing that these are bona fide parts of the proteins and are not cleaved prior to incorporation into the PFR. In support of this, a truncation mutant of TbADKA lacking the N terminus failed to localise to the PFR and remained in the cytoplasm. This N-terminal sequence also proved to be sufficient for targeting a GFP fusion protein to the flagellum. This localisation was sensitive to non-ionic detergent treatment suggesting that other factors are involved in the stable incorporation of these proteins into the PFR structure. No effect on the morphology or function of the flagellum was detected after RNAi against both proteins simultaneously, although AK activity was reduced by 80% in cytoskeletons. This may be a result of residual AK activity being sufficient for normal flagellar function or that the specific circumstances under which these function are not preserved in culture conditions. Bioinformatic analysis of the N-terminal sequences identified homologous sequences in both human and *Caenorhabditis elegans* genome projects. Crucially, in these organisms the positive matches were also associated with genes encoding putative adenylate kinases. Whether this N-

terminal sequence functions as a flagellar targeting signal in other organisms has yet to be determined, but the presence of a homologue of these unusual adenylate kinases in *C. elegans* may hint at a role in regulatory or signalling pathways, as all cilia produced by *C. elegans* are immotile. This proposed role may explain the lack of an observable phenotype in *T. brucei* when ADKs are ablated under culture conditions.

GRESAG4 adenylyl cyclase and the related bloodstream form calcium–regulated adenylyl cyclase ESAG4 have been shown to localise to the flagellar membrane of *T. brucei* (Paindavoine, Rolin et al. 1992). These enzymes have divergent extracellular N-termini, a transmembrane domain and an intracellular catalytic domain that, due to the location of the enzyme, may interact with components of the axoneme and/or PFR. An additional study (D'Angelo, Montagna et al. 2002) demonstrated the existence of a calcium-regulated adenylyl cyclase termed TczAC that is expressed in all life-cycle stages of *T. cruzi*. This enzyme exhibits dose-dependent stimulation by Ca^{2+} that is seemingly independent of calmodulin regulation despite lacking any identifiable calcium interacting domains. The authors showed that TczAC can dimerise via the catalytic domain and, interestingly, that it also interacts with either PFR1 or PFR2 by the same domain in Yeast-2-Hybrid analysis.

Further evidence for the role of cAMP in the Kinetoplastida flagellum, and particularly the PFR, came with the localisation of two cyclic nucleotide-specific phosphodiesterases to the PFR of *T. brucei* (Oberholzer, Marti et al. 2007). These proteins, PDEB1 and PDEB2, show high similarity to each other at the catalytic domain but are divergent at their N-termini. Interestingly, this coincides with a differential localisation of the two proteins with PDEB1 being restricted to the PFR and PDEB2 localising mainly to the cytoplasm with a small portion present in the PFR. The PFR localisation of epitope tagged versions of both proteins was determined by immunofluorescence and immunogold TEM. This localisation was resistant to treatment with non-ionic detergent. This is in agreement with the presence of both proteins in a *T. brucei* flagellum proteome (Broadhead, Dawe et al. 2006) generated from extracted flagella and suggests a tight association with the PFR. It has been shown

that RNAi ablation of PFR2 results in an accumulation of un-polymerised PFR proteins at the tip of the new flagellum called the 'blob' (Bastin, Pullen et al. 1999). After ablation of PFR2, epitope tagged versions of both PDEB1 and PDEB2 were seen to localise to the blob (Oberholzer, Marti et al. 2007). Importantly it was shown that ablation of both proteins by RNAi was lethal in the bloodstream form both in vitro (in culture) and in vivo (after infection into the mammalian host) although there was little effect on procyclic forms. This hypersensitivity of the bloodstream form is reminiscent of phenotypes resulting from the knockdown of other flagellar proteins in *T. brucei* (Broadhead, Dawe et al. 2006; Ralston and Hill 2006; Griffiths, Portman et al. 2007).

1.4.4. Calcium sensing

The role of Ca^{2+} signalling and calcium binding proteins in flagellar function has been well established over many years (Tamm 1994). One of the most widely known calcium binding proteins, calmodulin, while having no intrinsic enzymatic activity, acts to transduce calcium signals to other proteins via calmodulin binding domains. Calmodulin has been shown to function in many parts of the axoneme including the radial spokes (Dymek and Smith 2007) and central pair projections (Wargo, Dymek et al. 2005). Other predicted calcium and calmodulin binding proteins have been identified in the radial spoke (Patel-King, Gorbatyuk et al. 2004) and the outer dynein arm docking complex (Casey, Inaba et al. 2003)

A non-calmodulin calcium binding protein was identified as being a major antigen recognised by Chagasic serum (serum from individuals infected with *T. cruzi*) in several studies. This 24 kDa protein (FCaBP) was purified and localised to the *T. cruzi* flagellum (Engman, Krause et al. 1989). Further work in *T. brucei* (Wu, Haghighat et al. 1992; Wu, Deford et al. 1994) identified a family of related flagellar non-calmodulin EF-hand calcium binding proteins that were named calflagins. An antibody that recognises the calflagins was shown to decorate the blob that accumulates at the tip of the new flagellum as a result of RNAi ablation of PFR2 in *T. brucei* (Bastin, Pullen et al. 1999). This finding may implicate at least one of the calflagins as a component of the PFR. Both FCaBP and the calflagins are

dually acylated with myristoylate and palmitoylate and this was shown to be essential for localisation of FCaBP to the flagellar membrane (Godsel and Engman 1999). Recent work has gone on to show that myristoylation alone targets calflagin Tb44 to the pellicular membrane and that palmitoylation, specifically by the palmitoyl acyl transferase TbPAT7, is then necessary for localisation to the flagellar membrane (Emmer, Souther et al. 2009). Furthermore, work on calflagin Tb24 showed that this protein displays biochemical characteristics of lipid-raft association (Tyler, Fridberg et al. 2009). Lipid rafts are areas of membrane that have increased liquid order and are associated with increased concentrations of sterols and sphingolipids (Brown and London 2000). Tyler et al. (2009) provided evidence for increased liquid order in the *T. brucei* flagellar membrane and showed that in conditions under which lipid raft stability could be expected to be disrupted, flagellar localisation of calflagin Tb24 was also disrupted in both bloodstream form and procyclic form trypanosomes. As part of this study these authors also demonstrated an increased intensity of calflagin Tb24 staining in bloodstream forms at the anterior tip of the new flagellum where it contacts the old flagellum. This localisation at the tip of the new flagellum is consistent with the flagella connector of procyclic forms (Moreira-Leite, Sherwin et al. 2001) and with the predominant site at which new components are incorporated into the flagellar structure (Bastin, Ellis et al. 2000). It is not currently clear whether calflagins are transported to the growing tip of the flagellum in an intraflagellar transport (IFT)-dependent manner although data have been presented suggestive of a role for lipid rafts in IFT (Tyler, Fridberg et al. 2009). The membrane association of FCaBP has been shown to be dependent on the calcium binding state of the protein (Godsel and Engman 1999). In an environment in which calcium has been chelated, FCaBP dissociates from the membrane and enters the cytosolic fraction. This finding may provide an alternative explanation for the presence of calflagins in the flagellar blob after ablation of PFR2. It has been shown that PFR proteins such as PFR1 and the ROD1 antigen accumulate in the blob (Bastin, Pullen et al. 1999) and that numerous proteins with calcium binding ability are components of the PFR (Ridgley, Webster et al. 2000; Portman, Lacomble et al. 2009). A concentration of unregulated calcium binding proteins in the blob may therefore reduce the

available calcium and cause calflagins to dissociate from the membrane and concentrate in that area. If there is an increased localisation of calflagins to the tip of the new flagellum (although to my knowledge this has not been demonstrated in procyclic form *T. brucei*) this effect may be exacerbated.

Calmodulin itself has also been shown to be a component of the PFR in a series of experiments by Ridgley et al. (2000). An antibody that recognised *T. brucei* calmodulin (Tryp-calmodulin) labelled the flagellum in both bloodstream and procyclic life cycle stages with weaker signals associated with cytoplasmic vacuoles. Cryo-section immunogold showed that Tryp-calmodulin associates mainly with the PFR at the proximal and distal domains and on the filaments that connect the proximal domain to the FAZ. Gold particles were also observed along the axoneme consistent with localisation to the dynein arms and radial spokes. A possible interaction between Tryp-calmodulin and PFR1/2 was investigated by passing purified PFR proteins over a calmodulin-sepharose column in the presence of calcium. Approximately 60% of the protein pool associated with the column with the remainder washing through. When the eluate from this first round was passed over a second column all of the protein was bound. This suggests that there are two pools of PFR proteins that are differentiated by their ability to bind calmodulin, although the presence in the preparations of proteins of similar molecular weight such as PAR1 and PAR4 homologues may also explain these results. PFR protein binding by calmodulin-sepharose was sensitive to competition by the calmodulin binding peptide from calmodulin kinase II but not an irrelevant peptide, suggesting that there is a specific interaction between calmodulin and components of the PFR.

1.4.5. Functions of the PFR

The function of the PFR had been the subject of much conjecture. Early ideas tended to focus on concepts involving the PFR as a physical attribute to the flagellum i.e. as a thickening or stiffening agent (Fuge 1969). The PFR has been implicated in the ubiquitous attachment of kinetoplastid parasites to the insect host at some stage in their life-cycle. Attachment is achieved via electron-

dense hemi-desmosome-like plaques associated with the proximal portion of the flagellum which is enlarged and contains filaments that resemble PFR material and in some cases appear to emanate from the PFR structure (reviewed by Bastin, Matthews et al. 1996; Maga and LeBowitz 1999). Further investigation of the function of the PFR in this process requires cell lines competent for establishing an infection in the insect host.

Real progress on function was initiated with two studies in *Leishmania* and *T. brucei* using reverse genetics to ablate the PFR and hence address mutant phenotypes (Santrich, Moore et al. 1997; Bastin, Sherwin et al. 1998). A PFR2 null mutant in *L. mexicana* and a PFR2 RNAi knockdown mutant in procyclic *T. brucei* (named *snl1*) produced markedly similar phenotypes. Despite some important differences between these organisms and mutants, some overall general observations emerged. Cells showed a dramatic decrease in flagellar wave frequency and amplitude that corresponded to a loss of forward cell motility. Bending patterns became unstable and wavelengths were shortened although the tip-to-base wave propagation pattern exhibited by trypanosomes (Walker 1961) was preserved. TEM of each mutant revealed a loss of the bulk of the PFR structure corresponding to the distal and intermediate domains and part of the proximal domain where it was not attached to the axoneme. Immunofluorescence staining consistent with PFR1 being present in the PFR remnant was also observed. This result predicted that of the two most abundant PFR components only PFR1 was required to form the extreme proximal domain and a subsequent study (Maga, Sherwin et al. 1999) confirmed this using a PFR1 null mutant of *L. mexicana*. In this cell line, none of the domains of the PFR assembled and PFR2 protein was transported to the flagellum but not incorporated. The fibres that attach the axoneme to the PFR still formed and their presence in both null mutant cell lines as well as a double null mutant of PFR1 and PFR2 shows that these proteins are not involved in these structures. The blob that accumulates during new flagellum formation in the procyclic *T. brucei snl1* mutant was shown to be an accumulation of PFR proteins that included PFR1. This suggests that in the absence of PFR2, PFR1 and other PFR components cannot be correctly assembled and accumulate at the flagellar tip. These studies confirmed that a correctly assembled PFR was

necessary for normal flagellar function in these organisms. The availability of the mutant cell lines has enabled subsequent studies into the dynamics and regulation of flagellar assembly, the functions and components of the PFR and possible avenues of intervention against the pathologies of many trypanosomatid parasites.

It is important to note that both the original procyclic *T. brucei snl1* mutants and the inducible RNAi *snl2* mutant are viable (Bastin, Sherwin et al. 1998; Bastin, Ellis et al. 2000). However, Hunger-Glaser and Seebeck (Hunger-Glaser and Seebeck 1997) were unable to obtain a PFR2 double-knock-out cell line in procyclic *T. brucei*. This suggests a need for at least a low level of PFR2 expression in this organism that can still be achieved under RNAi conditions, although this protein was at levels undetectable by Western blot. Of course the failure to obtain knock-out of the second copy of a gene cannot prove its essential nature; however this experience may suggest an intrinsic difference in the essentiality of the PFR between procyclic *T. brucei* and *Leishmania*. In this respect the fact that *T. brucei* has a flagellum attached to its cell body along its length does offer an explanation for a difference. Until an inducible ectopic knock-out approach is used this must remain conjecture.

Trypanosomatids have an unusual tip-to-base flagellar beat initiation pattern (Walker 1961) and Branche et al. (2006) describe an essentially normal wave amplitude at the distal tip of the procyclic form *T. brucei* flagellum that is not effectively propagated to the base after PFR2 ablation. These authors also observed rapid alterations between forward and reverse waves with the previously observed lack of cellular displacement. Finally, cell morphology was altered whereby the majority of cells no longer display the characteristic left-handed helical twist of the flagellum around the cell body but rather show a planar 'L' shape as a result of a near 90 degree bend in the cell body and attached flagellum. This work in procyclic form trypanosomes led these authors to propose a role for the PFR in generating the helical path of the flagellum around the cell body. In contrast, in the absence of a PFR, *T. brucei* bloodstream form cells still maintain this helical pattern despite becoming monstrous and otherwise contorted (Broadhead, Dawe et al. 2006; Gadelha, Wickstead et

al. 2007). This difference between the life-cycle stages alerts us to the importance of paying particular attention to the life-cycle stage being studied when assessing the form, extent and penetrance of RNAi mutants in *T. brucei*. A recent study by Koyfman et al used a cryoelectron tomography approach to characterise the structure of the PFR as a function of the bending state of the flagellum (Koyfman, Schmid et al. 2011). This analysis showed that the various domains of the PFR lattice undergo compression and expansion under the influence of axonemal bending. By analysing the relative angles of the bending plane of the axoneme and the position of the PFR, these authors proposed a model whereby the PFR modifies the planar beat of the axoneme to generate the 3-dimensional helical beat so characteristic of *T. brucei*. Although this model is compelling at one level, it does not account for the planar beat of flagella in other kinetoplastids that possess a PFR. Indeed, another high resolution structural interrogation of the PFR, this time conducted on *T. cruzi* flagella, revealed similar patterns of contraction and expansion of the PFR lattice as a function of flagellar bending, as well as similar angles of incidence between the PFR and the axoneme (Rocha, Teixeira et al. 2010). The most prominent difference between flagella of *T. brucei* and those of *T. cruzi* and other kinetoplastids is the attachment to the cell body. This results in the flagellum following a left-handed helical path round the cell body, influenced by the helical arrangement of the subpellicular microtubule array via the FAZ, and any model of planar wave modulation must consider this important attribute.

In the general terms of the PFR, many studies using RNAi against PFR2 have shown that procyclic form cells exhibit a strong reduced-motility phenotype but are normal or near normal in their growth rate with no distinctive morphological defects other than the lack of a major portion of the PFR. However, recent work used doxycyclin-inducible RNAi against PFR2 in *T. brucei* to show that in contrast to the paralysed but viable procyclic form phenotype, ablation of PFR2 is lethal in the mammalian bloodstream form both in vitro in culture and in vivo in mouse infections (Broadhead, Dawe et al. 2006; Griffiths, Portman et al. 2007). When the PFR is not correctly assembled, bloodstream form cells progress through multiple rounds of organellar replication but are unable to

complete cytokinesis (Broadhead, Dawe et al. 2006). This results in monstrous cells with multiple nuclei, kinetoplasts and flagella. Analysis at an early timepoint in the induction showed that motility is compromised before cytokinesis defects become apparent in the culture (Griffiths, Portman et al. 2007). Mice infected with an inducible PFR2 RNAi mutant developed parasitaemia as normal but when doxycyclin was added to the drinking water, thus inducing RNAi, infections were cleared within 16 h and did not re-occur during a subsequent 7 day monitoring period (Griffiths, Portman et al. 2007). There are many examples from a variety of experimental organisms where alterations in culture conditions, turbulence and other physical and biochemical factors produce different phenotypes for the same mutant (for examples see De Lozanne and Spudich 1987; Larochelle, Vithalani et al. 1996; Brown, Fine et al. 2003; Ralston, Lerner et al. 2006). The in vivo experiments described by Griffiths et al. (2007) were therefore vitally important to establish that the different environmental conditions experienced by the parasite in the bloodstream, either in terms of turbulence in blood vessels or composition of growth medium, could not rescue the lethal phenotype observed in culture. The success of this study validates flagellar function as an important new target for possible intervention against *T. brucei* infections.

It has also been shown (Broadhead, Dawe et al. 2006) that RNAi mutants affecting four different axonemal components exhibit the differential phenotype between the bloodstream and procyclic forms observed after PFR2 ablation. This demonstration that individual ablation of different proteins in different flagellar compartments led to the same growth effect, cell morphogenesis defects and defined terminal phenotype argued for a general and critical requirement for normal flagellar function in the bloodstream form. Other work revealed a requirement for another axonemal protein, Trypanin (Ralston and Hill 2006), in the bloodstream but not procyclic form, and again demonstrated the strikingly different effects of PFR2 RNAi between the two life-cycle stages (Branche, Kohl et al. 2006). Recently ablation of the TAX-2 protein in the two life-cycle stages added another axonemal protein to this growing list presenting the differential phenotype (Farr and Gull 2009). The range of components for which this differential requirement has been observed adds

weight to the view that loss of normal flagellar function, and not a specific requirement for the PFR, is the major factor in the lethality of PFR2 ablation in the bloodstream form. It is important to note here that impairment of cytokinesis in the bloodstream form can be achieved by RNAi ablation of a wide range of flagellar proteins with a range of effects on the structures and functions of the flagellum. This reliance on correct flagellar function in the bloodstream form may reflect a dependency on either natural beat, the translation of natural beat to coordination of separation of a late dividing cell or possibly the dependence of an internal cytoskeletal structure on a physical flagellar component rather than progressive cell movement. Analysis of these phenotypes requires a reasonably sophisticated level of knowledge of the role of the ablated protein component in the parasite cytoskeleton. Again, the debate here has to recognise that explanations for a general collective category of 'bloodstream lethal but procyclic viable' may vary as discussed above. The restricted evolutionary distribution of the PFR structure and components compared to the more conserved structure and components of the axoneme makes the PFR a particularly valuable target possibility for therapeutic intervention.

1.4.7. Speculations on the role of the PFR in motility

The mechanisms underlying the role of the PFR in flagellar motility are becoming clearer as the result of recent component analyses. Ablation of the PFR in both *T. brucei* and *L. mexicana* demonstrated that this structure is essential for maintaining flagellar motility (Santrich, Moore et al. 1997; Bastin, Sherwin et al. 1998). Early proposals suggested that the PFR contributes to the flagellar beat by increasing stiffness (Fuge 1969). It is possible that recently identified signalling and metabolic enzymes built into the PFR lattice could induce conformational changes in the structure as a response to stimuli making it permissive for different forms of flagellar beat. As a possible counterpoint to this argument it has recently been shown that the flagellum of *C. deanei*, which possesses a reduced PFR alongside the proximal third of the axoneme, produces waveforms with comparable curvature and wavelength to that of *C. fasciculata* which possesses a PFR along the length of the flagellum (Gadelha, Wickstead et al. 2007). *Crithidia deanei* is capable of producing

both ciliary and flagellar beat patterns and there is no observable difference between the curvature of the beat at the proximal and distal ends of the flagellum (Gadelha, Wickstead et al. 2007). Another possible role for the PFR in flagellar motility is as a phosphotransfer relay to maintain the supply of ATP to the more distal portions of the flagellum more effectively than by diffusion from the cell body (for reviews see Oberholzer, Bregy et al. 2007; Ginger, Portman et al. 2008). The discovery of two PFR-specific adenylate kinases (Pullen, Ginger et al. 2004) supports this hypothesis. The specificity and effectiveness of signalling pathways is often reliant on the anchoring of effecter proteins into complexes or structures (reviewed by Pawson and Scott 1997) that can provide localised domains of messenger molecules and appropriately limit the signal cascade. Within the confined domain of the eukaryotic flagellum, the complex adenine nucleotide metabolism employed to fulfil regulatory, signalling and energy requirements suggests the need for a high level of order. One might predict that ablation of critical proteins within a potential PFR regulatory network would result in changes in the ability of the flagellum to propagate particular waveforms. However, previous studies of RNAi ablation of ADKA and ADKB in *T. brucei* did not detect any effects on the motility of the cells (Pullen, Ginger et al. 2004). It is likely that the techniques used to date to analyse motility have not been sufficiently sensitive to detect subtle changes in the motility of RNAi-induced cells. For example, most studies analyse progressive cell movement or sedimentation of cells rather than beat characteristics. It is conceivable that the 'default setting' for the PFR is to normal tip-to-base flagellar beating and that ablation of critical proteins in the PFR regulatory network causes an inability of the cell to produce rare waveforms such as ciliary beating and wave reversal (Gadelha, Wickstead et al. 2007). It is also possible that, given the apparent requirement for motility in certain life cycle stages, redundant systems are in place or that any changes in flagellar motility induced by ablation of PFR proteins are not observable in cultured cells. These questions remain to be answered and we are currently developing techniques to more fully explore the role of the PFR in motility.

1.4.8. Regulation of the PFR in the cell cycle and life cycle

Kinetoplastid parasites have a complex interaction of life-cycle and cell cycle, often involving both host and vector interactions. The PFR is a feature of all life-cycle stages with the exception of the amastigote form of *T. cruzi* and *Leishmania* spp. where the reduced flagellum does not emerge from the flagellar pocket and does not present a PFR. The flagellum of Kinetoplastida is built over only a proportion of the cell cycle. Thus both life-cycle and cell cycle considerations raise issues as to how regulation of gene expression is achieved. Are all flagellar proteins made even when not used or are there discrete life and cell cycle regulatory processes?

1.4.9. Cell cycle regulation

A new flagellum is built once during the trypanosomatid cell cycle while the existing (old) flagellum persists. The PFR begins to form after 0.52 of the cell cycle in *T. brucei* (Sherwin and Gull 1989). The dynamics of PFR formation and some of the factors involved have been investigated using the *snl1* constitutive PFR2 RNAi mutant (Bastin, Pullen et al. 1999) and an inducible Ty epitope tagged PFR2 cell line (Bastin, MacRae et al. 1999). As previously described, a striking feature of the *snl1* phenotype was the blob (Bastin, Pullen et al. 1999). Careful observation of the blob revealed that it increased in size as the new flagellum extended, suggesting the involvement of an IFT anterograde transport mechanism. At some point after cytokinesis, but before the formation of a new flagellum, the blob was removed (the new flagellum becoming the old flagellum in subsequent rounds of the cell cycle). Removal of the aggregate implicated the retrograde IFT process and a level of cell cycle regulation. An additional level of control may involve cell cycle control exercised over the synthesis of new flagellar components. Another interesting observation was that although PFR1 protein was still transported to the distal site of incorporation, other PFR components were not. The ROD1 antigen was almost completely absent from the new flagellum and rather remained in the cytoplasm at levels much reduced compared to wild-type. Stably transfected cell lines expressing an inducible Ty epitope tagged PFR2 allowed the pattern of tagged protein incorporation to be assessed (Bastin,

MacRae et al. 1999). The results point to a major site of new protein incorporation at the distal tip of the new flagellum and a minor site of incorporation along its length, as well as incorporation of new protein into the old flagellum that is consistent with a low level of protein turnover after the PFR has been built.

A question arises as to whether there are specific targeting or retention signals within the PFR or flagellar protein sequences. Tagged PFR2 deletion mutants indicate that a region of the PFR2 protein between amino acids 514 and 570 is necessary for flagellar localisation but is not sufficient to exclusively target GFP to the flagellum (Bastin, MacRae et al. 1999). A further set of deletion mutants defined a region of seven amino-acids between residues 564 and 571 that is required for incorporation at the distal tip of the new flagellum but not along the length. In subsequent work, this region was further refined to the tri-peptide HLA and was shown to also be necessary for targeting the axonemal component Tryp-ARP to the flagellum (Ersfeld and Gull 2001). The N-terminal sequences of the *T. brucei* adenylate kinases discussed earlier (Pullen, Ginger et al. 2004) have extended our knowledge of signals critical to flagellar localisation.

1.4.10. Life-cycle regulation

Gene regulation in Kinetoplastida is predominantly achieved post-transcriptionally and primary RNA transcripts are, in the main part, likely transcribed uniformly across the genome in a poly-cistronic manner (discussed by Clayton and Shapira 2007). The amastigote life-cycle stages of *T. cruzi* and *Leishmania* spp. lack a PFR and several studies have shown that PFR1 and PFR2 mRNA levels are enriched between 10- and 12-fold in *L. mexicana* promastigotes compared to amastigotes (Mishra, Holzer et al. 2003; Holzer, McMaster et al. 2006; Holzer, Mishra et al. 2008). In the first of these studies it was shown that transcription rates across the PFR2 locus (that contains three tandem copies of the PFR2 open reading frame in this organism) were nearly constant in both life-cycle stages supporting the unregulated production of a polycistronic precursor RNA. The half-life of the mature transcripts differed significantly between life-cycle stages, being 3.9 h in promastigotes and

0.8 h in amastigotes, suggesting that mRNA stability is an important regulatory mechanism. Analysis of mutant cell lines facilitated the definition of a 10 nucleotide element that was required for regulation of transcript level and was sufficient to confer regulation on a transcript with a vector-derived exogenous 3' untranslated region (UTR). This element was named the Paraflagellar Regulatory Element (PRE). This work continued with the screening of the *L. major* genome for instances of the PRE (Holzer, Mishra et al. 2008). A total of 343 occurrences in the genome were identified, 139 of which fell on the coding strand within 2,000 bp of an open reading frame stop codon. Of these, 78 were within 500 bp of a stop codon and are therefore very likely to be contained within the 3' UTR of the associated transcript. Not all of the genes associated with the PRE have a predicted function that is immediately consistent with the PFR although proteins involved in flagellar organisation and calcium or calmodulin binding were identified. Five of these proteins were selected for further study and all showed down-regulation in the amastigote form. The PRE is found in orthologous proteins from other *Leishmania* spp., which, together with the fact that not all of the open reading frames identified encode PFR proteins, points to a conserved mechanism for down-regulating a variety of mRNA transcripts in the amastigote form.

Further insights into the regulation of PFR proteins in the different life-cycle stages of *Leishmania* spp. have been provided in a series of recent reports from Wiese et al (Wiese, Kuhn et al. 2003; Wiese, Wang et al. 2003; Erdmann, Scholz et al. 2006). The mitogen activated protein kinase kinase, LmxMKK, was found to be down-regulated in the amastigote form of *L. mexicana*. LmxMKK null mutants showed a dramatic phenotype whereby cell motility was severely compromised and flagellar length was reduced by at least 80% with a majority lacking a PFR. These cells were able to form lesions after injection into mice and the resulting amastigotes presented the typical short flagellum. Null mutants of the kinase LmxMPK3, which has a similar expression profile to LmxMKK, also result in short flagella with either an absent or reduced PFR (Erdmann, Scholz et al. 2006). Interestingly no phosphorylated LmxMPK3 could be found in the LmxMKK null mutant, suggesting that these kinases operate in the same signalling pathway and that LmxMPK3 is a substrate of

LmxMKK. One of the main differences between the phenotypes of the null mutants was the presence of PFR2 protein. In the LmxMKK null mutant no PFR2 protein could be detected whereas in LmxMPK3 null variable amounts of PFR2 could be detected in the flagellum although evidently this was not assembled into a PFR. This raises an interesting question of whether LmxMKK has additional substrates, perhaps involved in the expression of proteins such as PFR2. I suggest that this could possibly be achieved through the inactivation in promastigotes of a factor responsible for degrading mRNA that carries the PRE discussed earlier.

Recent work from Tammana et al. (2008) proposes a role for actin in building the flagellum and particularly the PFR in *L. donovani*. Mutant cells carrying either a double or single knock-out of the *L. donovani* actin-depolymerising factor, LdCof, exhibit a similar phenotype to that observed for null mutants of LmxMKK and LmxMPK3. These authors propose that LdCof/actin dynamics are involved in the transport of flagellar components to the base of the flagellum prior to intraflagellar transport, hence the shortened flagellum phenotype observed in LdCof knock-out mutants, and that there is a specific role for LdCof in the formation of the PFR as this structure is completely absent from null mutant flagella. Based on the similarity of the LdCof null phenotype to those reported for LmxMKK and LmxMK3, these authors go on to hypothesise that in the absence of LIM kinase (an enzyme not coded in the *Leishmania* genome which is responsible for the reversible activation of ADF/cofilin in other eukaryotic systems) LdCof is a substrate of the MAP kinase pathway that includes homologues of LmxMKK and LmxMPK3.

1.4.11. Immunogenicity of PFR proteins

Infection by trypanosomatid parasites is endemic in many of the poorest areas of the world and existing treatments are associated with high toxicity and increasing drug resistance, leading to an urgent need for modern therapies (de Souza 2007; Checchi and Barrett 2008; Simarro, Jannin et al. 2008 for current perspectives). There are currently no vaccines available although work from several groups over the last decade or so has identified PFR proteins as attractive targets for generating

protective immunity against several species of trypanosome (Wrightsman, Miller et al. 1995; Miller, Wrightsman et al. 1996; Miller, Wrightsman et al. 1997; Wrightsman and Manning 2000; Wrightsman, Luhrs et al. 2002; Luhrs, Fouts et al. 2003; Michailowsky, Luhrs et al. 2003; Saravia, Hazbon et al. 2005). Immunisation with PFR proteins purified from *T. cruzi* epimastigotes was shown to completely protect mice from a subsequent challenge by an otherwise fatal dose of this parasite (Wrightsman, Miller et al. 1995). The protection conferred was dependent upon the delivery method of the PFR vaccine. Intraperatoneal injections completely failed to protect immunised mice while s.c. injections conferred immunity. Chagasic serum from human patients was also shown to contain antibodies that recognised PFR proteins (Wrightsman, Miller et al. 1995; Michailowsky, Luhrs et al. 2003). In a subsequent report (Wrightsman and Manning 2000) it was shown that PFR antigen co-adsorbed onto alum with recombinant IL-12 or adenovirus-expressed IL-12 could elicit a Th1-type cell-mediated immune response that provide protection against subsequent infection when delivered subcutaneously. The use of recombinant PFR proteins as antigens confirmed that it was these and not some previously unidentified contaminant of the preparations that conferred immunity (Luhrs, Fouts et al. 2003). Other recombinant PFR and DNA vaccine approaches have led to a deeper understanding of the cellular mechanisms of immunity to *T. cruzi* infection (Wrightsman, Luhrs et al. 2002; Michailowsky, Luhrs et al. 2003; Morell, Thomas et al. 2006).

PFR2 has also been shown to have potential as a vaccine against *Leishmania* infections (Saravia, Hazbon et al. 2005). A *pfr-2* DNA vaccination led to delayed lesion appearance or significant lesion reduction in male hamsters after subsequent challenge with 10,000 and 500 *L. mexicana* promastigotes. Interestingly this same treatment exacerbated subsequent lesions when applied to female hamsters. Immunisation with recombinant PFR2 protein prevented *Leishmania panamensis* lesion formation in female hamsters but was ineffective against *L. mexicana*. However, a prime boost immunisation regime using both DNA and recombinant protein reduced lesion size in female hamsters challenged with 500 *L. mexicana* promastigotes.

An interesting question arises as to how an intracellular antigen that is associated with a structure apparently not present in the mammalian form of the parasite can elicit an immune response. Serum from infected humans or animals can recognise PFR proteins and a mechanism has been proposed whereby the degradation of the flagellum and PFR during the promastigote to amastigote transition makes components available for recognition by the immune system (Michailowsky, Luhrs et al. 2003; Saravia, Hazbon et al. 2005). Another possibility is that lysis of a portion of the parasite cells could expose internal antigens to the host. This awaits experimental verification.

1.4.12. Wider perspectives on the PFR

Although the PFR is a unique structure restricted to Kinetoplastida and Euglenida, extra-axonemal structures in general are rather common. These structures can be symmetrically arranged around the axoneme or asymmetrically located as in the case of the PFR. In addition they can run along the full length or only a portion of the axoneme. They occur in many diverse organisms from mammalian and insect sperm to a range of protists such as dinoflagellates and *Giardia* (Talke and Preisfeld 2002; Elmendorf, Dawson et al. 2003; Werner and Simmons 2008). Perhaps the most intriguing extra-axonemal structure to compare with the kinetoplastid PFR is the mammalian sperm Outer Dense Fibres and fibrous sheath. Several components of the flagellar accessory structures of mouse sperm have been identified. These include adenylate kinase and proteins involved in cAMP signalling drawing intriguing parallels to the PFR (reviewed by Oberholzer, Bregy et al. 2007). Thus the concept of the PFR as a metabolic, homeostatic, regulatory and sensory platform may well turn out to be a conserved phenomenon among extra-axonemal structures in evolution.

Chapter 2

Materials and Methods

2.1. Molecular Biology

2.1.1. Bacterial transformation

XL1-blue strain of *Escherichia coli* (Stratagene) was made competent for transformation following the Inoue method (Inoue, Nojima et al. 1990). 50μl of competent cells were incubated with plasmid DNA or ligation mix at 4°C for 30 minutes before heat shock at 42°C for 1 minute. Cells were immediately transferred to 4°C for 2 minutes then incubated at 37°C overnight on plates consisting of Luria broth (LB - Sigma) supplemented with 12 mg ml^{-1} agar and 100 μg ml^{-1} ampicillin. For subsequent amplification of plasmids, single colonies were picked and incubated overnight in LB supplemented with 100 μg ml^{-1} ampicillin at 37°C with shaking.

2.1.2. Agarose gel electrophoresis

Samples were separated on a gel containing 0.5 - 1% w/v agarose/TAE (40mM Tris, 20mM acetic acid, 10mM EDTA (ethylenediaminetetraacetic acid)) and 1 μg ml^{-1} ethidium bromide. Bands were then visualised on a UV transilluminator.

2.1.3. Polymerase chain reaction

Primers were designed using Primer3 software (http://frodo.wi.mit.edu/primer3/) with typical limits being: length 18-23 bp; optimal melting temperature (T_{opt}) 58-62°C; GC content 20-80%. Primer pairs were based on a difference in T_{opt} of less than 1°C. For the purposes of subsequent insertion into vector backbones, sequences for restriction sites were added to the 5' end of each primer with an additional 3 AT dimers added upstream to ensure effective digestion.

A typical PCR reaction contained 2 ng μl^{-1} procyclic form *T. brucei* genomic DNA, dNTPs at 0.2mM each (dATP, dCTP, dGTP and dTTP), 0.2 μM of each primer, 1 U phusion DNA polymerase (NEB) and an appropriate volume of polymerase buffer. A typical thermo-cycling protocol consisted of incubation for 2 minutes at 95°C followed by 30 cycles of 95°C for 30 seconds, T_{opt} -2°C for 30 seconds and 72°C for 1 minute kbp^{-1} amplified product with a final incubation at 72°C for 2 minutes.

The success of amplification was determined by separation of the PCR reaction by agarose gel electrophoresis. PCR products were purified either by excision from a gel (QIAquick gel extraction kit, QIAGEN) or directly from the reaction mix using a silica column (QIAquick PCR purification kit, QIAGEN).

2.1.4. Plasmid generation

For restriction digestion, DNA was incubated with restriction enzymes (Roche, NEB) according to the manufacturer's instructions. Vectors were dephosphorylated after digestion by the addition of Calf intestinal alkaline phosphatase (Roche) and incubation at 37^{o}C for 30 minutes. Digestion products were separated by agarose gel electrophoresis and appropriate bands excised. DNA was purified from excised bands over a silica column (QIAquick gel extraction kit, QIAGEN). Fragments were ligated in a 1:3 vector backbone: insert molar ratio by the addition of T4-DNA ligase (Roche) and incubation at room temperature for 1 hour.

2.1.5. Vectors and strategies

Three vectors were used for the generation of plasmid constructs in this work. RNAi constructs were generated by amplification of 300-700 bp of the target open reading frame from genomic DNA and insertion between the XbaI sites of p2T7-177 (Wickstead, Ersfeld et al. 2002). Target sequences were compared to the *T. brucei* genome by BLASTN to determine specificity. For transfection into trypanosomes the construct was linearised at the NotI restriction site. For ectopic expression of recombinant proteins with an N terminal Ty::GFP tag the entire open reading frame of the gene of interest was amplified and inserted in frame between the XbaI and BamHI restriction sites of pDex577-G (Kelly, Reed et al. 2007). For transfection into trypanosomes the construct was linearised at the NotI restriction site. For the expression of chimeric proteins from endogenous loci with an N terminal Ty::YFP or Ty only tag, 150-250 bp of sequence from the 5' UTR directly upstream of the start codon and 150-250 bp of in-frame sequence from the 5' end of genes of interest were amplified and inserted in this order between the XbaI (to include YFP) or SpeI (to exclude YFP) and BamHI

restriction sites of pEnT6B-Ty::YFP::Ty (Kelly, Reed et al. 2007). UTR and ORF inserts were separated by an XhoI restriction site that was used to linearise plasmids prior to transfection. For the expression of chimeric proteins with a C terminal YFP::Ty tag from endogenous loci, 150-250 bp of in-frame sequence up to but not including the stop codon and 150-250 bp of the 3' UTR of genes of interest were amplified and inserted in this order between the HindIII and SpeI restriction sites of pEnT6B-Ty::YFP::Ty, again separated by an XhoI restriction site. One exception to this was the endogenous tagging of FCP1 (Chapter4) where a construct containing the necessary elements was ordered from Mr Gene (http://mrgene.com/desktopdefault.aspx/tabid-2/). The entire intergenic region downstream of the gene of interest was amplified and inserted between the BamHI and SphI restriction sites to preserve any regulatory elements in the 3' UTR. Plasmids were linearised with XhoI prior to transfection into trypanosomes. Oligonucleotides used in this study are detailed in appendix A.

2.1.6. Plasmid isolation

For small scale preparations plasmid DNA was isolated from 3ml bacterial culture using a silica column (QIAprep spin Miniprep kit, QIAGEN). For large scale preparations plasmid DNA was isolated from 50ml bacterial culture using an anion exchange column (QIAquick Midiprep kit, QIAGEN).

2.2. *T. brucei* strains, cell culture and genetic modification

2.2.1. Trypanosome cell culture

Procyclic forms were cultured at 28^{o}C in SDM-79 medium supplemented with 10% v/v foetal bovine serum (Gibco) (Brun and Jenni 1977). Bloodstream forms were cultured at 37^{o}C with 5% CO_2 in HMI-9 medium supplemented with 15% v/v foetal bovine serum (Gibco). Cells were diluted as necessary to maintain the culture in log-phase. Cell density was measured using a Casy-counter (Model TT; Sharfe systems). The cell lines used in each chapter were as follows.

Chapter 3: Procyclic form Lister-427; 29-13 (expressing T7-RNA polymerase and tetracycline repressor) and *snl2*.

Chapter 4 and 5: Procyclic form Smox2P9 (TREU-927 expressing T7-RNA polymerase and tetracycline repressor from a single plasmid insert – S. Kelly, unpublished). Bloodstream form Smox2B4 (Lister-427 expressing T7-RNA polymerase and tetracycline repressor from a single plasmid insert – S. Kelly, unpublished).

For cell lines with selectable markers the medium was supplemented with appropriate drugs as follows: Phleomycin – PCF 5 μg ml^{-1}, BSF 2.5 μg ml^{-1}; Blasticidin – PCF 10 μg ml^{-1}; BSF 5 μg ml^{-1}; Puromycin – PCF 1 μg ml^{-1}, BSF – 0.2 μg ml^{-1}; Hygromycin – PCF 50 μg ml^{-1}, BSF 5 μg ml^{-1}; G418 (Neomycin) – PCF 15 μg ml^{-1}.

Induction of RNAi or ectopic gene expression was achieved by the addition of doxycycline to the culture medium to a final concentration of 1μg ml^{-1}. For washout experiments, 10ml cell cultures were washed 5x 10ml complete medium and returned to fresh medium without doxycycline.

Differentiation of monomorphic bloodstream forms to procyclic forms was induced by the addition of 6mM cis-aconitate to the culture medium and transfer of the culture to 28^{o}C.

2.2.2. Transfection of trypanosomes

Plasmids for transfection were linearised and precipitated by the addition of 100% ethanol and incubation at -20^{O}C for 1 hour. Precipitated DNA was then washed once in 70% v/v ethanol, air dried and resupsended in 50 μl ddH_2O. 2.5x10^7 cells were harvested by centrifugation at 800g, washed once in Zimmerman's Post Fusion Medium (ZPFM: 132 mM NaCl; 8 mM Na_2HPO_4; 0.5 mM $Mg[CH_3COO]_2$; 0.09 mM $Ca[CH_3COO]_2$; pH 7.0; 50 mM glucose added for bloodstream form transfections) and resuspended in ZPFM to 5x10^7 cells ml^{-1}. Plasmid DNA was added to 0.5 ml cell suspension and electroporation carried out in a 4mm electroporation cuvette by applying 3x 100 ms square pulses of 1.7 kV separated by intervals of 200 ms. Cells were immediately transferred to warm medium and incubated overnight at 28^{o}C (PCF) or 37^{o}C (BSF). After a 16 hour recovery period, cultures were diluted 1:10 into fresh warm medium containing appropriate selection drugs.

2.3. Microscopy

2.3.1. Chemical fixation of cells for TEM

Cells were fixed in culture by addition to the growth medium of glutaraldehyde to a final concentration of 2.5% (w/v). Cells were collected by centrifugation and fixed again in 4% (w/v) formaldehyde, 2% (w/v) glutaraldehyde in 100 mM sodium phosphate buffer, pH 7.0 before post-fixation with 1% (w/v) osmium tetroxide in 100 mM sodium phosphate buffer. After several washes, cells were en bloc stained with 1% (w/v) aqueous uranyl acetate before dehydration. Dehydration was achieved by exposing samples to 30%, 50%, 70% and 90% v/v acetone for 15 minutes each then 3 exposures to 100% acetone for 30 minutes each. Samples were transferred to propylene oxide (PO) and embedded by progressive infiltration of epoxy resin (Agar) (2:1 PO: epoxy, 1 hour; 1:1 PO: epoxy, 1 hour; 1:2 PO: epoxy, 1 hour; 100% epoxy, overnight). Fresh epoxy was then added and polymerised overnight at 60^{o}C. Sections of nominal 80 nm thickness were cut and stained with aqueous uranyl acetate and Renyold's lead citrate. Sections were viewed in an FEI Tecnai-F12 electron microscope (FEI Company Ltd.) operating at 80 kV.

2.3.2. High pressure freezing of cells for electron tomography

For electron tomography, cells were harvested by centrifugation for 2 minutes at 600 g and a sample was removed from within the pellet. The sample was then subjected to high pressure freezing in an EM PACT2 (Leica Microsystems Ltd). Freeze substitution was achieved by the addition of 2% uranyl acetate (AMS Biotechnology) in dehydrated methanol at -90^{o}C for one hour in a Leica EM AFS1. Samples were washed twice in dehydrated acetone with a simultaneous increase in temperature to -50^{o}C at a rate of 20^{o}C hour^{-1}. Infiltration of the sample with Lowicryl HM20 resin was achieved by 1 hour incubations with stepwise increases of resin in dehydrated acetone (3:1 acetone: resin; 1:1 acetone: resin; 1:3 acetone: resin). This was followed by two changes of 100% resin before a final infiltration step with 100% resin overnight. Resin polymerisation was induced at -50^{o}C for 48 hours

by the application of UV-light. Over a further 48 hours the sample was raised to room temperature at $20^{o}C$ $hour^{-1}$ in the presence of UV-light.

350 nm thick serial sections were cut using a Leica UCT Ultramicrotome (Leica, Vienna, Austria) and poststained for 8 minutes in 2% UA and 1 minute in Reynold's lead citrate. Undiluted 15 nm colloidal gold (Ted Pella, Redding, CA, USA) was added to both sides of the grid. For tomography, a TF30 Tecnai electron microscope (FEI Company Ltd.) operated at 300 kV was used. An image was collected every degree ±60° in two axes at 23000x (1 nm pixel size on a 4 x 4 k Gatan CCD camera (binned by 2)). The images were aligned, and dual axis tomograms calculated using the 3dmod software (Kremer, Mastronarde et al. 1996). Serial sections were joined into larger volumes including the entire flagellar pocket and neck regions.

2.3.3. Preparation of negatively stained whole mount cytoskeletons

Cells were harvested by centrifugation at 800 g, washed once in PBS and resuspended in PBS to a density of $1x10^{7}$ cells ml^{-1}. Cells were then settled onto formvar coated, glow discharged nickel EM grids (Agar), washed once in PBS, then washed twice in 1% v/v Nonidet P40 (Sigma) in PEME (100mM PIPES, 2mM EGTA, 0.1mM EDTA, 1mM $MgSO_4$, pH 6.9). Cells were then washed 5x in PEME and fixed in 2% w/v paraformaldehyde in PEME for 20 minutes. Grids were washed 5x in PEME and incubated in 100mM glycine in PEME for 15 minutes followed by incubation in 1% w/v BSA in PBS. Primary antibody was diluted in PBS as necessary (see below for antibodies and dilutions used) and added to the grids for 30 minutes. After 5x washes in PBS, secondary antibody conjugated to 5 nm gold particles and diluted in PBS as necessary was added and grids were incubated for 30 minutes at room temperature. Grids were then washed 5x PBS and cells fixed in 2% w/v glutaraldehyde in ddH_2O for 30 minutes. The grids were then washed 10x ddH_2O and cells were negatively stained by the brief addition of 0.5% w/v goldthioglucose. Samples were then viewed were in an FEI Tecnai-F12 electron microscope (FEI Company Ltd.) operating at 80 kV.

2.3.4. Preparation of cells for light microscopy.

Cells were harvested by centrifugation at 800 g, washed once in PBS and resuspended in PBS to a density of $1x10^7$ cells ml^{-1}. Cells were then settled onto glass slides and washed once in PBS.

For whole cells: cells were fixed with 3.7% w/v paraformaldehyde for 20 minutes before permeabilisation by incubation in methanol for 20 minutes at -20°C.

For cytoskeletons: cells were washed once with 1% v/v Nonidet P40 (Sigma) in PEME and fixed by incubation in methanol for 20 minutes at -20°C.

Cells were then rehydrated in PBS at room temperature for 30 minutes. Slides were incubated with primary antibodies diluted in PBS as necessary and the washed 5x with PBS. Immunoglobulin isotype-specific secondary antibodies conjugated to either fluorophore 488 or fluorophore 594 (Alexafluor, Invitrogen) and diluted in PBS were added for 30 minutes and slides washed 5x in PBS. Samples were mounted in Vectashield mounting medium with 4', 6' - diamino-2-phenylindole (Vector Laboratories Inc) for visualisation of DNA and examined on a Leica DM5500B. Primary antibodies used in this study are as follows:

Name	Target	Type	Dilution	Reference
BB2	Ty epitope	IgG	1:10	(Bastin, Bagherzadeh et al. 1996)
L8C4	PFR	IgG	1:10	(Kohl, Sherwin et al. 1999)
L6B3	FAZ	IgM	1:2	(Kohl, Sherwin et al. 1999)
Rod1	PFR	IgM	1:10	(Woods, Sherwin et al. 1989)
AB1	FC	IgM	1:1	(Briggs, McKean et al. 2004)
WCB	Cell body	IgM	1:10	(Woods, Baines et al. 1992)
CAP5.5	Cell body (PCF)	IgG	1:10	(Hertz-Fowler, Ersfeld et al. 2001)
TgMORN1	TgMORN1/CMRP	IgG	1:100	(Heaslip, Dzierszinski et al. 2010)

2.3.5. Image processing and analysis

All image processing and analysis was performed in ImageJ (http://rsbweb.nih.gov/ij) using built in functions or custom scripts (see appendix C).

2.4 Protein biochemistry

2.4.1. Preparation of protein samples

Cells were harvested by centrifugation at 800 g and washed once in PBS.

For whole cell preparations: Samples were resuspended in an appropriate buffer (see below)

For cytoskeleton preparations: Samples were resuspended for 2 minutes in 1% v/v Nonidet P40 (Sigma) in PEME containing Focus protease arrest mixture (CalBiochem), 200 μg ml^{-1} DNaseI and 50 μg ml^{-1} RNase. Pellets were harvested by centrifugation at 3200 g in a benchtop microfuge, washed twice in PEME and resuspended in an appropriate buffer.

For flagella preparations: After treatment with PEME/NP40 as above, pellets were harvested by centrifugation at 3200 g in a benchtop microfuge and resuspended in 1M NaCl in PEME containing Focus protease arrest mixture (CalBiochem), 200 μg ml^{-1} DNaseI and 50 μg ml^{-1} RNase. Samples were incubated at 4^{o}C for 30 minutes and pellets harvested by centrifugation at maximum speed in a benchtop microfuge. Resulting pellets were washed twice in PEME and resuspended in an appropriate buffer.

2.4.2. SDS polyacrylamide gel electrophoresis

For standard SDS-PAGE either $5x10^6$ (whole cell), $1x10^7$ (cytoskeleton) or $5x10^7$ (flagella) cell equivalents were resuspended in 30 μl boiling Laemmli buffer (2% w/v SDS, 10% v/v glycerol, 100mM dithiothreitol (DTT), 50mM Tris-Cl pH 6.8, trace bromophenol blue) and incubated at 95^{o}C for 5 minutes. Resolving gels were prepared with 10% v/v acrylamide/bisarylamide (37.5:1), 375mM Tris-Cl pH8.8, 0.1% w/v SDS, 0.1% w/v ammonium persulfate (APS) and 0.0006% v/v *N,N,N',N'* – Tetramethylethylenediamine (TEMED) and polymerised at room temperature for 1 hour. Stacking

gels were prepared with 4% v/v acrylamide/bisarylamide (37.5:1), 125mM Tris-Cl pH6.8, 0.1% w/v SDS, 0.1% w/v APS and 0.0006% v/v TEMED and polymerised at room temperature for 1 hour. Proteins were separated at constant 180V in running buffer (25mM Tris, 250mM glycine, 0.1% w/v SDS) and apparent molecular weight was indicated by the use of Precision Plus protein markers (Bio-Rad).

2.4.3. Western blot and immuno-detection

Proteins were transferred to nitrocellulose membrane (Whatman) by semi-dry blot in Towbin transfer buffer (25mM Tris, 192mM glycine, 20% v/v methanol, 0.01% w/v SDS) at constant 12V for 45 minutes. Total protein was visualised by staining of the membrane with PonceauS (PonceauS staining solution, Sigma). For immuno-detection, membranes were incubated for 30 minutes in 5% w/v dried skimmed milk in TBS (10mM Tris, 150mM NaCl) and then for a further 30 minutes in primary antibody diluted in 1% w/v dried skimmed milk in TBS. Membranes were washed 5x 5 minutes in TBST (TBS, 0.1% v/v Tween 20) before application of the secondary antibody conjugated to horseradish peroxidase diluted in 1% w/v dried skimmed milk in TBS for 30 minutes. After a further 5 washes in TBST, the membrane was treated with Western Lightning chemoluminescence reagent (Perkin Elmer) and visualised by exposure to film (Kodak).

2.4.4. Difference gel electrophoresis

50 μg of each protein sample (around $1.5x10^8$ cell equivalents for flagella or $1.5x10^7$ cell equivalents for cytoskeletons) and a reference sample containing equal amounts of all samples in the analysis were incubated at -20°C in 50% v/v acetone for 1 hour then washed once in 100% acetone. Samples were resuspended to 5 mg ml^{-1} in labelling buffer (2M thiourea, 7M urea, 30mM Tris-Cl pH8.5, 4% w/v CHAPS) and incubated for 30 minutes at 4°C with 400 pmol cyDye (cy2, cy3 or cy5, GE Healthcare). 1 nM Lysine was then added to quench any unconjugated dye and 1 volume of addition buffer (2M thiourea, 7M urea, 2% w/v CHAPS, 130mM DTT, 1% v/v ampholine (IPG buffer, GE Healthcare), trace bromophenol blue) was added to each sample. Paired samples were pooled and

one volume of reference sample added to each pooled sample. Loading buffer (2M thiourea, 7M urea, 3% w/v CHAPS, 65mM DTT, 0.5% v/v ampholine (IPG buffer, GE Healthcare), trace bromophenol blue) was added to the volume specified for the Immobilised pH gradient strip (IPG strips, GE Healthcare) to be used (in this work typically 340 µl for 18 cm pH3-11 non-linear strips). IPG strips were rehydrated in the presence of the samples for 20 h before first dimension focusing (50 µA strip^{-1} limited current; 10–500 V gradient for 4 h; 500–8000 V gradient for 5 h; 8000 V hold for 6 h). Strips were then equilibrated in 50mM Tris-Cl pH8.8, 6M Urea, 30% v/v glycerol for 15 minutes with 65mM DTT then a further 15 minutes with 135 µM iodoacetamide. Second dimension separation was performed using SDS-PAGE with 10% w/v acrylamide/bisacrylamide (37.5:1) gels (1 Watt gel^{-1} for 1 h and then 13 Watt gel^{-1} for 4–5 h) on an Ettan DALT6 system (GE Healthcare) cooled to 20^{o}C. Spots were visualized separately in each spectral channel using a Typhoon scanner (GE Healthcare) and analyzed using DeCyder software (GE Healthcare). Spots of interest (criteria in main text) were excised, and proteins identification was performed as below.

2.4.5. Tryptic digests and identification of peptides

Excised spots and bands were washed twice in 25 mM ammonium bicarbonate in 50% v/v acetonitrile. They were then dehydrated by washing with acetonitrile and reduced in 10 mM DTT for 30 min before being washed again and dehydrated prior to alkylation with 55 mM iodoacetamide for 60 min. Proteins in the gel pieces were digested with 200 ng of trypsin at 37 °C overnight. Peptides were acidified using 1 µl of trifluoroacetic acid and extracted with a wash of 0.1% v/v trifluoroacetic acid in 50% v/v acetonitrile and a wash of 0.1% v/v trifluoroacetic acid in acetonitrile. Pooled supernatants were dried in a SpeedVac (Thermo). Peptides were purified using home-made C18 purification tips (B. Thomas,The Sir William Dunn School of Pathology central proteomics facility). Peptides were spotted using α-cyano-hydoxycinnamic matrix and analyzed on an Applied Biosystems 4800 MALDI-TOF-TOF. Data were searched using MASCOT (MatrixScience) against an in-house curated *T. brucei* database (*T. brucei* genome version 4.0) containing trypsin and human keratin.

Tolerance was set at 50 ppm for MS and 0.1 Da for MS/MS. Carbamidomethylation of cysteine was set as a fixed modification, and methionine oxidation was set as a variable modification. Positive identifications were accepted with a confidence interval of 99% or greater and two unique peptides.

2.4.6. iTRAQ and Liquid Chromatography MALDI

50μg of each protein sample was solubilised and denatured then reduced and cysteines blocked according to the manufacturer's protocols (iTRAQ quadruplex starter kit, Applied Biosystems). Trypsin was added at 1mg per 10mg sample and incubated overnight at 37^{o}C. Peptides in each sample were then labelled with one of 4 isobaric stable isotope tags (114, 115, 116 or 117, Applied Biosystems) and labelled peptides were purified on an SCX cartridge (Applied Biosystems). The iTRAQ-labelled peptides were fractionated by C18 reverse phase HPLC using a Dionex U3000 nano-HPLC coupled to a Probot spotting robot. A 100-min gradient was used, and fractions were spotted, along with MALDI matrix, directly onto the MALDI target at 15-s intervals. The liquid chromatography run was analysed on an Applied Biosystems 4800 MALDI-TOF-TOF mass spectrometer, and the data were analysed using GPS Explorer (Applied Biosystems) and MASCOT against the in-house curated *T. brucei* database. Tolerance was set at 50 ppm for MS and 0.1 Da for MS/MS. Positive identifications were accepted with a confidence interval of 99% or greater and two unique peptides.

Chapter 3

The paraflagellar rod

The work presented here was published in research papers in The Journal of Biological Chemistry and PLoS ONE (Lacomble, Portman et al. 2009; Portman, Lacomble et al. 2009)

3.1. Combining comparative proteomics and the snl2 RNAi mutant cell line to identify novel components of the PFR

In the *snl2* cell line, ablation of a single major component of the PFR, PFR2, results in a failure of the structure to assemble (Bastin, Ellis et al. 2000). I have used two complementary comparative proteomic techniques, iTRAQ and DIGE, to identify proteins that are absent from flagella purified from the *snl2* induced cells but present in non-induced flagellum samples and hence to infer a PFR proteome (Figure 3.1.A).

3.1.1. Comparative proteomic analysis of the *snl2* RNAi mutant cell line identifies known and putative PFR components.

Using iTRAQ, I analysed three independent sample pairs, each consisting of a non-induced and 72 hour RNAi induced purified flagella preparation. Two sample pairs were analysed in a quadruplex experiment using four iTRAQ labels while the remaining sample pair was analysed in a duplex iTRAQ experiment utilising two of the available labels. In total, 239 proteins were identified in these samples of which 53% were present in a recent *T. brucei* flagellum proteome (Broadhead, Dawe et al. 2006). An advantage of using a quadruplex design for two of the pairs is the ability to obtain abundance ratios between the non-induced samples of each pair. When plotted as a frequency distribution of $\log_2$ ratios this shows a near symmetrical distribution with 98% of $\log_2$ ratios falling between -1 and +1 (i.e. a less than twofold change in either direction) (Figure 3.1.B). When average $\log_2$ ratios of the RNAi induced to non-induced samples are plotted in the same way a shoulder is observed on the distribution for values of $\log_2$ ratio less than -1 (Figure 3.1.C). With reference to the ratio distribution obtained by comparison of the two non-induced samples I defined proteins of interest as those with $\log_2$ ratio of less than -1 in either iTRAQ experiment (i.e. a greater than twofold reduction after PFR2 ablation). In cases where ratios passed this test in one experiment and failed in the other, the ratio generated by the highest number of peptides was accepted. If this occurred between samples in the quadruplex iTRAQ I applied a stringent approach and did not classify the

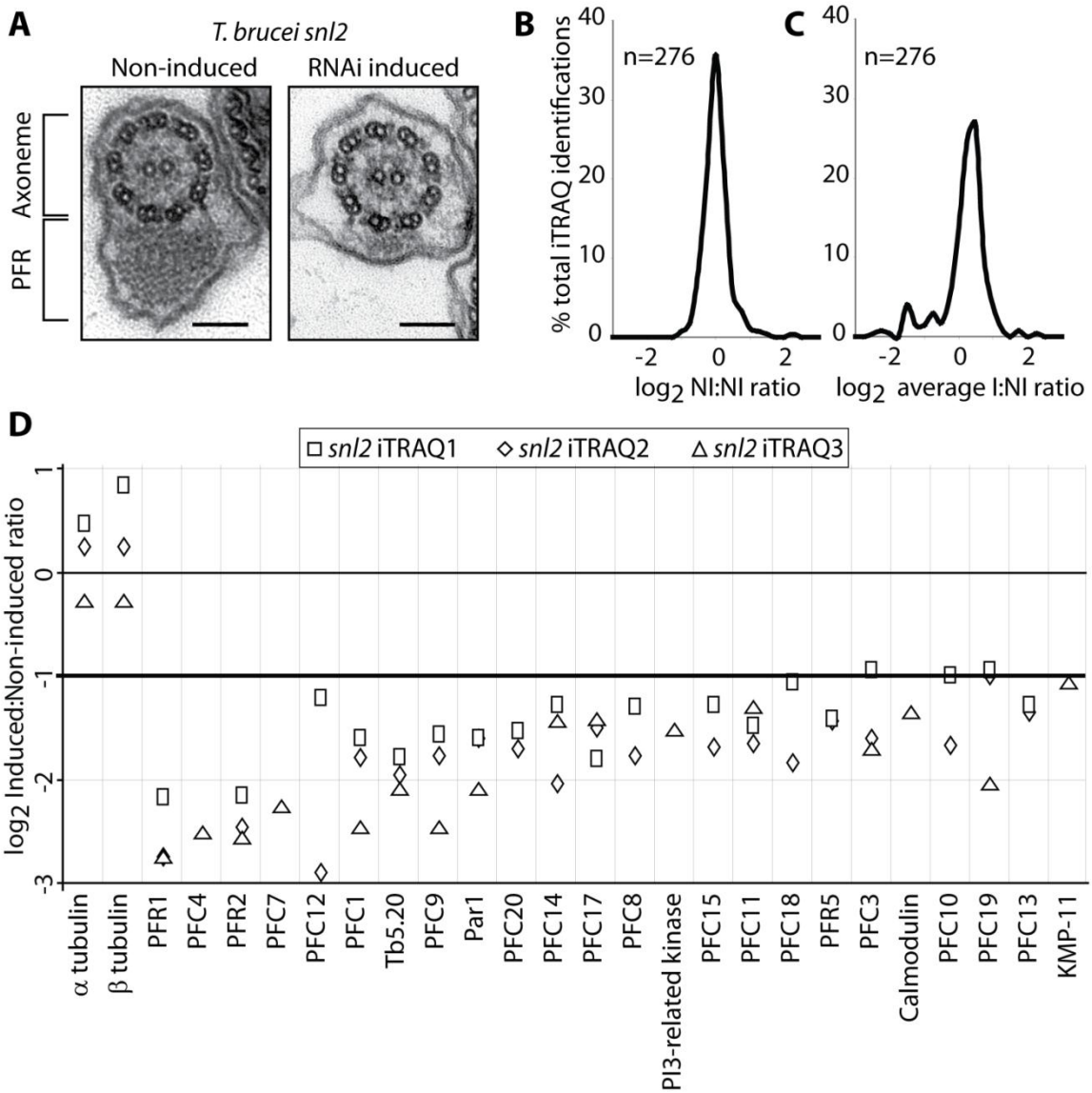

Figure 3.1. iTRAQ analysis of the *snl2* mutant. A) electron microscopy images of *T. brucei snl2* noninduced and RNAi-induced flagellar transverse sections shows the loss of a large part of the PFR structure. Bar, 100 nm. B) frequencies (resolution 0.25) of $\log_2$ protein abundance ratios of noninduced to noninduced samples from quadruplex iTRAQ. C) averaged frequencies (resolution 0.25) of $\log_2$ protein abundance ratios of induced to noninduced samples from quadruplex iTRAQ. D) $\log_2$ protein abundance ratios of induced to noninduced samples from all iTRAQ experiments for all proteins that show at least a 2-fold decrease after RNAi induction of *snl2*. α- and β-tubulin show a less than 2-fold change as expected. The results of individual sample pairs are graphed separately as per key.

protein as of interest. The portfolio of PFR candidates generated by this approach consists of 24 proteins and results from each sample pair are plotted separately in (Figure 3.1.D).

I also performed a comparative analysis on the *snl2* mutant using DIGE, another established proteomic technology, in three experiments using two independent paired samples (non-induced and 72 hour RNAi induced) in each experiment. The resulting gels were analysed using DeCyder software and spots were selected on the basis of a fold change in spot volume greater than two (consistent with the criteria applied to the iTRAQ results) (Figure 3.2.). Spots which exhibited this fold modulation were excised from the gels and subjected to tandem MS protein identification. In total 62 spots were sequenced and 36 proteins were identified. In cases where multiple identifications were forthcoming from a single spot, I again applied a conservative criterion and did not classify these as proteins of interest as the specific contribution of each protein to the reduction in spot volume cannot be readily assessed. It is likely however that at least some of these excluded 20 proteins are *bona fide* PFR components and await further investigation for confirmation. Although one specific group of spots did show an increase in spot volume after induction, no protein identifications were forthcoming from MS/MS analysis. The observation that several spots increased in abundance as a result of PFR2 ablation may be due to differences in post-translational modification altering the mobility of proteins in either one or both of the electrophoresis dimensions. There is no evidence of any other spots increasing in abundance or appearing as a consequence of PFR2 ablation so it is likely that the majority of the changes observed are due to the absence of proteins in the sample. In total 16 proteins were identified as PFR candidates in this screen; 10 of which were also identified by iTRAQ.

In summary these two proteomic approaches identified 30 proteins as PFR candidates (Table 3.1) of which twenty are novel. These novel proteins are named here as paraflagellar rod proteome component (PFC) 1 to 20. Two proteins in the dataset have existing annotations but have not previously been associated with the PFR. KMP-11 has been shown to be differentially expressed

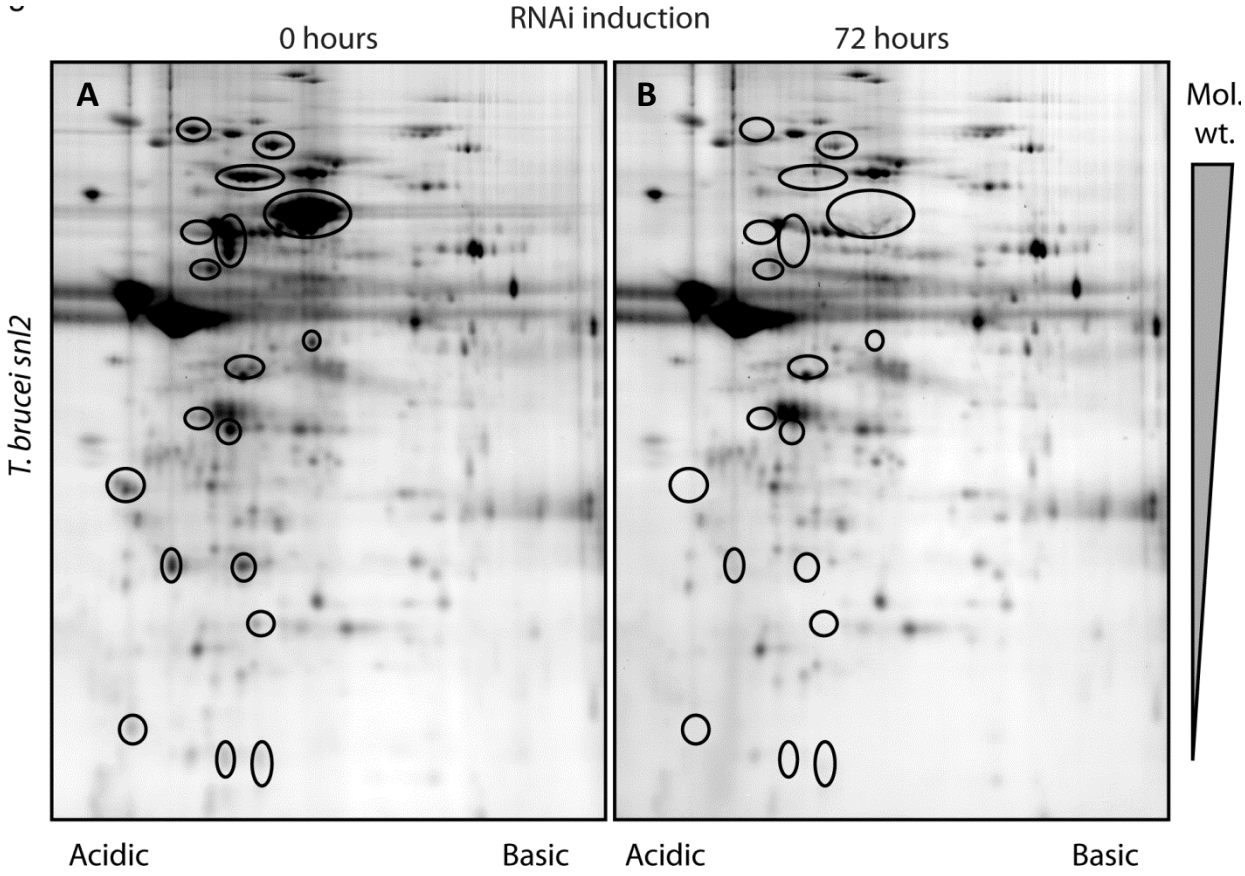

Figure 3.2. DiGE analysis of the *snl2* mutant. Comparison of purified flagella from A) noninduced and B) induced cells. Spots showing a greater than twofold change in abundance between the two samples are circled

Accession Number	Annotation	DIGE peptides for identification	Log_2 average Ind:Non DIGE ratio	iTRAQ Quadruplex peptides	iTRAQ Duplex peptides	Log_2 average Ind:Non ratio	
Tb927.3.4290	PFR1	35	-2.72	28	30	-2.53	A
Tb927.8.4970	PFR2	38	-2.72	27	32	-2.38	
Tb11.01.5100	Par1	38	-2.78	8	6	-1.75	
Tb927.2.4330	PFR5			3		-1.42	
Tb11.01.6740	Tb5.20			4	2	-1.94	
Tb927.2.5660	ADKA	15	-3.38			-1.63	
Tb10.70.7330	ADKB	13	-2.12			0.00	
Tb11.01.4623	Calmodulin				3	-1.34	
Tb09.211.4513	KMP-11				10	-1.06	B
Tb11.01.6300	PI3-related kinase				2	-1.52	
Tb927.8.6660	PFC1	14	-1	9	2	-1.90	C
Tb927.8.3790	PFC2	9	-2.63			-2.45	
Tb927.8.1550	PFC3	33	-2.13	9	8	-1.38	
Tb927.6.4140	PFC4				2	-2.51	
Tb927.7.1920	PFC5	14	-1.77			0.00	
Tb927.3.3770	PFC6	20	-1.84		2	-0.66	
Tb927.3.3750	PFC7	8	-2.84		2	-2.25	
Tb927.6.3670	PFC8			2		-1.51	
Tb11.01.6510	PFC9			3		-1.88	
Tb927.2.3660	PFC10			2		-1.30	
Tb927.2.2160	PFC11	24	-1.11	3	2	-1.47	
Tb11.02.2350	PFC12			2		-1.83	
Tb927.2.950	PFC13			2		-1.31	
Tb10.6k15.0810	PFC14	27	-2.24	7	2	-1.56	
Tb10.61.1260	PFC15			6		-1.47	
Tb10.26.0680	PFC16	7	-2.79			0.00	
Tb11.01.3000	PFC17	4	-1.38	3		-1.57	
Tb10.6k15.1510	PFC18			2		-1.40	
Tb10.6k15.0140	PFC19	16	-1.42	3	2	-1.24	
Tb10.389.0100	PFC20			2		-1.61	

Table 3.1. Summary of all candidate identifications made by iTRAQ and DiGE. 8 known PFR components (A), 2 annotated proteins not previously described as PFR components (B) and 20 novel PFR components (C - PFC proteins) were identified.

during the life cycle of several kinetoplastids and has been localised to the flagellum (Stebeck, Beecroft et al. 1995; Berberich, Machado et al. 1998). Tb11.01.6300 is annotated as a PI3-related kinase by homology and my analysis of the predicted domain architecture and size of the protein are consistent with this automated annotation (see below). 15 proteins have been identified as PFR components by previous studies and eight of these proteins are present in this dataset. These are the major PFR proteins PFR1 and PFR2 (Hyams 1982; Russell, Newsam et al. 1983; Cunha, De Souza et al. 1984; Birkett, Parma et al. 1992; Deflorin, Rudolf et al. 1994), PAR1 (Saborio, Manuel Hernandez et al. 1989; Fouts, Stryker et al. 1998), PFR5 (Clark, Kovtunovych et al. 2005), Tb5.20 (Woodward, Carden et al. 1994), calmodulin (Ridgley, Webster et al. 2000) and the PFR adenylate kinases ADKA and ADKB (Pullen, Ginger et al. 2004).

3.1.2. Bioinformatics analysis of PFR proteins.

As the PFR is an extra-axonemal structure specific to trypanosomes and related protozoa it might be expected that many of the PFR proteins will be restricted to this lineage. Indeed *in silico* analysis using a reciprocal BLASTP methodology (Figure 3.3.) revealed that 25 of the proteins identified are either restricted to *T. brucei* or have a corresponding gene in the *Leishmania major* genome but cannot be found in either the *Homo sapiens* or *C. reinhardtii* genomes. However, homologues were detected in either *H. sapiens*, *C. reinhardtii* or both for five of these proteins. In some cases, for example calmodulin, this may be as a result of other functions in the cell but it may also give an insight into conserved flagellar functions, albeit built into variable flagellar structures (Oberholzer, Bregy et al. 2007).

The portfolio of proteins generated in this analysis contains eight proteins previously proposed as PFR components. These initial descriptions have come from a number of kinetoplastids (Deflorin, Rudolf et al. 1994; Woodward, Carden et al. 1994; Fouts, Stryker et al. 1998; Ridgley, Webster et al. 2000; Pullen, Ginger et al. 2004) and are supported by variable levels of evidence. Where necessary the annotation of these proteins in the *T. brucei* dataset has been inferred from bioinformatics using

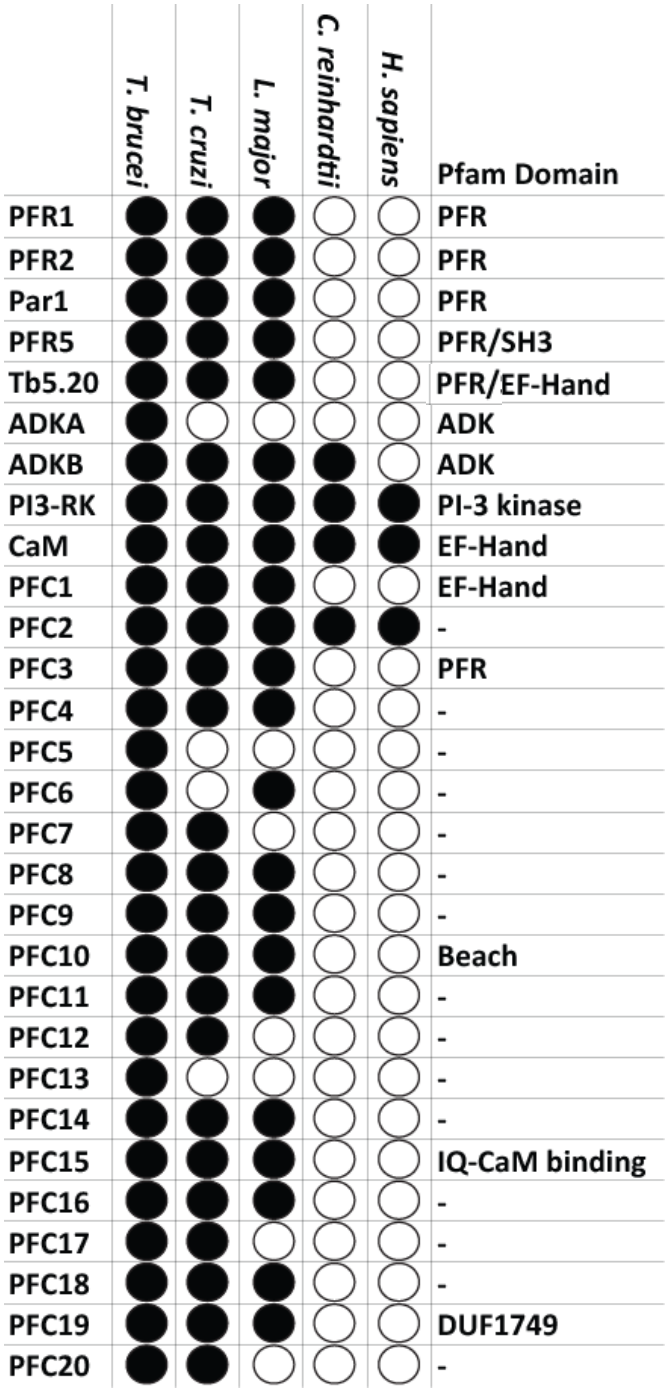

Figure 3.3. Comparative genomics analysis of PFC proteins using reciprocal best BLASTP. The majority of PFC proteins are restricted to the kinetoplastid lineage and are not found in the genomes of other flagellates. The PFR cohort contains proteins with domains involved in adenine nucleotide homeostasis and calcium signalling. Filled circle – orthologue detected, open circle – no orthologue detected.

the TriTryp genome projects (Berriman, Ghedin et al. 2005; El-Sayed, Myler et al. 2005; Ivens, Peacock et al. 2005). In order to consolidate the nomenclature of existing and newly identified PFR components I conducted a reciprocal best BLASTP analysis of all of the currently identified PFR components against six kinetoplastids species with complete or nearly complete genome sequencing projects (Table 3.2.). This analysis revealed that the majority of identified PFR components are encoded in the genome of all species interrogated. However, a subset of proteins were restricted to *T. brucei* and the closely related *T. congolense* (PFC5 and PFC13) and the two pairs of related proteins identified in the PFR (ADKA/ ADKB and PDEB1/ PDEB2) were found only as single copies in the *Leishmania* lineage. I17, PFC7, PFC12 and PFC20 were also not found in *Leishmania spp.*. These results demonstrate that the core composition of the PFR is conserved amongst kinetoplastids but that there are also lineage specific elaborations around this core proteome, perhaps reflecting the different challenges facing parasites with different life cycles.

An analysis of protein domains identified several previously predicted Pfam motifs (Figure 3.3.). As previously reported the PFR domain (PF05149) was identified in PFR1, PFR2, PFR5 and PAR1 (Clark, Kovtunovych et al. 2005) but I also detected an additional novel occurrence of this domain in Tb5.20. A motif corresponding to the EF hand domain (PF00036) was detected in three proteins (Tb5.20, PFC1 and calmodulin) and one corresponding to the leucine rich repeat domain (PF00560) was present in four proteins (PFC13, PFC14, PFC2 and PFC5). As expected, motifs consistent with adenylate kinase signatures were detected for ADKA and ADKB. A Pfam analysis of the dataset also identified two IQ calcium-independent calmodulin binding motifs (PF00612) in PFC15, a Beige/BEACH domain (PF02138) in PFC10, as previously reported (Clark, Kovtunovych et al. 2005) an SH3 (PF00018) domain in PFR5 and a Phosphatidylinositol 3- and 4-kinase (PF00454) and FATC (PF02260) domain in Tb11.01.6300, consistent with the automatic PI3-related kinase annotation.

Name	*T. brucei*	*T. congolense**	*T. cruzi*	*L. major*	*L. braziliensis*	*L. infantum*
PFR1	Tb927.3.4290	1193c01.q1k_17	XP_809830	LmjF29.1750	LbrM31_V2.0160	LinJ29_V3.1890
PFR2	Tb927.8.4970	1087c12.p1k_0	XP_814169	LmjF16.1430	LbrM16_V2.1480	LinJ16_V31510
PAR1	Tb11.01.5100	Not found	XP_818742	LmjF09.1320	LbrM09_V2.1380	LinJ09_V3.1390
PAR4	Tb927.5.4480	865g03.q1k_12	XP_805825	LmjF05.0040	LbrM05_V2.0040	LinJ05_V3.0040
PFR5	Tb927.2.4330	999f08.p1k_5	XP_816074	LmjF27.1850	LbrM27_V2.1990	LinJ27_V3.1750
PFR6	Tb927.7.6970	1341e03.p1k_4	XP_819921	LmjF05.0920	LbrM05_V2.0900	LinJ05_V3.0920
Calmodulin	Tb11.01.4621	528h03.p1k_2	XP_808089	LmjF09.0910	LbrM09_V2.0960	LinJ09_V3.0980
ADKA	Tb927.2.5660	1144b06.p1k_5	Not found	Not found	Not found	Not found
ADKB	Tb10.70.7330	1389a06.q1k_3	XP_810144	LmjF21.1250	LbrM21_V2.1450	LinJ21_V3.1490
Gamma Tubulin	Tb927.3.910	526h04.q1k_1	XP_814966	LmjF25.0960	LbrM25_V2.0840	LinJ25_V3.0990
KMP-11	Tb09.211.4512	Not found	XP_810488	LmjF35.2210	LbrM34_V2.2150	LinJ35_V3.2250
Myosin XXI	Tb11.01.7990	Not found	XP_809654	LmjF32.3870	LbrM32_V2.4110	LinJ32_V3.4020
PDEB1	Tb09.160.3590	857h01.q1ka_11	XP_820270	Not found	LbrM15_V2.1250	Not found
PDEB2	Tb09.160.3630	Not found	XP_804464	LmjF15.1480	LbrM15_V2.1480	LinJ15_V3.1550
Tb5.20	Tb11.01.6740	1557c01.q1k_0	XP_817636	LmjF32.1910	LbrM32_V2.2100	Not found
TbI17	Tb10.26.0960	1023a12.q1k_9	XP_811780	Not found	Not found	Not found
TbI2	Tb927.3.5310	1411c01.q1k_2	XP_811482	LmjF29.0350	LbrM29_V2.0290	LinJ29_V3.0360
PI3K-related kinase	Tb11.01.6300	Not found	XP_812942	LmjF32.1460	LbrM32_V2.1620	LinJ32_V3.1520
PFC1	Tb927.8.6660	1023a07.q1k_7	XP_806248	LmjF24.1560	LbrM24_V2.1300	LinJ24_V3.1630
PFC2	Tb927.8.3790	1148b02.q1k_15	XP_802628	LmjF10.0180	LbrM10_V2.0180	LinJ10_V3.0160
PFC3	Tb927.8.1550	1291d12.q1k_4	XP_816963	LmjF07.0310	LbrM07_V2.0320	LinJ07_V3.0470
PFC4	Tb927.6.4140	1085c12.p1k_4	XP_809400	LmjF30.2850	LbrM30_V2.2830	LinJ30_V3.2870
PFC5	Tb927.7.1920	1126c02.q1k_2	Not found	Not found	Not found	Not found
PFC6	Tb927.3.3770	1124g03.p1k_0	XP_808170	LmjF29.1170	Not found	LinJ29_V3.1260
PFC7	Tb927.3.3750	1407h03.q1k_4	XP_813907	Not found	Not found	Not found
PFC8	Tb927.6.3670	1335c05.q1k_7	XP_819095	LmjF30.2390	LbrM30_V2.2340	LinJ30_V3.2400
PFC9	Tb11.01.6510	Not found	XP_804149	LmjF32.1680	LbrM32_V2.1850	LinJ32_V3.1760
PFC10	Tb927.2.3660	1130f02.p1k_3	XP_812725	LmjF33.2780	LbrM33_V2.3060	LinJ33_V3.2920
PFC11	Tb927.2.2160	171e08.q1k_13	XP_807404	LmjF02.0310	LbrM02_V2.0360	LinJ02_V3.0280
PFC12	Tb11.02.2350	1278f02.q1k_13	XP_817448	Not found	Not found	Not found
PFC13	Tb927.2.950	771g11.q1k_1	Not found	Not found	Not found	Not found
PFC14	Tb10.6k15.0810	1004e12.q1k_6	XP_812195	LmjF36.4230	LbrM35_V2.4480	LinJ36_V3.4440
PFC15	Tb10.61.1260	Not found	XP_817255	LmjF19.0520	LbrM19_V2.0840	LinJ19_V3.0520
PFC16	Tb10.26.0680	1069e05.p1k_0	XP_819848	LmjF33.0610	LbrM33_V2.0650	LinJ33_V3.0660
PFC17	Tb11.01.3000	Not found	XP_803930	Not found	Not found	Not found
PFC18	Tb10.6k15.1510	410c11.p1k_1	XP_815947	LmjF36.5870	LbrM35_V2.6170	LinJ36_V3.6130
PFC19	Tb10.6k15.0140	758b01.p1k_15	XP_817130	LmjF36.4780	LbrM35_V2.5030	LinJ36_V3.5010
PFC20	Tb10.389.0100	1205b11.p1k_21	XP_819266	Not found	Not found	Not found
TczAC/GRESAG 4	Tb10.61.0280	189g01.p1k_3	XP_806389	LmjF17.0190	LbrM17_V2.0130	LinJ17_V3.0130
FCaBP	Tb927.8.5440	20a04.p1k_4	XP_808305	Not found	LbrM16_V2.0930	LinJ16_V30930
LdCof	Tb927.3.5180	1379b03.q1k_1	XP_810628	LmjF29.0510	LbrM29_V2.0450	LinJ29_V3.0520
LmxMKK	Tb927.3.4860	1242a01.q1k_13	XP_822045	LmjF29.2320	LbrM29_V2.2290	LinJ29_V3.2430
LmxMPK3	Tb927.8.3550	1097a03.q1k_20	XP_807815	LmjF10.0490	LbrM10_V2.0620	LinJ10_V3.0540

Table 3.2. Consolidated nomenclature of all identified PFR components using a reciprocal best BLASTP approach. Where multiple identical orthologues were found in a single genome (as for PFR1 and PFR2) a single representative accession number is provided. *When interpreting 'Not found' statements it is important to take into account the completeness of the relevant genome project.

3.1.3. PFC proteins localise to the PFR

The presence of previously identified PFR proteins in this dataset (representing over 25% of the identifications) is comforting and shows that this RNAi mutant/comparative proteomic method is capable of identifying genuine PFR components and supports the annotation of PFR proteins previously identified only by bioinformatics. In order to validate the remaining proteins in the dataset four novel proteins were selected that were representative of the methodologies used to identify them (PFC5 identified only by DIGE; PFC15 identified only by iTRAQ; PFC3 and PFC14: identified by both methods) for subcellular localisation by epitope tagging and immunofluorescence microscopy. Transgenic cell lines were generated in which one of the endogenous copies of the gene of interest carried the in-frame coding sequence for the Ty epitope tag (Bastin, Bagherzadeh et al. 1996) immediately downstream of the start codon. Trypanosome cells were fixed and assayed by immuno-double labelling using antibodies against the Ty epitope tag and the flagellum attachment zone (FAZ) (Kohl, Sherwin et al. 1999). In *T. brucei*, the PFR lies alongside the axoneme from a point after the flagellum exits the flagellar pocket, beyond the start-point of the FAZ, to a point beyond the region of attachment to the cell body. In all cases the tagged protein localised in a portion of the flagellum (Figure 3.4.) with a labelling pattern consistent with the PFR. All proteins were distributed along the length of the flagellum as either a continuous or punctate line. Including the known PFR proteins in this dataset, and two novel components (PFC11, PFC4 and PFC16) localised to the PFR by Sylvain Lacomble (as part of this project) (Portman, Lacomble et al. 2009) there is now strong evidence for PFR localisation of 50% of the proteins identified (and 100% of those tested), suggesting that this is a robust dataset that contains a very high proportion of *bona fide* PFR proteins.

3.2. Comparative proteomics and RNAi identifies subgroups, dependencies and interactions within the cohort of PFR proteins.

The presence of calmodulin, and the calcium and calmodulin recognition domains in the PFC proteins, is indicative of a calcium regulated system operating within the PFR. In order to investigate interactions of components within this potential calcium signalling pathway I conducted

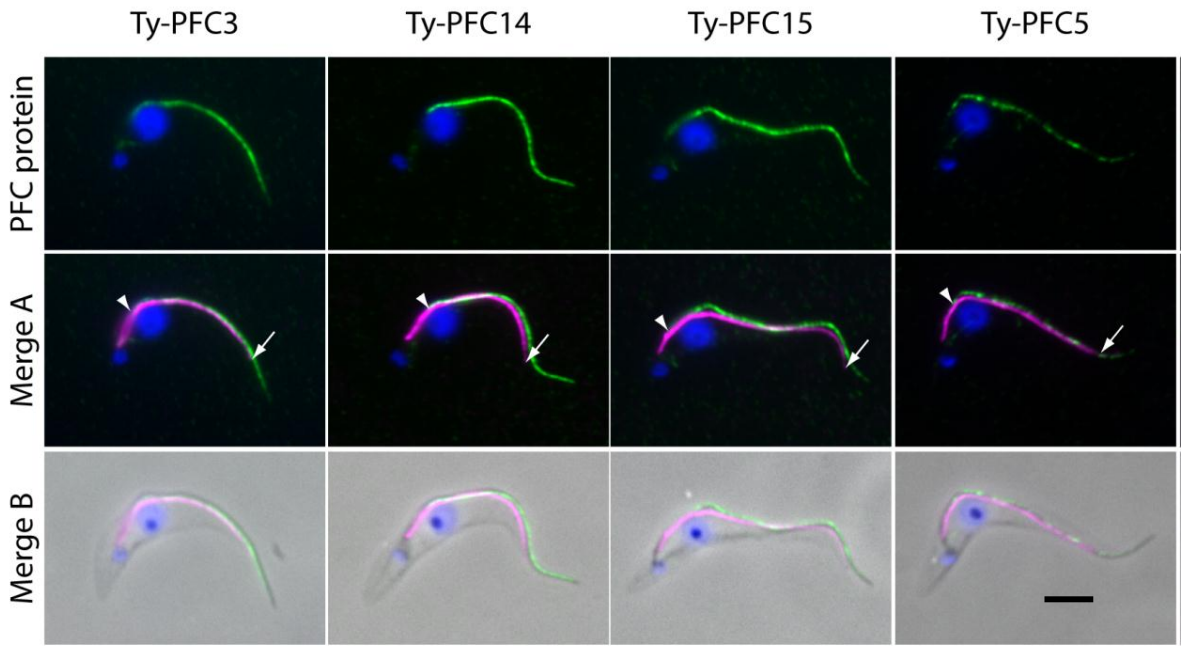

Figure 3.4. Localisation of novel PFR components. 5 cell lines expressing a Ty epitope tagged PFC protein from one of the endogenous loci of endogenous loci were generated. Chimeric proteins were localised using BB2 and the FAZ was visualised with L6B3. All protein localisations are consistent with a position in the PFR. Green – Ty::PFC protein, magenta – FAZ, blue DAPI, bar = 5μm

RNAi/comparative proteomic analyses using DIGE against two cryptic proteins with predicted domains involved in calcium signalling; PFC1 (EF-Hand calcium binding domain) and PFC15 (IQ-Calmodulin binding domain).

3.2.1. PFC1 and PFC5 form a dependency subgroup with PFR adenylate kinases

A number of spots showed volume reductions following RNAi mediated ablation of PFC1 and PFC15 and, by reference to *snl2* DIGE gels (Figure 3.5.), the identities of the corresponding proteins were determined to be PFC1, ADKA and ADKB. ADKA spot volumes decreased significantly as a result of RNAi against either PFC1 (log_2 ratio ADKA: -0.84) or PFC15 (log_2 ratio ADKA: -2.22). PFC1 spot volume was reduced as effectively by PFC15 RNAi (log_2 ratio PFC1: -1.50) as it was by PFC1 RNAi (log_2 ratio PFC1: -1.53), however the effect on ADKB spot volume in these RNAi backgrounds differed with a significant reduction only observed after PFC15 RNAi (PFC1 RNAi log_2 ratio: -0.37, PFC15 RNAi log_2 ratio: -1.25) (Figure 3.5.A). Although the reasons for this are not immediately clear, it may suggest a role for other proteins in this complex or transport into the flagellum/PFR as a factor. PFC15 has not been detected in DIGE analyses, possibly due to its highly basic nature (predicted pI 10.4). In order to determine the fate of PFC15 in these RNAi cell lines, I tagged one of the endogenous copies of the gene with a Ty epitope in both PFC1 and PFC15 RNAi backgrounds. RNAi induced and non-induced detergent-extracted pellets derived from each cell line were compared by Western blot using an antibody that recognises the Ty epitope (Figure 3.5.B). This revealed that, as expected, Ty-PFC15 is readily detectable in non-induced samples and is not present after PFC15 RNAi. However, this analysis also showed that the Ty-PFC15 protein is not correctly assembled into the flagellum after RNAi against PFC1 (Figure 3.5.B). Overall these results show the interdependency of PFC1 and PFC15 and suggest a possible role for calcium regulation of adenylate kinase function in the PFR. In contrast to the severe motility consequences following ablation of PFR2 and the gross reduction in the PFR structure (Bastin, Sherwin et al. 1998) RNAi against either PFC1 or PFC15 did not obviously affect the motility of the cells under culture conditions, as similarly reported previously following RNAi ablation of both ADKA and ADKB (Pullen, Ginger et al. 2004).

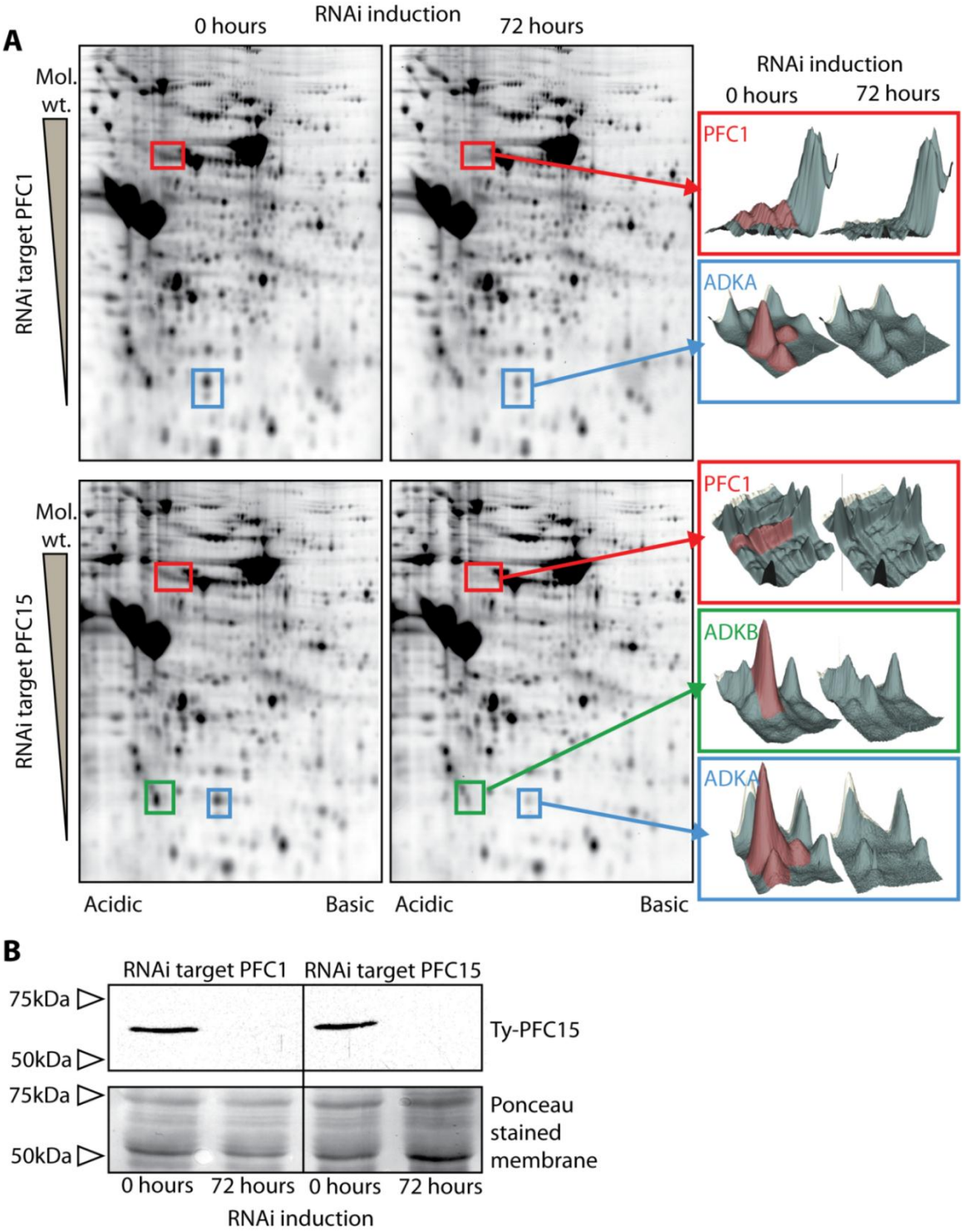

Figure 3.5. 2D- DIGE analysis of PFC1 and PFC15 noninduced and induced flagella. A) The gels were analyzed using Decyder software (GE Healthcare), which was used to generate three-dimensional representations of the spots that show a change in volume after induction. In both RNAi environments, significant reductions in volume were seen for spots corresponding to PFC1 and ADKA. An equally significant volume decrease was observed for ADKB after PFC15 RNAi, but this was not observed after PFC1 RNAi. B) Western blot showing the absence of Ty epitope-tagged PFC15 from the detergent-resistant fraction following RNAi against PFC15 and against PFC1. Ponceau-stained membrane is shown as a loading control.

3.2.2. Proteomic analysis reveals dependencies supporting the identified interactions.

Having demonstrated the power of combining RNAi ablation of key proteins with comparative proteomics techniques to identify dependent sub-groups of proteins within the larger complex of the PFR I applied this method to test interactions (PFC3/PAR1) detected in a yeast two-hybrid screen of identified PFR components (Lacomble, Portman et al. 2009). Resulting spot patterns were matched using Decyder software to a reference 2D gel map of PFR proteins within the context of purified flagella. Samples prepared 72 hours after RNAi induction against PFC3 showed a number of spots with a twofold or greater decrease in volume when compared to non-induced samples (consistent with criteria applied previously) (Figure 3.6.). As expected a group of five spots of approximately 80kDa that correspond to PFC3 showed two- to four-fold reduction in volume (3.8, 3.7, 3.1, 2.8 and 2.3-fold reductions). Interestingly the volume of a spot of approximately 65kDa that corresponds to PAR1 also showed a 2.1-fold decrease. This result shows that PAR1 is not stably incorporated into the structure of the flagellum in the absence of PFC3 protein and supports the interaction of these two proteins observed in the yeast two-hybrid screen. Greater than twofold reductions in spot volumes following PFC3 RNAi were also observed for three other spots. These correspond to PFC5 (two spots – 2.1-fold and 2.7-fold reductions in volume) and PFC17 (one spot – 2.1-fold reduction in volume). PFC3 or PAR1 interactions with either PFC5 or PFC17 were not observed by yeast two-hybrid analysis. Reciprocal experiments showed that RNAi induction for 72 hours against PAR1 phenocopies the PFC3 result with spot volume reductions for PAR1 (3.7-fold reduction), PFC3 (3.1, 4.9, 4.5, 3.2 and 2.2-fold reductions), PFC5 (2.1 and 2.7-fold reductions) and PFC17 (2.1-fold reduction) (Figure 3.6.B). RNAi against PFC5, however, only resulted in a reduction in volume of the two spots corresponding to PFC5 itself (1.5 and 2.0 -fold reductions) (Figure 3.6.C). Taken together these data suggest a hierarchical dependency sub-network whereby PAR1 and PFC3 are both necessary for the incorporation of all four proteins into the PFR. Using immunofluorescence light microscopy of detergent extracted cells, I analysed cell lines containing a Ty epitope tagged copy of PFC3 at one of the endogenous alleles (18) and inducible RNAi against PFC3, PAR1 or PFC5 with the BB2 antibody.

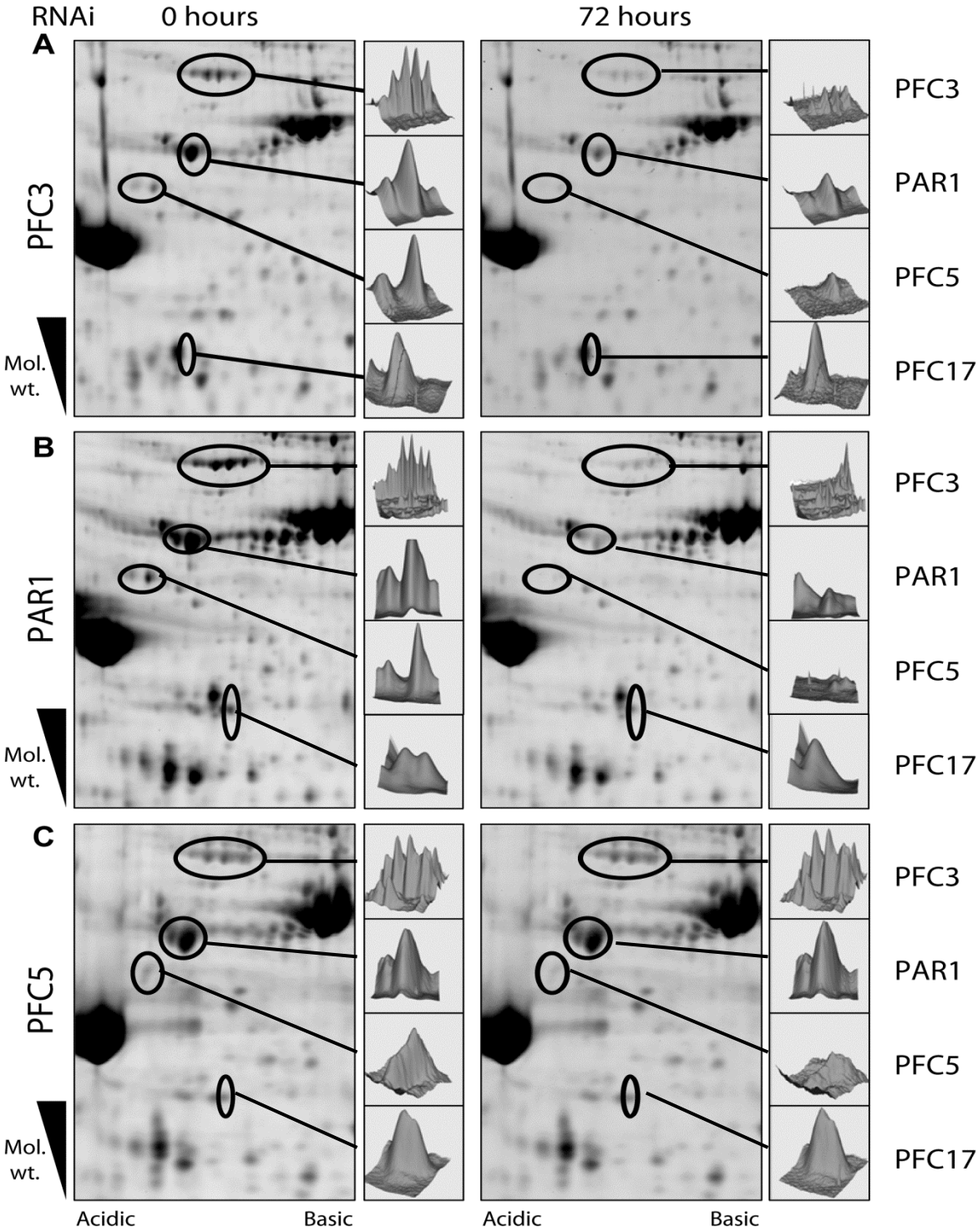

Figure 3.6. DiGE analysis of the PFC3/PAR1 network. A) ablation of PFC3 results in a decrease in spot volume for PAR1, PFC5 and PFC17. B) ablation of PAR1 results in a decrease in spot volume for PFC3, PFC5 and PFC17. C) ablation of PFC5 only results in a decrease in spot volume for PFC5. 3D spot maps generated in DeCyder software (GE Healthcare) are shown beside the relevant gels.

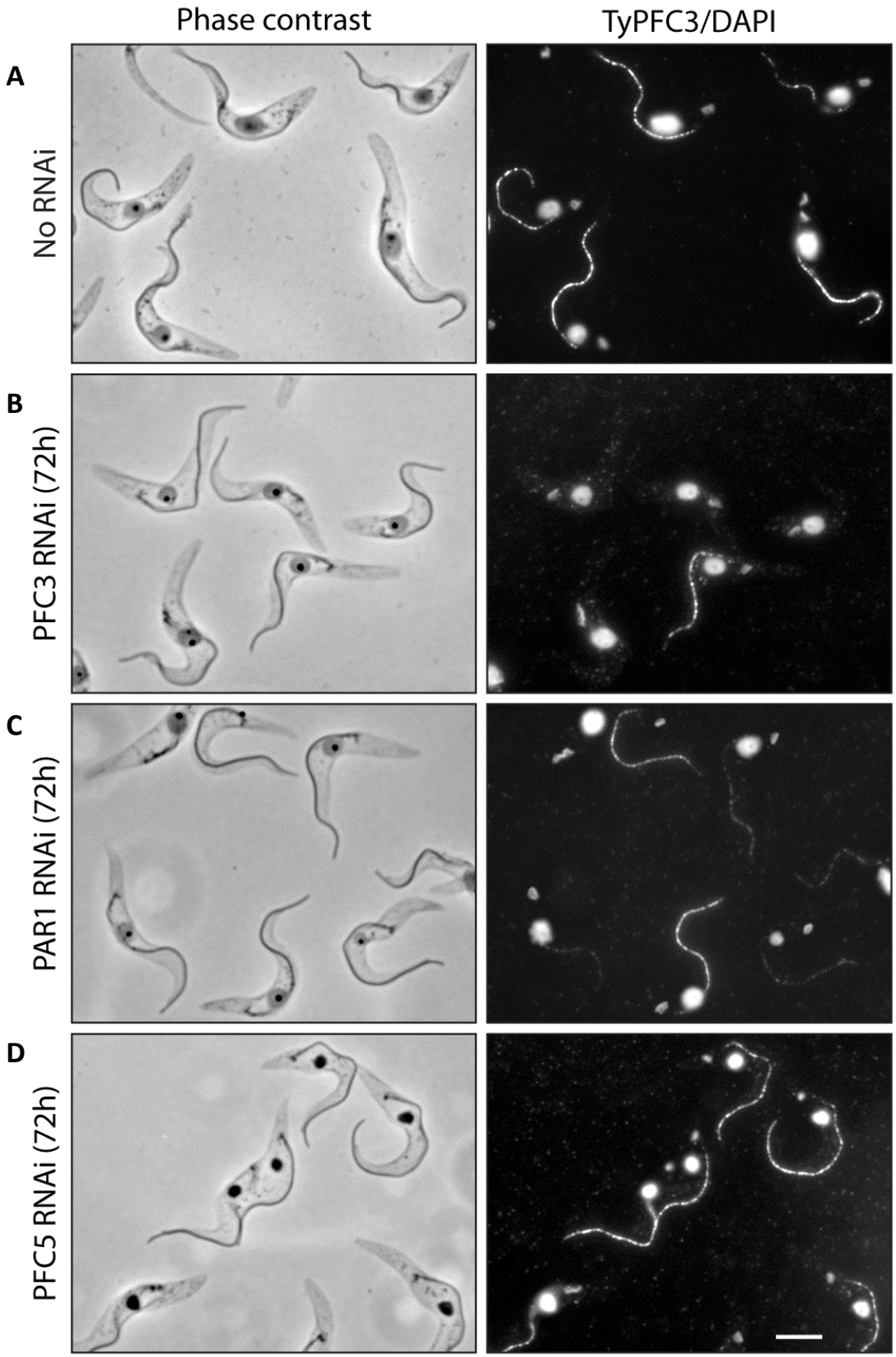

Figure 3.7. RNAi of the PFC3/PAR1 network. A) cells expressing Ty::PFC3 from one of the endogenous loci with B) RNAi against PFC3, C) RNAi against PAR1 and D) RNAi against PFC5. Cells were extracted in PEME-1% NP40 and fixed in methanol. Nucleus and kinetoplast were visualised with DAPI. Bar = 5 μm

Comparison of cells 72 hours after RNAi induction with non-induced controls showed no gross morphological changes (Figure 3.7.). In addition, consistent with my previous results, PFC3 signal was absent in the majority of cells following PFC3 RNAi and was greatly reduced following PAR1 RNAi. Furthermore, RNAi against PFC5 did not affect PFC3 localisation.

Chapter 4

Identification of life-cycle stage-specific cytoskeletal proteins in *T. brucei*

As discussed above there are numerous differences between the morphology, metabolism and proteomic makeup of bloodstream and procyclic form *T. brucei* reflecting the very different environments inhabited by the two forms. In this part of my project I identify novel cytoskeletal and flagellar proteins with stage-specific patterns of protein expression.

4.1. Comparison of bloodstream form and procyclic form purified flagella

4.1.1. Candidate flagellar proteins identified using comparative proteomics

In order to identify components of the flagellar complex with life-cycle stage-specific expression I used the gel-based comparative proteomic technique DIGE to compare the protein composition of detergent and salt extracted bloodstream form cells to that of procyclic form cells prepared in the same way (Figure 4.1.). The resulting gels were scanned and spots showing differential abundance between the two samples were detected by overlaying the gel images. Numerous spots showed a difference in spot volume between the two samples and a total of 35 were cut from the gel for mass spectrometric analysis. 62 identifications were made with a confidence interval greater than 99% and identification by at least two unique peptides. A total of 46 non-redundant identifications were made (Table 4.1.). One set of spots were identified as VSG221, the VSG variant expressed by the bloodstream cell line used (Figure 4.1.C). Reassuringly these spots were only present in the bloodstream form sample but do demonstrate the need for caution when analysing proteomic data as VSG would be expected to be washed out of the preparation under the extraction conditions used. That VSG was observed in this preparation is likely to be a function of the large number of VSG molecules present in a bloodstream form cell. Six proteins were identified for which a role in the flagellum has not been shown or would seem unlikely (Table 4.1.). Another set of proteins constitute those for which a role in the flagellum is known or has been postulated. These include alpha and beta tubulin, several dynein heavy chains, the axonemal components trypanin and PF16 and several PFR components. Stage specific expression of most of these seems unlikely. However, it is interesting to note that one of the spots present only in the bloodstream form sample yielded a single identification of beta tubulin (Figure 4.1.A - *). The location on the gel suggests that the protein in

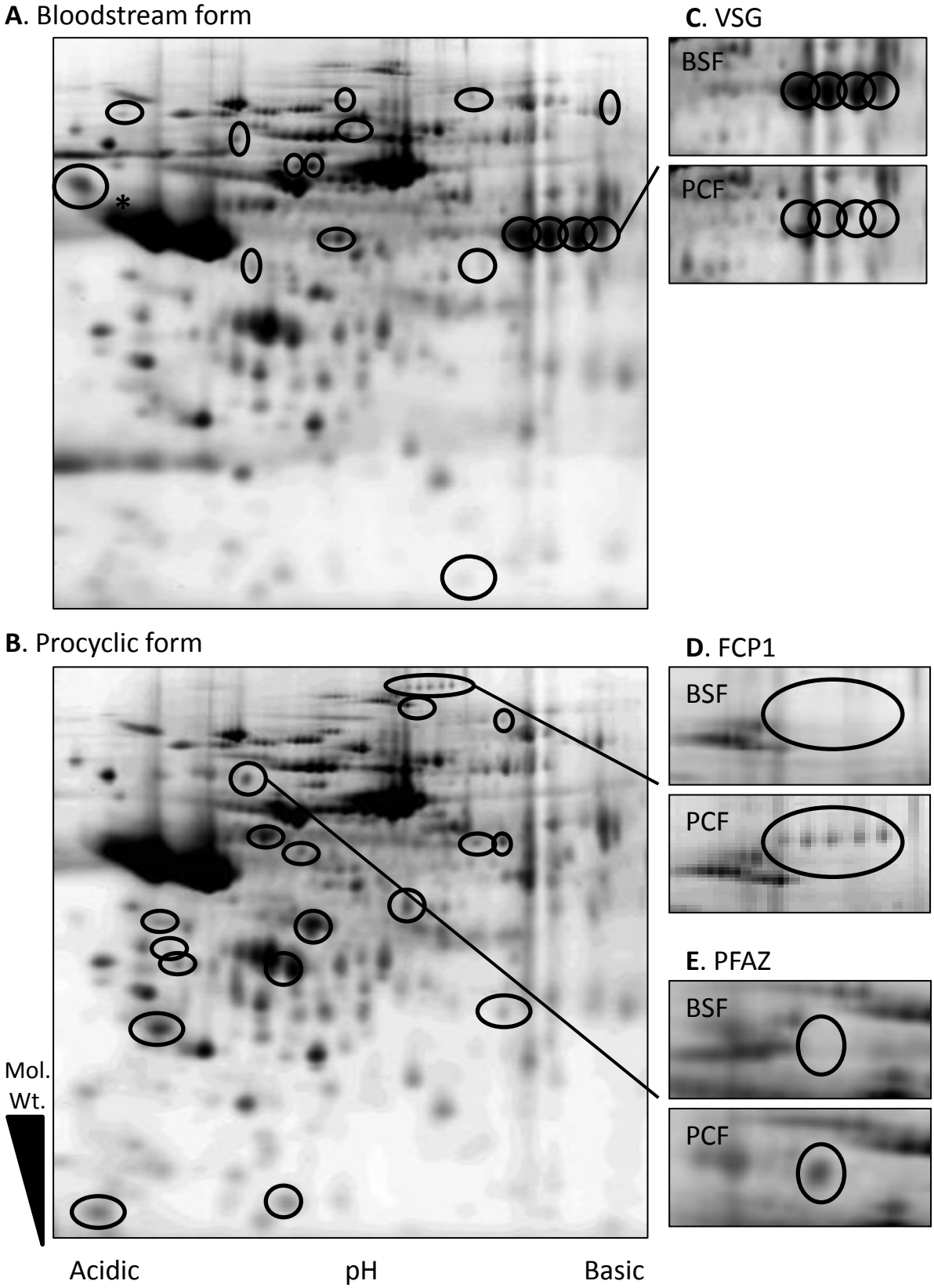

Figure 4.1. 2D-DIGE comparison of purified flagella from A) Bloodstream forms and B) Procyclic forms. Spots that showed a twofold or greater change between the samples are circled. C - E) close up views of the gel regions corresponding to VSG, FCP1 and PFAZ respectively. A) * = spot identified as beta tubulin.

Table 4.1. Comparison of bloodstream form and procyclic form flagella.

Accession	TM	pI	Mr	Annotation	Up in sample	
Tb927.8.7590	1	8.23	139526	GRESAG4	B/P	A
Tb11.01.3000	0	5.18	41941	PFC17	B/P	
Tb927.3.2600	0	6.09	244997	RNA helicase	B/P	
Tb927.1.2330	0	4.46	49705	beta tubulin	B	B
Tb11.02.5450	0	5.12	71436	BiP	B	
Tb11.02.0760	0	5.12	531191	dynein heavy chain	B	
Tb927.10.10980	0	4.81	80794	HSP83	B	
Tb09.160.1160	0	4.4	85915	NOP86	B	
Tb11.03.0810	0	5.37	109767	Nucleoporin	B	
Tb11.01.5100	0	5.13	68351	PAR1	B	
Tb927.1.2670	0	6.67	56127	PF16	B	
Tb927.8.1550	0	5.6	88180	PFC3	B	
Tb927.8.4970	0	5.89	69598	PFR2	B	
Tb927.10.6350	0	6.88	53925	trypanin	B	
Tb927.2.3020	0	5.44	118834	Hypothetical	B	
Tb927.4.4130	0	7.26	100041	Hypothetical	B	
Tb927.6.4520	0	8.15	52590	Hypothetical	B	
Tb927.8.4580	0	7.56	58086	Hypothetical	B	
Tb927.8.8200	0	7.28	99868	Hypothetical	B	
Tb927.10.15760	0	4.63	36412	Hypothetical	B	
Tb11.01.0510	0	6.8	46475	Hypothetical	B	
Tb09.211.0620	0	5.3	41896	actin A	P	C
Tb927.1.2340	0	4.69	49788	alpha tubulin	P	
Tb927.1.2100	0	4.44	126155	calpain-like cysteine peptidase	P	
Tb927.10.8710	0	4.42	18802	centrin	P	
Tb927.6.4670	0	5.2	40687	CMRP	P	
Tb11.01.3010	0	6.01	480264	dynein heavy chain	P	
Tb927.10.6510	0	5.06	59504	HSP60	P	
Tb927.7.3440	0	4.46	27050	I/6 autoantigen	P	
Tb927.2.2160	0	5.04	37732	PFC11	P	
Tb927.10.10140	0	5.16	37014	PFC19	P	
Tb927.7.1920	0	4.95	59272	PFC5	P	
Tb927.3.3750	0	5.33	19860	PFC7	P	
Tb11.02.2210	0	5.01	56735	PKA-R	P	
Tb927.1.4800	0	10.06	51502	Hypothetical	P	
Tb927.2.4810	0	5.89	150503	Hypothetical	P	
Tb927.4.630	0	6.69	33880	Hypothetical	P	
Tb927.5.3330	0	7.08	521771	Hypothetical	P	
Tb927.7.3310	0	6.51	38536	Hypothetical	P	
Tb927.7.4840	0	4.46	38168	Hypothetical	P	
Tb927.8.940	2	5.25	237466	Hypothetical	P	
Tb927.8.4050	2	4.83	83065	Hypothetical	P	
Tb927.8.8170	0	9.79	100405	Hypothetical	P	
Tb09.160.0350	0	6.39	59815	Hypothetical	P	
Tb11.02.0880	0	6.82	486557	Hypothetical	P	

Table 4.1. Comparison of bloodstream form and procyclic form flagella. A) proteins identified from multiple spots showing different specificity. B) proteins identified from spots more abundant in the bloodstream sample. C) proteins identified from spots more abundant in the procyclic sample. PFAZ and FCP1 are shaded blue

this spot has an apparent molecular weight between 5 and 10 kDa greater than that of beta tubulin with a slightly more acidic isoelectric point. If the identification is genuine and not the result of contamination due to proximity to the main tubulin spot this may represent a stage specific modification of beta tubulin. Finally 16 of the identified proteins were annotated as hypothetical (Table 4.1.) and I took these forward for bioinformatic analysis.

4.1.2. Bioinformatic characterisation of candidate proteins

Two flagellar associated structures in particular are likely to contain proteins with stage-specific expression patterns, the FAZ and the flagella connector. As discussed above stage-specific expression of FAZ proteins has previously been demonstrated and a flagella connector has only been observed in procyclic form cells. Both of these structures are involved in connecting cytoskeletal components across membranes so I hypothesised that some components of these would likely contain transmembrane domains and/or signal peptides. I submitted the accession numbers of the hypothetical proteins as a query at tritrypdb (www.tritrypdb.org) to search for predicted transmembrane domains. This search identified two proteins from my dataset with predicted transmembrane domains, Tb927.8.4050 and Tb927.8.940, both of which were present only in the procyclic form sample.

4.1.3. Bioinformatic analysis of Tb927.8.4050

Tb927.8.4050, which I have called PFAZ (Procyclic FAZ) , is a 750 amino acid protein with a calculated molecular weight of 83kDa and a predicted isoelectric point of pH4.8, which are consistent with the area of the gel from which the spot was cut (Figure 4.1.E). The protein has two predicted transmembrane domains at residues 21-43 and 688-710 (Figure 4.2.) and a low scoring prediction of a signal anchor (SignalP probability 0.571) at the N terminus. A second identical copy of the gene is also located on chromosome 8 (Tb927.8.4100) approximately 10kb downstream. Interestingly these two copies of PFAZ are located in the same repeat unit that contains the fla family discussed above

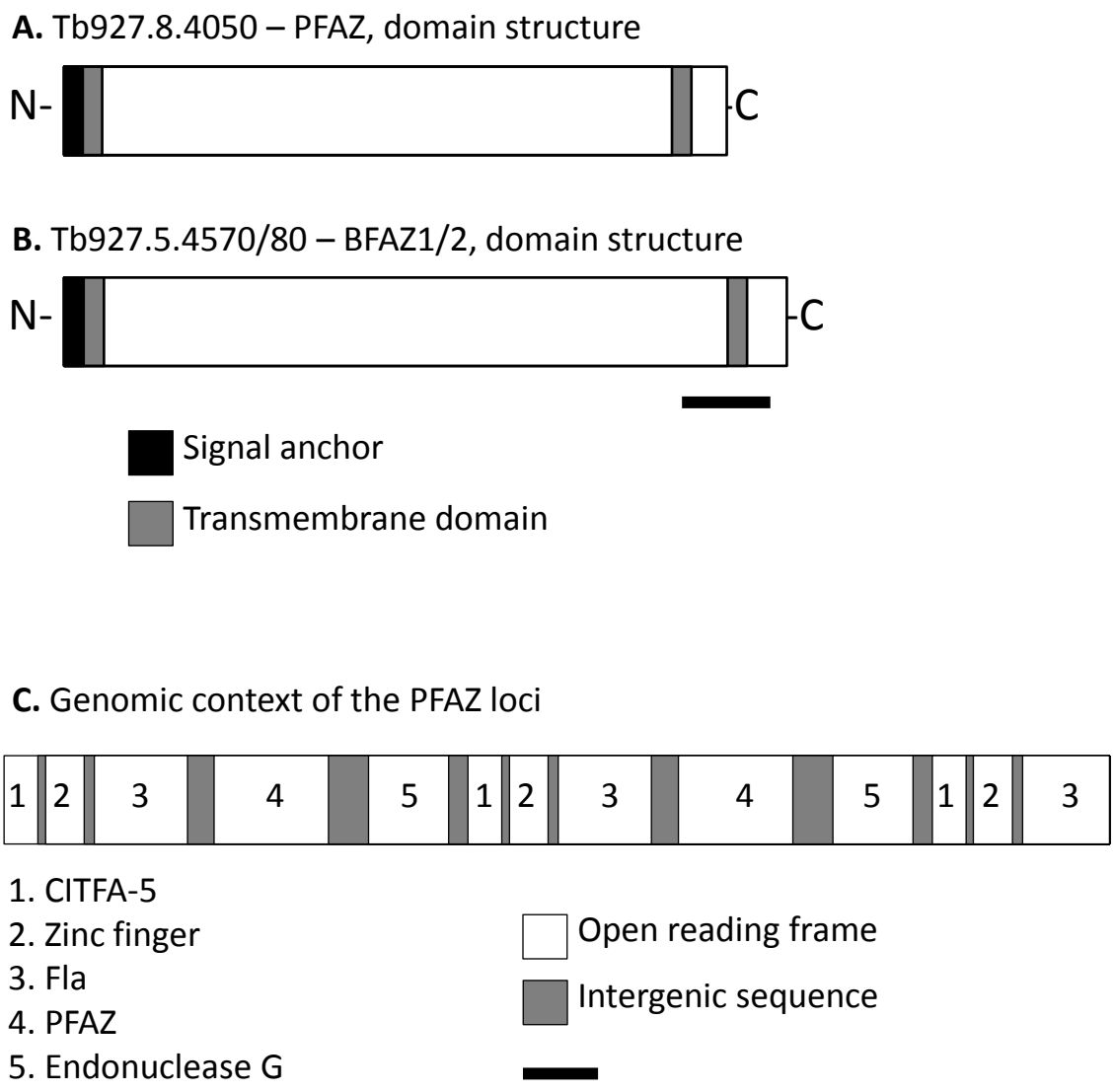

Figure 4.2. Cartoon of the protein domain structure and genomic context of PFAZ. PFAZ (A), BFAZ1 and BFAZ2 (B) proteins share a common domain architecture with a signal anchor at the N terminus (black) associated with a single transmembrane domain (grey) with a second transmembrane domain at the C terminus. Bar = 100 residues. C) PFAZ is encoded by two identical open reading frames within a five open reading frame repeat region on chromosome 8. White = open reading frame with 5'UTR, grey = intergenic sequence, bar = 1 kpb.

(Figure 4.2.). The repeat unit consists of a class1 transcription factor A subunit (CITFA-5) followed by a small zinc finger domain containing protein, a fla protein, PFAZ and endonucleaseG. There are two full repeats followed by a partial repeat that terminates with fla1. At the protein level both copies of PFAZ are identical as are all three copies of the zinc finger domain containing protein while the endonuclease G repeats differ at only a single residue. The first two copies of CITFA-5 are identical whereas the third is 71% identical and 80% similar to the other two with all of the differences located in the C terminal half of the protein. Finally fla3 and fla2 are 97% identical but only 65% identical to fla1. The first 100 residues of all three proteins are identical and fla2 and fla3 contain a 44 residue proline-rich region beginning at amino acid 340 that is not present in fla1.

By alignment of the PFAZ sequence to the translated *T. brucei* genome using BLASTP I identified a further two open reading frames, Tb927.5.4570 and Tb927.5.4580 which I have named BFAZ1 and BFAZ2 (Bloodstream FAZ 1,2), that are 90% identical to each other and likely in-paralogues of PFAZ to which they are around 50% identical (Figure 4.3.). Both proteins are predicted to be 818 amino acids long with two predicted transmembrane domains between residues 23-45 and residues 751-773 (Figure 4.2.B). The open reading frames are located in tandem adjacent to the sub telomeric array of VSG pseudogenes on chromosome 5. Interestingly, given my prediction that PFAZ is a procyclic form stage protein, a recent genome wide screen of RNAi phenotypes found that ablation of BFAZ1 and BFAZ2 led to abnormal growth in bloodstream form cultures but not in procyclic form cultures although ablation of PFAZ did not result in abnormal growth in either life cycle stage (Alsford, Turner et al. 2011).

4.1.4. Localisation of PFAZ

In order to determine the localisation of PFAZ I generated a procyclic form cell line expressing C terminal CFP::Ty tagged PFAZ from one of the endogenous loci. Native fluorescence was examined by immunofluorescence microscopy which showed a continuous line of fluorescence with bright foci

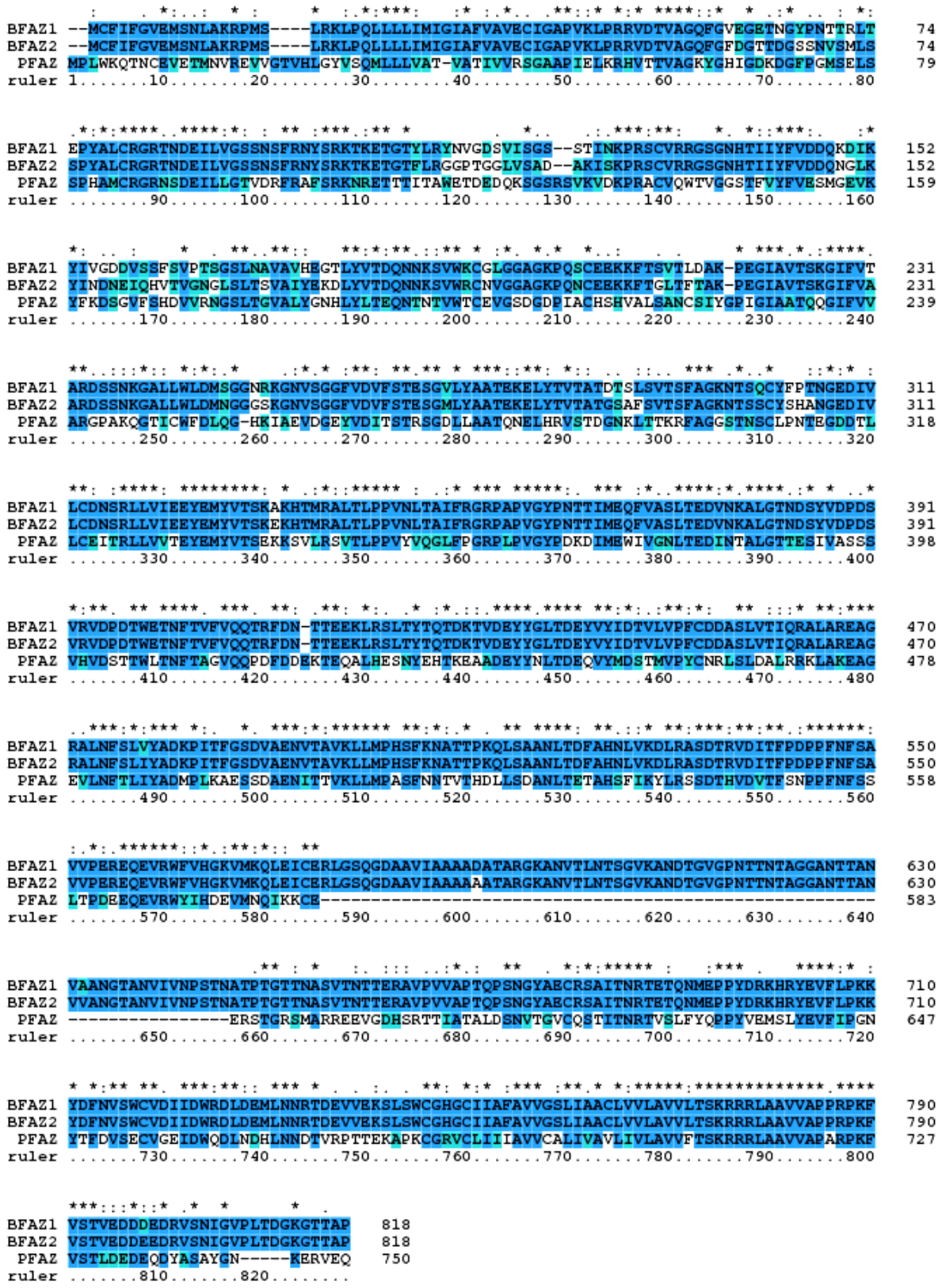

Figure 4.3. BFAZ1, BFAZ2 and PFAZ aligned using Clustal. BFAZ1 and BFAZ2 are 90% identical and 50% identical to PFAZ. BFAZ1 and BFAZ2 contain a 75 residue insert beginning at residue 575 that is not present in PFAZ. Dark blue represents identity, light blue functional similarity

at each end along the length of the cell from a point consistent with the flagellar exit point to the anterior tip of the cell body (Figure 4.4.). Immunofluorescence using the antibody L6B3 showed that the PFAZ signal colocalises with the FAZ. PFAZ fluorescence was present in both whole cell preparations and in cells after detergent extraction suggesting that the protein is strongly associated with the cytoskeletal structure.

4.1.5. Bioinformatic analysis of Tb927.8.940

Tb927.8.940 which I have called FCP1 (flagella connector protein 1) is a 2194 amino acid protein located on chromosome 8 with a calculated molecular weight of 237kDa and a predicted isoelectric point of pH5.37, which are consistent with the area of the gel from which the protein was identified. A single identification of FCP1 was made from this gel slice that encompassed five discreet spots with equivalent apparent molecular mass but small stepwise increments of iso-electric point (Figure 4.1.D). This pattern of spots resulting in a single identification is consistent with post-translational modification of the protein and is most likely due to the presence of a series of phosphorylation sites. The protein has two predicted transmembrane domains at residues 36-58 and 1819-1841 and a high probability of a signal anchor sequence at the N terminus (SignalP probability 0.96) (Figure 4.5). A second identical copy of the open reading frame (Tb927.8.960) is located approximately 5kb upstream. The FCP1 open reading frames are separated by an open reading frame for a hypothetical protein (Tb927.8.950) a further two copies of which flank the FCP1 loci on both sides (Figure 4.5.B). Alignment to the translated *T. brucei* genome using BLASTP revealed no additional copies of FCP1 and no other open reading frames with significant homology in the genome. BLASTP alignment to the translated genome databases for *T.* cruzi and *L. major* revealed a single copy homologue in the *T. cruzi* genome (TcCLB.503733.80) and four homologues in the *L. major* genome (LmjF.07.0820, LmjF.07.0830, LmjF.07.0840 and LmjF.34.0460) (Figure 4.5.A). The *T. cruzi* protein has similar features to FCP1 with two predicted transmembrane domains and a signal anchor predicted with

A.

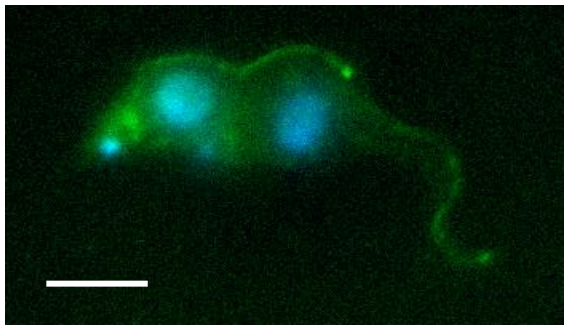

PFAZ::Ty

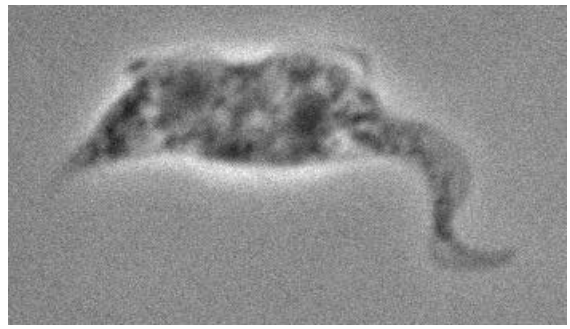

Phase contrast

B.

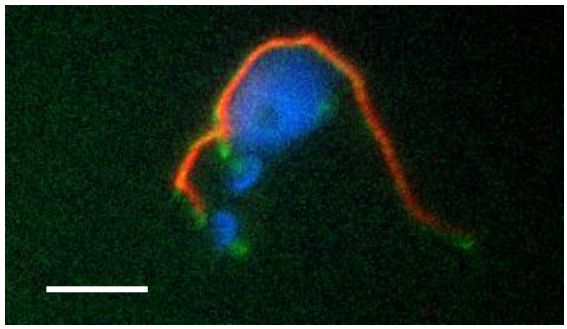

PFAZ::Ty, FAZ

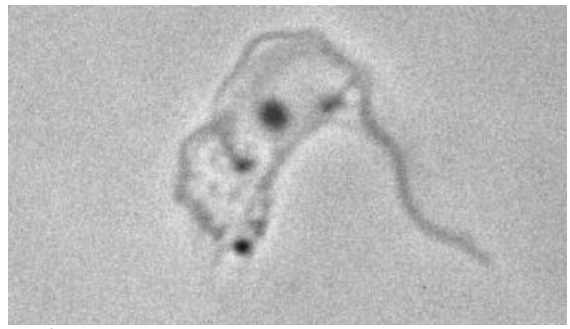

Phase contrast

Figure 4.4. PFAZ localises to the FAZ. C terminal Ty epitope tagged PFAZ (green) expressed from one of the endogenous loci localises to the FAZ in A) whole cell procyclic forms fixed in methanol and B) is still present after detergent extraction and methanol fixation. The signal forms an unbroken line along the FAZ with bright foci at each end. Red = FAZ (L6B3), blue = DAPI, bar = 5μm.

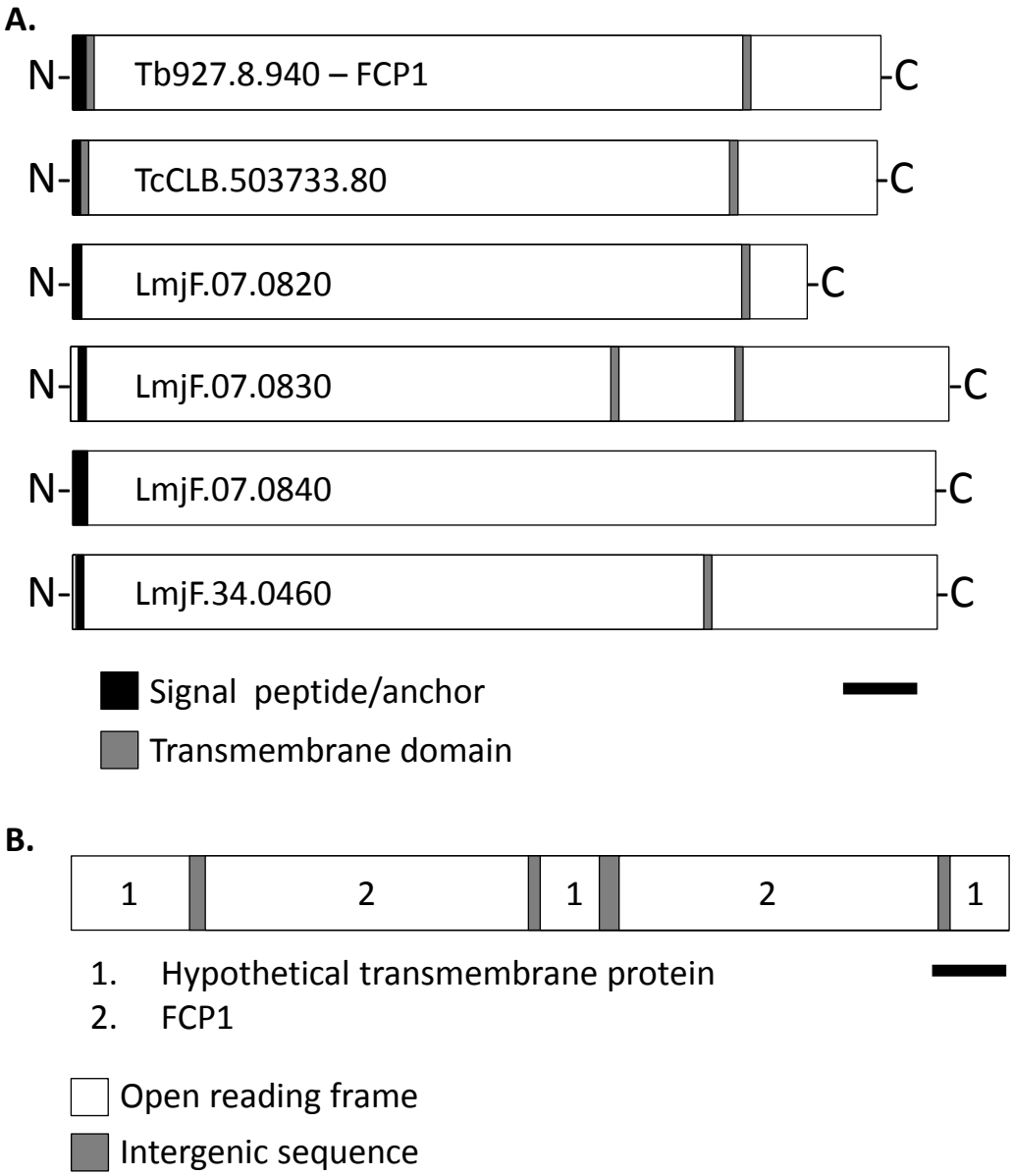

Figure 4.5. Cartoon of the protein domain structure of FCP1 and its orthologues in other kinetoplastids and the genomic context of FCP1. A) FCP1 has an N terminal signal anchor (black) with an associated transmembrane domain (grey) and a second transmembrane domain 375 residues from the C terminus. The *T. cruzi* orthologue has a similar domain architecture while the expanded family of orthologues in *L. major* have variable numbers of transmembrane domains and are predicted to contain N terminal signal peptides rather than signal anchors. Bar = 200 residues. B) Two identical copies of FCP1 are arrayed with three identical copies of a hypothetical protein of unknown function. White = open reading frame plus 5' UTR, grey = intergenic sequence, bar = 2 kbp.

high probability (SignalP probability 0.952). One of the *L. major* homologues is present on chromosome 34 whilst the remaining three are in adjacent loci on chromosome 7 in a region syntenic with the FCP1 locus in *T. brucei*. LmjF.07.0820 and LmjF.34.0460 have two predicted transmembrane domains and signal peptides (unlike the signal anchor on FCP1) predicted with high probability (SignalP probability 0.936 and 0.998). There is a likely miscalled start codon for LmjF.34.0460 in the genome database as using an alternative upstream in-frame start codon includes the sequence that contains the N terminal transmembrane domain and signal peptide. LmjF.07.0830 has three predicted transmembrane domains and again a predicted signal peptide (SignalP probability 0.984). Finally, LmjF.07.0840 is not predicted to contain transmembrane domains but does have a highly probable signal peptide motif (SignalP probability 0.995). Alignment of FCP1 to the non-redundant database of protein sequences at http://www.ncbi.nlm.nih.gov/ identified no further homologues outside the kinetoplastid lineage.

4.1.6. FCP1 is the first component of the flagella connector to be identified

I next generated a procyclic form cell line expressing FCP1 with a C terminal YFP::Ty tag from one of the endogenous loci. The choice of a C terminal tag was made to circumvent any possible effects associated with interfering with the predicted signal anchor at the N terminus. Analysis of native fluorescence by fluorescence microscopy showed that FCP1 colocalised with the tip of the new flagellum but never the old flagellum, a localisation consistent with the position of the flagella connector (Figure 4.6.). FCP1 signal could be detected from the earliest point of new flagellum formation and remained associated with the tip of the new flagellum for the remainder of the cell cycle. 70% of 1K1N cells were negative for FCP1 compared to 0% of 2K1N and 2K2N cells (Figure 4.7.B). This is consistent with a model whereby FCP1 incorporation occurs at or shortly after the beginning of new flagellum formation and that the protein is removed following cytokinesis which reflects the known behaviour of the flagella connector.

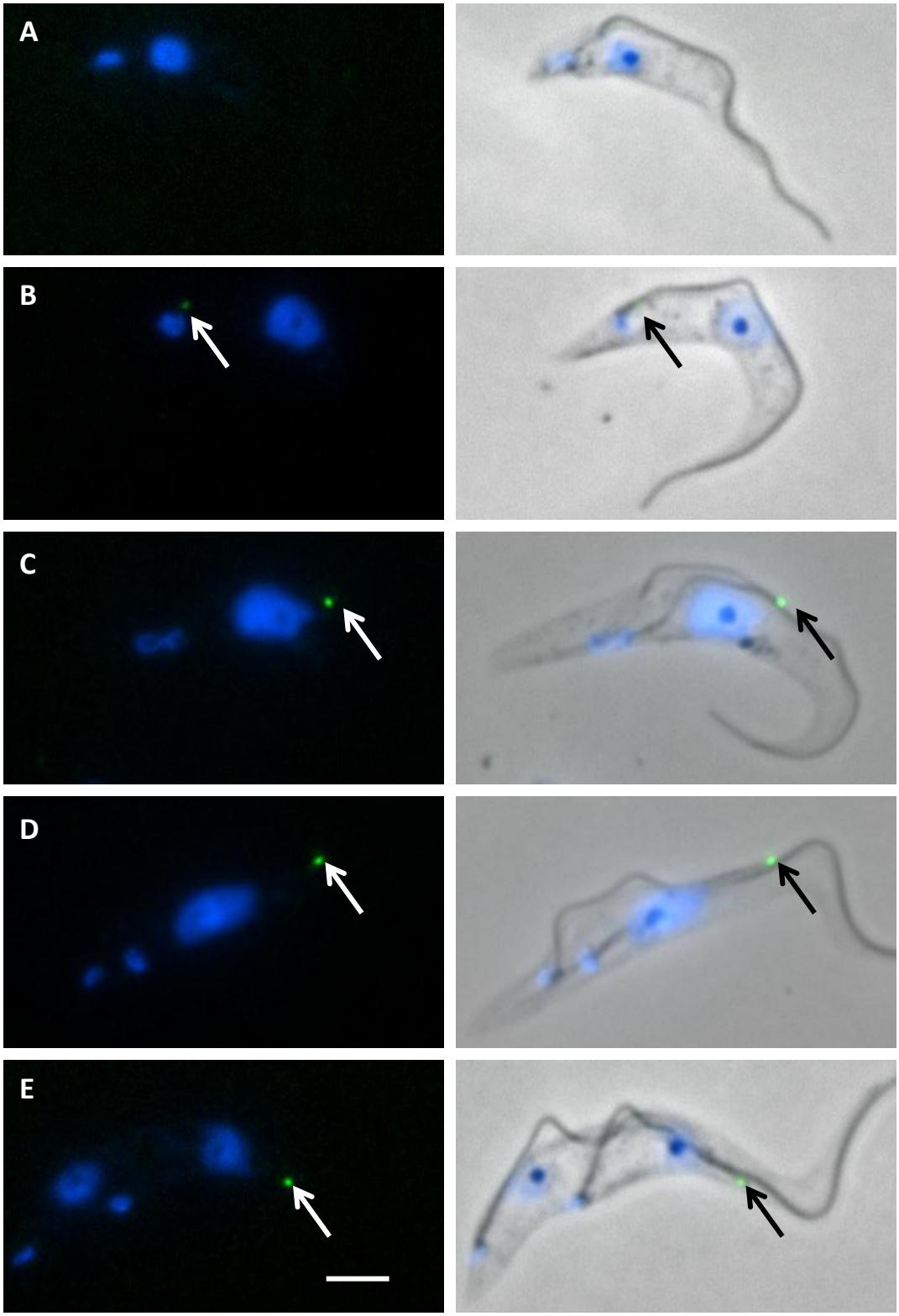

Figure 4.6. FCP1 localises to the tip of the new flagellum in procyclic forms. Cells were extracted with detergent and fixed in methanol. C terminal YFP tagged FCP1 expressed from one of the endogenous loci is not observed in A) cells with a single flagellum but is present B) once the new flagellum starts to form and remains associated with the tip of the new flagellum in C) late 1K1N cells, D) 2K1N cells and E) 2K2N cells. Green = FCP1::YFP, blue = DAPI, bar = 5mm.

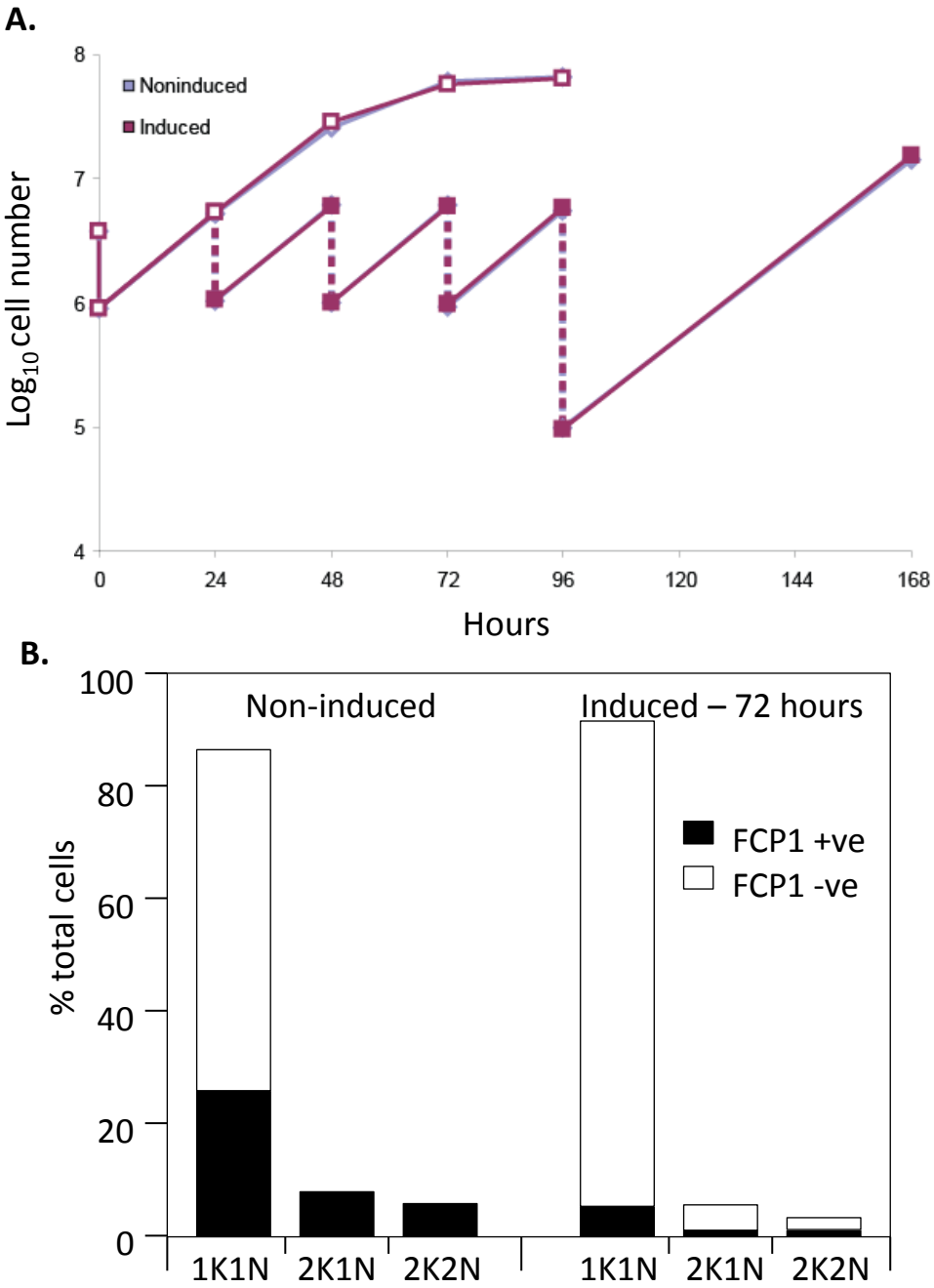

Figure 4.7. RNAi mediated ablation of FCP1 has no effect on the growth or nucleus/kinetoplast number of procyclic forms. A) Population growth was measured for cells expressing YFP tagged FCP1 from one of the endogenous loci and with inducible RNAi against FCP1 mRNA in the presence or absence of doxycycline. Cells were counted every 24 hours in continuous and diluted cultures and no growth defect was observed. B) The cell populations grown with dilution were sampled at 72 hours post induction and nucleus/kinetoplast number per cell was counted and cells scored for the presence or absence of FCP1::YFP. In non-induced cells around 80% of 1K1N cells were YFP negative (white) whilst 100% of 2K1N and 2K2N cells were YFP positive. In the induced sample there was no significant difference in the number of cells in each category although the reduction in the number of YFP positive cells demonstrated that the RNAi was effective in the majority of the population.

4.1.7. RNAi ablation of FCP1

I generated a procyclic form cell line with inducible RNAi against FCP1 in a background of YFP::Ty tagged FCP1 expressed from one of the endogenous loci. Induction of RNAi over 168 hours resulted in no reduction of population growth rate (Figure 4.7.A) and no accumulation of aberrant cells as assessed by KN count and visual inspection (Figure 4.7.B) although analysis of cells by fluorescence microscopy showed that ablation of FCP1 was successful in the majority of cells. This result was somewhat surprising given the postulated importance of the flagella connector in cell patterning and organelle segregation but immunofluorescence analysis of induced cells using the AB1 antibody, which recognises a currently unknown component of the flagella connector, showed that at least some components of the connector are still assembled (Figure 4.8.). This lack of gross RNAi phenotype is also supported by evidence from the genome-wide RNAi screen (discussed above) which reported normal growth in procyclic cells following ablation of FCP1. However, this study did report abnormal growth in bloodstream form cells following ablation of FCP1, an intriguing result given that bloodstream forms do not possess a recognisable flagella connector, particularly when taken together with the presence of FCP1 homologues in *Leishmania sp.* and *T. cruzi* for which the existence of a flagellar connector has also not been reported.

4.2. Comparison of bloodstream form and procyclic form cytoskeletons

4.2.1. Candidate cytoskeletal proteins identified using comparative proteomics

It has previously been shown that the cytoskeleton contains several sets of paralogous proteins that show complementary life-cycle stage-specific expression (Vedrenne, Giroud et al. 2002; Olego-Fernandez, Vaughan et al. 2009). The reasons for these differences so far remain unclear as the available evidence suggests that in all cases the paralogous proteins perform equivalent functions in their respective life-cycle stages. It is also currently unclear to what extent the composition of the cytoskeleton is life-cycle stage specific. It could be that the majority of cytoskeletal components are shared in common between the two life cycle stages and that only a small number of proteins have

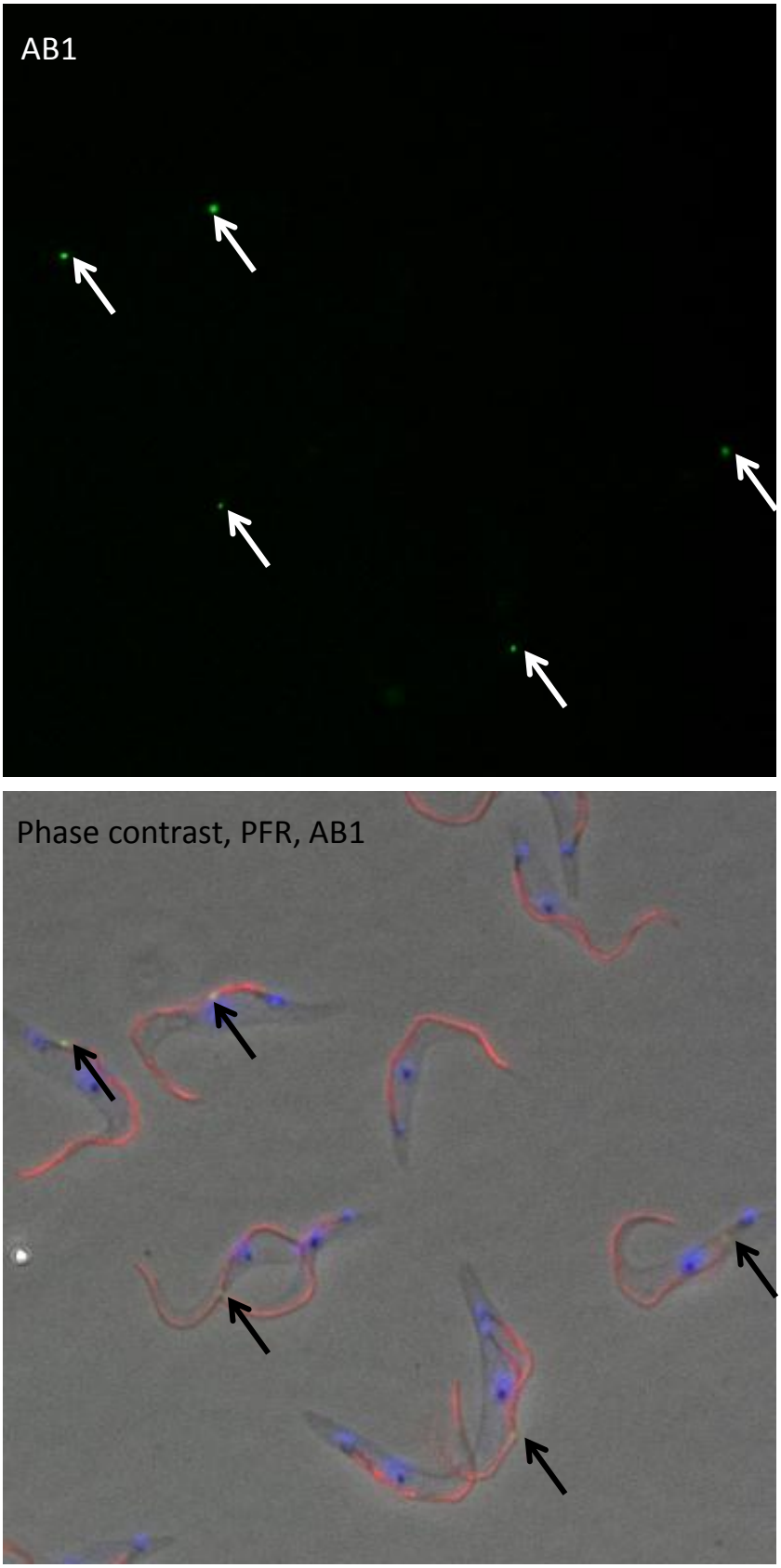

Figure 4.8. 72 hours after induction of RNAi against FCP1, the connector component recognised by AB1 (green) is still present at the tip of new flagella in detergent extracted cells fixed in methanol. Red = PFR (L8C4), blue = DAPI.

been required to adapt to the specific intra-and extracellular environments of the two forms. Another possibility would be that only a small conserved core of cytoskeletal components are shared by the two forms and that the majority of components are specific to a given life-cycle stage, perhaps resulting in the generation of paralogous stage-specific sets of proteins needed to perform common functions in different molecular environments. In either case the generation of paralogous sets is likely to be a result of the lack of alternative splicing and transcriptional regulation in the *T. brucei* genome meaning that alternative transcripts must be encoded as discreet genes.

In order to identify paralogous sets of cytoskeletal proteins with life-cycle stage-specific expression I used DIGE to compare the protein composition of detergent extracted bloodstream form cells to that of detergent extracted procyclic form cells (Figure 4.9.). The resulting gels were scanned and spots showing differential abundance between the two samples were detected by overlaying the gel images. A total of 36 spots showing a difference in spot volume between the two samples were cut from the gel for mass spectrometric analysis (Table 4.2.). This yielded 71 identifications with a confidence interval greater than 99% and two unique peptides which formed a non-redundant candidate set of 49 proteins. As before a set of known proteins were present in the dataset that likely represent contaminants of the preparation and another set of proteins that are likely to be contaminants of the picked spot. Both CAP5.5 and CAP5.5V were identified in this way and showed greater abundance in samples from the appropriate life-cycle stage. A total of 18 proteins were identified that were annotated as hypothetical.

I entered my set of hypothetical proteins as a query at TritrypDB to determine the orthologue group assigned to each protein. In this way I identified two pairs of proteins that were assigned to the same orthologue groups; Tb927.4.4130 and Tb927.8.8200, and Tb927.7.2640 and Tb927.7.2650. The mass spectrometric identifications for the two proteins in the first group both came from the same spot and the proteins themselves are 94% identical making it difficult to determine if one or both

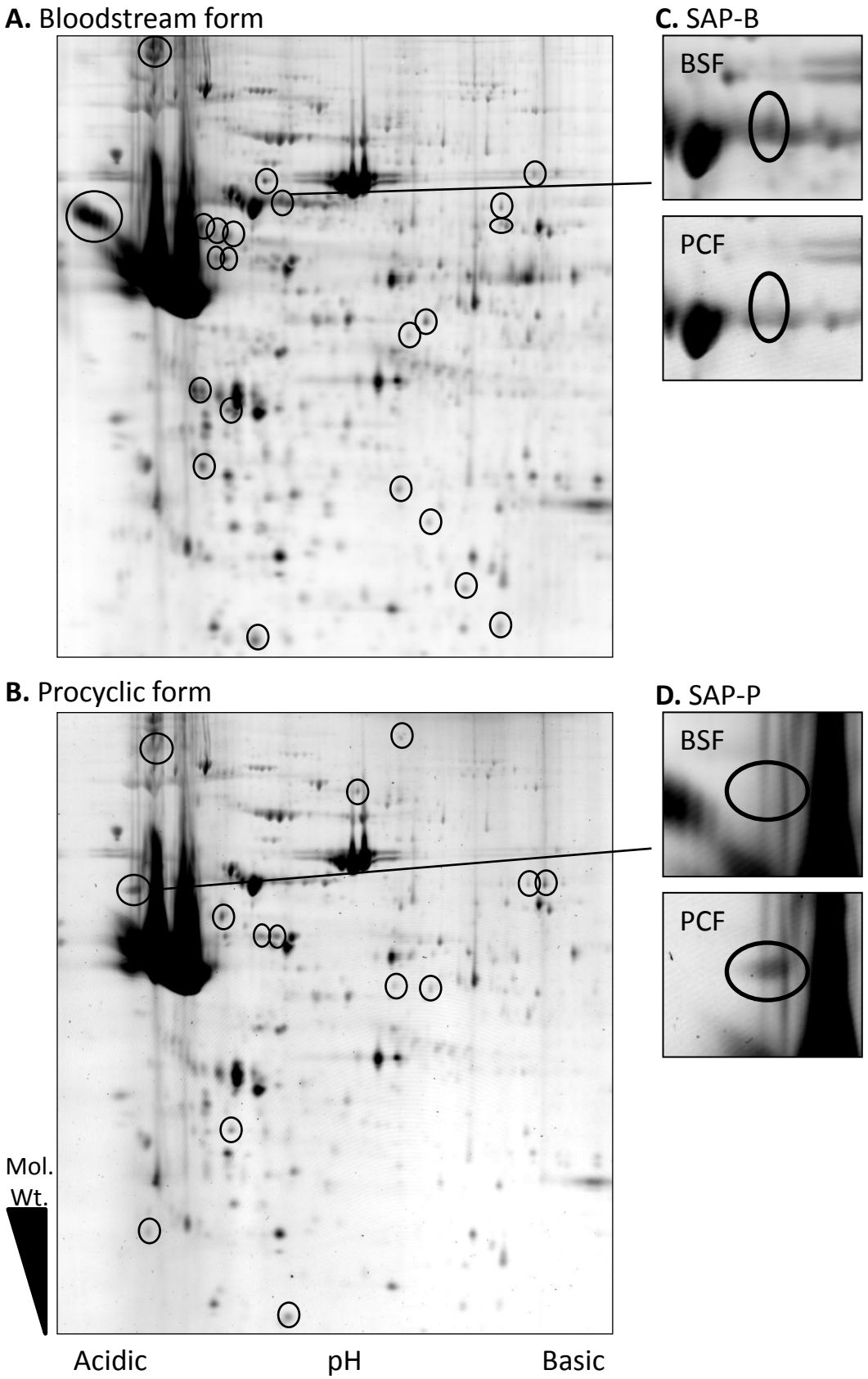

Figure 4.9. 2D-DIGE comparison of detergent extracted A) Bloodstream forms and B) Procyclic forms. Spots that showed a twofold or greater change between the samples are circled. C) and D) show close up views of the gel regions corresponding to SAP-B and SAP-P respectively.

proteins were present on the gel or whether one or both contributed to the difference in spot volume observed. I did not pursue these candidates further although it is interesting to note that the formation of this paralogous set occurred in the same duplication event that gave rise to CAP5.5 and CAP5.5V. The other pair of candidate proteins did show the pattern I was looking for. The spot corresponding to Tb927.7.2640 showed a 4.1-fold greater volume in the procyclic form sample while the spot corresponding to Tb927.7.2650 showed a 3.6-fold greater volume in the bloodstream form sample. These proteins are encoded by open reading frames that are adjacent to one another on chromosome 7 and that are related but not identical. I named these proteins SAP-P and SAP-B respectively (Subpellicular Associated Protein - Procyclic/Bloodstream).

4.2.2. Bioinformatic analysis of SAP proteins

A two-way alignment of the SAP protein sequences showed that they were orthologous with four distinct regions identifiable based on the level of identity (Figure 4.10.A). Beginning at the N terminus, domain 1 consists of 34 residues with 95% identity and is followed by domain 2, a region of very low similarity, around 120 residues long in SAP-P and 195 residues long in SAP-B. Domain 2 includes a complex lysine rich repetitive element in SAP-B that is not found at all in SAP-P. Domain 3 is a 160 residue region with 90% identity and the 150 residue domain 4 extends to the C terminal with 57% identity between the two proteins. The proteins contain no known functional domains but are predicted to form similar patterns of coiled-coils in domains 3 and 4 (Figure 4.10.B). The 5' UTRs of the SAP genes are identical for around 200bp upstream of the open reading frames but no significant similarity could be found between the 3'UTRs. Alignment to the NCBI non-redundant protein database by BLASTP showed that homologues to these proteins are restricted to kinetoplastids, with both *L. major* (LmjF.22.0730) and *T. cruzi* (Tc00.1047053506859.170) genomes encoding a single SAP homologue (Figure 4.10.C).

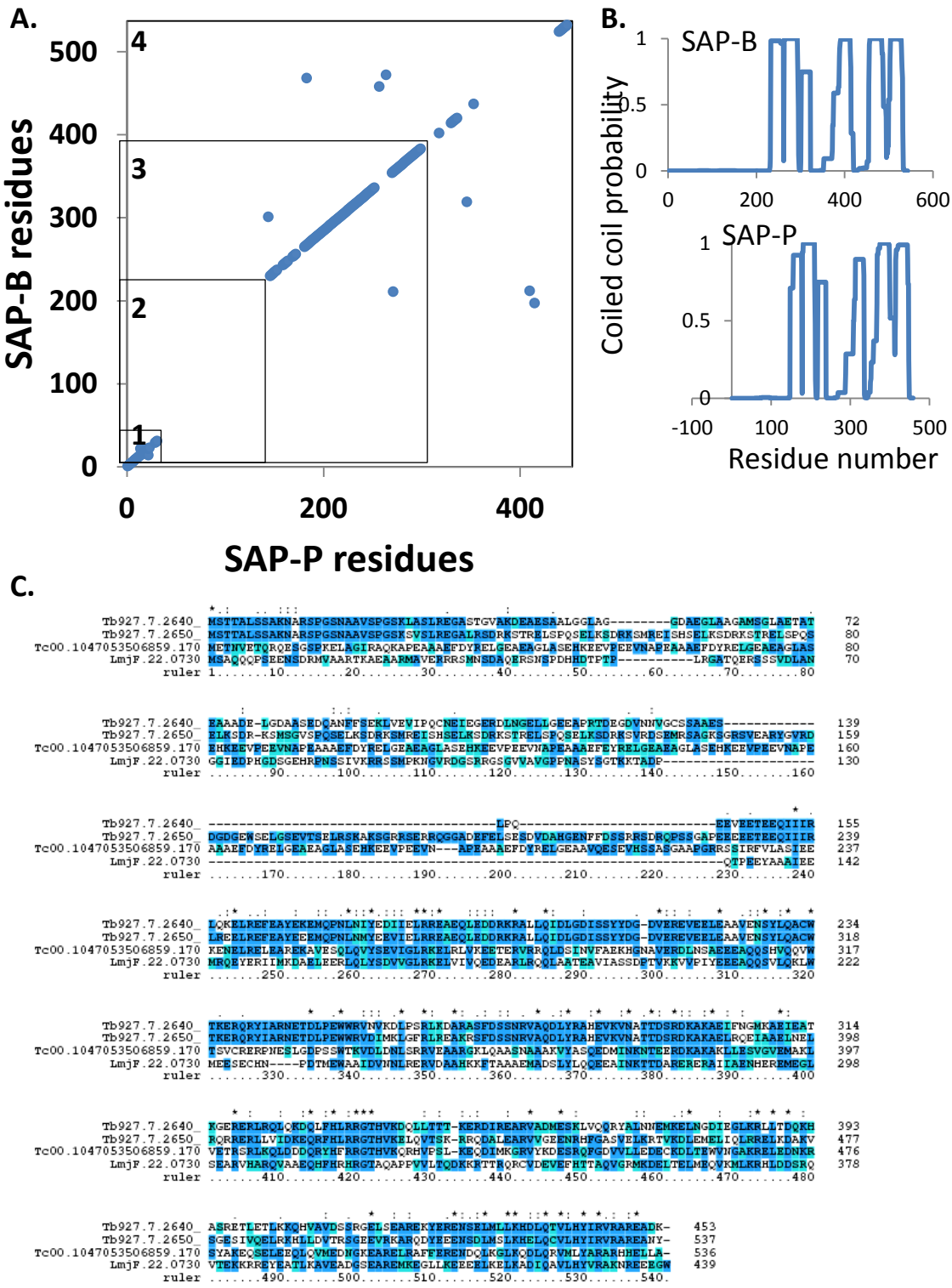

Figure 4.10. SAP-P and SAP-B are paralogous proteins. A) Dotplot alignment of SAP-P (x) and SAP-B (y) protein sequences using a 5 residue window. Domains 1-4 are shown and are defined by the level of similarity between the two proteins. Domain 2 of SAP-B contains a 75 residue lysine rich insert that is not present in SAP-P. B) Coils prediction for the two proteins shows similar patterns of predicted coiled-coils in domains 3 and 4 of both proteins C) Clustal alignment of SAP-P, SAP-B and the single orthologues detected in *T. cruzi* and *L. major.*

4.2.3. Localisation of SAP proteins

To determine the localisation and expression patterns of the SAP proteins I introduced a C terminal YFP::Ty tag into one of the endogenous alleles for both proteins individually in both bloodstream and procyclic form cells in such a way as to preserve the endogenous 3' UTRs of the genes. Specific N terminal tagging of the endogenous alleles using this method was not possible due to the high conservation of sequence between the 5' end of the genes and between the last 200bp of the 5' UTRs. Western blot analysis of whole cell extracts from each of these cell lines using BB2 confirmed that SAP-P is expressed in procyclic forms but is not expressed above the level of detection in bloodstream forms and that SAP-B is expressed in bloodstream forms but is not detected in procyclic forms (Figure 4.11.A). Analysis of native YFP in whole cells and detergent extracted cells by fluorescence microscopy with co-staining for WCB showed that both proteins localise to the subpellicular corset in their respective life cycle stages (Figure 4.11.B). The YFP signal in both lifecycle stages decorated the subpellicular corset evenly throughout the cell cycle with the exception of the extreme posterior end of procyclic form cells where no signal is detected (Figure 4.11.C). No SAP::YFP was detected in the flagellum in either life cycle stage.

4.2.4. Analysis of SAP protein function

To investigate the functions of the SAP proteins I generated cell lines in both bloodstream and procyclic form cells with inducible RNAi against each SAP message individually. To ensure specific knockdown of the target protein only, RNAi was targeted against the region of low similarity towards the N terminus for each coding sequence. RNAi was induced by the addition of doxycycline to the culture medium and population growth was measured for induced and non-induced cell lines for each SAP in both life-cycle stages over a period of 96 hours. RNAi against both SAPs resulted in a dramatic decrease in population growth rate compared to noninduced cells in their respective life cycle stages (Figure 4.12.). This decrease was readily detectable 24 hours after induction of SAP-B RNAi in bloodstream forms and by 48 hours after induction of SAP-P RNAi in procyclic forms. RNAi

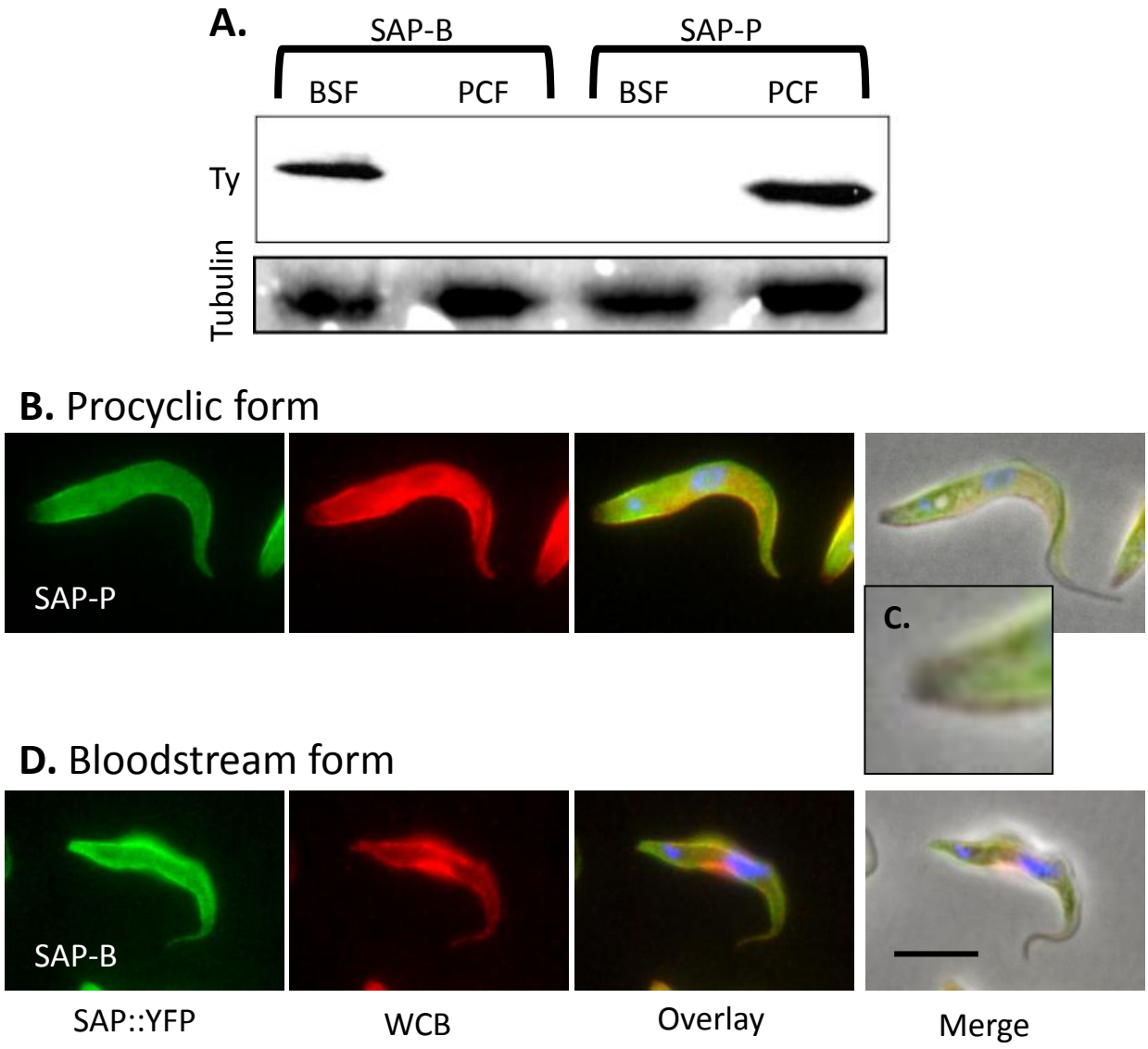

Figure 4.11. Expression profile and localisation of SAP-P and SAP-B. A) Western blot of detergent extracted bloodstream (BSF) and procyclic (PCF) form cells expressing C terminal YFP::Ty tagged SAP-B or SAP-P from one of the endogenous loci. SAP-B is expressed only in the bloodstream form and SAP-P only in the procyclic form. A ponceau stain of the membrane showing the tubulin region is included as an indication of relative loading. B) Procyclic form cells expressing SAP-P::YFP::Ty from one of the endogenous loci. Cells were fixed in paraformaldehyde and permeabilised using methanol. SAP-P localises to the whole of the subpellicular corset apart from the extreme posterior end of the cell (C) and is not present on the flagellum. D) Bloodstream form cells expressing SAP-B::YFP::Ty from one of the endogenous loci prepared as above. SAP-B localises to the subpellicular corset with no signal detected on the flagellum. Red = whole cell body (WCB), blue = DAPI, bar = 5μm.

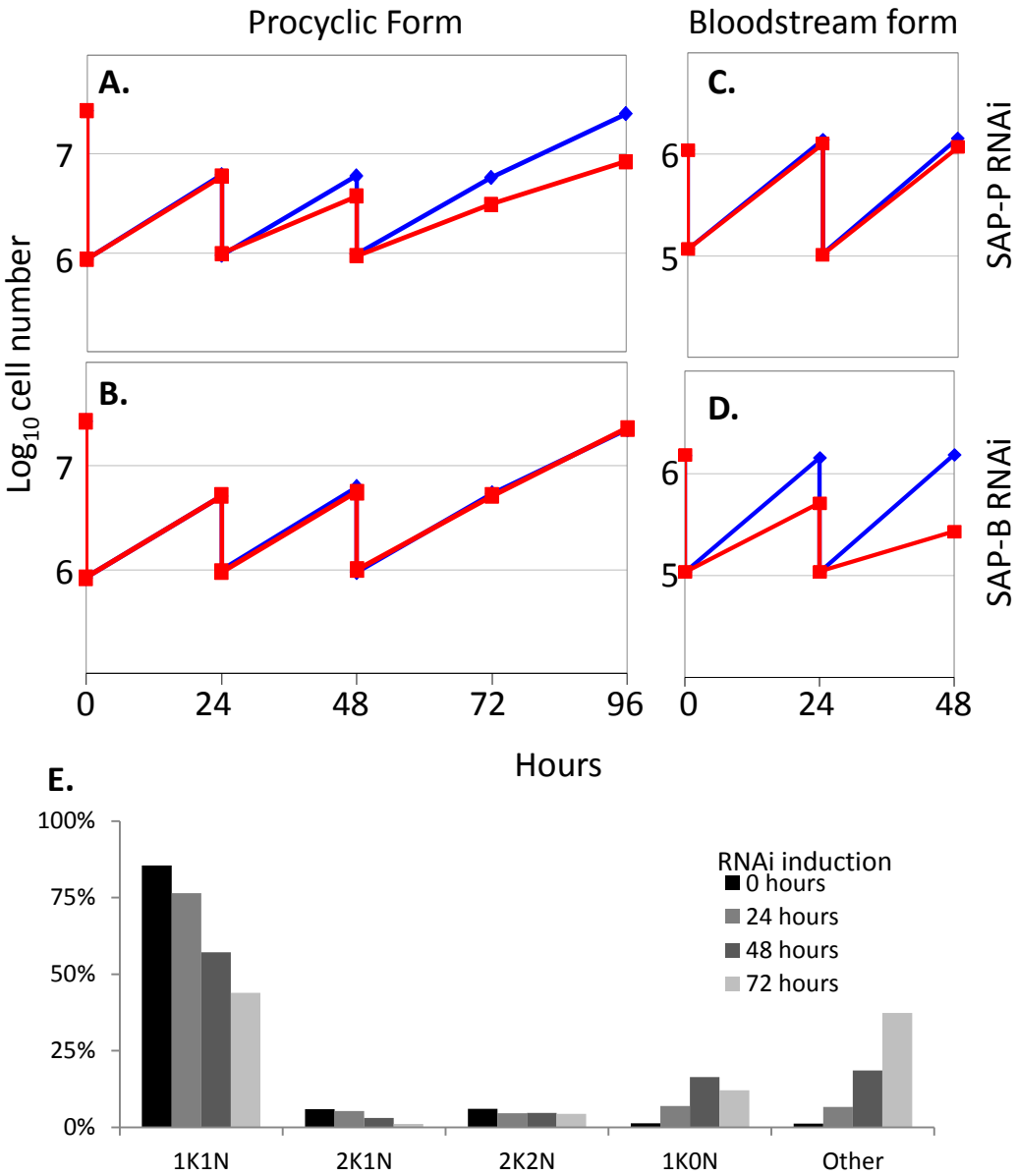

Figure 4.12. RNAi mediated ablation of SAP-P and SAP-B cause defects in growth in their respective life-cycle stages. RNAi against SAP-P results in a decreased growth rate in A) procyclic but not B) bloodstream forms. Ablation of SAP-B has no effect on the growth of C) procyclic forms but causes a decrease in growth rate in D) bloodstream forms. E) ablation of SAP-P in procyclic forms results in an accumulation of cells with aberrant nucleus/kinetoplast numbers including the production of 1K0N zoids.

against SAP-B in the procyclic form or SAP-P in the bloodstream form had no effect on population growth rates. Addition of a YFP::Ty C terminal tag at one of the endogenous alleles of SAP-P in the procyclic form SAP-P RNAi cell line followed by fluorescence microscopy based analysis of the morphology of RNAi induced cells showed that by 48 hours post-induction SAP-P protein was lost preferentially from the posterior end of the cell (Figure 4.13.). Loss of SAP protein did not affect the distribution of the cytoskeletal markers CAP5.5 in procyclic form or WCB in either life cycle stage (Figure 4.13.A&B). SAP-P ablation in procyclic forms resulted in cells exhibiting distorted morphology such that the diameter of the cell at the midpoint was abnormally large by 48 hours after induction (Figure 4.13.A&B). Cells with abnormal nuclear and kinetoplast DNA content including monstrous multinucleate cells and anucleate zoids began to accumulate by 72 hours after RNAi induction (Figure 4.13.C). In bloodstream forms, multinucleate cells (Figure 4.13.F) and cells undergoing aberrant cytokinesis (Figure 4.13. D&E) were evident by 24 hours after induction of SAP-B RNAi and cytoplasts with no detectable DNA content appeared (Figure 4.13. E - *). It is likely that the aberrant cytokinesis events apparent in the cells shown in Figure 4.13. D&E lead to the production of cytoplasts such as that shown in Figure 4.13. E. Examination of bloodstream form cells 24 hours after induction of RNAi against SAP-B and procyclic form cells 48 hours after induction of RNAi against SAP-P by thin section electron microscopy showed that the tight organisation of the subpellicular array of microtubules is lost as a result of RNAi in both life cycle stages (Figure 4.14.). In wild-type cells the subpellicular microtubules form a regularly spaced single layer array closely apposed to the plasma membrane. In induced bloodstream form cells 83% of cross sections that contained a nucleus and in which clear cross-sections of individual microtubules could be seen (n = 72) showed microtubules that were associated with the array but were not intercalated correctly into the microtubule sheet, although inter-microtubule spacing appeared to be preserved (Figure 4.14.A). These perturbations in the microtubule array occurred in short runs and other areas of the array in the same cross-section often appeared normal. In 93% of cross sections whose width and possession of an associated flagellar profile suggested an anterior position in the cell (and again in which clear microtubule cross sections

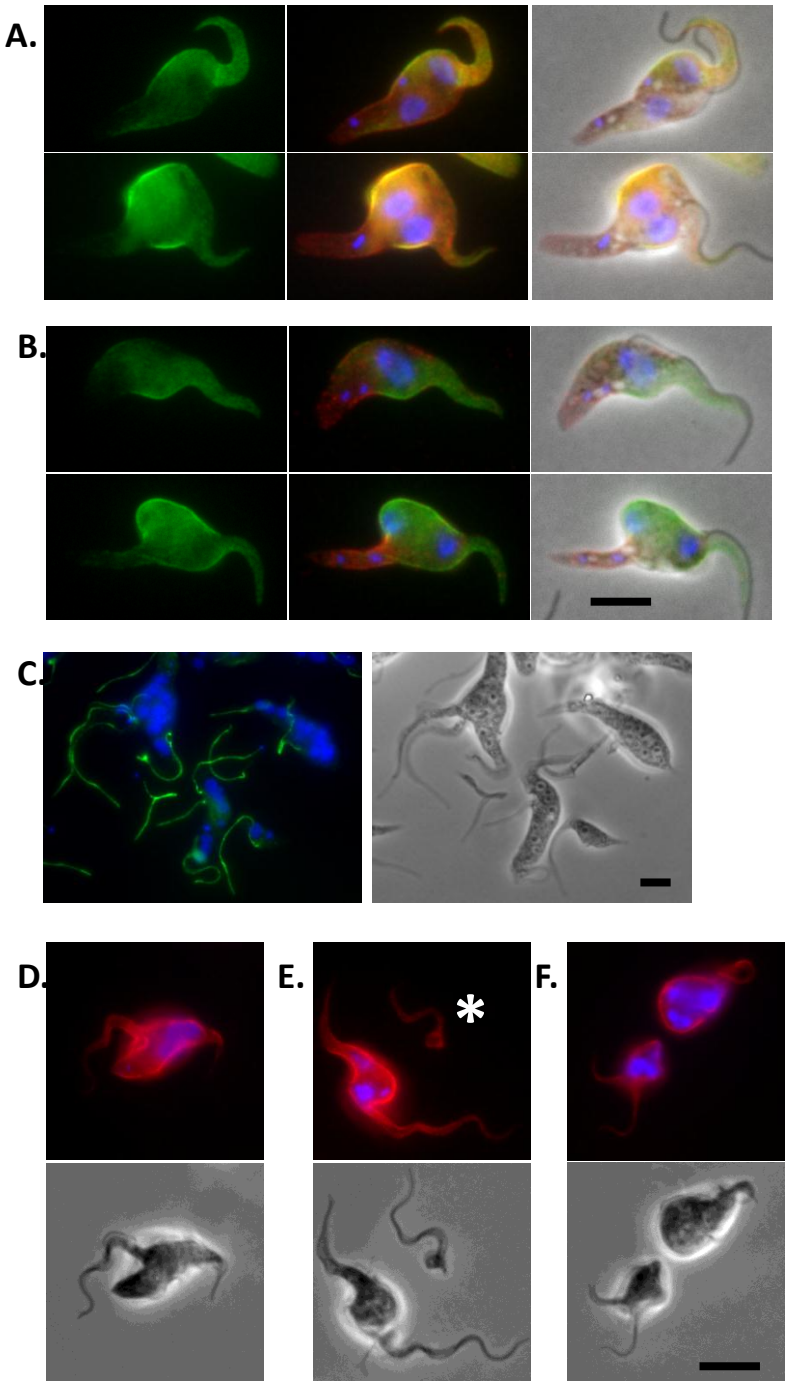

Figure 4.13. RNAi against SAP-P results in SAP-P::YFP::Ty being lost preferentially from the posterior end of the cell. A & B) SAP-P::YFP::Ty (green) fluorescence is still visible at the anterior end of the cell 24 hours after RNAi induction but is lost from the posterior. The posterior of the cell is still positive for other markers of the subpellicular corset WCB (A - red) and CAP5.5 (B - red). C) 72 hours after induction of RNAi, multinucleate cells with multiple kinetoplasts and flagella and 1K0N zoids can readily be observed, green = PFR (L8C4). D-E) a similar situation occurs in the bloodstream form 24 hours after the induction of RNAi against SAP-B. Cells undergoing aberrant cytokinesis (D & E) and multi-nucleate cells (F) are observed. Cytoplasts that contain no nuclear or kinetoplast DNA (E - *) can also be seen and may be the result of aberrant cytokinesis events such as those shown in D & E, red = WCB. Cells were fixed in paraformaldehyde and permeabilised with methanol. Blue = DAPI, bar = 5μm.

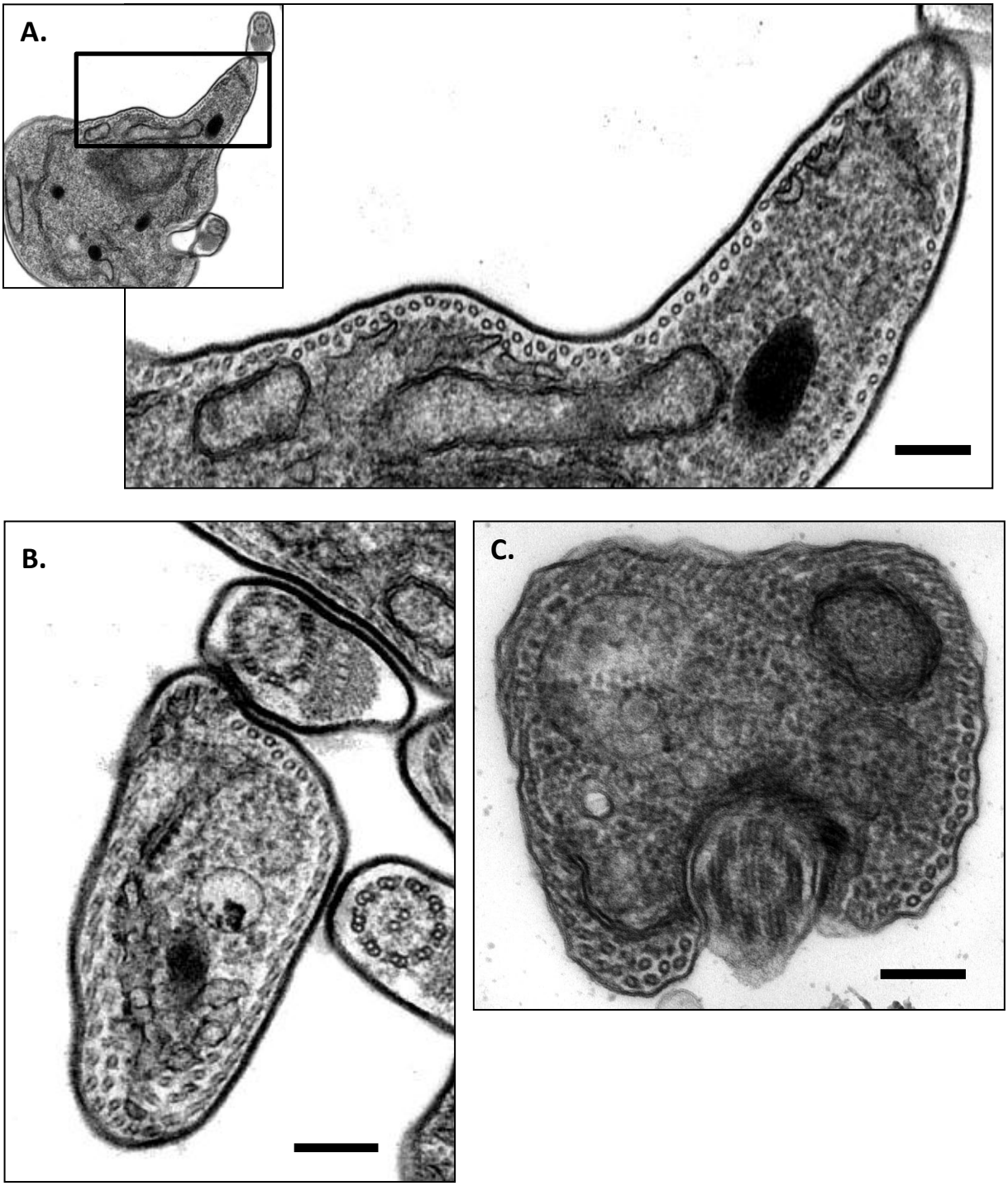

Figure 4.14. Ablation of SAP proteins disrupts the organisation of the microtubule corset. A & B) bloodstream forms. Thin section TEM of transverse sections through A) the anterior of a cell and B) the mid part of a cell 24 hours after induction of RNAi against SAP-B. A) a double layer of microtubules can be seen underlying the plasma membrane. B) Numerous microtubules can be seen that are not correctly incorporated into the array. C) similar disruptions can also be seen in procyclic form sections 48 hours after induction of RNAi against SAP-P. Cells were chemically fixed as described in Materials and Methods. Bar = 200nm.

could be seen, n=56), the microtubule disorganisation was more pronounced with layered sheets of microtubules apparent (Figure 4.14.B). Disorganisation of the microtubule array was observed rarely in cross sections without an associated flagellar profile (12%, n=76) which presumably correspond to positions on the cell posterior to the flagellar pocket. In procyclic form sections, similar disorganisations of the microtubular array were observed (Figure 4.14.C) although at a lower frequency than in bloodstream forms – anterior 33% (n=75), midsection 27% (n=85) and posterior 3% (n=59). Membrane blebbing of the type previously reported as a consequence of ablation of WCB was not observed (Baines and Gull 2008).

4.2.5. SAP functions are complementary

Although I have shown that the SAP proteins perform an important role in the organisation of the microtubule array, the phenotypes associated with RNAi ablation of these proteins were similar in the two life-cycle stages which suggests that the two proteins have similar functions. This raises the question of why the cell needs two versions of this protein. One possibility is that there are other life-cycle specific elements in the subpellicular array that necessitate alternative SAPs for localisation to or function within the cytoskeleton. In order to address this I ectopically expressed Ty::GFP::SAP-B in procyclic forms and Ty::GFP::SAP-P in bloodstream forms from an inducible promoter. I found that in both cases cells grew normally after induction and the ectopic protein still localised to the subpellicular array (Figure 4.15.). The brighter edge effect indicative of localisation to the subpellicular corset was clearly visible in procyclic forms expressing GFP::SAP-B (Figure 4.15.A) although this was obscured to some extent in bloodstream forms expressing GFP::SAP-P due to the presence of the protein in the cytoplasm as evidenced by the areas with less GFP fluorescence that correspond to the position of the nucleus (Figure 4.15.B). Detergent extraction of bloodstream form cells removed the cytoplasmic pool of GFP::SAP-P and showed a clear localisation to the subpellicular array (Figure 4.15. C). Having determined that the ability of SAPs to associate with the subpellicular array is independent of life-cycle stage, I next asked whether the same is true for SAP function. Using a parental cell line with inducible RNAi against SAP-P I generated a cell line in which ectopic

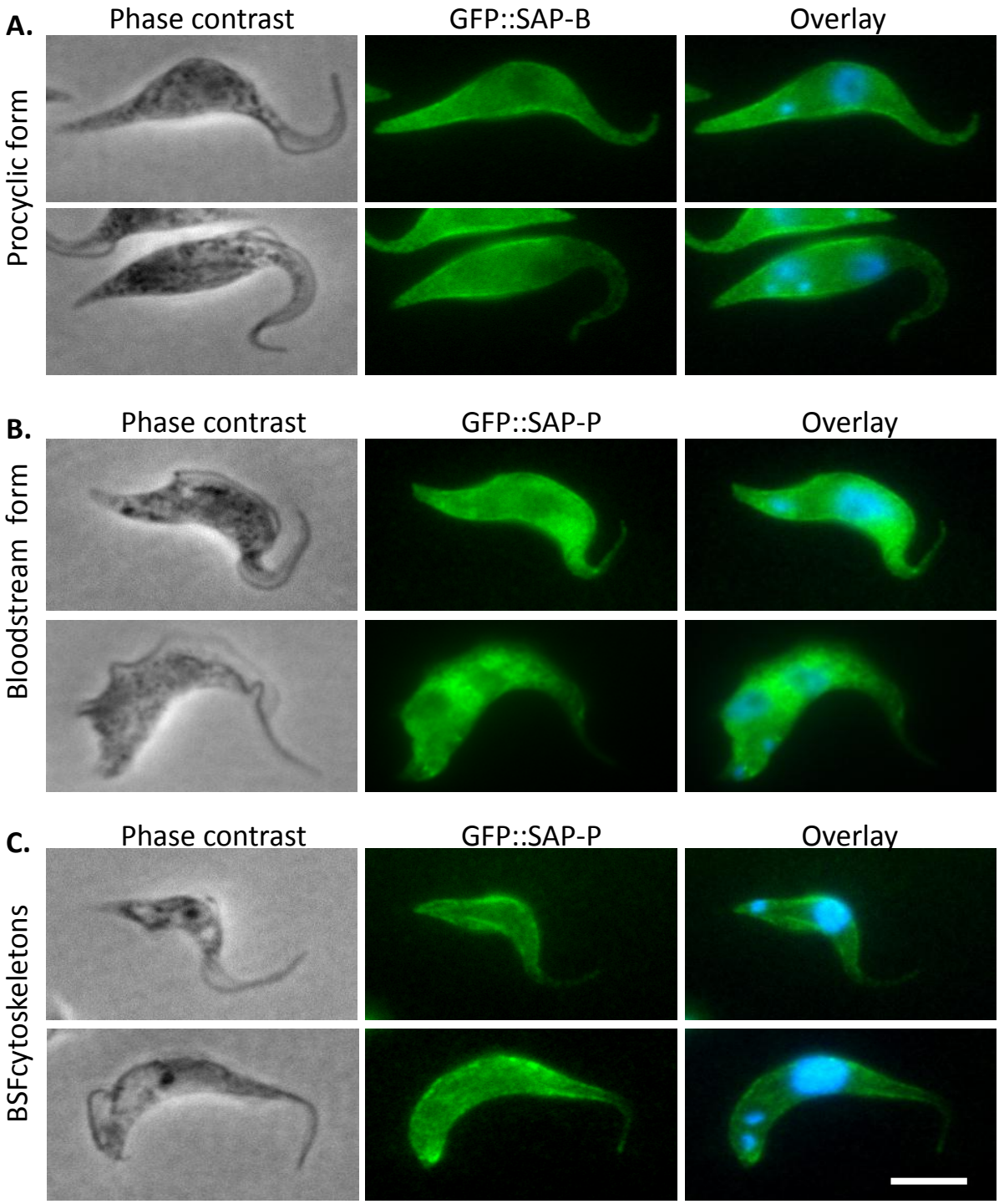

Figure 4.15. Localisation of SAP proteins to the subpellicular microtubule array is not life-cycle stage dependant. A) GFP::SAP-B (green) expressed from an inducible ectopic locus for 24 hours localises to the subpellicular array of procyclic form cells. B) GFP::SAP-P (green) expressed from an inducible ectopic locus for 24 hours localises to the subpellicular array of bloodstream form cells and C) is resistant to detergent extraction. Expression of the ectopic protein does not disrupt positioning of the nuclei and kinetoplasts of 2K2N cells in either life-cycle stage. Cells were fixed in methanol (A & B) or (C) extracted with detergent and fixed in methanol. Blue = DAPI, bar = 5μm.

expression of Ty::GFP::SAP-B and RNAi against SAP-P could be induced simultaneously by the addition of doxycycline to the culture medium. At the same time I also generated bloodstream form cells for the reciprocal experiment in a parental line with inducible RNAi against SAP-B. In both cases expression of the ectopic protein completely rescued the growth rate/cell division defect experienced by the parental cell lines after ablation of the endogenous protein (Figure 4.16.A&B). Examination of the cells by fluorescence microscopy showed that as before the ectopic protein localised to the subpellicular microtubule array and that no defects in the positioning of nuclei or kinetoplasts could be detected (Figure 4.16.C&D). In a second set of experiments simultaneous induction of RNAi against the endogenous protein and inducible ectopic expression of the RNAi target protein failed to rescue the phenotype in either life-cycle stage (Figure 4.16.E&F).

4.2.6. SAPs during differentiation

To determine the behaviour of SAP proteins during differentiation I incubated the monomorphic bloodstream form cell lines with tagged SAP-P and SAP-B at 28^{O}C in the presence of 6mM cis-aconitate, a treatment that has been shown to induce differentiation to procyclic forms in culture conditions. I examined the cells using fluorescence microscopy at 0, 24 and 48 hours after induction (Figure 4.17 A&B). In SAP-P::YFP expressing cells at 0 hours no fluorescence above background was detected but after 24 hours bright fluorescence was visible at the posterior end of the cell that gradually lessened towards the anterior (Figure 4.17.A), an almost direct reversal of the situation seen at early timepoints after RNAi against SAP-P in procyclic forms. By 48 hours after induction the pattern was similar: SAP-P::YFP fluorescence was still brighter towards the posterior of the cell but the overall intensity and spread of tagged protein across the subpellicular array had increased. At 0 hours, SAP-B::YFP expressing cells showed uniform fluorescence across the microtubule corset as described above which persisted through 24 and 48 hours but at a steadily decreasing intensity. (Figure 4.17.B). Samples of the cell line expressing tagged SAP-B were removed at 0, 24 and 48 hours after induction of differentiation and analysed by Western blot using BB2 (Figure 4.17.C). Tagged SAP-B was present as a single band of the correct apparent molecular weight at 0 hours but by 24

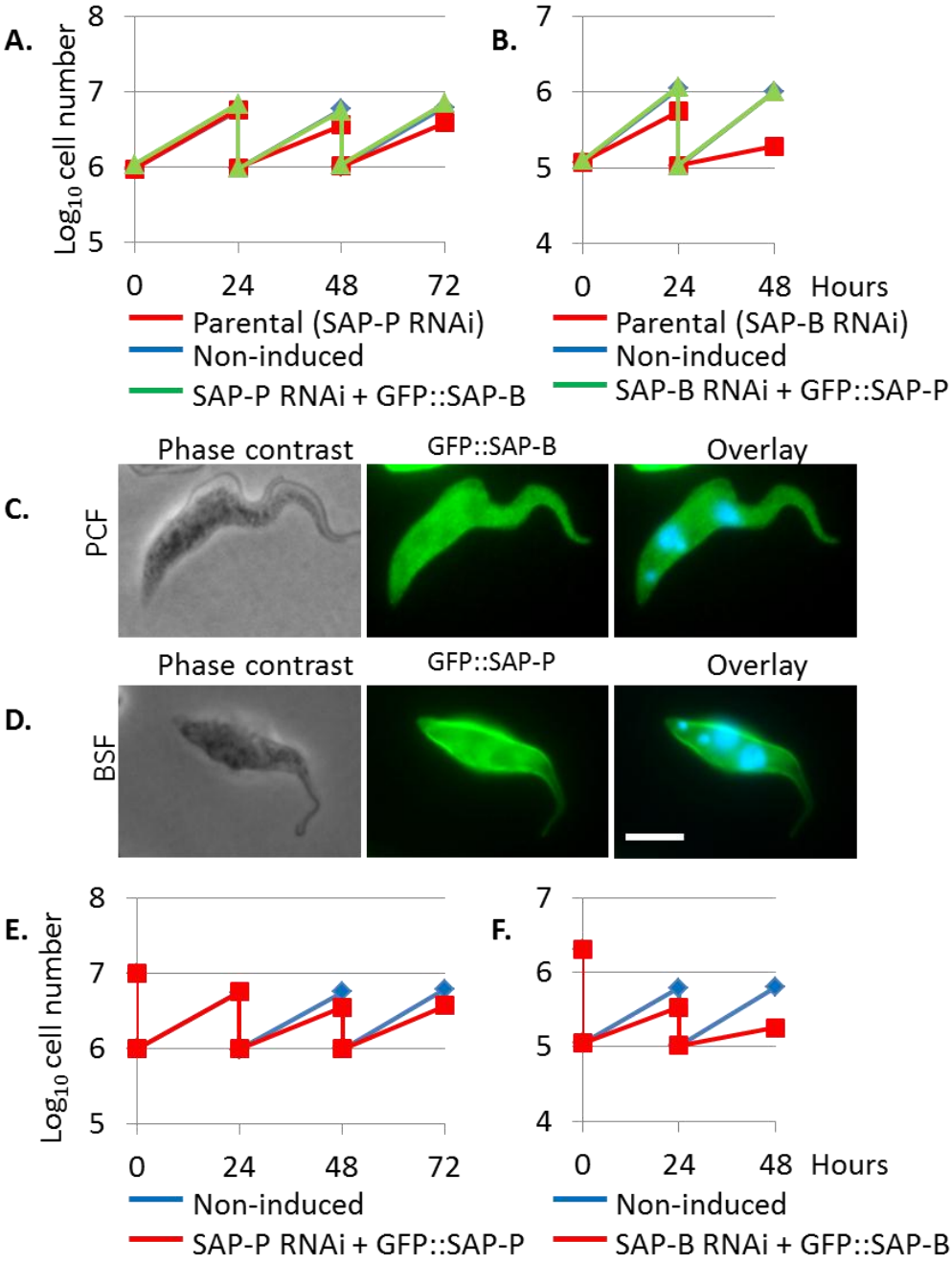

Figure 4.16. SAP protein functions are complementary. A) simultaneous induction of RNAi against SAP-P and inducible ectopic expression of GFP::SAP-B in procyclic forms rescues the growth defect observed in the parental cell line with RNAi induction alone. B) simultaneous induction of RNAi against SAP-B and inducible ectopic expression of GFP::SAP-P in bloodstream forms is also able to rescue the growth defect observed in the parental RNAi only cells. Red = parental (RNAi only), blue = non-induced, green = RNAi plus ectopic expression. Both C) procyclic forms and D) bloodstream forms show normal morphologies 96 hours after induction of RNAi and ectopic expression as described above. Ectopic protein localises to the subpellicular microtubule array. Green = GFP::SAP-B (C) or GFP::SAP-B (D), blue = DAPI, bar = 5μm. Simultaneous induction of RNAi against the endogenous protein and inducible expression of the endogenous protein with an N terminal GFP tag from an inducible ectopic locus does not rescue the growth defect in E) procyclic form or F) bloodstream form cells. Red = parental (RNAi only), blue = non-induced, green = RNAi plus ectopic expression.

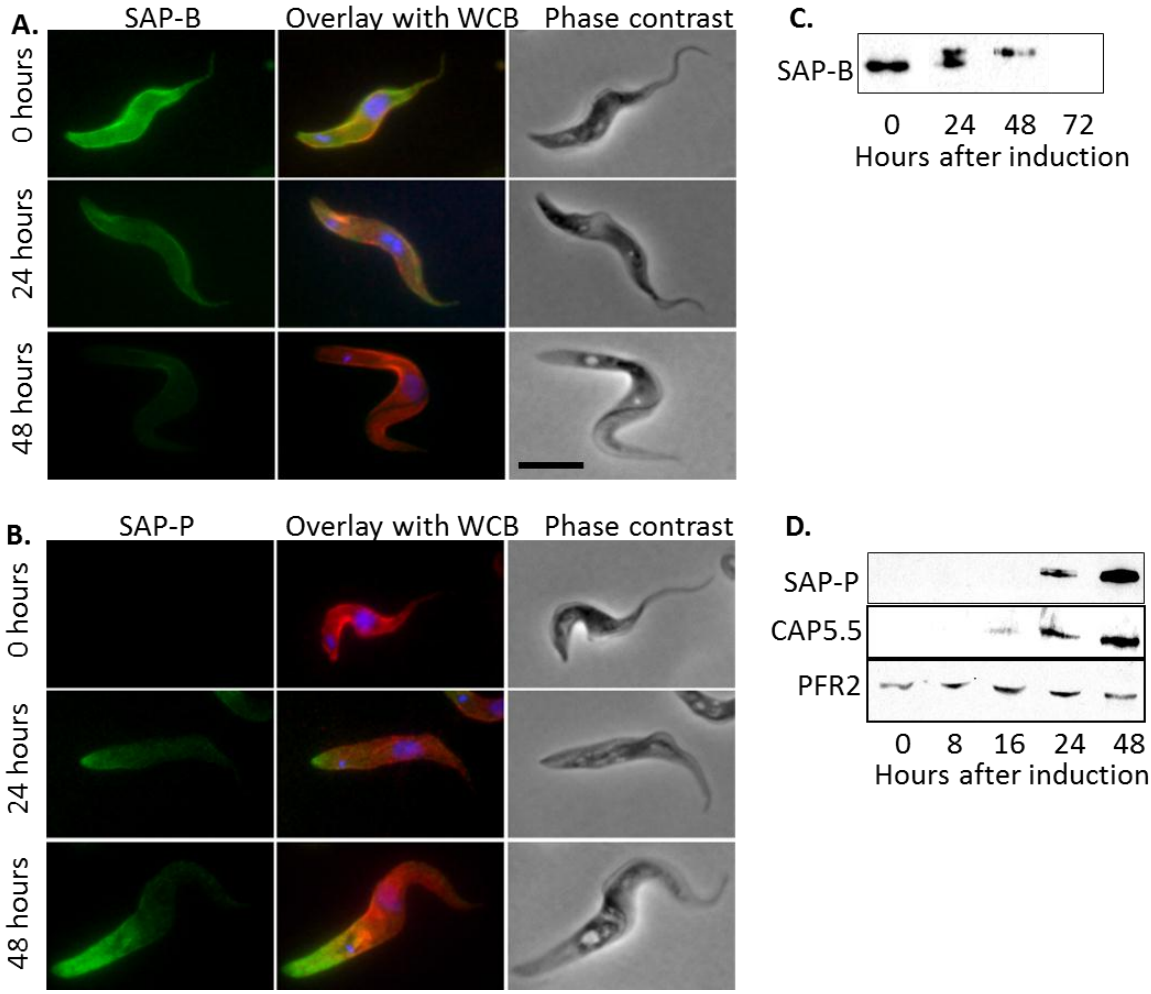

Figure 4.17. SAP proteins during differentiation. Monomorphic bloodstream form cells with C terminal YFP::Ty tagged SAP-B (A) or SAP-P (B) expressed from an endogenous locus were induced to differentiate into procyclic forms by the addition of cis-aconitate and incubation at 28ºc. A) SAP-B::YFP signal (green) gradually disappears uniformly across the cell body during differentiation. B) SAP-P::YFP signal (green) intrudes from the posterior end of the cell during the course of the differentiation. Cells were fixed in paraformaldehyde and permeablised with methanol. Red = WCB, blue = DAPI, bar = 5μm. C) Western blot of SAP-B::YFP::Ty on detergent extracted cells using BB2. In non-induced cells SAP-B initially appears as a single band of the predicted apparent molecular mass. During differentiation a second band approximately 15kDa larger than the first appears. Neither form of SAP-B is detectable by 72 hours after induction. D) Western blot of SAP-P::YFP::Ty on detergent extracted cells using BB2. SAP-P is undetectable in non-induced cells. A band of the correct predicted molecular mass appears by 24 hours, slightly later than the first detection of CAP5.5 (detected with the CAP5.5 antibody) at 16 hours. A blot of PFR2 (L8C4) is shown as an indication of relative loading.

hours a second, larger band appeared. By 48 hours only the higher molecular weight band was detectable and this too was absent by 72 hours. The apparent difference in molecular weight of these two bands was approximately 10kDa. Samples of the cell line expressing tagged SAP-P were taken at 0, 4, 8, 16, 24 and 48 hours after induction and analysed by Western blot with BB2 and the CAP5.5 antibody. Tagged SAP-P protein was undetectable at the early timepoints but appeared between 16 and 24 hours after differentiation was induced (Figure 4.17.D). This is in accordance with the immunofluorescence analysis and is slightly later than the appearance of CAP5.5 that was first detected 16 hours after induction of differentiation.

Chapter 5

The flagellar pocket collar

The flagellar pocket collar has previously been described as a ring or horseshoe structure that either partially or entirely surrounds and constricts the neck region of the flagellar pocket (Figure 5.1.). The FPC is located on the cytoplasmic face of the neck region but remains associated with the insoluble flagellum even after extraction with detergent and depolymerisation of the subpellicular array with high salt. Four distinct external membrane domains exist within *T. brucei* cells; the plasma membrane, the flagellar pocket neck, the flagellar pocket, and the flagellar membrane. The FPC is located at the boundary between the flagellar pocket neck region and the flagellar pocket membrane and is essential for the formation of a new flagellar pocket, and hence cell viability, during the cell cycle.

5.1. Investigation of the morphology and biogenesis of the flagellar pocket collar

5.1.1. The morphology of the flagellar pocket collar

The flagellar pocket is a structurally complex part of the cell and the precise morphology of the FPC and its relationship with other structures such as the flagellar pocket membrane and microtubule quartet have not so far been fully determined. To begin to address this I captured a series of 12 tomograms of high pressure frozen whole procyclic form cells containing the flagellar pocket and neck region of which 3 contained the entire FPC structure within a single slice volume. Analysis of these tomograms revealed that the electron dense FPC material extends from the microtubule quartet and completely encircles the neck of the flagellar pocket (Figure5.2. A) with electron density visible between the microtubules of the quartet. The FPC maintains an almost constant distance from the neck membrane for most of its circuit and discreet connections are visible between the FPC and the membrane (Figure 5.2.C). The FPC deviates from this constant distance in a specific area adjacent to the position of the neck microtubule at which point there is no distinguishable gap between the FPC material and the neck membrane and no discreet connecting structures can be seen (Figure 5.2.D).

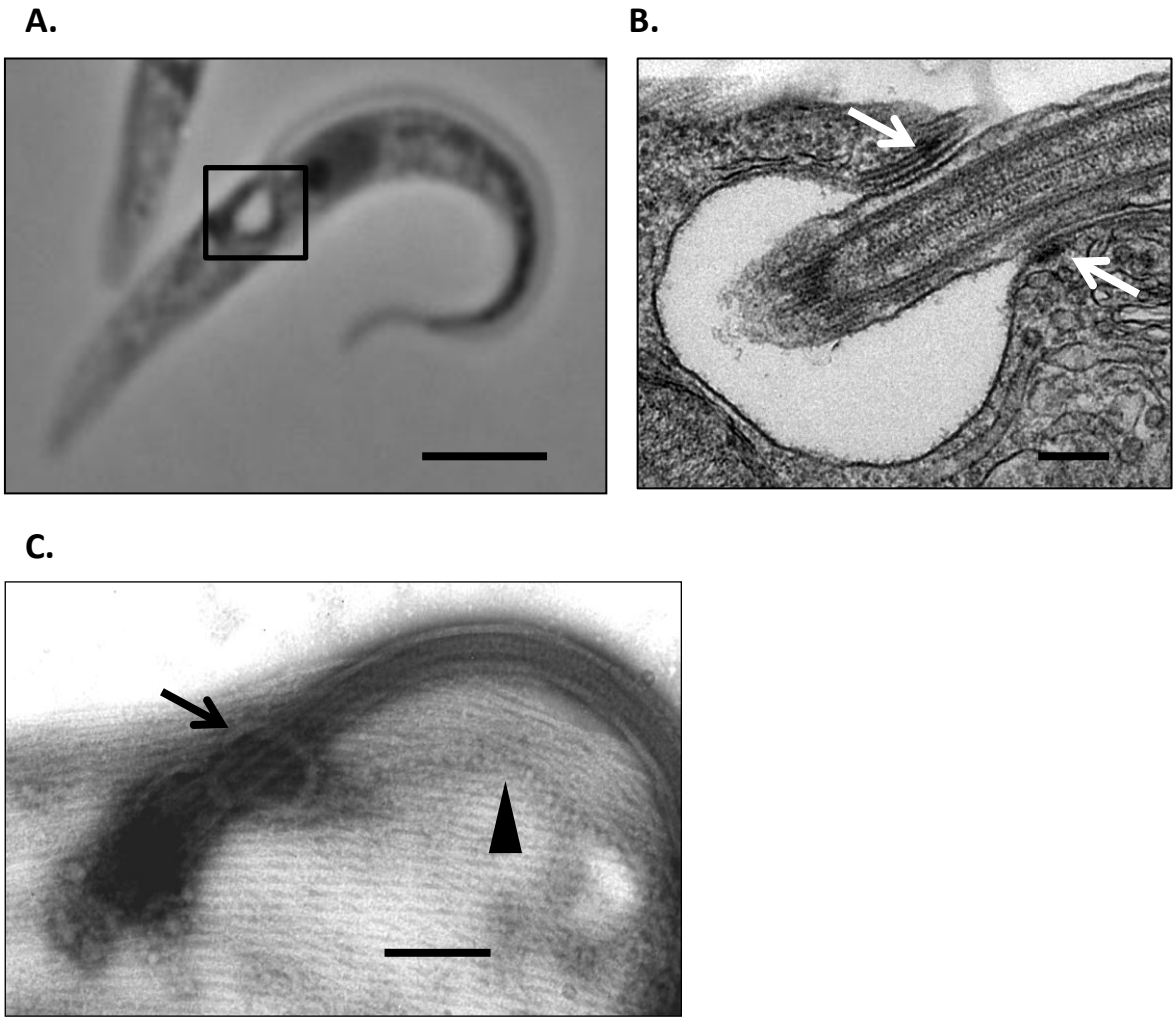

Figure 5.1. The flagellar pocket collar. The collar is defined as the electron density surrounding the neck of the flagellar pocket. A) Phase contrast image of procyclic form *T. brucei* fixed in paraformaldehyde. Bar = 5μm B) Chemically fixed procyclic form *T. brucei* in longitudinal section by thin section TEM, arrows show the position of the collar. Bar = 200nm. C) Negatively stained whole mount cytoskeleton of procyclic form *T. brucei*. Arrow shows the collar, arrowhead marks the FAZ. Bar = 200nm.

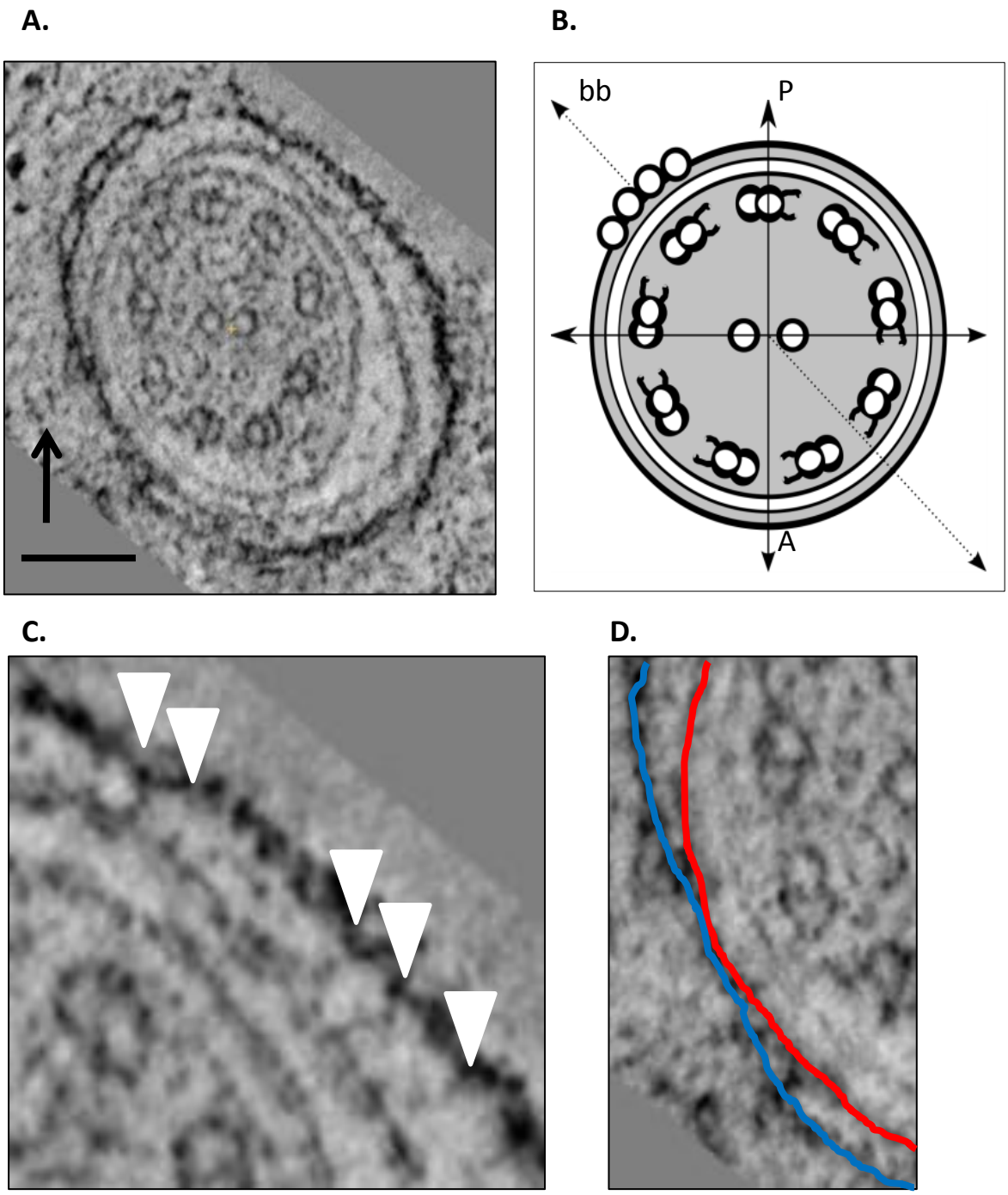

Figure 5.2. The morphology of the flagella pocket collar. A) 1nm nominal thickness pseudo-section from a tomographic reconstruction of high pressure frozen procyclic form *T. brucei*. The collar forms a continuous ring around the flagellar pocket neck which it contacts at a point adjacent to the neck microtubule (arrow). Bar = 100nm. B) Schematic representation of the orientation of the collar shown in A. A = anterior of the cell, P = posterior of the cell, bb = basal body of the flagellum. C) High magnification image of the connections between the collar and the neck membrane (arrowheads). D) High magnification image of the section of the collar (blue) that approaches the neck membrane (red).

5.1.2. Biogenesis of the flagellar pocket collar

There are currently two apparently contradictory models of FPC biogenesis in the literature (Figure 5.3.). In order to test these two models I generated a procyclic form cell line that expressed BILBO1 protein with an N terminal Ty epitope tag from one of the endogenous loci. The resulting cells grew normally and did not display any of the adverse phenotypes previously associated with overexpression of a GFP tagged BILBO1 (but not overexpression of untagged BILBO1) (Bonhivers, Nowacki et al. 2008). Interestingly I was unable to generate a cell line expressing GFP tagged BILBO1 from the endogenous locus which supports the hypothesis that incorporation of a GFP tag confers a toxic effect on BILBO1.

Tagged cells were examined by immunofluorescence microscopy using a monoclonal antibody against the Ty epitope. As previously described I was able to observe cells early in the cell cycle with a single discreet ring or horseshoe signal and cells later on in the cell cycle with two discreet signals (Figure 5.4.). Interestingly I did not observe any cells with the elongated FPC configuration previously described (Bonhivers, Nowacki et al. 2008) but did identify a third type of BILBO1 localisation on cells in the early stages of new flagellum formation and flagellar pocket biogenesis. The Ty::BILBO1 signal localised to the exit point of the old flagellum as seen before, however, from this structure two lines of fluorescence were seen to extend around or through the flagellar pocket to a point close to the basal bodies where two additional foci were observed (Figure 5.5.). In Figure 5.5.A the new basal body has docked with the flagellar pocket membrane but extension of the new flagellum into the lumen of the pocket has not yet begun (or rather, not to the extent at which it is detectable in these images). Figure 5.5.B shows a cell slightly later in the cell cycle where the new flagellum has invaded the lumen of the flagellar pocket but is still positioned to the anterior of the old flagellum. The extensions from the old FPC are consistent with the position of the old and new microtubule quartets so to interrogate this further I performed immunogold labelling of the Ty epitope on negatively stained whole mount cytoskeletons of the tagged cell line. Figure 5.6. shows gold labelling of the FPC

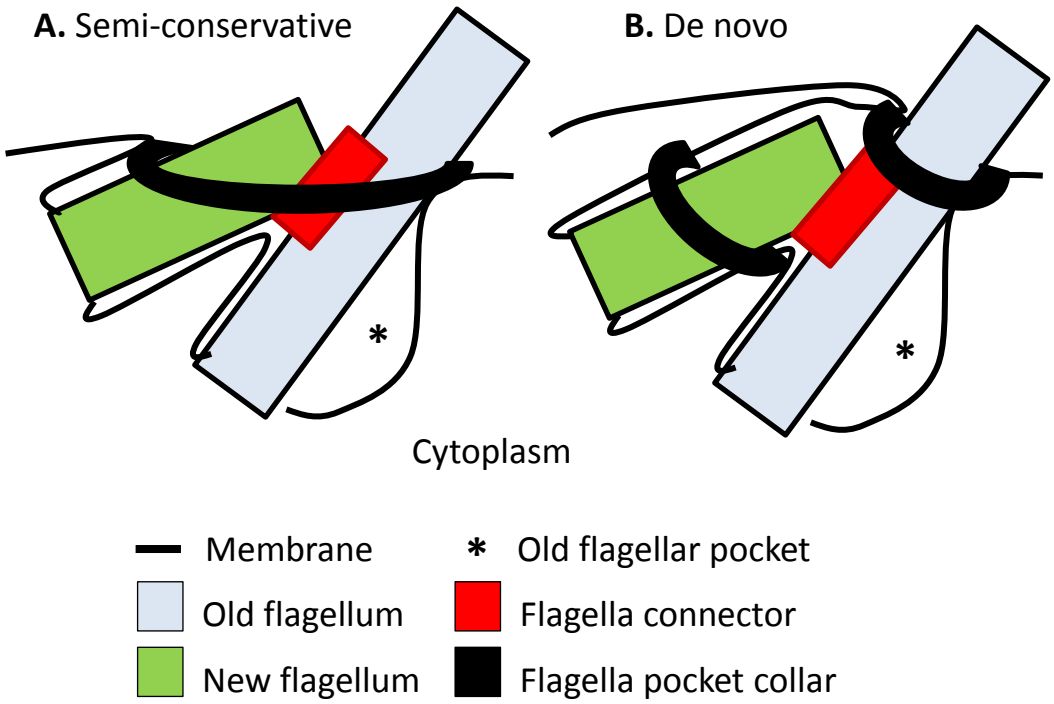

Figure 5.3. Two models of new collar formation. A cartoon representation of the semi-conservative (A) and de novo (B) models of new collar formation. In the semi-conservative model the old collar extends to encompass the emerging new flagellum and is subsequently constricted to form two discreet collar structures. In this model the flagella connector passes through the extended collar before separation into two collars. In the de novo model the new collar forms independently of the old collar around the nascent neck region. This model is supported by evidence from tomographic reconstructions of the dividing pocket but raises the question of how the flagella connector negotiates passage through the old collar. The cartoons are orientated such that the posterior of the cell is to the left and the cytoplasm is at the bottom. Thin black line, membrane; thick black line, collar; red box, flagella connector; green box, new flagellum; blue box, old flagellum; * marks the old flagellar pocket separated from the forming new pocket by a cell body intrusion into the lumen known as the ridge.

and the microtubule quartets on a cell at approximately the same stage as that shown in Figure 5.5.B.

5.1.3. Incorporation of new BILBO1 protein into the flagellar pocket collar

Although the precise role of BILBO1 in the FPC has not yet been determined, it is currently the best molecular marker available to interrogate the nature of FPC biogenesis. I generated a procyclic form cell line with inducible expression of Ty::GFP tagged BILBO1 from an ectopic locus and expression of Ty epitope tagged BILBO1 from one of the endogenous loci. To address the fate of new BILBO1 protein during FPC biogenesis, expression of GFP::BILBO1 was induced for four hours (approximately half a cell cycle) and the resulting cells were examined using fluorescence microscopy (Figure 5.7.). At the time of induction the culture was asynchronous so cells at all stages of the cell cycle were present. In *T. brucei* the cell cycle stage can be determined quite accurately by the position and morphology of the nucleus (or nuclei) – N - and kinetoplast(s) - K. I did not observe any GFP fluorescence in cells that possessed two discreet FPCs and had progressed beyond nuclear M phase (2K2N) or in cells with a single discreet FPC (early stage 1K1N cells). These are likely to represent cells that had not progressed sufficiently far through the cell cycle to begin FPC biogenesis during the course of the induction (1K1N) or had completed FPC biogenesis prior to induction (2K2N). In cells exhibiting the particular extended FPC morphology described above (late stage 1K1N cells) GFP::BILBO1 localised to the entire structure decorating both the partial ring and extensions. In cells in which two discreet FPCs could be observed but nuclear G2 phase was not complete (late stage 1K1N and 2K1N) GFP::BILBO1 localised to both the old and new FPC equally. Cells exhibiting GFP::BILBO1 localisation correspond to a two to three hour portion of the cell cycle, consistent with the timing of the induction. These results demonstrate that new BILBO1 protein is incorporated into both old and new FPCs and that even when expressed from an ectopic promoter system, BILBO1 is only assembled into a FPC during new FPC formation suggesting that there is little turnover of protein once a FPC is assembled.

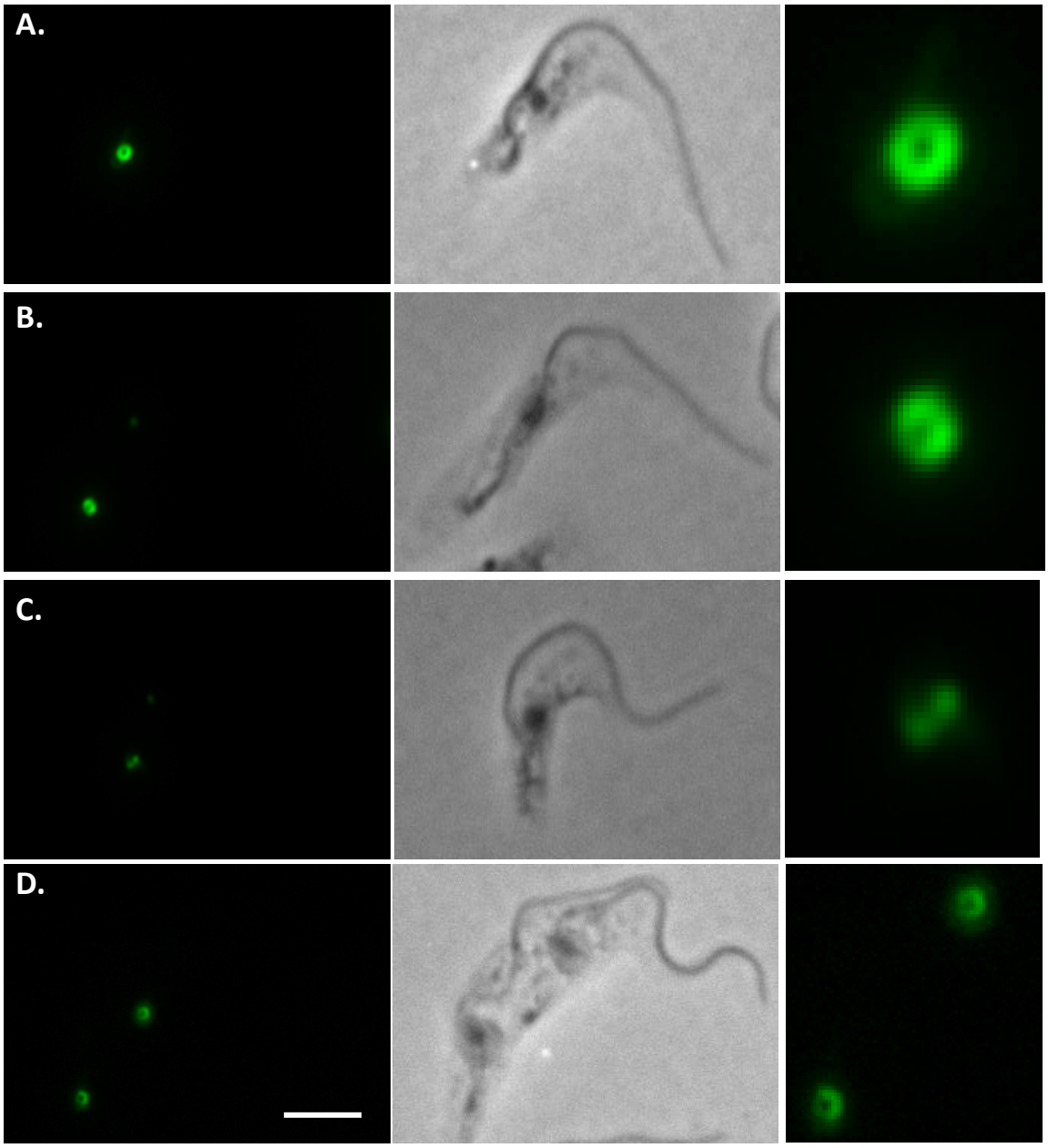

Figure 5.4. BILBO1 can be observed as A) a ring, B) a horseshoe or C) two adjacent foci or D) as a pair of these structures in cells with two external flagella. These different appearances are the result of viewing the same ring structure in different orientations relative to the viewer.

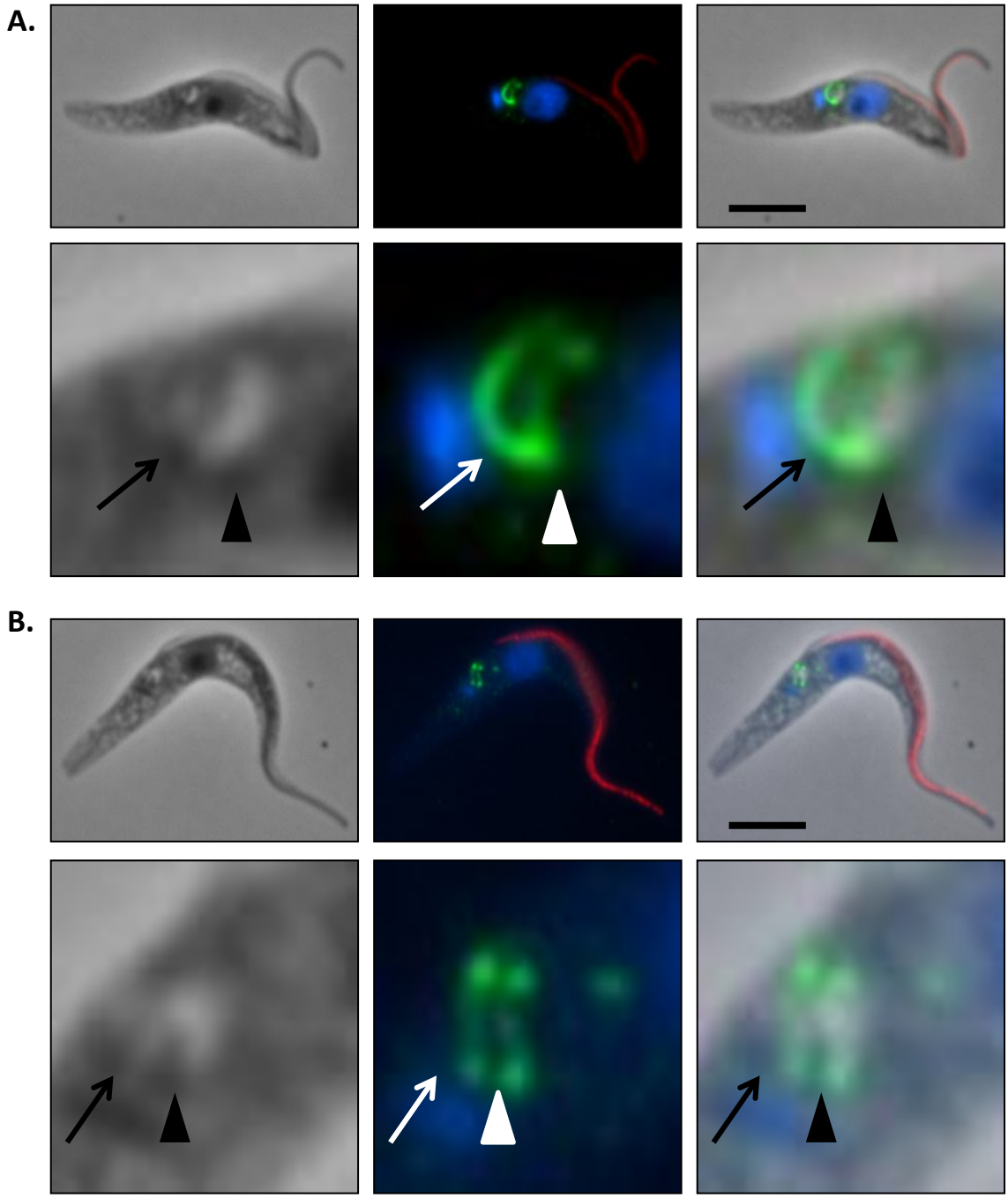

Figure 5.5. The extended collar phenotype. Prior to duplication of the collar, BILBO1 localises around the flagellar pocket. A) shows a cell in the earliest stages of new flagellum formation. The new basal body (arrowhead) has docked with the flagellar pocket membrane but the new flagellum has not begun to extend into the pocket. Ty::BILBO1 recognised by BB2 (green) surrounds the posterior side of the pocket in two lines of fluorescence that terminate at points adjacent to the old basal body (arrow) and the new basal body, consistent with the location of the old and new microtubule quartets. B) shows a cell slightly later in the cell cycle with the new flagellum visible in the flagellar pocket lumen but still on the anterior side of the old flagellum and the extended BILBO1 localisation is still observed. Cells expressing Ty::BILBO1 from one of the endogenous loci were fixed in paraformaldehyde and permeablised with methanol. Red = PFR (Rod1), blue = DAPI, bar = 5μm.

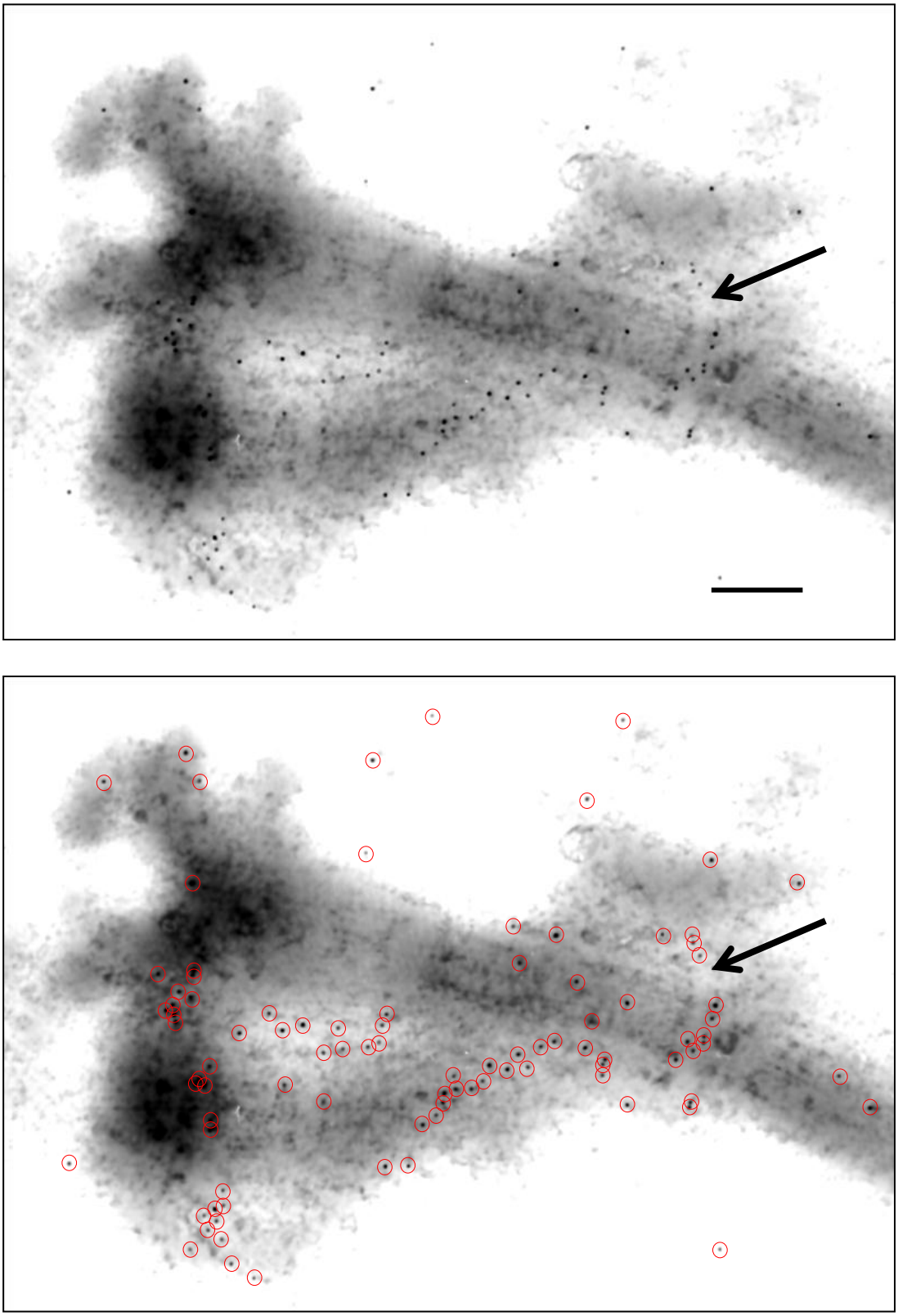

Figure 5.6. Negatively stained whole mount procyclic form cell expressing Ty::BILBO1 from one of the endogenous loci. The cell shown is at approximately the same stage as that in Figure 5.5 B with an extended new flagellum on the anterior side of the old flagellum. A single collar can be observed (arrow) and immunogold localisation of Ty::BILBO1 using BB2 (red circles) labels the collar and both microtubule quartets. Bar = 200nm.

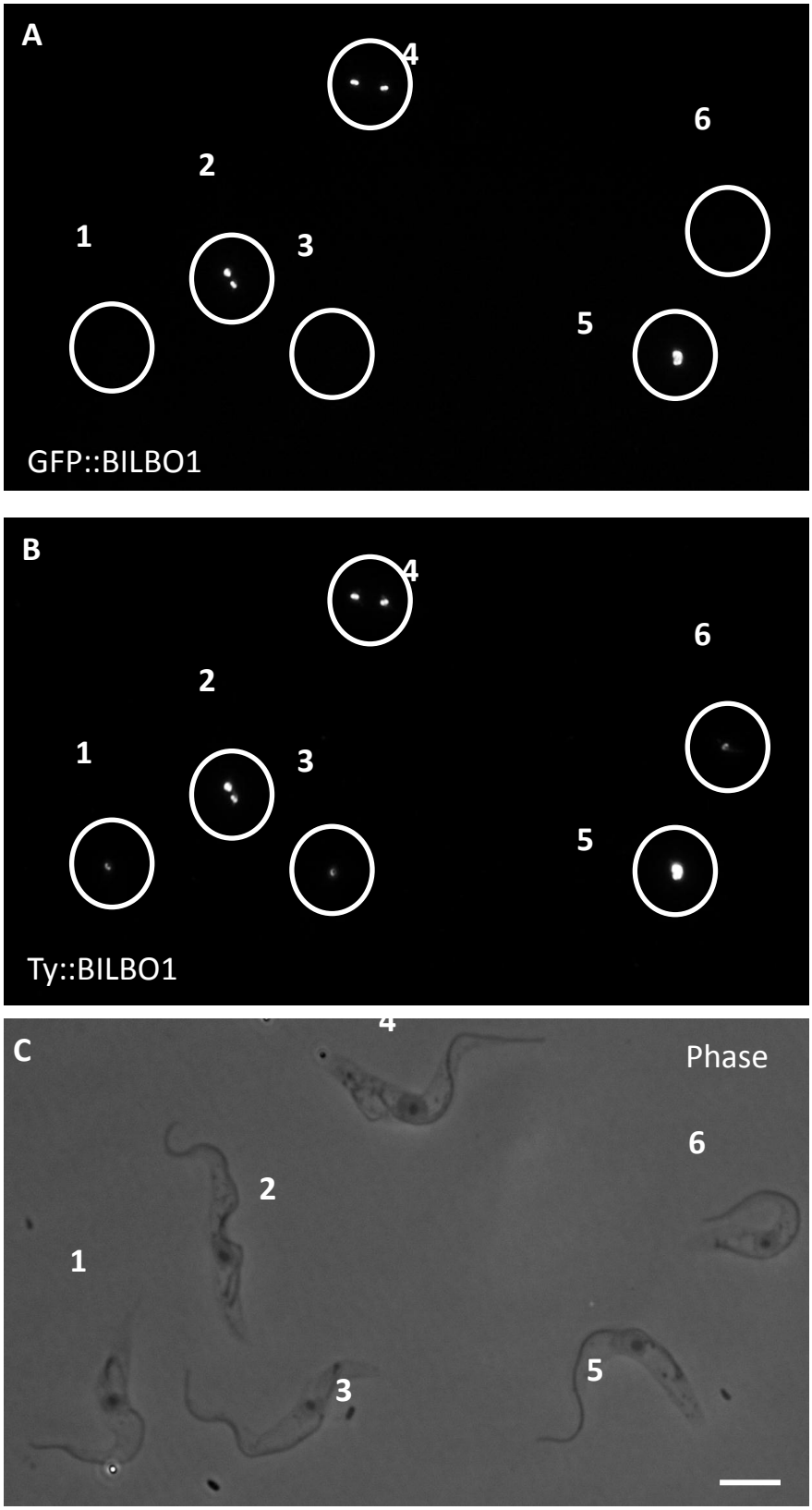

Figure 5.7. Incorporation of new GFP::BILBO1 protein. Cells expressing Ty::BILBO1 (A) from one of the endogenous loci with an inducible ectopic copy of GFP::BILBO1 (B) were induced for 4 hours. Only cells with two collars (2,4) or with a collar in the extended format (5) described above were positive for GFP. All collars were positive for Ty::BILBO1 detected by BB2. Cells were extracted with detergent and fixed with methanol. Green = GFP::BILBO1, red = Ty::BILBO1, blue = DAPI, bar = 10μm.

5.1.4. The fate of old BILBO1 protein during formation of the new flagellar pocket collar

Having determined the fate of new BILBO1 protein I next asked what happened to old protein (protein that was present before the beginning of FPC biogenesis) during FPC duplication. I induced the expression of Ty::GFP::BILBO1 for 24 hours in cells expressing Ty::BILBO1 from one of the endogenous loci. Samples of the population were analysed using fluorescence microscopy and all FPCs observed contained GFP tagged BILBO1 (Figure 5.8.A). The cells were then repeatedly washed and grown under non-inducing conditions for a further 48 hours. During this period population doubling times were equivalent to non-induced cells and no accumulation of cells with morphological abnormalities was observed. Again samples of the population were taken and examined using fluorescence microscopy. Cells with two FPCs (as assessed by immunolocalisation of Ty::BILBO1 with BB2) showed GFP fluorescence in both the old and new FPCs (Figure 5.8.B). The images were analysed using a custom macro script for ImageJ that identified FPC boundaries based on the BB2 signal and quantified the fluorescence intensity of GFP within these boundaries, pairing old and new FPCs from individual cells. The GFP intensities determined in this way demonstrated that the old FPC contained slightly more GFP::BILBO1 than the new FPC within a single cell (paired T test, P=0.028) (Figure 5.8.C) and that the average GFP intensity of FPCs following washout (average normalised GFP intensity 0.34, n = 173 FPCs) was threefold less than that measured before washout (average normalised GFP intensity set at 1, n = 164 FPCs). FPCs in the extended format exhibited a very particular distribution of old and new protein and were not included in the above analysis. GFP tagged BILBO1 localised to the anterior portion of the old FPC in a discrete semi-circle open towards the posterior (Figure 5.8.D). This gap in labelling when applied to a hypothetical ring was larger than that observed for FPCs in the horseshoe configuration in cells not undergoing FPC biogenesis. Little GFP signal could be detected in the extensions around or through the pocket indicating that these structures contained predominantly new BILBO1 protein.

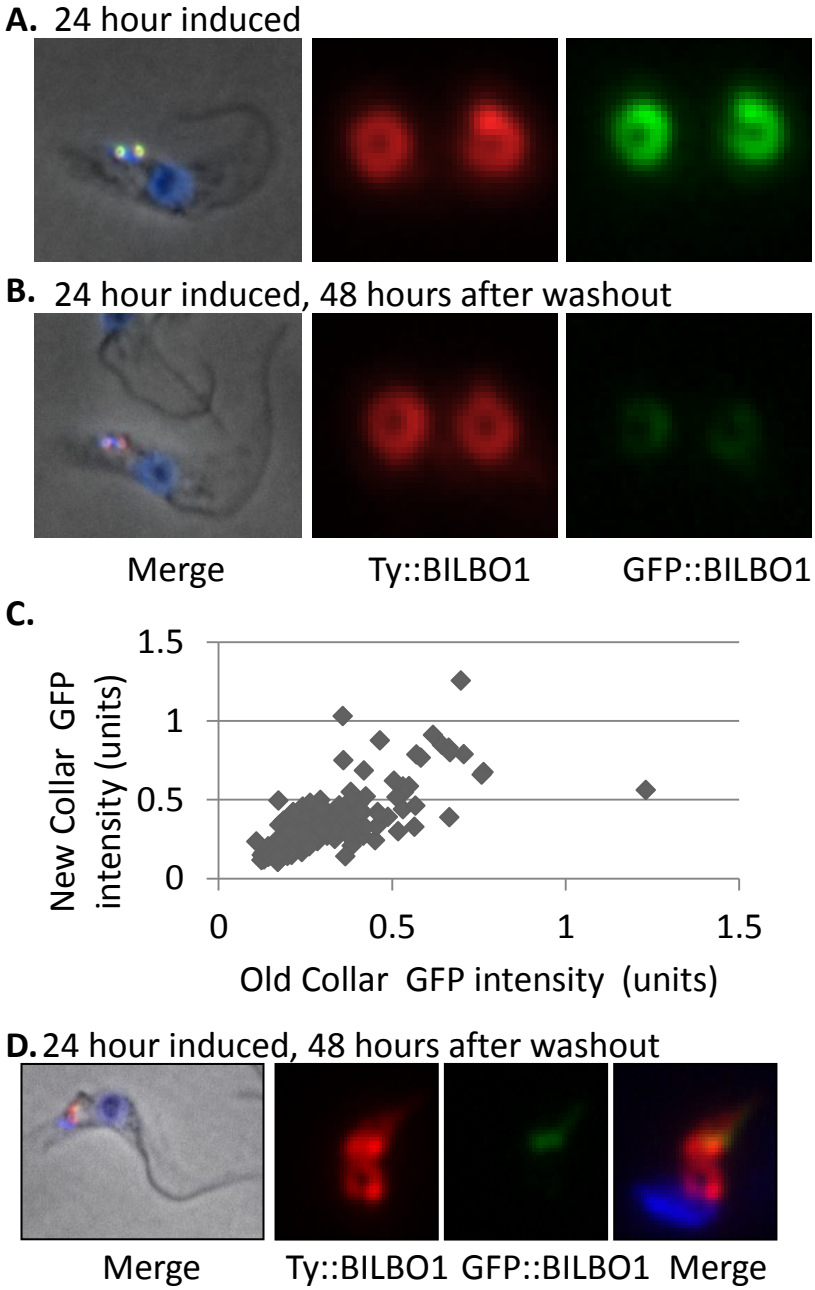

Figure 5.8. Localisation of old BILBO1 protein. 24 hours after induction, cells described in 5.6. above were washed and incubated under non-inducing conditions for a further 48 hours. After this time cells were extracted and fixed in methanol for analysis using fluorescence microscopy. This showed that after washout cells with 2 collars showed GFP fluorescence in both old and new collars (B) although the intensity was lower than that observed prior to washout (A). BB2 was used to detect Ty::BILBO1 (red) as a marker for the collar and all images were captured and processed using identical settings. C) a custom scripted image analysis tool (see supplementary methods) was used to identify and delimit collars based on the BB2 signal and to measure GFP fluorescence within the resulting boundary. A plot of old and new collar intensity for each 2 collar cell showed that the new collar contained slightly more GFP::BILBO1 than the old collar (paired 2-tailed T-test, P=0.03). D) 48 hours after washout, in cells with the extended collar format the majority of old (GFP labelled) BILBO1 localised to the anterior portion of the collar and not the extensions along the microtubule quartets. Red = Ty::BILBO1, green = GFP::BILBO1, blue = DAPI.

5.2. Characterisation of a novel flagellar pocket collar component

Note: *The description and localisation of CMRP was published independently by Morriswood et al (Morriswood, He et al. 2009) who identified it as a component of the golgi-associated bilobe structure. Differences and similarities between this analysis and my own are addressed in the discussion for this section.*

TgMORN1 (AAZ99885) is a defining component of the basal complex in the apicomplexan parasite *Toxoplasma gondii* (Gubbels, Vaishnava et al. 2006; Heaslip, Dzierszinski et al. 2010). The basal complex is detected as a TgMORN1-containing ring at the basal end of daughter cell cortical cytoskeletons and is maintained throughout daughter cell development. Disruption of the basal complex via TgMORN1 knockout leads to the disruption of cytoskeleton formation and defects in daughter cell separation. TgMORN1 protein consists entirely of repeated MORN (Membrane Occupation and Recognition Nexus) domains, a highly conserved sequence motif that is found across the eukaryotic and bacterial lineages, often in combination with other domains and motifs and is thought to mediate protein interactions with membranes.

The *T. brucei* protein CMRP (Tb927.6.4670) has previously been shown to associate strongly with the flagellum, remaining with the flagellar fraction after detergent and high salt treatment of cells (Broadhead, Dawe et al. 2006). CMRP protein is 358 amino acids long and bioinformatic analysis shows that it is a clear homologue of TgMORN1 with 52% identity and 72% similarity (Figure 5.9.A). Like TgMORN1, CMRP also consists entirely of MORN repeats (Figure 5.9.B).

A polyclonal antibody raised against the TgMORN1 protein decorates an area corresponding to the FPC and proximal portion of the FAZ by immunogold thin section TEM on chemically fixed whole *T. brucei* procyclic forms (pers. comm. Prof David Ferguson, Univ. Oxford) and by Western blot recognises a single band with an apparent molecular mass of just over 35kDa, only slightly smaller than the calculated molecular mass of CMRP (40kDa) (Figure 5.9.C). In this part of my project I sought to determine whether CMRP is a novel component of the flagellar pocket collar.

5.2.1. Localisation of CMRP

In order to determine the localisation of CMRP I generated a cell line expressing N-terminal Ty epitope tagged CMRP from one of the endogenous loci. Analysis of cells by immunofluorescence microscopy showed that tagged protein localised to the area corresponding to the flagellar exit point with a particular pattern of fluorescence that I have termed 'ring and finger' (Figure 5.10.A). As with BILBO1, either one or two ring and finger structures are visible in a cell-cycle dependant manner that correlates with the number of external flagella visible. This demonstrates that the CMRP-containing structure duplicates by some method early in the process of new flagellum formation which is consistent with the known behaviour of the FPC during the cell cycle. The more posterior or ring part of the signal occurs around the flagellum at a point on the cell consistent with the flagellar exit point and is seen as either two adjacent foci, a ring or a horseshoe, a localisation that is consistent with the FPC and is comparable to that observed for BILBO1. The anterior or finger localisation extends from the ring and lies alongside the flagellum for approximately 1μm, terminating while still posterior to the nucleus. Costaining with BB2 and the TgMORN1 antibody showed that the two signals colocalised at the ring and finger with an additional focus of fluorescence at the extreme posterior of the cell that was recognised only by the TgMORN1 antibody (Figure 5.10.A, arrowheads). Interestingly, in 2K2N cells an additional α-TgMORN1 signal is visible located between the separated kinetoplasts. It is possible that this marks the position of a new posterior structure that will be inherited by the daughter cell that inherits the old flagellum following cytokinesis. Double staining of cells expressing Ty epitope tagged BILBO1 from one of the endogenous loci with BB2 and the TgMORN1 antibody showed that the ring recognised by the TgMORN1 antibody colocalises with BILBO1 (Figure 5.11.A-E). Finally, immunogold labelling via BB2 of negatively stained whole mount cytoskeletons of cells expressing tagged CMRP showed localisation to the FPC and proximal portion of the FAZ (Figure 5.10.B).

Interestingly, the distinct pattern of localisation of BILBO1 extending around the flagellar pocket during flagellar pocket biogenesis described above is also observed with the TgMORN1 antibody

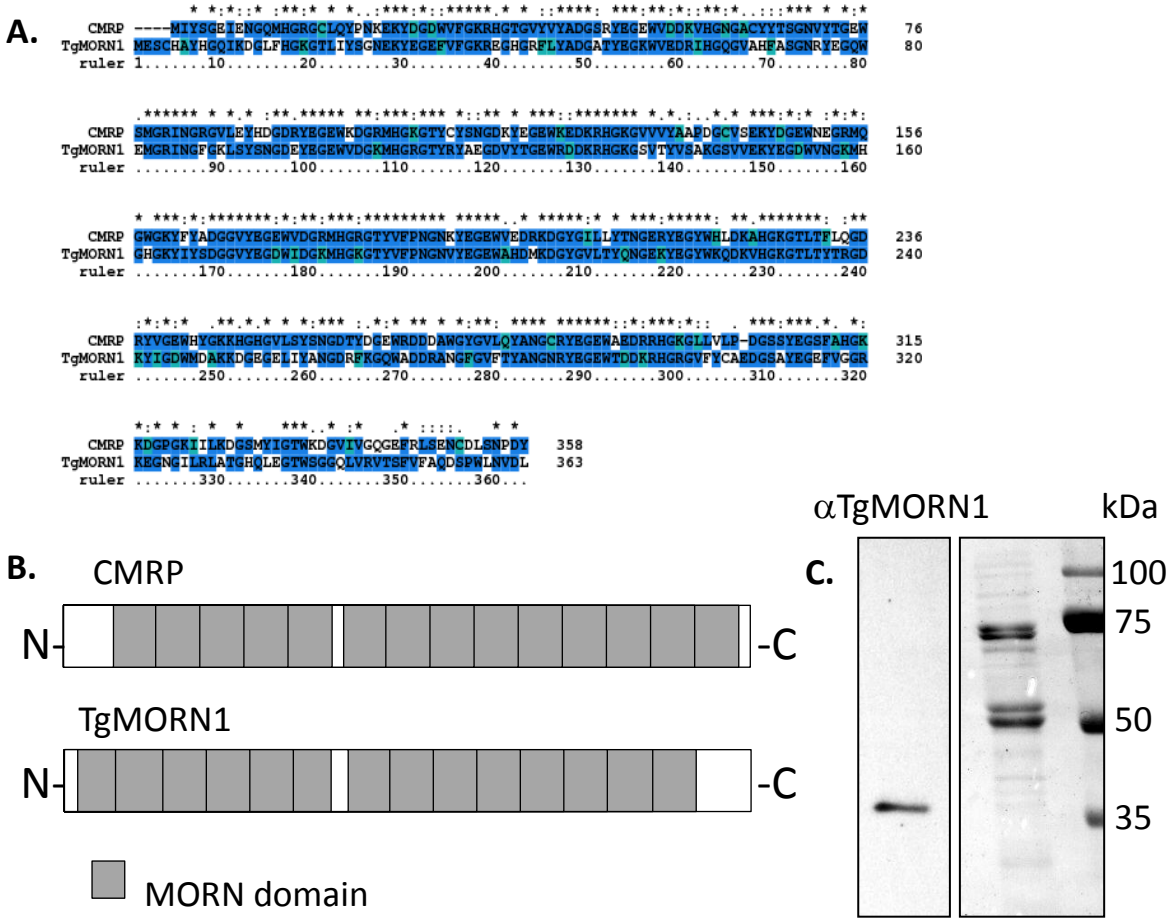

Figure 5.9. CMRP and TgMORN1. A) clustal alignment of CMRP and TgMORN1. B) a cartoon representation of the domain architecture of CMRP and TgMORN1. Both proteins are almost entirely composed of MORN repeat motifs. C) Western blot of purified flagella from wild type procyclic form cells. The TgMORN1 antibody recognises a single band with an apparent molecular weight consistent with that calculated for CMRP. Ponceau stained membrane with molecular weight markers is shown for reference.

(Figure 5.11.B&C) and by using BB2 on cells expressing tagged CMRP (Figure 5.11.G&H). In both cases lines of fluorescence extend from the ring through or around the flagellar pocket to points adjacent to the basal bodies, again consistent with an association with the old and new microtubule quartets. Double labelling of cells expressing epitope tagged BILBO1 using the TgMORN1 antibody and BB2 showed that the extensions detected by the TgMORN1 antibody colocalise with the extensions of BILBO1 (Figure 5.11.A).

5.2.2. Analysis of CMRP function

In order to determine the function of CMRP I generated a cell line with inducible RNAi against CMRP in a background of epitope tagged CMRP at one of the endogenous loci. The growth of cell populations was measured in the presence and absence of RNAi induction and no significant decrease in growth rates was found as a result of ablation of CMRP over a period of 96 hours (Figure 5.12.A). Although the growth rate of cell populations was not affected by RNAi against CMRP, counts of the number of kinetoplasts and nuclei per cell showed a small increase in the number of cells with abnormal KN morphology (Figure 5.12.B). By 96 hours after induction of RNAi, 15% of cells (n=234) contained more than the normal maximum of two nuclei. This was not observed in non-induced cells or in parental cells treated with doxycycline, strongly suggesting that aberrant morphologies were the result of ablation of CMRP. Analysis of cells 72 hours after induction of RNAi by thin section electron microscopy showed phenotypes reminiscent of those observed after ablation of BILBO1. A proportion of the population produced flagella that were either associated with a reduced flagellar pocket (Figure 5.13. A&B) or emerged directly from the cell body with no associated flagellar pocket (Figure 5.13.C). Interestingly the collarrette, an intriguing structure with nine-fold symmetry that normally surrounds the external surface of the flagellar membrane where it emerges into the lumen of the flagellar pocket, can still be observed associated with flagella that emerge without a flagellar pocket. Immunofluorescence examination of cells induced for 72 hours, a timepoint before significant numbers of multi-nucleate cells are apparent, showed that 7.2% cells (n=127) had at least one detached flagellum with either no FAZ or a much reduced FAZ associated with it (Figure 5.13.D).

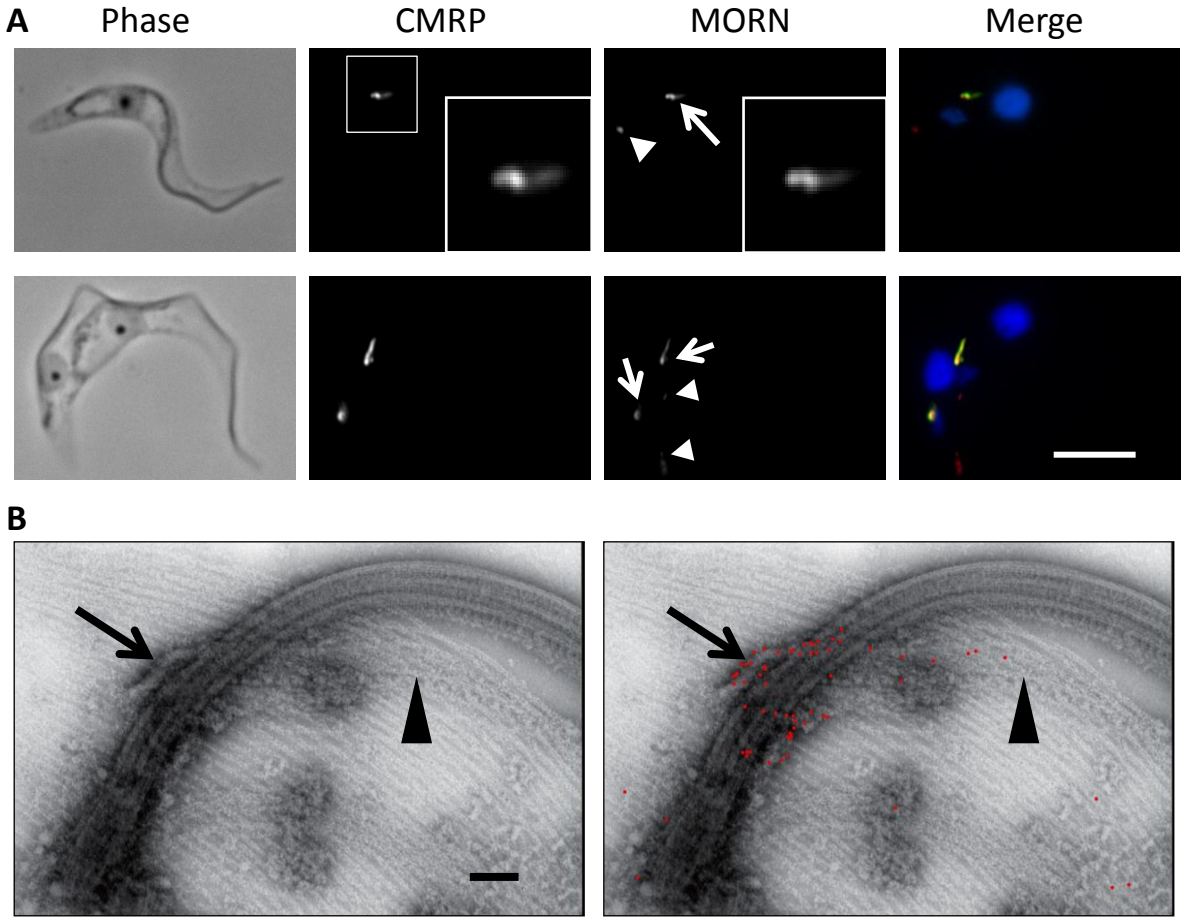

Figure 5.10. Localisation of CMRP. A) cells expressing Ty::CMRP from one of the endogenous loci were extracted with detergent and fixed in methanol and then co-stained with BB2 and a-TgMORN1. Both signals colocalised at the flagellar exit point with a particular ring and finger conformation. The ring localises to the flagellar exit point and the finger extends from here alongside the flagellum for approximately 1mm at the ring and finger structure. a-TgMORN1 labelled an additional structure at the posterior of the cell. Interestingly, in 2K2N cells, a-TgMORN1 also labelled a point on the cytoskeleton located between the separated kinetoplasts. It is possible that this corresponds to the position of the new posterior end of the daughter cell that will inherit the old flagellum. Green = a-TgMORN1, red = PFR (L8C4), blue = DAPI, bar = 5mm. B) Negatively stained whole mount cytoskeletons were prepeared from cells expressing Ty::CMRP. Immunogold localisation using BB2 (red circles) labelled the collar (arrow) and the proximal portion of the FAZ (arrowhead). Bar = 200nm.

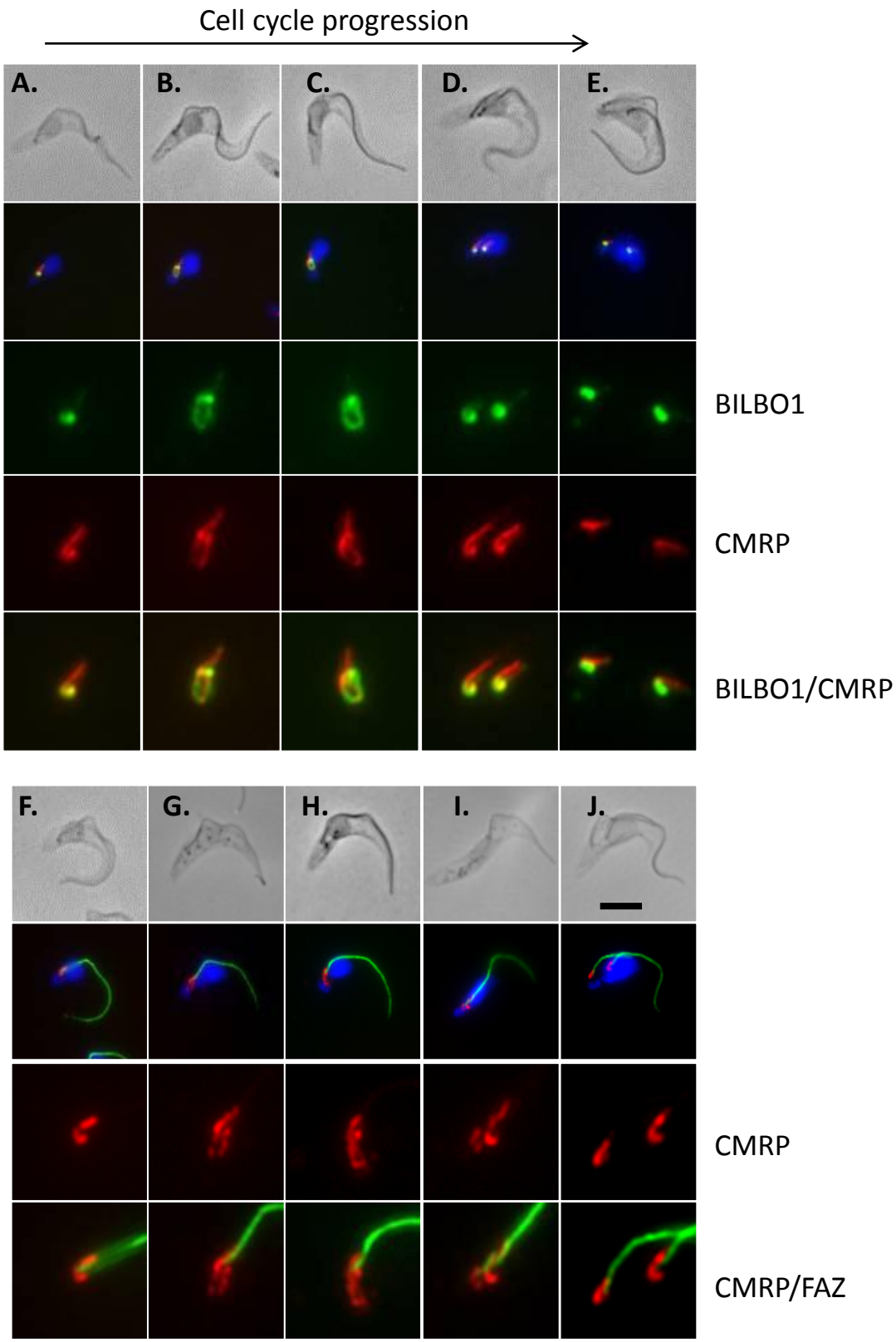

Figure 5.11. CMRP localisation during the cell cycle. A-E) Cells expressing TY::BILBO1 from one of the endogenous loci were extracted with detergent and fixed with methanol and costained with BB2 (green) and a-TgMORN1 (red) before analysis by fluorescence microscopy. The ring detected by a-TgMORN1 colocalised with BILBO1 throughout the collar duplication cycle including the adoption of the extended format described above. F-G) Cells expressing TY::CMRP from one of the endogenous loci were extracted with detergent and fixed with methanol and costained with BB2 (red) and L6B3 (green) before analysis by fluorescence microscopy. CMRP also localises to the extended ring formation. Blue = DAPI, bar = 5μm.

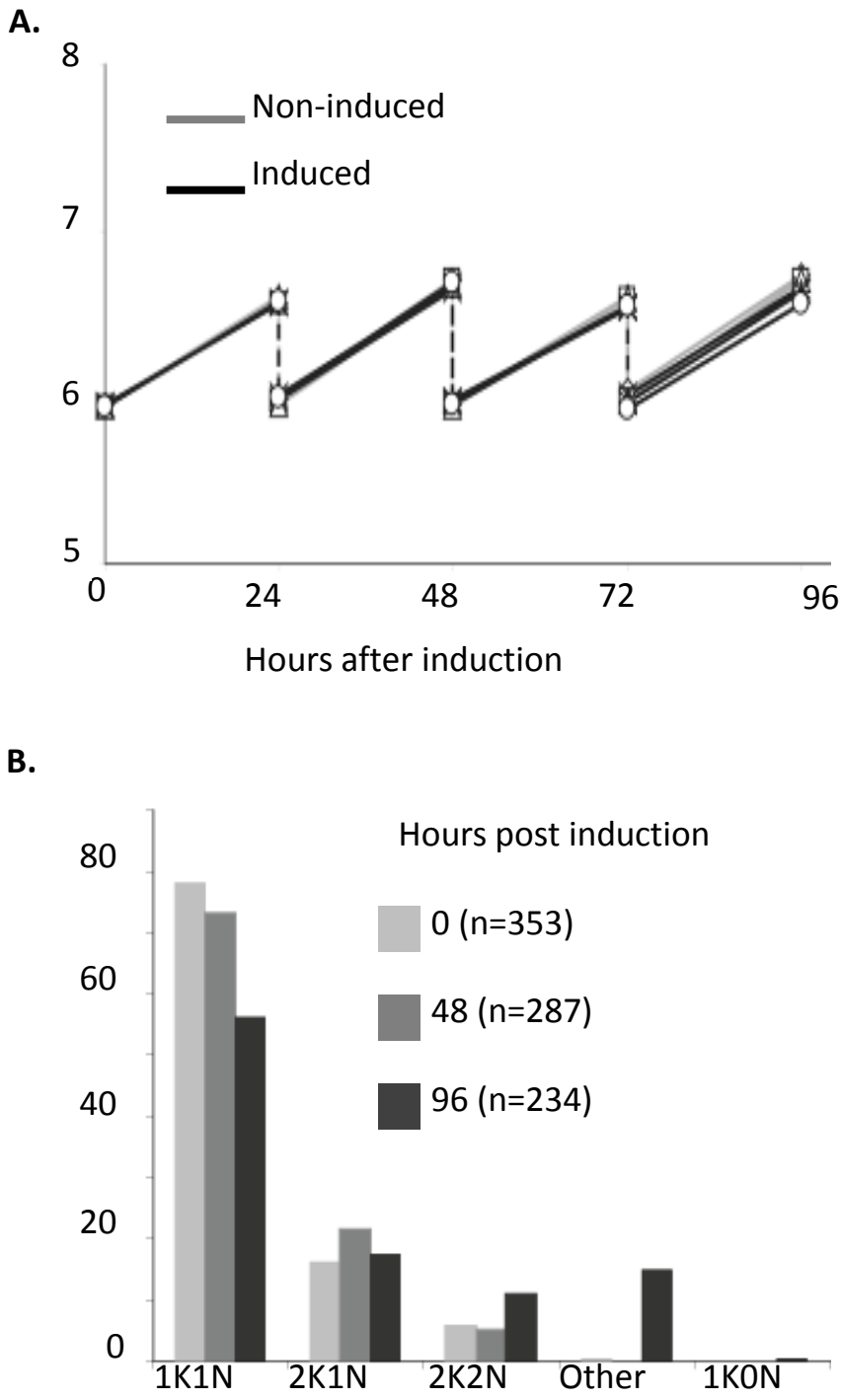

Figure 5.12. RNAi against CMRP. A) population growth of cells undergoing inducible RNAi mediated ablation of CMRP measured at 24 hour intervals for 96 hours shows no significant deviation from that of non-induced cells. B) however, analysis of the KN numbers at 0, 48 and 96 hours after induction reveals a slight accumulation of cells with aberrant KN morphology by 96 hours with a concomitant reduction in the proportion of 1K1N cells

In these cells flagellar and kinetoplast segregation was also compromised with both flagella emerging close together in 2N cells. This is similar to the phenotype observed after ablation of BILBO1 (Bonhivers, Nowacki et al. 2008), albeit affecting a smaller percentage of the population, and is consistent with the phenotype observed for CMRP RNAi by thinsection TEM above. Interestingly, when induced cells were assayed using TgMORN1 antibody, the ring and finger was absent but the posterior end signal remained suggesting that TgMORN1 does indeed recognise CMRP and an additional protein located at the posterior of the cell (Figure 5.13.E). Although the consequences of losing CMRP can be devastating and presumably lethal to the cell, the majority of cells show normal morphologies despite loss of detectable levels of protein. It is possible that CMRP function may be partially redundant or that stochastic events during the tectonic changes associated with flagellar pocket biogenesis strongly influence the fate of any given cell following loss of CMRP.

5.2.3. CMRP and BILBO1

Given the similarities in localisation and RNAi phenotype between CMRP and BILBO1 I next investigated the impact of BILBO1 RNAi on the localisation of CMRP. I generated a cell line with inducible RNAi against BILBO1 in a background expressing epitope tagged CMRP from one of the endogenous loci. Induction of RNAi yielded phenotypes qualitatively similar to those previously described. When cells were examined by immunofluorescence microscopy using the BB2 antibody, the ring and finger localisation was undetectable. Instead, longer strings of fluorescence were observed alongside the FAZ if it was present (Figure 5.14.A) or bending around into the cell body from a point close to the base of the flagellum in the absence of a FAZ (Figure 5.14.B). This loss of the ring and finger morphology was associated with all flagella observed, even though it has been reported that BILBO1 protein is still present at the old FPC after ablation of new protein by RNAi. These results show that CMRP depends upon incorporation of BILBO1 for correct localisation but also suggests that even where BILBO1 protein is still present, CMRP localisation is still disrupted in the absence of new BILBO1. Interestingly, although the ring and finger localisation was lost, CMRP still localised to the correct part of the cell (ie. in the vicinity of the proximal region of the flagellum),

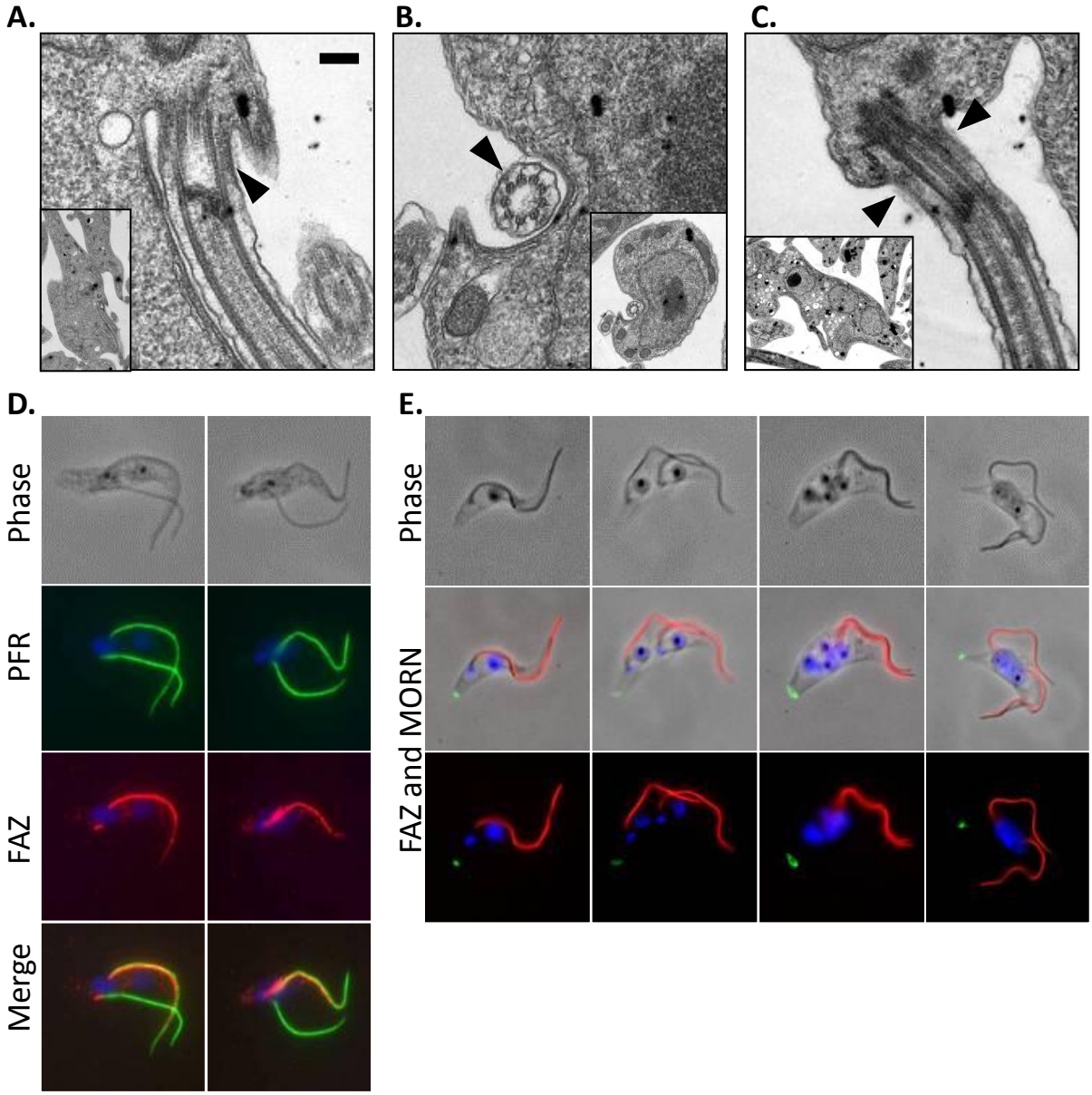

Figure 5.13. A-C) Analysis of chemically fixed 72 hour induced cells by thin section TEM shows that a proportion of the population have flagella associated with aberrant flagellar pocket morphology (A,B) or with no discernible flagellar pocket at all (C), a phenotype consistent with that observed after ablation of BILBO1, albeit affecting a smaller proportion of the population. Interestingly, even flagella with no associated flagellar pocket still possess a collarette (arrowhead). Bar = 200nm. D) samples of the same population were also examined by fluorescence microscopy which showed that 7.6% of cells had at least one detached flagellum, a phenotype consistent with the aberrant flagellar pocket morphology observed by TEM. Costaining with markers for the PFR (L8C4, green) and FAZ (L6B3, red) showed that detached flagella were associated with a reduced FAZ or in some cases with no FAZ at all. E) Costaining of induced cells with L8C4 (red) and a-TgMORN1 (green) showed that in all cells the ring and finger localisation of a-TgMORN1 was absent although the posterior signal remained, acting as a serendipitous marker for antibody efficacy in these samples. Blue = DAPI, bar = 5μm.

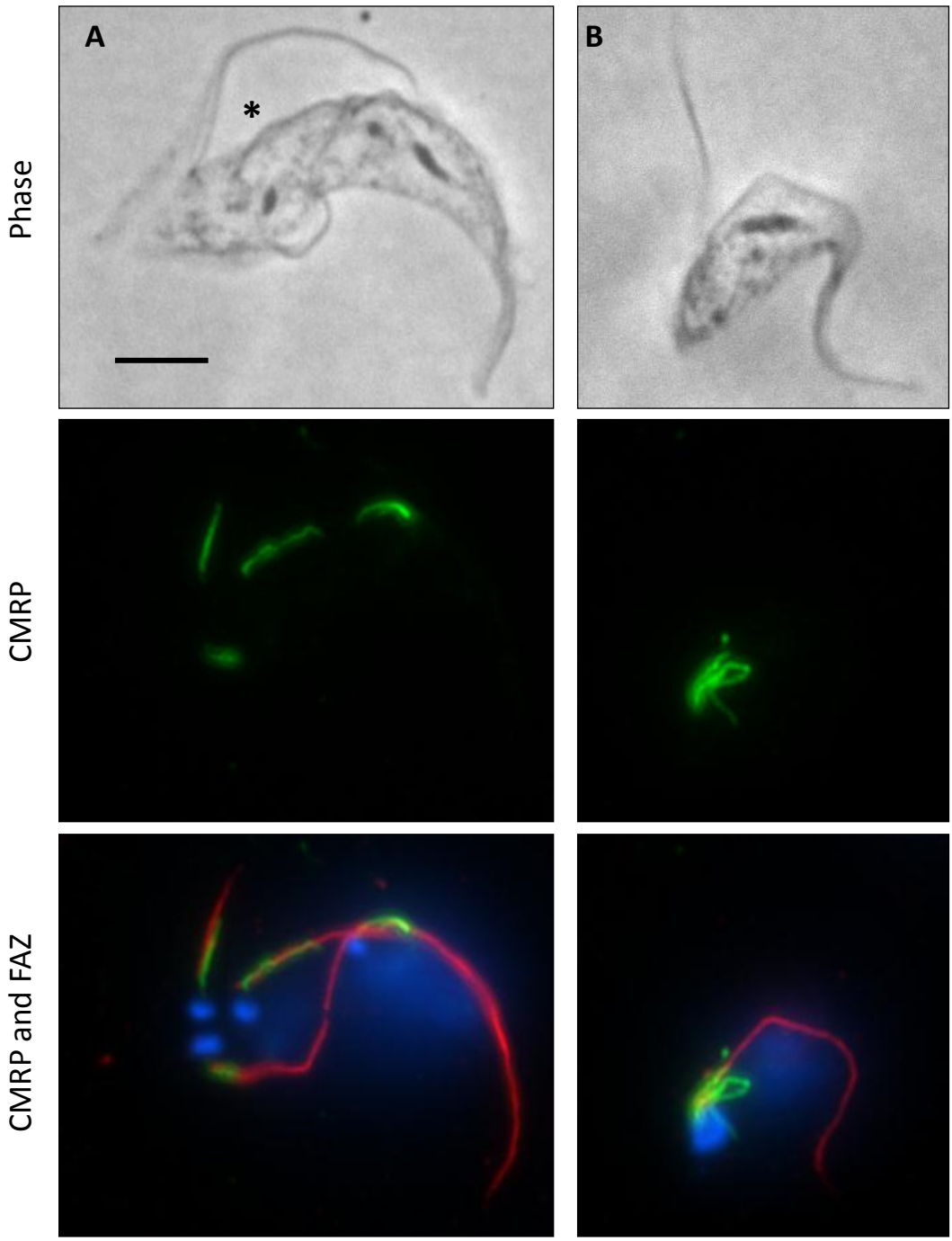

Figure 5.14. Ablation of BILBO1 causes mislocalisation of CMRP. RNAi against BILBO1 was induced for 48 hours in cells expressing Ty::CMRP from one of the endogenous loci. The cells were extracted with detergent and fixed in methanol before examination by fluorescence microscopy with costaining for Ty::CMRP (BB2, green) and the FAZ (L6B3, red). Loss of BILBO1 protein resulted in the loss of the CMRP ring and finger morphology. Instead, CMRP formed strings of fluorescence either A) along a FAZ where one is present or B) folding back into the cell body in the vicinity of the base of the flagellum in the absence of a FAZ structure. Interestingly, these strings of fluorescence were observed to be associated with all flagella, including those which had presumably been formed with intact flagellar pockets before RNAi induction (A - *). Blue = DAPI, bar = 5μm.

albeit in an aberrant configuration. This suggests that at least part of the transport or retention machinery required for the correct localisation of CMRP is not dependent on the presence of BILBO1.

Chapter 6

Discussion

6.1. Discussion of Chapter 3 – The PFR

The aim of this work was to establish a method that combines RNAi ablation of proteins of interest with comparative proteomics techniques to generate proteomes for flagellar substructures and provide additional information about protein-protein interactions within these sub-structures. Applying this protocol to the well characterised *T. brucei* PFR mutant *snl2* has identified 30 proteins as components of the PFR. Furthermore, this process of RNAi ablation and comparative proteomics has been iterated with novel PFR proteins to define a subset of interdependent components within the cohort. Whether the detected dependencies are due to interactions in the final PFR structure or are a result of the process of transporting proteins to the flagellum remains to be determined. Studies in *T. brucei* benefit from the availability of a completed and well annotated genome (Berriman, Ghedin et al. 2005) as well as a wealth of functional genomics tools. This organism is an excellent model for the study of many eukaryotic cell processes, such as flagellar function, as well as being an important parasite in its own right. For general future use, the reiteration of this RNAi mutant/proteomic approach at the level of individual proteins shows it to have high sensitivity in revealing sub-cohort protein dependencies.

6.1.1. Previously identified PFR components.

Previous studies have identified 15 proteins as PFR components in Trypanosome or *Leishmania* species, based either on interactions, localisation, bioinformatics or a combination of these approaches (Saborio, Manuel Hernandez et al. 1989; Woodward, Carden et al. 1994; Imboden, Muller et al. 1995; Fouts, Stryker et al. 1998; Ridgley, Webster et al. 2000; Libusova, Sulimenko et al. 2004; Pullen, Ginger et al. 2004; Clark, Kovtunovych et al. 2005; Oberholzer, Marti et al. 2007). Eight of these previously identified PFR proteins were identified in the analysis presented here along with an additional 20 previously hypothetical proteins and two annotated proteins that have not previously been identified as PFR components (KMP-11 and PI3 related-kinase). As PFR2 was the RNAi target in the snl2 cell line it was expected that the level of PFR2 protein would be significantly

reduced and this was indeed the case, both by DIGE and iTRAQ analyses. The other major component of the PFR, PFR1 is also reduced and although it is difficult to resolve these two proteins using 2D-DIGE the average $\log_2$ ratios of induced to non-induced samples detected by iTRAQ were -2.4 (PFR1) and -2.6 (PFR2) which is consistent with a near stoichiometric loss of these two proteins after PFR2 RNAi. Four other proteins have previously been given the soubriquet PFR (or PAR) (Saborio, Manuel Hernandez et al. 1989; Fouts, Stryker et al. 1998; Clark, Kovtunovych et al. 2005) and of these PAR1 and PFR5 are both present in the dataset.

Calmodulin has been shown to localise to the proximal and distal domains of the PFR as well as to the fibres attaching the PFR to the axoneme (Ridgley, Webster et al. 2000). Consistent with this, calmodulin was identified using iTRAQ as being reduced following RNAi ablation of the PFR structure in the *snl2* cell line. There is evidence that calmodulin interacts directly with one of the major PFR components (Ridgley, Webster et al. 2000) and several novel proteins described in this analysis have pfam motifs (http://pfam.sanger.ac.uk/) predicted as calmodulin- or calcium-binding domains. In the original proteomic analysis of the *snl2* mutant (Pullen, Ginger et al. 2004) two novel adenylate kinases were identified as PFR components. These two proteins, designated ADKA and ADKB, have an unusual N-terminal extension that is both necessary and sufficient for localisation to the PFR. Interestingly, neither ADKA nor ADKB were observed by iTRAQ within the criteria used in this analysis but both were identified in the DIGE comparisons and are included in the final dataset on this basis. Similarly a number of proteins were detected only by iTRAQ which supports the use of both comparative methods to more fully explore the samples. The final previously known PFR component detected in this screen is the repetitive protein known as Tb5.20. This protein was isolated from a cDNA library using a complex antisera raised against *T. brucei* cytoskeletons and specific antibodies to Tb5.20 (Woodward, Carden et al. 1994) localise along the whole length of the PFR.

Seven proteins that have previously been proposed as PFR components are not in the final dataset: gamma tubulin, PAR4, PFR5, TbI2, TbI17, PDEB1 and PDEB2 (Imboden, Muller et al. 1995; Fouts,

Stryker et al. 1998; Libusova, Sulimenko et al. 2004; Clark, Kovtunovych et al. 2005; Oberholzer, Marti et al. 2007). Their absence could be due to sampling variations, low protein abundance, masking by other proteins in the case of DIGE or physical properties that may be refractory to MS identification. However, such absences might indicate discreet localisation in the PFR substructures that are not ablated by RNAi against PFR2 such as the proximal domain or the links to the axoneme and FAZ (Bastin, Sherwin et al. 1998).

6.1.2. Novel PFR components.

Two proteins identified in this dataset have a pre-existing annotation but have not previously been identified as PFR components. KMP-11 is a conserved membrane protein of kinetoplastids that is mainly associated with the developmental form present in the insect vector where it has been localised to the flagellum and flagellar pocket (Stebeck, Beecroft et al. 1995; Berberich, Machado et al. 1998). A recent examination of the KMP-11 RNAi phenotype in *T. brucei* has suggested a role for this protein in regulating basal body segregation with additional consequences for nuclear and cell division (Li and Wang 2008). Interestingly, a feature of this phenotype was the inability of cells to correctly assemble the FAZ filament in the procyclic but not the bloodstream form. A FAZ is still made in the *snl2* mutant as evidenced by the attachment of flagella to the cell body and so this suggests that KMP-11 may have a complex localisation within the PFR such that only a portion of the protein is lost after PFR2 ablation. Tb11.01.6300 is annotated in the *T. brucei* genome as a PI3-related kinase by homology and my analysis of the predicted physical properties of the protein would support this. The family of PI3-related kinases do not phosphorylate lipids but instead have a ser/thr protein kinase activity (Abraham 2004). A function for this protein in the PFR has not yet been determined but a number of proteins identified in this analysis migrate on 2D gels with a multi-spot pattern that suggests a role for protein phosphorylation in the PFR.

I have also identified 20 proteins previously annotated as conserved hypothetical as components of the PFR and have verified seven of these by immuno-localisation at the light microscope level.

Various bioinformatics strategies were used as an initial screen to probe for possible functions for these novel proteins and identified a number of interesting patterns. Six PFR proteins, representing 20% of the dataset and including previously known components, have domains associated with calcium sensing and taken together with the previously published interactions of calmodulin with PFR1/2 (Ridgley, Webster et al. 2000) this suggests an important role for calcium regulation in the PFR. Five of the identified proteins contain the PFR domain, an automatic annotation based on homology between PFR1 and PFR2. Perhaps unsurprisingly, PFR5, which was first identified as a PFR protein based on its homology to PFR1/2, contains this domain but it is also present in PAR1 and Tb5.20. An intriguing domain found in this bioinformatics analysis is the Beige/BEACH pfam domain of PFC10. In humans a protein containing this domain is implicated in Chediak-Higashi syndrome, an autosomal recessive disease likely resulting from abnormalities in vesicular transport. However none of the pathology associated with this syndrome is likely to be caused as a result of flagella/cilia dysfunctions.

6.1.3. Interactions and dependencies within the PFR

In a recent study conducted by Sylvain Lacomble (Lacomble, Portman et al. 2009), eight novel protein-protein interactions within the PFR were discovered using a yeast two hybrid screen of 28 PFR components. All of the interactions identified fall into two clusters. The smaller cluster consists of PFC4 and PFC16 that share a 21 amino acid motif. RNAi/epitope tagging analyses revealed an intriguing relationship between these two proteins in that absence of one results in an additional higher mobility band for the other by Western blot. The larger cluster involves eight proteins (one fifth of all identified PFR proteins including several that contain the automatically predicted PFR domain) centred around two main hub interacting proteins, PFC3 and PFR5 which interact directly with each other. PFC3 also interacts with two PFR domain containing proteins (PAR1, PFR5) as well as interacting with itself. I went on to investigate the key interaction partnership of PFC3/PAR1 by RNAi/DiGE analysis which has the power to provide context to the yeast two-hybrid data. While yeast two-hybrid analysis showed an interaction between PFC3 and PAR1, RNAi/DiGE provided an insight

into the nature of this interaction in that PFC3 and PAR1 are mutually dependent on each other for correct assembly into the PFR structure. My RNAi/DiGE analyses also revealed dependency relationships not detected in the yeast two-hybrid screen with incorporation of both PFC5 and PFC17 being dependent upon the presence of PFC3/PAR1. RNAi ablation of PFC5 did not affect the assembly of PFC3, PAR1 or PFC17 which suggests a hierarchical directionality to this dependency network.

One surprising, and likely significant result from this analysis is that a successful ablation by RNAi of the PFC3/PAR1 network results in no gross changes in the morphology of the PFR polymeric structure. This may represent evidence that the three major zones of the PFR and their distinct morphologies are heavily reliant for their formation on only a relatively few structural proteins, perhaps PFR1 and PFR2 (the only proteins that have been shown to localise to the PFR whose ablation results in a failure of PFR assembly). A picture then emerges of these few structural proteins being responsible for the major PFR lattice structure onto which is built a cohort of numerous other proteins with domain architectures suggesting a role in metabolism, signalling and regulation. It seems unlikely that abundant proteins such as PFC3 and PAR1, that are important enough to be conserved in the genomes of every sequenced trypanosomatid, lack a function. In these terms insights into the functions of these network proteins must await the development of more sensitive phenotype tests.

6.1.4. Dependency subgroups provide clues about the role of the PFR in the regulation of flagellar motility.

In this work I have also demonstrated a reciprocal dependency relationship between two novel PFR proteins; PFC1 and PFC15. These two proteins were chosen for further study as domain predictions suggested a role in a potential PFR calcium signalling network as also suggested by the localisation of calmodulin to the PFR and the finding that it interacts with the major PFR components (Ridgley, Webster et al. 2000). Intriguingly, the PFC1/PFC15 relationship involves the previously identified PFR-specific adenylate kinases ADKA and ADKB (Pullen, Ginger et al. 2004). Roles for calcium signalling

and adenine nucleotides (in addition to the role of ATP as an energy source) in the regulation of flagellar and dynein arm function are well established and the results presented here may point towards these two systems being linked in the trypanosome PFR. I hypothesise that adenylate kinase function in the PFR responds to changes in calcium concentration to regulate adenine nucleotide homeostasis in the flagellar compartment. This could function to directly regulate the activity of dynein arms (Yagi 2000; Inoue and Shingyoji 2007) or perhaps provide and/or limit substrates for calcium regulated cyclic nucleotide signalling pathways that have been described in the flagellum, and shown to influence the mode of flagellar motility (Bonini and Nelson 1988; Bonini, Evans et al. 1991). This could then provide a mechanism for calcium regulated control of flagellar waveform. Flagellar wave reversal, changes in wave form and regulation of microtubule sliding as a response to changes in calcium concentration have been described in a number of organisms, including trypanosomes (Naitoh and Kaneko 1972; Holwill and McGregor 1976; Hyams and Borisy 1978; Brokaw 1979; Johnson and Brokaw 1979; Okuno and Brokaw 1979; Bessen, Fay et al. 1980; Cosson, Tang et al. 1983; Kamiya and Witman 1984; Omoto and Brokaw 1985; Bannai, Yoshimura et al. 2000; Smith 2002) and recent work has demonstrated the switching from flagellar to ciliary waveform in three species closely related to *T. brucei* (Gadelha, Wickstead et al. 2007). Calcium regulation is also an important factor in the hyperactivation of mammalian sperm which involves changes in the flagellar beat (Quill, Sugden et al. 2003). Substantial evidence points to the central pair complex and radial spokes as key transducers of calcium signals to the dynein arms in *C. reinhardtii* (Smith and Yang 2004) and calmodulin has been localised to both of these structures (Wargo, Dymek et al. 2005; Dymek and Smith 2007). Analysis of *C. reinhardtii* mutants suggests that the outer dynein arms control the beat frequency of the flagellum whereas the inner dynein arms are responsible for the shape of the waveform (Brokaw and Kamiya 1987). In trypanosomes, however, it appears that beat frequency can be maintained in the absence of outer dynein arms, although the direction of wave propagation is reversed (Branche, Kohl et al. 2006). This highlights differences in the regulation of

flagellar motility between these organisms, another example being the fixed central pair position of trypanosomes compared to the rotating central pair of *Chlamydomonas*.

Regulation of adenylate kinase function by calcium has previously been reported in other organisms, including in the flagellum of sea-urchin sperm (Notari, Pepe et al. 2001; Notari, Morelli et al. 2003; Kinukawa and Vacquier 2007) and two adenylate kinases have been localised to the fibrous sheath of mouse sperm flagella (Cao, Gerton et al. 2006), a structure to which a number of intriguing parallels can be drawn to the PFR (Oberholzer, Bregy et al. 2007), suggesting that this could be a more general feature of flagellar beat regulation in other eukaryotes.

Recent work has shown that the mammalian bloodstream form of *T. brucei* is exquisitely sensitive to loss of the PFR as a result of RNAi ablation of PFR2 (Broadhead, Dawe et al. 2006). In the procyclic form loss of the PFR results in severely impaired flagellar motility leading to a loss of cell motility but the cells continue to divide normally and are viable in culture for extended periods (Bastin, Sherwin et al. 1998). In the bloodstream form loss of the PFR rapidly leads to a failure in cytokinesis and accumulation of monstrous cells with multiple nuclei, kinetoplasts and flagella. Infecting mice with such cells and then inducing RNAi allows the animal to completely clear a normally lethal challenge by this parasite (Griffiths, Portman et al. 2007). RNAi mutants affecting axonemal components give a similar phenotype in the bloodstream form suggesting that impaired motility is the major factor in this phenotype and not a specific effect of PFR ablation. The RIT-seq study conducted by Horn and co-workers (Alsford, Turner et al. 2011) confirmed the particular importance of flagellar function in the bloodstream form in terms of cell viability. However, the restricted evolutionary distribution of the PFR structure compared to the more conserved components of the axoneme makes this a particularly valuable result from the viewpoint of therapeutic potential.

6.2. Discussion of Chapter 4 – Comparison of BSF and PCF cytoskeletons

The aim of this part of the project was to take advantage of the structural differences between long slender bloodstream form trypomastigotes and procyclic form trypomastigotes to identify novel components of life-cycle stage-specific structures with particular focus on the identification of components of the elusive flagella connector.

6.2.1. Mechanisms of false discovery in gel-based comparative proteomics

In comparisons of both flagella and cytoskeletons from bloodstream form and procyclic form cells a number of the identified proteins are unlikely to be bona fide regulated cytoskeletal proteins. There are numerous possible explanations for the presence of such proteins in the lists. Some proteins, such as VSG, do show life-cycle stage specific expression but are highly unlikely to be components of the cytoskeleton. It is likely that such proteins, being very highly abundant, are inevitable contaminants of the preparation. Other proteins that are highly abundant in the cell may also contaminate the preparations in a stochastic manner, appearing more strongly in some preparations than others. In using a gel-based method there is also the risk of contaminating identifications, i.e. multiple identifications from a single spot. In some cases this may be from different proteins genuinely running together so as to be unresolved under the conditions used. In these cases it becomes difficult to determine which proteins contributed to any observed differences between the samples being analysed. In other cases, highly abundant proteins that are 'legitimately' present in the preparation, such as alpha and beta tubulin in the case of cytoskeletal preparations, may also contaminate other spots. These can often be detected in the list of identifications from a spot if the molecular weight and/or isoelectric point of the protein do not match the area of the gel from which the spot was cut, although post-translational modifications and break-down products can complicate this approach in terms of the identification of both false positives and false negatives. Another form of possible contamination is from misidentified peptides. The algorithms used in peak matching software yield probability-based peptide identifications and therefore some level of false discovery is inevitable. Again, checking the position of the spot on the gel relative to the predicted mass and

isoelectric point of an identified protein and the requirement for at least two unique peptide identifications go some way towards ameliorating this problem.

6.2.2. Exploiting life-cycle stage specificity: an approach to the interrogation of the flagella connector

The flagella connector is a mobile transmembrane junction that connects the tip of the growing new flagellum to the lateral face of the old flagellum in procyclic form cells (and probably mesocyclic forms prior to asymmetric division). In this way it transmits positional information from the old flagellum to the new one in a form of cytotaxis (Moreira-Leite, Sherwin et al. 2001; Briggs, McKean et al. 2004). No such structure has been described in bloodstream form trypomastigotes which may reflect the immune evasion strategy of the parasites which functions by limiting the exposure of invariant surface antigens to the host immune system. I exploited this difference in the cell biology of the two forms to attempt to identify novel components of the flagella connector. By conducting a proteomic comparison of flagella from procyclic forms to that of bloodstream forms I generated a list of 46 candidate proteins. Based on the observation that the flagella connector has domains inside both the old and new flagellar membranes as well as spanning the gap between these membranes, I hypothesised that some flagella connector proteins would contain transmembrane domains and used this criterion to screen the list of candidates. This identified two of the candidate proteins as potential transmembrane proteins, with each predicted to contain two transmembrane domains. I tagged both of these proteins at the C terminus to avoid any possible interference with signal peptides and found that one of them, FCP1, localised to the flagella connector and the other, PFAZ, localised to the FAZ in procyclic forms.

6.2.3. Identification of the first component of the flagella connector.

The presence of FCP1 as five spots on 2D gels with a similar apparent molecular weight but incrementally different isoelectric points suggests that the protein is modified, most likely given the spot pattern by phosphorylation. It has previously been shown that the anti-phosphoprotein

antibody MPM2 recognises epitopes at the flagella connector, demonstrating the presence of phosphorylation in this structure (Davidge, Chambers et al. 2006). Given the hypothesis that the flagella connector plays an important role in the segregation of basal bodies in procyclic forms (Briggs, McKean et al. 2004; Davidge, Chambers et al. 2006), it was somewhat surprising to find that RNAi-mediated ablation of FCP1 had no apparent effect on the morphology or growth of cells. The antigen recognised by the AB1 antibody still localised to the flagella connector, however, suggesting that a connector still forms and retains its function. The RIT-seq screen recently conducted by Horn and co-workers (Alsford, Turner et al. 2011) supported my finding that loss of FCP1 in procyclic forms had no effect on the growth rate of populations. Interestingly, this study also found that loss of FCP1 did have an effect on the fitness of bloodstream form cells. It is possible that FCP1 functions in an as yet unidentified flagella connector structure in the bloodstream form, possibly a transitory connection perhaps only present while the tip of the new flagellum is still contained within the flagellar pocket. Another possibility, supported by the presence of FCP1 homologues in *Leishmania spp.* and *T. cruzi*, which are not known to form a flagella connector, is that FCP1 performs a different function in bloodstream forms, perhaps not related to flagellar function or growth, and that its presence in the flagella connector is a secondary adaptation. Both of these possibilities would account for the observed absence (or reduction below the level of detection in the case of a transitory flagella connector) of FCP1 in flagella purified from bloodstream form cells. Horn and co-workers measured the fitness costs of RNAi within a mixed population of cells and therefore did not analyse the particular morphologies of mutants associated with a loss of fitness. Targeted studies of the FCP1 RNAi phenotype in bloodstream form cells are likely to yield further insights into the functions of this protein.

6.2.4. PFAZ, a novel component of the FAZ

The second protein identified in this analysis, PFAZ, localised alongside the flagellum between markers for the cell body component of the FAZ and the PFR in procyclic form cells. This is consistent with a position in the extracellular portion of the FAZ between the plasma membrane and the

flagellar membrane, supported by the presence of predicted transmembrane domains within the protein sequence. Unfortunately I was unable to recover bloodstream form transfectants with tagged PFAZ and was therefore unable to confirm the life-cycle stage specificity suggested by the comparative proteomics approach. Interestingly, my bioinformatics analysis of the PFAZ sequence identified a pair of paralogous proteins in the *T. brucei* genome which I have tentatively named BFAZ based on their apparent requirement in the bloodstream form but not the procyclic form as demonstrated in the RIT-seq screen discussed earlier (Alsford, Turner et al. 2011). Again, my efforts to tag BFAZ1 or BFAZ2 in the bloodstream form proved futile and further analysis must await a more successful tagging strategy or the development of specific antibodies to the proteins. It is interesting to note, however, that there is precedent for life-cycle stage-specific proteins in the FAZ. There is evidence that one of the most well-known and well-studied of the identified FAZ proteins, fla1, is procyclic form specific (or is at least more abundant in the procyclic form than the bloodstream form) and that one or both of its paralogues in the *T. brucei* genome, fla2 and fla3, are expressed mainly in the bloodstream form (Koumandou, Natesan et al. 2008). Recent work from Bastin and co-workers (Rotureau, Subota et al. 2011) has also provided evidence for a remodelling of the FAZ during the life-cycle transition from mesocyclic to epimastigote forms in the tsetse proventriculus. In this work, two components of the FAZ, FAZ1 (Vaughan, Kohl et al. 2008) and the as yet unidentified DOT1 antigen, were shown to drop below detectable levels during the morphological remodelling preceding the asymmetric division that forms the long and short epimastigotes. Both proteins were subsequently detectable in the short daughter cell but remained absent in the long daughter cell. These authors hypothesised that this remodelling of the FAZ may be linked to the migration of the nucleus (which remains attached to the FAZ after detergent extraction) towards the posterior of the cell in the mesocyclic form.

6.2.4. Novel paralogous cytoskeletal proteins with life-cycle stage-specificity

The finding over recent years of several sets of paralogous cytoskeletal proteins with life-cycle stage-specificity prompted me to extend my comparison of bloodstream and procyclic forms to an analysis

of cytoskeletal components. Using DIGE I identified numerous proteins that showed greater abundance in one or other of the two lifecycle stages analysed. These included both CAP5.5 and CAP5.5V that comfortingly showed greater abundance in samples from the appropriate life-cycle stage (procyclic form and bloodstream form respectively) (Olego-Fernandez, Vaughan et al. 2009). 18 of the identified proteins were annotated as hypothetical and the curated orthologue group for each of these was obtained from TriTrypDB. Two pairs of proteins in the dataset shared an orthologue group and of these SAP-P and SAP-B exhibited a pattern of life-cycle stage expression whereby one (SAP-P) was identified from a spot that was more abundant in procyclic from samples and the other (SAP-B) was identified from a spot that was more abundant in bloodstream form samples. The primary sequences of the two proteins could be divided into four domains based on the level of homology. Domain 1 and domain 3 share significant identity whereas domain 4 is more divergent. No significant homology could be detected in domain 2. This domain contains an insert in the bloodstream form protein that consists of a complicated lysine-rich repeat unit. No annotated functional domains could be detected other than a predicted propensity to form coiled-coils in domains 3 and 4. The genomes of *L. major* and *T. cruzi* both encode a single SAP orthologue and BLASTP analysis detected no related proteins outside the *Kinetoplastida*.

By fluorescently tagging each protein in each life-cycle stage I was able to confirm life-cycle stage-specific expression and localise the proteins to the cytoskeletal microtubule array in their respective life-cycle stages. Both proteins decorated the array evenly throughout the cell cycle, with the exception of the extreme posterior end of procyclic form cells where no SAP-P was detected. Several studies have shown that there are differences in the regulation of microtubules at the posterior end of procyclic and bloodstream form cells, strikingly displayed by the nozzle phenotype in the procyclic form (Hendriks, Robinson et al. 2001; Hammarton, Engstler et al. 2004). Overexpression of the small CCCH-zinc finger protein, TbZFP2, or RNAi-mediated ablation of the cyclin CYC2, results in a polar extension of microtubules at the posterior end of procyclic form but not bloodstream cells. This extension specifically increases the length of the posterior end of the cells (to form a ‘nozzle’)

without affecting any other cell dimensions or organelle positioning. RNAi ablation of TbZFP2 in the bloodstream form inhibits subsequent differentiation to the procyclic form whereas CYC2 plays a role in cell cycle progression in both bloodstream and procyclic form cells. Although further characterisation of the functions of SAP-P would be required to more fully explore any relationship between the absence of this protein from the posterior end of procyclic form cells and the specific regulation of microtubule extension in this life-cycle stage, it is possible that this life-cycle stage-specific regulation requires the exclusion of certain cytoskeletal components from the posterior end of the cell.

RNAi-mediated knockdown of both SAP proteins in their respective life-cycle stages resulted in a slow growth phenotype accompanied by the accumulation of cells with aberrant morphologies. SAP proteins were lost preferentially from the posterior end of cells during the induction. As discussed above, during the cell cycle, cells become both longer and wider prior to cell division. This mechanism may go some way to explain the pattern of loss of SAP proteins in that within a single cell cycle microtubules at the posterior of the cell extend in the absence of new protein. The apparent loss of protein at the posterior of the cell would therefore more properly be considered a loss of gain of protein and would argue for a very low turnover of existing protein already associated with the cytoskeleton. Although the loss of gain would also presumably be occurring at the sites (or potential sites) of new microtubule intercalation, this may be disguised at the level of immunofluorescence analysis by the presence of old protein associated with the existing microtubule array. An opposing model would be that during the extensive remodelling associated with cell growth and division, cytoskeletal proteins are actively stripped from microtubules during microtubule elongation and intercalation and rapidly replaced. In this way an absence of new protein would be most readily observed at the dynamic posterior end of the cell. This pattern of protein loss is consistent with that previously described for RNAi against other cytoskeletal proteins such as CAP5.5 and WCB (Baines and Gull 2008; Olego-Fernandez, Vaughan et al. 2009).

In the procyclic form, at timepoints prior to the appearance of large numbers of multi-nucleate cells, 2N cells exhibited a particular morphology characterised by a distortion of the cell shape such that the diameter of the mid-portion of the cell appeared abnormally large. Thinsection TEM analysis of cells from the same population revealed distortions to the microtubule array and the presence of individual microtubules that were associated with, but not intercalated into the array. Taken together these data are consistent with a model whereby intercalation of short new microtubules into the array during the cell cycle occurs (increasing the mid-point diameter of the cell) but that when these microtubules subsequently extend the growing ends are not able to intercalate into the array (Sherwin and Gull 1989). The mechanism whereby short microtubules intercalate into the array is not currently known although it is thought that proteins associated with the existing microtubules mark the sites where this integration will occur. The connections between existing microtubules must be severed to accommodate the growing ends of the new microtubules during their extension into the array. I hypothesise that the SAP proteins play a role in this severing of inter-microtubule connections during the process of cell volume increase, perhaps in conjunction with the calpain-like CAP5.5 and CAP5.5V proteins that also show life-cycle stage specificity and ablation of which results in a similar phenotype to that described here (Hertz-Fowler, Ersfeld et al. 2001; Olego-Fernandez, Vaughan et al. 2009). Loss of the inter-microtubule connection severing function could prevent the intercalation of the growing ends of new microtubules, but not necessarily the incorporation of the short nucleating microtubules. This could then lead to the distortions in cell morphology seen in both life cycle stages and the subsequent accumulation of monstrous cells and zoids due to organelle and cleavage furrow mispositioning.

By tagging both proteins in the bloodstream form I was able to assay the loss of SAP-B and gain of SAP-P during in vitro differentiation to procyclic forms. SAP-P first appeared at the posterior end of cells between 16 and 24 hours after induction of differentiation, a pattern consistent with that observed previously for CAP5.5 (Matthews and Gull 1994). By contrast, SAP-B disappeared evenly across the whole cell body during differentiation and analysis of the cells by western blot showed

that this was accompanied by an apparent increase in the molecular weight of a proportion of the protein by 24 hours with all remaining protein present at the higher molecular weight by 48 hours. This shift in mobility on the gel corresponds to an increase in molecular weight of approximately 10kDa which is consistent with the approximate shift that would result from a mono-ubiquitination event. Ubiquitination is associated with marking proteins for degradation or for relocation in the cell and this would certainly correlate with the observed behaviour of SAP-B during differentiation.

6.2.5. Why does the cell require two versions of some cytoskeletal components?

I have also shown that expressing SAP-B in procyclic forms or SAP-P in bloodstream forms from ectopic loci in parental backgrounds with RNAi against the endogenous protein completely rescues the RNAi phenotype. The ectopic protein localises to the subpellicular array and rescued cells exhibit normal morphologies in terms of nucleus and kinetoplast positioning. Initial results from experiments which are not included here suggest that bloodstream form cells expressing ectopic SAP-P in a SAP-B RNAi background are still able to differentiate into procyclic forms.

The results from this section raise the question of why two versions of this protein with such strict life-cycle stage regulation are needed in the cell if localisation and function are not life-cycle stage specific. It is possible that over time small, initially undetectable aberrant phenotypes will accumulate although rescued cells have been kept in culture under induction for several weeks with no apparent detrimental effects. It is also possible that residual expression of the endogenous protein, bolstered by the presence of ectopic protein, is sufficient for normal cell functions. Full gene conversions of both alleles for the endogenous protein would be needed to address this and these experiments are currently on-going. Another possibility is that differential SAP functions are actually required in life-cycle stages that were not examined in this study and that the expression pattern observed is actually a residual effect from a previous life-cycle stage or a pre-adaptation in preparation for a forthcoming differentiation event. For technical reasons this study was carried out using monomorphic bloodstream form cells that are able to differentiate into procyclic forms

without the need to pass through the intervening stumpy form phenotype exhibited by wild type pleomorphic cells (Li, Li et al. 2003). The differentiation from proliferative long-slender to growth arrested stumpy bloodstream forms involves significant changes to cell shape which necessitates restructuring of the cytoskeletal array (Tyler, Matthews et al. 2001). Similarly, the transition from procyclic form to mesocyclic form in the tsetse proventriculus involves a drastic change in cell morphology, again mediated by restructuring of the cytoskeleton (Sharma, Peacock et al. 2008). It is possible that it is during such restructuring processes during the life-cycle rather than those that occur in the individual cell cycles that a difference in SAP functions might be required.

6.3. Discussion of Chapter 5 – The Flagellar pocket collar

Although the existence of the FPC has been known about for many years and several recent papers have included partial descriptions of the morphology of the FPC or have identified novel FPC components, a full description of the FPC at the EM level has not yet been forthcoming. In this work I have provided the first full description of the morphology of the FPC in procyclic form *T. brucei* using electron tomography. Originally described as a ring surrounding the flagellar exit point, the FPC has also been identified as horseshoe shaped. This discrepancy is due to uncertainty over whether the FPC is a continuous ring that encompasses the mtq as it passes through the neck region. I have shown here that the electron dense material of the FPC directly abuts the mtq on both sides and that further electron dense material exists between the microtubules of the quartet specifically where they pass through the FPC. Currently the FPC is defined as the electron dense structure visible in thin section electron microscopy and the debate over whether the material I have observed associated with the mtq should properly be considered to be bona fide FPC material, and hence whether the FPC should be thought of as ring shaped or horseshoe shaped, will doubtless continue amongst interested parties until the composition of the FPC can be more fully defined at the molecular level.

6.3.1. FPC substructure and shape

Although the precise molecular composition of the FPC remains to be defined, my tomographic analysis has identified novel complexity in the morphology of the structure. For most of its circuit around the neck, the FPC maintains an approximately constant distance from the neck membrane and within the resulting gap, including the area adjacent to the mtq, discreet pillar-like connections can be observed. Further connections can be detected crossing the neck lumen to connect the neck membrane to the flagellar membrane although it is not clear whether these are a direct continuation of the connections from the FPC. This correlates with the finding of rings of intramembrane particles in the neck membrane that correspond to the position of the FPC (Henley, Lee et al. 1978; Gadelha, Rothery et al. 2009) and reinforces the hypothesis that the FPC associates directly with the flagellum. The function of these connections has yet to be determined; they could generate the tight

membrane junction necessary to restrict ingress and egress to the flagellar pocket or perhaps serve as a marker for the flagellar membrane to differentiate between cell body internal and external domains. They may even mark the position of the initiation of PFR assembly, although this last can be largely discounted due to the finding that the position of PFR assembly is preserved in the absence of a FPC (Bonhivers, Nowacki et al. 2008).

I have also shown that the main FPC structure directly contacts the neck membrane in an area adjacent to the microtubule quartet and directly opposite the position of the neck microtubule (Lacomble, Vaughan et al. 2009). The recently described neck microtubule follows the helical progress of the microtubule quartet around the neck from a point adjacent to the FPC to where the quartet joins the subpellicular array. The maculae and filament of the FAZ initiate just beyond the FPC and lie between the quartet and the neck microtubule. So far the function of the neck microtubule has not been determined, it may stabilise the neck or perhaps serve as part of a transport machinery in this region. A distinctive aspect of the FPC at this position is the lack of distance from the membrane and hence the lack of discreet identifiable connections to the membrane. Intriguingly, in the characterisation of BILBO1, Bonhivers et al (Bonhivers, Nowacki et al. 2008) presented immunogold labelling of BILBO1 that showed that, whilst most of the FPC was BILBO1 positive, two regions lacked any labelling. The first of these corresponds to the position of the microtubule quartet and the second corresponds to the area where I have shown that the FPC directly contacts the membrane. Given these data I propose that BILBO1 may be a component of the connections between the FPC and the membrane or, more likely given the lack of any identifiable membrane recognition motifs in BILBO1, an intermediary between the FPC proper (as defined by TEM) and the connections. The lack of BILBO1 labelling associated with the mtq would therefore suggest that the composition of the connections between the mtq and the neck membrane is distinct from those of the FPC or that different components are required to mediate their attachment to microtubules as opposed to FPC material.

6.3.2. FPC biogenesis: de novo or semi-conservative?

There are currently two proposed models of FPC duplication in the literature: a semi-conservative model involving elongation of the existing FPC followed by constriction to generate two FPCs proposed by Bonhivers et al (Bonhivers, Nowacki et al. 2008) and based on immunofluorescence localisation of BILBO1; and a de novo model whereby a new FPC forms around the neck of the nascent pocket after relocation of the new flagellum to the posterior side of the old flagellum proposed by Lacomble et al (Lacomble, Vaughan et al. 2010) and based on the presence of electron dense material at the nascent neck region observed in tomographic reconstructions. Given that the FPC is currently defined on the basis of its structural appearance and not its molecular composition, in the first instance the second of these models should be given priority. The semi-conservative model is compelling in its simplicity, avoiding as it does the issue of how two discreetly formed FPCs would resolve to accommodate the fact that the tip of the new flagellum is attached to the old flagellum via the flagella connector. In the semi-conservative model, the tip of the new flagellum would simply extend through a single elongated FPC which would then resolve into two discreet FPCs behind it. However, the semi-conservative model is based almost entirely on the observation of elongated FPCs by Bonhivers and co-workers. In this work I have provided an alternative interpretation of this phenotype. I have shown that the elongation of the FPC is in fact consistent with localisation of BILBO1 (and other FPC components) to the old and new mtq. At the light microscope level these extensions could easily be interpreted as an extension of the FPC proper along the long principle axis of the cell. These extensions can be observed in cells at the earliest stages of new flagellum formation, consistent with the finding by Lacomble et al (Lacomble, Vaughan et al. 2010) that initiation of the new microtubule quartet is the earliest identified event in the process of flagellar pocket biogenesis and new flagellum formation. Given the supposed role of the FPC in constricting and restricting access to or egress from the flagellar pocket, doubling the size of the FPC at this early stage in new flagellum formation would seem to be an unlikely strategy. Localisation of FPC components to the microtubule quartet could indicate a transport system for

newly synthesised FPC components along these specialised microtubules in preparation for new FPC formation, as I have shown here that the extensions contain primarily new BILBO1 protein. Perhaps a more intriguing possibility (that does not exclude an additional role as a transport system) is that these FPC components may actually perform a function at this location specifically during biogenesis of the new flagellar pocket. Lacomble et al proposed, and provided compelling evidence in support of, a model of new pocket formation whereby translocation of the new flagellum and its associated new microtubule quartet divides the existing pocket into two partially separate entities (Lacomble, Vaughan et al. 2010). The new flagellum moves from the anterior to the posterior side of the old flagellum in a rotary motion which folds the pocket over the old microtubule quartet to generate a new pocket that exits into the lumen of the existing (old) pocket. It is possible that certain FPC components (maybe those also involved in creating the connections between the FPC and the neck membrane) localise to both quartets during this process to further stabilise the interaction between the quartets and the flagellar pocket membrane to ensure faithful segregation into old and new pockets. If this were the case a failure in this regard would also provide an alternative explanation for the lack of new pocket formation observed as a result of RNAi against BILBO1 (and CMRP as described in this work).

If we consider the model that the new FPC is formed de novo, this presents the problem of how the tip of the new flagellum passes through the old FPC while attached to the lateral aspect of the old flagellum via the flagella connector. It is well established that the flagella connector is formed before translocation of the new flagellum when both flagella still invade a single pocket (Briggs, McKean et al. 2004; Lacomble, Vaughan et al. 2010). There are four possible models whereby negotiation of the old FPC by the flagella connector might occur. Firstly, the tip of the new flagellum and the connector could simply pass through the material of the old FPC. This seems unlikely given the apparent solidity of the structures involved as evidenced by their resistance to detergent and high salt treatment. Another possibility is that the flagella connector itself breaks down and reforms after the tip of the new flagellum has extended past the old FPC. Again, this seems unlikely. All of the currently available

evidence, including my own tomographic analysis and localisation of a novel component of the connector, suggests that once the connector is formed it persists through the remainder of the cell cycle until the new flagellum detaches from the old flagellum. The third possibility is that the FPC itself breaks down. Bonhivers and co-workers (Bonhivers, Nowacki et al. 2008) showed that following ablation of BILBO1 by RNAi, the old FPC remains BILBO1 positive. Although not conclusive, and given the caveat that the behaviour of BILBO1 is not necessarily indicative of the behaviour of the electron density observed by electron microscopy, this argues against a situation whereby the old FPC completely breaks down during new FPC formation. Finally the old FPC may undergo restructuring so as to 'open' and in this study I have provided some evidence that this may indeed be the case. Unfortunately I was unable to demonstrate using tomography that this situation occurs. However, examination of the fate of 'old' BILBO1 protein during FPC biogenesis is informative. Here I have shown that old BILBO1 protein accumulates on the anterior face of the old flagellum exit point in cells exhibiting the extended FPC morphology. This gives a semi-circular localisation of BILBO1 that is distinct from the horseshoe localisation seen in resolved FPCs. This leaves the posterior side of the old flagellum exit point devoid of BILBO1 signal and, if indicative of the behaviour of the FPC as a whole, would provide the necessary 'opening' to allow passage of the extending new flagellum and flagella connector which occurs on the posterior face of the old flagellum. A restructuring event to open the old FPC addresses the major concern raised by the de novo model of new FPC formation and the preservation of at least part of the old FPC correlates with the presence of BILBO1 here after ablation by RNAi. However, I have also shown that both old and new FPCs contain approximately equal amounts of old and new BILBO1 within an individual cell. Under the de novo model of new FPC formation the presence of new protein in the old FPC can be explained if a restructuring of the FPC involves the removal of protein that must then be replaced. The presence of old protein in the new FPC is slightly more problematic and appears to support the proposition of a semi-conservative pattern of inheritance. There are three possible explanations for this observation that are consistent with the de novo model. Although the population of BILBO1 localising to the extensions along the

mtq was predominantly composed of new protein, a low level of GFP signal could still be observed. It is possible that during a restructuring of the old FPC, protein is recycled onto the quartet and is later incorporated into the new FPC. To fully explain the observed results, the protein redistributed in this way would have to be approximately equal to that maintained in the old FPC. Another possibility is that switching off ectopic expression of BILBO1 by removal of the inducing agent is not 100% efficient and that residual amounts of GFP-tagged BILBO1 are still produced. In this situation the loss of GFP intensity at the old FPC would suggest that old protein is lost (but not recycled) and replaced by new protein at the old FPC and the apparently equal level of GFP labelling of the old and new FPC would demand that the residual expression level of GFP tagged BILBO1 correlates with the loss of old protein from the old FPC. An unambiguous two state expression system would be required to more conclusively differentiate between these possibilities. The final possibility is that FPC duplication proceeds by a hybrid form of semi-conservative and de novo mechanisms, dependent upon which component is being observed. Although it is somewhat difficult to reconcile the observation that two discreet regions of FPC material are present before the final resolution of two flagella exit points with a situation whereby these two bodies interact to a degree that they are able to directly share components, a definitive answer must await the identification and precise characterisation of additional components encompassing the full structure of the FPC.

6.3.3. CMRP as a component of the FPC

In this study I have provided an initial characterisation of a novel component of the FPC, CMRP. CMRP has a complex localisation consisting of a ring or horseshoe that colocalises with BILBO1 at the FPC with a finger-like projection extending from here in an anterior direction that colocalises with the posterior portion of the FAZ. Identical localisations were observed using epitope tagged CMRP or by using a polyclonal antibody raised against the *T. gondii* protein TgMORN1 (Gubbels, Vaishnava et al. 2006) which also recognised a single band with an apparent molecular weight by Western blot consistent with that predicted for CMRP. CMRP and TgMORN1 share significant homology and are both composed entirely of MORN domain repeats. TgMORN1 is associated with numerous structures

in *T. gondii* cells that play roles in cytokinesis, daughter cell formation and mitosis where it is thought to mediate interactions between membranes and the cytoskeleton (Gubbels, Vaishnava et al. 2006; Heaslip, Dzierszinski et al. 2010). The MORN domain itself is an intriguing motif that occurs in a range of proteins in both eukaryotes and bacteria and is often associated with other protein domains involved in metabolic functions or protein-protein interactions. The domain was first described as a conserved motif in a family of proteins known as junctophilins (Takeshima, Komazaki et al. 2000), which form transmembrane junctional complexes between the ER and plasma membrane in mammalian cells, and has since been well studied in a family of phosphatidylinositol phosphate kinases in plants in which an N terminal MORN repeat regulates the metabolic function and localisation of the proteins (Im, Davis et al. 2007). In both of these cases the MORN domain is involved in interactions with the plasma membrane. These data are consistent with a role for CMRP in the FPC in its role as a critical junction in the trypanosome cell that imposes a cytoskeletal influence on the adjacent membranes. In these terms it is also interesting to consider the particular localisation of CMRP during the formation of the new flagellum. As I have shown here for BILBO1, CMRP also forms two extensions around the flagellar pocket consistent with the position of the old and new mtq during the early stages of new flagellum formation and flagellar pocket biogenesis. Again as for BILBO1 this could be new protein being transported along the mtq in preparation for new FPC formation but it could also play a role in stabilising the connection of the mtq to the membrane of the flagellar pocket during this process. A protein containing motifs associated with membrane-cytoskeleton interactions would be a very attractive candidate for a role in this hypothetical scenario.

Unfortunately I was unable to determine a precise function for CMRP. RNAi-mediated ablation of the protein had no effect on the growth rate of populations over a 96 hour period and the majority of cells exhibited normal morphologies. Immunofluorescence analysis of induced cells with tagged CMRP or using the TgMORN1 antibody showed that knockdown was effective, and in these terms the additional posterior end signal exhibited by the TgMORN1 antibody served as a serendipitous

internal control, demonstrating that labelling was effective in the absence of the ring and finger signal. This posterior end signal has been observed with a number of rabbit polyclonal antibodies (Gull lab, anecdotal evidence) but has so far resisted attempts to identify the relevant antigen. In contrast to the situation following ablation of BILBO1 where protein persists at the old FPC, CMRP is absent from all FPCs by 72 hours after ablation. This could be due to turnover of assembled CMRP or dilution of the available protein by a semi-conservative inheritance during cell division. A third possibility is that as the majority of cells appear to continue to divide normally during the course of the RNAi induction, by 72 hours the majority of flagellar pockets/FPCs have formed in the absence of CMRP protein. I did, however, observe a moderate increase in the number of cells with abnormal numbers of nuclei and kinetoplasts at later timepoints in the induction as well as the appearance of cells with detached flagella, reduced FAZ and little or no kinetoplast segregation. These aberrant cells correlate with the morphologies observed by thinsection TEM where flagella were seen to emerge from the cell body directly from the cell surface or in association with a reduced flagellar pocket. Structures such as the collarette and transition zone of the basal body, normally contained well within the volume of the flagellar pocket, were present on the exterior of the cell. This phenotype is very reminiscent of that observed following ablation of BILBO1 and has been interpreted as a failure in flagellar pocket biogenesis as a result of a failure in FPC formation (Bonhivers, Nowacki et al. 2008). Although CMRP does not appear to be essential during the biogenesis of the flagellar pocket complex, it does appear to play an important role in this process. The relatively low penetrance of abnormal phenotypes caused by a loss of CMRP does not appear to be a result of heterogeneity in the effectiveness of the RNAi which suggests that there may be some redundancy to CMRP function or that the detrimental consequences of loss of CMRP are heavily influenced by other factors affecting the cell. Flagellar pocket biogenesis is a complex and highly regulated process that requires the precise coordination of numerous structures and organelles in both time and space. All structures must be faithfully duplicated and segregated and this must be accomplished in the context of at least one actively motile flagellum and a flagellar pocket that is still functioning as the sole site

for endo- and exocytosis. Although loss of CMRP does not guarantee a detrimental outcome of cell division, it does seem to make this more likely.

6.3.4. CMRP, the FPC and the bilobe

CMRP has also recently been described independently by Warren and co-workers (Morriswood, He et al. 2009) who identified a similar localisation pattern at the FPC and FAZ as shown here, but did not report a localisation to the mtq during flagellar pocket biogenesis. Interestingly, these researchers also reported a partial colocalisation of the CMRP (which they called TbMORN1) finger with the Golgi-associated bilobe, an enigmatic structure defined by a particular localisation of TbCentrin2 adjacent to the flagellar pocket neck region on the anterior side of the flagellar pocket (He, Pypaert et al. 2005). RNAi-mediated ablation of TbCentrin2 results in a failure in Golgi duplication and in basal body duplication and kinetoplast segregation. The additional localisation of TbCentrin2 to the basal bodies complicates the interpretation of this phenotype, but ablation of TbCentrin1, which localises to the basal bodies but not the bilobe, results in a similar failure in basal body duplication and kinetoplast segregation with no associated loss of Golgi duplication (He, Pypaert et al. 2005). This suggests that TbCentrin2 and by extension the bilobe plays an important role in Golgi duplication. To date no specific structure has been identified in ultrastructural studies of *T. brucei* cells that would correspond to the bilobe, but a number of other proteins have also now been identified that localise to this area. The first of these was TbCentrin4 (Shi, Franklin et al. 2008) and more recently a protein now known as TbLRRP1 which colocalises with CMRP (Zhou, Gheiratmand et al. 2010). Ablation of TbLRRP1 resulted in a similar phenotype to that which I have described here for CMRP, albeit affecting a larger proportion of cells. Basal body and kinetoplast segregation were compromised and detached flagella and reduced FAZ were observed. No gross morphological changes to the flagellar pocket were reported in this work, although the published ultrastructural examination of cells was conducted at 48 hours after induction of RNAi and it is possible that abnormalities of the flagellar pocket may occur later, as is the case for CMRP. The single *T. brucei* polo-like kinase (TbPLK) homologue also localises to this part of the cell in a cell-cycle

dependant manner (de Graffenried, Ho et al. 2008). During new flagellum biogenesis, TbPLK first appears associated with the basal bodies and the posterior lobe of the bilobe, relocating entirely to the neck region during bilobe duplication. TbPLK then appears to track the tip of the growing new FAZ and becomes undetectable at some point prior to the completion of cytokinesis and is not observed again until daughter cells begin a new round of duplication.

The lack of any ultrastructural definition of the bilobe as a discreet entity causes some problems in defining what constitutes a bilobe protein although it has become convenient shorthand for proteins that localise to the flagellar pocket neck region. The close proximity of numerous critical structures in this part of the cell means that care must be taken when assigning proteins to individual structures, particularly those defined only at the resolution of the light microscope. There is colocalisation of proteins such as CMRP and TbLRRP1 with parts of the TbCentrin2 signal, but equally these proteins colocalise with parts of the FAZ and the FPC. It is clear that there is a specialised domain at the proximal end of the FAZ that links the FAZ, FPC and Golgi although whether this is the bilobe as defined by TbCentrin2, an as yet undefined structure or a specialised portion of the FAZ or FPC has yet to be determined. It is this interconnectedness and interdependence of many of the critical structures of the cell that complicates analysis of the function of proteins involved in these structures. It has been hypothesised that the bilobe plays a crucial role in FAZ formation based on the reduction of the FAZ in TbLRRP1 RNAi mutants (Zhou, Gheiratmand et al. 2010). However, a similar reduction in the FAZ is seen after ablation of the FPC protein BILBO1, a phenotype that also results in a failure in flagellar pocket biogenesis, or after ablation of IFT components to prevent flagellum formation. The interconnectedness renders the determination of causes, direct effects and indirect effects incredibly complicated. Ablation of CMRP or TbLRRP1 results in detached flagella, but is this due to the failure of the FAZ to form as a consequence of disrupting the bilobe or is FAZ failure a consequence of flagellar detachment? Is the bilobe a critical organiser of structures in the flagellar pocket neck region or does it merely suffer the consequences of disrupting these structures? My finding that correct morphology of the CMRP-containing structure is dependent upon the presence

of BILBO1 but that CMRP still assembles with aberrant morphology in its absence demonstrates some of the complications that must be considered. The next step towards addressing questions such as these will require the integration of proteomic data, high resolution imaging, interaction mapping, phenotype analysis and further analysis of the processes and events of the cell cycle and the implications of these results when considered in terms of the spatial and temporal organisation of events and structures across multiple cell cycles.

6.4. General conclusions

Over recent years high-throughput and whole-cell analysis techniques have advanced rapidly, aided in no small part by equally rapid advancements in the speed and processing power of modern microprocessors. These advancements enable the kind of proteomic and tomographic studies that I have conducted here. As a model organism *T. brucei* is almost uniquely suited to these types of approaches. The high level of temporal and spatial organisation of the cell lends itself incredibly well to interrogation at the ultrastructural level using electron tomography and the availability of a completed and well annotated genome, in conjunction with the inherent lack of introns in the genome, are a boon to both genomic and proteomic analyses. The well-established and widely available molecular biological toolkit enables the rapid translation of candidate screens into analyses of protein localisations, functions and interactions. Numerous high-throughput screens have provided cellular level analyses of proteomic composition, mRNA level and protein function, incredibly valuable data that are actively curated and included in readily accessible databases such as GeneDB and TriTrypDB.

In this project I sought to determine some of the components and functions of several *T. brucei* cytoskeletal structures associated with the flagellum. I have employed comparative proteomics approaches combined with RNAi mutants or the naturally occurring differences in *T. brucei* life-cycle stages to identify novel components of the PFR, FAZ and flagella connector and have identified a number of interdependent sub-groups of proteins within the PFR structure. I have provided the first full description of the morphology of the flagella pocket FPC and provided new data that will advance

the debate over the composition of the FPC, its functions and its biogenesis. In a slight digression from the flagellum-associated cytoskeleton I have also identified novel components of the subpellicular array that show life-cycle stage-dependent expression. This adds to a growing body of work that seeks to address the differences and similarities between life-cycle stages and raises intriguing questions concerning the requirement for stage-specific protein variants in the cytoskeleton.

Chapter 7

References

Abraham, R. T. (2004). "PI 3-kinase related kinases: 'big' players in stress-induced signaling pathways." DNA Repair (Amst) **3**(8-9): 883-887.

Absalon, S., T. Blisnick, et al. (2008). "Intraflagellar transport and functional analysis of genes required for flagellum formation in trypanosomes." Mol Biol Cell **19**(3): 929-944.

Alsford, S., D. J. Turner, et al. (2011). "High-throughput phenotyping using parallel sequencing of RNA interference targets in the African trypanosome." Genome Res **21**(6): 915-924.

Baines, A. and K. Gull (2008). "WCB is a C2 domain protein defining the plasma membrane - sub-pellicular microtubule corset of kinetoplastid parasites." Protist **159**(1): 115-125.

Bannai, H., M. Yoshimura, et al. (2000). "Calcium regulation of microtubule sliding in reactivated sea urchin sperm flagella." J Cell Sci **113 (Pt 5)**: 831-839.

Baron, D. M., K. S. Ralston, et al. (2007). "Functional genomics in *Trypanosoma brucei* identifies evolutionarily conserved components of motile flagella." J Cell Sci **120**(Pt 3): 478-491.

Barry, J. D. and R. McCulloch (2001). "Antigenic variation in trypanosomes: enhanced phenotypic variation in a eukaryotic parasite." Adv Parasitol **49**: 1-70.

Bastin, P., Z. Bagherzadeh, et al. (1996). "A novel epitope tag system to study protein targeting and organelle biogenesis in *Trypanosoma brucei*." Mol Biochem Parasitol **77**(2): 235-239.

Bastin, P., K. Ellis, et al. (2000). "Flagellum ontogeny in trypanosomes studied via an inherited and regulated RNA interference system." J Cell Sci **113 (Pt 18)**: 3321-3328.

Bastin, P., T. H. MacRae, et al. (1999). "Flagellar morphogenesis: protein targeting and assembly in the paraflagellar rod of trypanosomes." Mol Cell Biol **19**(12): 8191-8200.

Bastin, P., K. R. Matthews, et al. (1996). "The paraflagellar rod of kinetoplastida: solved and unsolved questions." Parasitol Today **12**(8): 302-307.

Bastin, P., T. J. Pullen, et al. (1999). "Protein transport and flagellum assembly dynamics revealed by analysis of the paralysed trypanosome mutant snl-1." J Cell Sci **112 (Pt 21)**: 3769-3777.

Bastin, P., T. Sherwin, et al. (1998). "Paraflagellar rod is vital for trypanosome motility." Nature **391**(6667): 548.

Basu, R., S. Bhaumik, et al. (2005). "Kinetoplastid membrane protein-11 DNA vaccination induces complete protection against both pentavalent antimonial-sensitive and -resistant strains of Leishmania donovani that correlates with inducible nitric oxide synthase activity and IL-4 generation: evidence for mixed Th1- and Th2-like responses in visceral leishmaniasis." J Immunol **174**(11): 7160-7171.

Beattie, P. and K. Gull (1997). "Cytoskeletal architecture and components involved in the attachment of Trypanosoma congolense epimastigotes." Parasitology **115 (Pt 1)**: 47-55.

Berberich, C., G. Machado, et al. (1998). "The expression of the Leishmania infantum KMP-11 protein is developmentally regulated and stage specific." Biochim Biophys Acta **1442**(2-3): 230-237.

Berriman, M., E. Ghedin, et al. (2005). "The genome of the African trypanosome Trypanosoma brucei." Science **309**(5733): 416-422.

Bessen, M., R. B. Fay, et al. (1980). "Calcium control of waveform in isolated flagellar axonemes of Chlamydomonas." J Cell Biol **86**(2): 446-455.

Birkett, C. R., A. E. Parma, et al. (1992). "Isolation of cDNA clones encoding proteins of complex structures: analysis of the *Trypanosoma brucei* cytoskeleton." Gene **110**(1): 65-70.

Bonhivers, M., S. Nowacki, et al. (2008). "Biogenesis of the trypanosome endo-exocytotic organelle is cytoskeleton mediated." PLoS Biol **6**(5): e105.

Bonini, N. M., T. C. Evans, et al. (1991). "The regulation of ciliary motility in *Paramecium* by Ca2+ and cyclic nucleotides." Adv Second Messenger Phosphoprotein Res **23**: 227-272.

Bonini, N. M. and D. L. Nelson (1988). "Differential regulation of *Paramecium* ciliary motility by cAMP and cGMP." J Cell Biol **106**(5): 1615-1623.

Borst, P. (2002). "Antigenic variation and allelic exclusion." Cell **109**(1): 5-8.

Branche, C., L. Kohl, et al. (2006). "Conserved and specific functions of axoneme components in trypanosome motility." J Cell Sci **119**(Pt 16): 3443-3455.

Briggs, L. J., J. A. Davidge, et al. (2004). "More than one way to build a flagellum: comparative genomics of parasitic protozoa." Curr Biol **14**(15): R611-612.

Briggs, L. J., P. G. McKean, et al. (2004). "The flagella connector of Trypanosoma brucei: an unusual mobile transmembrane junction." J Cell Sci **117**(Pt 9): 1641-1651.

Broadhead, R., H. R. Dawe, et al. (2006). "Flagellar motility is required for the viability of the bloodstream trypanosome." Nature **440**(7081): 224-227.

Brokaw, C. J. (1979). "Calcium-induced asymmetrical beating of triton-demembranated sea urchin sperm flagella." J Cell Biol **82**(2): 401-411.

Brokaw, C. J. and R. Kamiya (1987). "Bending patterns of Chlamydomonas flagella: IV. Mutants with defects in inner and outer dynein arms indicate differences in dynein arm function." Cell Motil Cytoskeleton **8**(1): 68-75.

Brown, D. A. and E. London (2000). "Structure and function of sphingolipid- and cholesterol-rich membrane rafts." J Biol Chem **275**(23): 17221-17224.

Brown, J. M., N. A. Fine, et al. (2003). "Hypoxia regulates assembly of cilia in suppressors of *Tetrahymena* lacking an intraflagellar transport subunit gene." Mol Biol Cell **14**(8): 3192-3207.

Brun, R. and L. Jenni (1977). "A new semi-defined medium for Trypanosoma brucei sspp." Acta Trop **34**(1): 21-33.

Cao, W., G. L. Gerton, et al. (2006). "Proteomic profiling of accessory structures from the mouse sperm flagellum." Mol Cell Proteomics **5**(5): 801-810.

Carrillo, E., M. Crusat, et al. (2008). "Immunogenicity of HSP-70, KMP-11 and PFR-2 leishmanial antigens in the experimental model of canine visceral leishmaniasis." Vaccine **26**(15): 1902-1911.

Casey, D. M., K. Inaba, et al. (2003). "DC3, the 21-kDa subunit of the outer dynein arm-docking complex (ODA-DC), is a novel EF-hand protein important for assembly of both the outer arm and the ODA-DC." Mol Biol Cell **14**(9): 3650-3663.

Chaves, I., G. Rudenko, et al. (1999). "Control of variant surface glycoprotein gene-expression sites in Trypanosoma brucei." EMBO J **18**(17): 4846-4855.

Checchi, F. and M. P. Barrett (2008). "African sleeping sickness." BMJ **336**(7646): 679-680.

Clark, A. K., G. Kovtunovych, et al. (2005). "Cloning and expression analysis of two novel paraflagellar rod domain genes found in *Trypanosoma cruzi*." Parasitol Res **96**(5): 312-320.

Clayton, C. and M. Shapira (2007). "Post-transcriptional regulation of gene expression in trypanosomes and leishmanias." Mol Biochem Parasitol **156**(2): 93-101.

Cosson, M. P., W. J. Tang, et al. (1983). "Modification of flagellar waveform and adenosine triphosphatase activity in reactivated sea-urchin sperm treated with N-ethylmaleimide." J Cell Sci **60**: 231-249.

Cross, G. A. (1977). "Antigenic variation in trypanosomes." Am J Trop Med Hyg **26**(6 Pt 2): 240-244.

Cunha, N. L., W. De Souza, et al. (1984). "Isolation of the flagellum and characterization of the paraxial structure of *Herpetomonas megaseliae*." J Submicrosc Cytol **16**(4): 705-713.

D'Angelo, M. A., A. E. Montagna, et al. (2002). "A novel calcium-stimulated adenylyl cyclase from *Trypanosoma cruzi*, which interacts with the structural flagellar protein paraflagellar rod." J Biol Chem **277**(38): 35025-35034.

Davidge, J. A., E. Chambers, et al. (2006). "Trypanosome IFT mutants provide insight into the motor location for mobility of the flagella connector and flagellar membrane formation." J Cell Sci **119**(Pt 19): 3935-3943.

Dawe, H. R., H. Farr, et al. (2005). "The Parkin co-regulated gene product, PACRG, is an evolutionarily conserved axonemal protein that functions in outer-doublet microtubule morphogenesis." J Cell Sci **118**(Pt 23): 5421-5430.

Dawe, H. R., M. K. Shaw, et al. (2007). "The hydrocephalus inducing gene product, Hydin, positions axonemal central pair microtubules." BMC Biol **5**: 33.

de Graffenried, C. L., H. H. Ho, et al. (2008). "Polo-like kinase is required for Golgi and bilobe biogenesis in Trypanosoma brucei." J Cell Biol **181**(3): 431-438.
De Lozanne, A. and J. A. Spudich (1987). "Disruption of the *Dictyostelium* myosin heavy chain gene by homologous recombination." Science **236**(4805): 1086-1091.
de Souza, W. (2007). "Chagas' disease: facts and reality." Microbes Infect **9**(4): 544-545.
de Souza, W. and T. Souto-Padron (1980). "The paraxial structure of the flagellum of trypanosomatidae." J Parasitol **66**(2): 229-236.
Deflorin, J., M. Rudolf, et al. (1994). "The major components of the paraflagellar rod of *Trypanosoma brucei* are two similar, but distinct proteins which are encoded by two different gene loci." J Biol Chem **269**(46): 28745-28751.
Drain, J., J. R. Bishop, et al. (2001). "Haptoglobin-related protein mediates trypanosome lytic factor binding to trypanosomes." J Biol Chem **276**(32): 30254-30260.
Dymek, E. E. and E. F. Smith (2007). "A conserved CaM- and radial spoke associated complex mediates regulation of flagellar dynein activity." J Cell Biol **179**(3): 515-526.
El-Sayed, N. M., P. J. Myler, et al. (2005). "The genome sequence of *Trypanosoma cruzi,* etiologic agent of Chagas disease." Science **309**(5733): 409-415.
Elmendorf, H. G., S. C. Dawson, et al. (2003). "The cytoskeleton of *Giardia lamblia*." Int J Parasitol **33**(1): 3-28.
Emmer, B. T., C. Souther, et al. (2009). "Identification of a palmitoyl acyltransferase required for protein sorting to the flagellar membrane." J Cell Sci **122**(Pt 6): 867-874.
Engman, D. M., K. H. Krause, et al. (1989). "A novel flagellar Ca2+-binding protein in trypanosomes." J Biol Chem **264**(31): 18627-18631.
Engstler, M., T. Pfohl, et al. (2007). "Hydrodynamic flow-mediated protein sorting on the cell surface of trypanosomes." Cell **131**(3): 505-515.
Erdmann, M., A. Scholz, et al. (2006). "Interacting protein kinases involved in the regulation of flagellar length." Mol Biol Cell **17**(4): 2035-2045.
Ersfeld, K. and K. Gull (2001). "Targeting of cytoskeletal proteins to the flagellum of *Trypanosoma brucei*." J Cell Sci **114**(Pt 1): 141-148.
Farina, M., M. Attias, et al. (1986). "Further Studies on the Organization of the Paraxial Rod of Trypanosomatids." Journal of Protozoology **33**(4): 552-557.
Farr, H. (2007). The Eukaryotic Flagellum in Health and Disease. The Sir William Dunn School of Pathology, University of Oxford. **DPhil**.
Farr, H. and K. Gull (2009). "Functional studies of an evolutionarily conserved, cytochrome b5 domain protein reveal a specific role in axonemal organisation and the general phenomenon of post-division axonemal growth in trypanosomes." Cell Motil Cytoskeleton **66**(1): 24-35.
Fenn, K. and K. R. Matthews (2007). "The cell biology of Trypanosoma brucei differentiation." Curr Opin Microbiol **10**(6): 539-546.
Ferrante, A. and A. C. Allison (1983). "Alternative pathway activation of complement by African trypanosomes lacking a glycoprotein coat." Parasite Immunol **5**(5): 491-498.
Field, M. C. and J. C. Boothroyd (1996). "Sequence divergence in a family of variant surface glycoprotein genes from trypanosomes: coding region hypervariability and downstream recombinogenic repeats." J Mol Evol **42**(5): 500-511.
Field, M. C. and M. Carrington (2009). "The trypanosome flagellar pocket." Nat Rev Microbiol **7**(11): 775-786.
Field, M. C., S. K. Natesan, et al. (2007). "Intracellular trafficking in the trypanosomatids." Traffic **8**(6): 629-639.
Fouts, D. L., G. A. Stryker, et al. (1998). "Evidence for four distinct major protein components in the paraflagellar rod of *Trypanosoma cruzi*." J Biol Chem **273**(34): 21846-21855.
Freymuller, E. and E. P. Camargo (1981). "Ultrastructural differences between species of trypanosomatids with and without endosymbionts." J Protozool **28**(2): 175-182.

Fuge, H. (1969). "Electron microscopic studies on the intra-flagellar structures of trypanosomes." J Protozool **16**(3): 460-466.
Gadelha, C., J. H. LeBowitz, et al. (2004). "Relationships between the major kinetoplastid paraflagellar rod proteins: a consolidating nomenclature." Mol Biochem Parasitol **136**(1): 113-115.
Gadelha, C., S. Rothery, et al. (2009). "Membrane domains and flagellar pocket boundaries are influenced by the cytoskeleton in African trypanosomes." Proc Natl Acad Sci U S A **106**(41): 17425-17430.
Gadelha, C., B. Wickstead, et al. (2005). "Cryptic paraflagellar rod in endosymbiont-containing kinetoplastid protozoa." Eukaryot Cell **4**(3): 516-525.
Gadelha, C., B. Wickstead, et al. (2007). "Flagellar and ciliary beating in trypanosome motility." Cell Motil Cytoskeleton **64**(8): 629-643.
Gadelha, C., B. Wickstead, et al. (2006). "Basal body and flagellum mutants reveal a rotational constraint of the central pair microtubules in the axonemes of trypanosomes." J Cell Sci **119**(Pt 12): 2405-2413.
Gallo, J. M. and J. Schrevel (1985). "Homologies between paraflagellar rod proteins from trypanosomes and euglenoids revealed by a monoclonal antibody." Eur J Cell Biol **36**(2): 163-168.
Gerdes, J. M., E. E. Davis, et al. (2009). "The vertebrate primary cilium in development, homeostasis, and disease." Cell **137**(1): 32-45.
Gibbons, B. H. and I. R. Gibbons (1973). "The effect of partial extraction of dynein arms on the movement of reactivated sea-urchin sperm." J Cell Sci **13**(2): 337-357.
Gibbons, I. R. and A. J. Rowe (1965). "Dynein: A Protein with Adenosine Triphosphatase Activity from Cilia." Science **149**(3682): 424-426.
Ginger, M. L., N. Portman, et al. (2008). "Swimming with protists: perception, motility and flagellum assembly." Nat Rev Microbiol **6**(11): 838-850.
Gluenz, E., M. L. Povelones, et al. (2011). "The kinetoplast duplication cycle in Trypanosoma brucei is orchestrated by cytoskeleton-mediated cell morphogenesis." Mol Cell Biol **31**(5): 1012-1021.
Godsel, L. M. and D. M. Engman (1999). "Flagellar protein localization mediated by a calcium-myristoyl/palmitoyl switch mechanism." EMBO J **18**(8): 2057-2065.
Griffiths, S., N. Portman, et al. (2007). "RNA interference mutant induction in vivo demonstrates the essential nature of trypanosome flagellar function during mammalian infection." Eukaryot Cell **6**(7): 1248-1250.
Gubbels, M. J., S. Vaishnava, et al. (2006). "A MORN-repeat protein is a dynamic component of the Toxoplasma gondii cell division apparatus." J Cell Sci **119**(Pt 11): 2236-2245.
Gull, K. (1999). "The cytoskeleton of trypanosomatid parasites." Annu Rev Microbiol **53**: 629-655.
Hammarton, T. C., M. Engstler, et al. (2004). "The Trypanosoma brucei cyclin, CYC2, is required for cell cycle progression through G1 phase and for maintenance of procyclic form cell morphology." J Biol Chem **279**(23): 24757-24764.
Han, Y. G., B. H. Kwok, et al. (2003). "Intraflagellar transport is required in Drosophila to differentiate sensory cilia but not sperm." Curr Biol **13**(19): 1679-1686.
He, C. Y., M. Pypaert, et al. (2005). "Golgi duplication in Trypanosoma brucei requires Centrin2." Science **310**(5751): 1196-1198.
Heaslip, A. T., F. Dzierszinski, et al. (2010). "TgMORN1 is a key organizer for the basal complex of Toxoplasma gondii." PLoS Pathog **6**(2): e1000754.
Hendriks, E. F., D. R. Robinson, et al. (2001). "A novel CCCH protein which modulates differentiation of Trypanosoma brucei to its procyclic form." EMBO J **20**(23): 6700-6711.
Henley, G. L., C. M. Lee, et al. (1978). "Electron microscopy observations on Trypanosoma brucei: freeze-cleaving and thin-sectioning study of the apical part of the flagellar pocket." Z Parasitenkd **55**(3): 181-187.

Hertz-Fowler, C., K. Ersfeld, et al. (2001). "CAP5.5, a life-cycle-regulated, cytoskeleton-associated protein is a member of a novel family of calpain-related proteins in Trypanosoma brucei." Mol Biochem Parasitol **116**(1): 25-34.

Hill, K. L. (2003). "Biology and mechanism of trypanosome cell motility." Eukaryot Cell **2**(2): 200-208.

Holwill, M. E. and J. L. McGregor (1976). "Effects of calcium on flagellar movement in the trypanosome Crithidia oncopelti." J Exp Biol **65**(1): 229-242.

Holzer, T. R., W. R. McMaster, et al. (2006). "Expression profiling by whole-genome interspecies microarray hybridization reveals differential gene expression in procyclic promastigotes, lesion-derived amastigotes, and axenic amastigotes in *Leishmania mexicana*." Mol Biochem Parasitol **146**(2): 198-218.

Holzer, T. R., K. K. Mishra, et al. (2008). "Coordinate regulation of a family of promastigote-enriched mRNAs by the 3'UTR PRE element in *Leishmania mexicana*." Mol Biochem Parasitol **157**(1): 54-64.

Hung, C. H., X. Qiao, et al. (2004). "Clathrin-dependent targeting of receptors to the flagellar pocket of procyclic-form Trypanosoma brucei." Eukaryot Cell **3**(4): 1004-1014.

Hunger-Glaser, I. and T. Seebeck (1997). "Deletion of the genes for the paraflagellar rod protein PFR-A in *Trypanosoma brucei* is probably lethal." Mol Biochem Parasitol **90**(1): 347-351.

Hutchings, N. R., J. E. Donelson, et al. (2002). "Trypanin is a cytoskeletal linker protein and is required for cell motility in African trypanosomes." J Cell Biol **156**(5): 867-877.

Hutchinson, O. C., K. Picozzi, et al. (2007). "Variant Surface Glycoprotein gene repertoires in Trypanosoma brucei have diverged to become strain-specific." BMC Genomics **8**: 234.

Hyams, J. S. (1982). "The *Euglena* paraflagellar rod: structure, relationship to other flagellar components and preliminary biochemical characterization." J Cell Sci **55**: 199-210.

Hyams, J. S. and G. G. Borisy (1978). "Isolated flagellar apparatus of Chlamydomonas: characterization of forward swimming and alteration of waveform and reversal of motion by calcium ions in vitro." J Cell Sci **33**: 235-253.

Im, Y. J., A. J. Davis, et al. (2007). "The N-terminal membrane occupation and recognition nexus domain of Arabidopsis phosphatidylinositol phosphate kinase 1 regulates enzyme activity." J Biol Chem **282**(8): 5443-5452.

Imboden, M., N. Muller, et al. (1995). "Repetitive proteins from the flagellar cytoskeleton of African trypanosomes are diagnostically useful antigens." Parasitology **110 (Pt 3)**: 249-258.

Inoue, H., H. Nojima, et al. (1990). "High efficiency transformation of Escherichia coli with plasmids." Gene **96**(1): 23-28.

Inoue, Y. and C. Shingyoji (2007). "The roles of noncatalytic ATP binding and ADP binding in the regulation of dynein motile activity in flagella." Cell Motil Cytoskeleton **64**(9): 690-704.

Ivens, A. C., C. S. Peacock, et al. (2005). "The genome of the kinetoplastid parasite, *Leishmania major*." Science **309**(5733): 436-442.

Johnson, R. E. and C. J. Brokaw (1979). "Flagellar hydrodynamics. A comparison between resistive-force theory and slender-body theory." Biophys J **25**(1): 113-127.

Kamiya, R. and G. B. Witman (1984). "Submicromolar levels of calcium control the balance of beating between the two flagella in demembranated models of Chlamydomonas." J Cell Biol **98**(1): 97-107.

Katta, S. S., A. A. Sahasrabuddhe, et al. (2009). "Flagellar localization of a novel isoform of myosin, myosin XXI, in *Leishmania*." Mol Biochem Parasitol **164**(2): 105-110.

Kelly, S., J. Reed, et al. (2007). "Functional genomics in Trypanosoma brucei: a collection of vectors for the expression of tagged proteins from endogenous and ectopic gene loci." Mol Biochem Parasitol **154**(1): 103-109.

Kilburn, C. L., C. G. Pearson, et al. (2007). "New Tetrahymena basal body protein components identify basal body domain structure." J Cell Biol **178**(6): 905-912.

Kinukawa, M., S. Oda, et al. (2006). "Roles of cAMP in regulating microtubule sliding and flagellar bending in demembranated hamster spermatozoa." FEBS Lett **580**(5): 1515-1520.

Kinukawa, M. and V. D. Vacquier (2007). "Recombinant sea urchin flagellar adenylate kinase." J Biochem **142**(4): 501-506.
Kohl, L., T. Sherwin, et al. (1999). "Assembly of the paraflagellar rod and the flagellum attachment zone complex during the Trypanosoma brucei cell cycle." J Eukaryot Microbiol **46**(2): 105-109.
Koumandou, V. L., S. K. Natesan, et al. (2008). "The trypanosome transcriptome is remodelled during differentiation but displays limited responsiveness within life stages." BMC Genomics **9**: 298.
Koyfman, A. Y., M. F. Schmid, et al. (2011). "Structure of Trypanosoma brucei flagellum accounts for its bihelical motion." Proc Natl Acad Sci U S A **108**(27): 11105-11108.
Kozminski, K. G., K. A. Johnson, et al. (1993). "A motility in the eukaryotic flagellum unrelated to flagellar beating." Proc Natl Acad Sci U S A **90**(12): 5519-5523.
Kremer, J. R., D. N. Mastronarde, et al. (1996). "Computer visualization of three-dimensional image data using IMOD." J Struct Biol **116**(1): 71-76.
Lacomble, S., N. Portman, et al. (2009). "A protein-protein interaction map of the Trypanosoma brucei paraflagellar rod." PLoS One **4**(11): e7685.
Lacomble, S., S. Vaughan, et al. (2009). "Three-dimensional cellular architecture of the flagellar pocket and associated cytoskeleton in trypanosomes revealed by electron microscope tomography." J Cell Sci **122**(Pt 8): 1081-1090.
Lacomble, S., S. Vaughan, et al. (2010). "Basal body movements orchestrate membrane organelle division and cell morphogenesis in Trypanosoma brucei." J Cell Sci **123**(Pt 17): 2884-2891.
LaCount, D. J., B. Barrett, et al. (2002). "Trypanosoma brucei FLA1 is required for flagellum attachment and cytokinesis." J Biol Chem **277**(20): 17580-17588.
Landfear, S. M. and M. Ignatushchenko (2001). "The flagellum and flagellar pocket of trypanosomatids." Mol Biochem Parasitol **115**(1): 1-17.
Larochelle, D. A., K. K. Vithalani, et al. (1996). "A novel member of the rho family of small GTP-binding proteins is specifically required for cytokinesis." J Cell Biol **133**(6): 1321-1329.
Li, Y., Z. Li, et al. (2003). "Differentiation of Trypanosoma brucei may be stage non-specific and does not require progression of cell cycle." Mol Microbiol **49**(1): 251-265.
Li, Z. and C. C. Wang (2008). "KMP-11, a basal body and flagellar protein, is required for cell division in Trypanosoma brucei." Eukaryot Cell **7**(11): 1941-1950.
Libusova, L., T. Sulimenko, et al. (2004). "gamma-Tubulin in *Leishmania*: cell cycle-dependent changes in subcellular localization and heterogeneity of its isoforms." Exp Cell Res **295**(2): 375-386.
Luhrs, K. A., D. L. Fouts, et al. (2003). "Immunization with recombinant paraflagellar rod protein induces protective immunity against *Trypanosoma cruzi* infection." Vaccine **21**(21-22): 3058-3069.
Maga, J. A. and J. H. LeBowitz (1999). "Unravelling the kinetoplastid paraflagellar rod." Trends Cell Biol **9**(10): 409-413.
Maga, J. A., T. Sherwin, et al. (1999). "Genetic dissection of the *Leishmania* paraflagellar rod, a unique flagellar cytoskeleton structure." J Cell Sci **112 (Pt 16)**: 2753-2763.
Matthews, K. R. (2005). "The developmental cell biology of Trypanosoma brucei." J Cell Sci **118**(Pt 2): 283-290.
Matthews, K. R., J. R. Ellis, et al. (2004). "Molecular regulation of the life cycle of African trypanosomes." Trends Parasitol **20**(1): 40-47.
Matthews, K. R. and K. Gull (1994). "Evidence for an interplay between cell cycle progression and the initiation of differentiation between life cycle forms of African trypanosomes." J Cell Biol **125**(5): 1147-1156.
McCulloch, R. (2004). "Antigenic variation in African trypanosomes: monitoring progress." Trends Parasitol **20**(3): 117-121.
McGhee, R. B. and W. B. Cosgrove (1980). "Biology and physiology of the lower Trypanosomatidae." Microbiol Rev **44**(1): 140-173.

McKean, P. G., A. Baines, et al. (2003). "Gamma-tubulin functions in the nucleation of a discrete subset of microtubules in the eukaryotic flagellum." Curr Biol **13**(7): 598-602.

Michailowsky, V., K. Luhrs, et al. (2003). "Humoral and cellular immune responses to *Trypanosoma cruzi*-derived paraflagellar rod proteins in patients with Chagas' disease." Infect Immun **71**(6): 3165-3171.

Miller, M. J., R. A. Wrightsman, et al. (1996). "*Trypanosoma cruzi*: protective immunity in mice immunized with paraflagellar rod proteins is associated with a T-helper type 1 response." Exp Parasitol **84**(2): 156-167.

Miller, M. J., R. A. Wrightsman, et al. (1997). "Protection of mice against *Trypanosoma cruzi* by immunization with paraflagellar rod proteins requires T cell, but not B cell, function." J Immunol **158**(11): 5330-5337.

Mishra, K. K., T. R. Holzer, et al. (2003). "A negative regulatory element controls mRNA abundance of the *Leishmania mexicana* Paraflagellar rod gene PFR2." Eukaryot Cell **2**(5): 1009-1017.

Moreira-Leite, F. F., W. de Souza, et al. (1999). "Purification of the paraflagellar rod of the trypanosomatid *Herpetomonas megaseliae* and identification of some of its minor components." Mol Biochem Parasitol **104**(1): 131-140.

Moreira-Leite, F. F., T. Sherwin, et al. (2001). "A trypanosome structure involved in transmitting cytoplasmic information during cell division." Science **294**(5542): 610-612.

Morell, M., M. C. Thomas, et al. (2006). "The genetic immunization with paraflagellar rod protein-2 fused to the HSP70 confers protection against late *Trypanosoma cruzi* infection." Vaccine **24**(49-50): 7046-7055.

Morgan, G. W., B. S. Hall, et al. (2002). "The kinetoplastida endocytic apparatus. Part I: a dynamic system for nutrition and evasion of host defences." Trends Parasitol **18**(11): 491-496.

Morrison, L. J., P. Majiwa, et al. (2005). "Probabilistic order in antigenic variation of Trypanosoma brucei." Int J Parasitol **35**(9): 961-972.

Morriswood, B., C. Y. He, et al. (2009). "The bilobe structure of Trypanosoma brucei contains a MORN-repeat protein." Mol Biochem Parasitol **167**(2): 95-103.

Naitoh, Y. and H. Kaneko (1972). "Reactivated triton-extracted models o paramecium: modification of ciliary movement by calcium ions." Science **176**(34): 523-524.

Notari, L., A. Morelli, et al. (2003). "Studies on adenylate kinase isoform bound to disk membranes of the rod outer segment of bovine retina." Photochem Photobiol Sci **2**(12): 1299-1302.

Notari, L., I. M. Pepe, et al. (2001). "Adenylate kinase activity in rod outer segments of bovine retina." Biochim Biophys Acta **1504**(2-3): 438-443.

Nozaki, T., P. A. Haynes, et al. (1996). "Characterization of the Trypanosoma brucei homologue of a Trypanosoma cruzi flagellum-adhesion glycoprotein." Mol Biochem Parasitol **82**(2): 245-255.

Oberholzer, M., P. Bregy, et al. (2007). "Trypanosomes and mammalian sperm: one of a kind?" Trends Parasitol **23**(2): 71-77.

Oberholzer, M., G. Marti, et al. (2007). "The Trypanosoma brucei cAMP phosphodiesterases TbrPDEB1 and TbrPDEB2: flagellar enzymes that are essential for parasite virulence." FASEB J **21**(3): 720-731.

Ogbadoyi, E. O., D. R. Robinson, et al. (2003). "A high-order trans-membrane structural linkage is responsible for mitochondrial genome positioning and segregation by flagellar basal bodies in trypanosomes." Mol Biol Cell **14**(5): 1769-1779.

Okuno, M. and C. J. Brokaw (1979). "Inhibition of movement of trition-demembranated sea-urchin sperm flagella by Mg2+, ATP4-, ADP and P1." J Cell Sci **38**: 105-123.

Olego-Fernandez, S., S. Vaughan, et al. (2009). "Cell morphogenesis of Trypanosoma brucei requires the paralogous, differentially expressed calpain-related proteins CAP5.5 and CAP5.5V." Protist **160**(4): 576-590.

Omoto, C. K. and C. J. Brokaw (1985). "Bending patterns of Chlamydomonas flagella: II. Calcium effects on reactivated Chlamydomonas flagella." Cell Motil **5**(1): 53-60.

Ostrowski, L. E., K. Blackburn, et al. (2002). "A proteomic analysis of human cilia: identification of novel components." Mol Cell Proteomics **1**(6): 451-465.

Overath, P. and M. Engstler (2004). "Endocytosis, membrane recycling and sorting of GPI-anchored proteins: Trypanosoma brucei as a model system." Mol Microbiol **53**(3): 735-744.

Paindavoine, P., S. Rolin, et al. (1992). "A gene from the variant surface glycoprotein expression site encodes one of several transmembrane adenylate cyclases located on the flagellum of *Trypanosoma brucei*." Mol Cell Biol **12**(3): 1218-1225.

Pan, J. and W. Snell (2007). "The primary cilium: keeper of the key to cell division." Cell **129**(7): 1255-1257.

Patel-King, R. S., O. Gorbatyuk, et al. (2004). "Flagellar radial spokes contain a Ca2+-stimulated nucleoside diphosphate kinase." Mol Biol Cell **15**(8): 3891-3902.

Pawson, T. and J. D. Scott (1997). "Signaling through scaffold, anchoring, and adaptor proteins." Science **278**(5346): 2075-2080.

Pazour, G. J., N. Agrin, et al. (2005). "Proteomic analysis of a eukaryotic cilium." J Cell Biol **170**(1): 103-113.

Pedersen, L. B. and J. L. Rosenbaum (2008). "Intraflagellar transport (IFT) role in ciliary assembly, resorption and signalling." Curr Top Dev Biol **85**: 23-61.

Porter, M. E. and W. S. Sale (2000). "The 9 + 2 axoneme anchors multiple inner arm dyneins and a network of kinases and phosphatases that control motility." J Cell Biol **151**(5): F37-42.

Portman, N. and K. Gull (2010). "The paraflagellar rod of kinetoplastid parasites: from structure to components and function." Int J Parasitol **40**(2): 135-148.

Portman, N., S. Lacomble, et al. (2009). "Combining RNA interference mutants and comparative proteomics to identify protein components and dependences in a eukaryotic flagellum." J Biol Chem **284**(9): 5610-5619.

Pullen, T. J., M. L. Ginger, et al. (2004). "Protein targeting of an unusual, evolutionarily conserved adenylate kinase to a eukaryotic flagellum." Mol Biol Cell **15**(7): 3257-3265.

Quill, T. A., S. A. Sugden, et al. (2003). "Hyperactivated sperm motility driven by CatSper2 is required for fertilization." Proc Natl Acad Sci U S A **100**(25): 14869-14874.

Ralston, K. S. and K. L. Hill (2006). "Trypanin, a component of the flagellar Dynein regulatory complex, is essential in bloodstream form African trypanosomes." PLoS Pathog **2**(9): e101.

Ralston, K. S., Z. P. Kabututu, et al. (2009). "The *Trypanosoma brucei* Flagellum: Moving Parasites in New Directions." Annu Rev Microbiol **63**: 335-362.

Ralston, K. S., N. K. Kisalu, et al. (2011). "Structure-function analysis of dynein light chain 1 identifies viable motility mutants in bloodstream-form Trypanosoma brucei." Eukaryot Cell **10**(7): 884-894.

Ralston, K. S., A. G. Lerner, et al. (2006). "Flagellar motility contributes to cytokinesis in *Trypanosoma brucei* and is modulated by an evolutionarily conserved dynein regulatory system." Eukaryot Cell **5**(4): 696-711.

Raynaud-Messina, B. and A. Merdes (2007). "Gamma-tubulin complexes and microtubule organization." Curr Opin Cell Biol **19**(1): 24-30.

Reuner, B., E. Vassella, et al. (1997). "Cell density triggers slender to stumpy differentiation of Trypanosoma brucei bloodstream forms in culture." Mol Biochem Parasitol **90**(1): 269-280.

Ridgley, E., P. Webster, et al. (2000). "Calmodulin-binding properties of the paraflagellar rod complex from *Trypanosoma brucei*." Mol Biochem Parasitol **109**(2): 195-201.

Robinson, D. R. and K. Gull (1991). "Basal body movements as a mechanism for mitochondrial genome segregation in the trypanosome cell cycle." Nature **352**(6337): 731-733.

Robinson, D. R., T. Sherwin, et al. (1995). "Microtubule polarity and dynamics in the control of organelle positioning, segregation, and cytokinesis in the trypanosome cell cycle." J Cell Biol **128**(6): 1163-1172.

Rocha, G. M., D. E. Teixeira, et al. (2010). "Structural changes of the paraflagellar rod during flagellar beating in Trypanosoma cruzi." PLoS One **5**(6): e11407.

Rotureau, B., I. Subota, et al. (2011). "Molecular bases of cytoskeleton plasticity during the Trypanosoma brucei parasite cycle." Cell Microbiol **13**(5): 705-716.

Russell, D. G., R. J. Newsam, et al. (1983). "Structural and biochemical characterisation of the paraflagellar rod of *Crithidia fasciculata*." Eur J Cell Biol **30**(1): 137-143.

Saborio, J. L., J. Manuel Hernandez, et al. (1989). "Isolation and characterization of paraflagellar proteins from *Trypanosoma cruzi*." J Biol Chem **264**(7): 4071-4075.

Sale, W. S. and P. Satir (1977). "Direction of active sliding of microtubules in Tetrahymena cilia." Proc Natl Acad Sci U S A **74**(5): 2045-2049.

Sant'Anna, C., L. Campanati, et al. (2005). "Improvement on the visualization of cytoskeletal structures of protozoan parasites using high-resolution field emission scanning electron microscopy (FESEM)." Histochem Cell Biol **124**(1): 87-95.

Santrich, C., L. Moore, et al. (1997). "A motility function for the paraflagellar rod of *Leishmania* parasites revealed by PFR-2 gene knockouts." Mol Biochem Parasitol **90**(1): 95-109.

Saravia, N. G., M. H. Hazbon, et al. (2005). "Protective immunogenicity of the paraflagellar rod protein 2 of *Leishmania mexicana*." Vaccine **23**(8): 984-995.

Schlaeppi, K., J. Deflorin, et al. (1989). "The major component of the paraflagellar rod of *Trypanosoma brucei* is a helical protein that is encoded by two identical, tandemly linked genes." J Cell Biol **109**(4 Pt 1): 1695-1709.

Schneider, A., H. U. Lutz, et al. (1988). "Spectrin-like proteins in the paraflagellar rod structure of *Trypanosoma brucei*." J Cell Sci **90 (Pt 2)**: 307-315.

Scholey, J. M. (2003). "Intraflagellar transport." Annu Rev Cell Dev Biol **19**: 423-443.

Scholey, J. M. and K. V. Anderson (2006). "Intraflagellar transport and cilium-based signaling." Cell **125**(3): 439-442.

Sharma, R., E. Gluenz, et al. (2009). "The heart of darkness: growth and form of Trypanosoma brucei in the tsetse fly." Trends Parasitol **25**(11): 517-524.

Sharma, R., L. Peacock, et al. (2008). "Asymmetric cell division as a route to reduction in cell length and change in cell morphology in trypanosomes." Protist **159**(1): 137-151.

Sherwin, T. and K. Gull (1989). "The cell division cycle of Trypanosoma brucei brucei: timing of event markers and cytoskeletal modulations." Philos Trans R Soc Lond B Biol Sci **323**(1218): 573-588.

Sherwin, T. and K. Gull (1989). "Visualization of detyrosination along single microtubules reveals novel mechanisms of assembly during cytoskeletal duplication in trypanosomes." Cell **57**(2): 211-221.

Sherwin, T., A. Schneider, et al. (1987). "Distinct localization and cell cycle dependence of COOH terminally tyrosinolated alpha-tubulin in the microtubules of Trypanosoma brucei brucei." J Cell Biol **104**(3): 439-446.

Shi, J., J. B. Franklin, et al. (2008). "Centrin4 coordinates cell and nuclear division in T. brucei." J Cell Sci **121**(Pt 18): 3062-3070.

Simarro, P. P., J. Jannin, et al. (2008). "Eliminating human African trypanosomiasis: where do we stand and what comes next?" PLoS Med **5**(2): e55.

Smith, E. F. (2002). "Regulation of flagellar dynein by calcium and a role for an axonemal calmodulin and calmodulin-dependent kinase." Mol Biol Cell **13**(9): 3303-3313.

Smith, E. F. and P. Yang (2004). "The radial spokes and central apparatus: mechano-chemical transducers that regulate flagellar motility." Cell Motil Cytoskeleton **57**(1): 8-17.

Smith, J. C., J. G. Northey, et al. (2005). "Robust method for proteome analysis by MS/MS using an entire translated genome: demonstration on the ciliome of Tetrahymena thermophila." J Proteome Res **4**(3): 909-919.

Stebeck, C. E., R. P. Beecroft, et al. (1995). "Kinetoplastid membrane protein-11 (KMP-11) is differentially expressed during the life cycle of African trypanosomes and is found in a wide variety of kinetoplastid parasites." Mol Biochem Parasitol **71**(1): 1-13.

Steverding, D. (2000). "The transferrin receptor of Trypanosoma brucei." Parasitol Int **48**(3): 191-198.

Takeshima, H., S. Komazaki, et al. (2000). "Junctophilins: a novel family of junctional membrane complex proteins." Mol Cell **6**(1): 11-22.

Talke, S. and A. Preisfeld (2002). "Molecular Evolution of Euglenozoan Paraxonemal Rod Genes *par1* and *par2* Coincides With Phylogenetic Reconstruction Based on Small Subunit rDNA DATA." Journal of Phycology **38**(5): 995-1003.

Tamm, S. (1994). "Ca2+ channels and signalling in cilia and flagella." Trends Cell Biol **4**(9): 305-310.

Tammana, T. V., A. A. Sahasrabuddhe, et al. (2008). "Actin-depolymerizing factor, ADF/cofilin, is essentially required in assembly of *Leishmania* flagellum." Mol Microbiol **70**(4): 837-852.

Tetley, L. and K. Vickerman (1985). "Differentiation in Trypanosoma brucei: host-parasite cell junctions and their persistence during acquisition of the variable antigen coat." J Cell Sci **74**: 1-19.

Tyler, K. M., A. Fridberg, et al. (2009). "Flagellar membrane localization via association with lipid rafts." J Cell Sci **122**(Pt 6): 859-866.

Tyler, K. M., K. R. Matthews, et al. (2001). "Anisomorphic cell division by African trypanosomes." Protist **152**(4): 367-378.

Vanhollebeke, B., G. De Muylder, et al. (2008). "A haptoglobin-hemoglobin receptor conveys innate immunity to Trypanosoma brucei in humans." Science **320**(5876): 677-681.

Vassella, E., B. Reuner, et al. (1997). "Differentiation of African trypanosomes is controlled by a density sensing mechanism which signals cell cycle arrest via the cAMP pathway." J Cell Sci **110 (Pt 21)**: 2661-2671.

Vaughan, S., L. Kohl, et al. (2008). "A repetitive protein essential for the flagellum attachment zone filament structure and function in Trypanosoma brucei." Protist **159**(1): 127-136.

Vaughan, S., M. Shaw, et al. (2006). "A post-assembly structural modification to the lumen of flagellar microtubule doublets." Curr Biol **16**(12): R449-450.

Vedrenne, C., C. Giroud, et al. (2002). "Two related subpellicular cytoskeleton-associated proteins in Trypanosoma brucei stabilize microtubules." Mol Biol Cell **13**(3): 1058-1070.

Vickerman, K. (1962). "The mechanism of cyclical development in trypanosomes of the *Trypanosoma brucei* sub-group: an hypothesis based on ultrastructural observations." Trans R Soc Trop Med Hyg **56**: 487-495.

Vickerman, K. (1965). "Polymorphism and mitochondrial activity in sleeping sickness trypanosomes." Nature **208**(5012): 762-766.

Vickerman, K. (1969). "On the surface coat and flagellar adhesion in trypanosomes." J Cell Sci **5**(1): 163-193.

Vickerman, K. (1973). "The mode of attachment of Trypanosoma vivax in the proboscis of the tsetse fly Glossina fuscipes: an ultrastructural study of the epimastigote stage of the trypanosome." J Protozool **20**(3): 394-404.

Vickerman, K. (1985). "Developmental cycles and biology of pathogenic trypanosomes." Br Med Bull **41**(2): 105-114.

Walker, P. J. (1961). "Organization of function in trypanosome flagella." Nature **189**: 1017-1018.

Wargo, M. J., E. E. Dymek, et al. (2005). "Calmodulin and PF6 are components of a complex that localizes to the C1 microtubule of the flagellar central apparatus." J Cell Sci **118**(Pt 20): 4655-4665.

Werner, M. and L. W. Simmons (2008). "Insect sperm motility." Biol Rev Camb Philos Soc **83**(2): 191-208.

Wickstead, B., K. Ersfeld, et al. (2002). "Targeting of a tetracycline-inducible expression system to the transcriptionally silent minichromosomes of Trypanosoma brucei." Mol Biochem Parasitol **125**(1-2): 211-216.

Wiese, M., D. Kuhn, et al. (2003). "Protein kinase involved in flagellar-length control." Eukaryot Cell **2**(4): 769-777.

Wiese, M., Q. Wang, et al. (2003). "Identification of mitogen-activated protein kinase homologues from *Leishmania mexicana*." Int J Parasitol **33**(14): 1577-1587.

Woods, A., A. J. Baines, et al. (1992). "A high molecular mass phosphoprotein defined by a novel monoclonal antibody is closely associated with the intermicrotubule cross bridges in the Trypanosoma brucei cytoskeleton." J Cell Sci **103 (Pt 3)**: 665-675.

Woods, A., T. Sherwin, et al. (1989). "Definition of individual components within the cytoskeleton of Trypanosoma brucei by a library of monoclonal antibodies." J Cell Sci **93 (Pt 3)**: 491-500.

Woodward, R., M. J. Carden, et al. (1994). "Molecular characterisation of a novel, repetitive protein of the paraflagellar rod in *Trypanosoma brucei*." Mol Biochem Parasitol **67**(1): 31-39.

Woodward, R. and K. Gull (1990). "Timing of nuclear and kinetoplast DNA replication and early morphological events in the cell cycle of Trypanosoma brucei." J Cell Sci **95 (Pt 1)**: 49-57.

Wrightsman, R. A., K. A. Luhrs, et al. (2002). "Paraflagellar rod protein-specific CD8+ cytotoxic T lymphocytes target *Trypanosoma cruzi*-infected host cells." Parasite Immunol **24**(8): 401-412.

Wrightsman, R. A. and J. E. Manning (2000). "Paraflagellar rod proteins administered with alum and IL-12 or recombinant adenovirus expressing IL-12 generates antigen-specific responses and protective immunity in mice against *Trypanosoma cruzi*." Vaccine **18**(14): 1419-1427.

Wrightsman, R. A., M. J. Miller, et al. (1995). "Pure paraflagellar rod protein protects mice against *Trypanosoma cruzi* infection." Infect Immun **63**(1): 122-125.

Wu, Y., J. Deford, et al. (1994). "The gene family of EF-hand calcium-binding proteins from the flagellum of *Trypanosoma brucei*." Biochem J **304 (Pt 3)**: 833-841.

Wu, Y., N. G. Haghighat, et al. (1992). "The predominant calcimedins from *Trypanosoma brucei* comprise a family of flagellar EF-hand calcium-binding proteins." Biochem J **287 (Pt 1)**: 187-193.

Yagi, T. (2000). "ADP-dependent microtubule translocation by flagellar inner-arm dyneins." Cell Struct Funct **25**(4): 263-267.

Yamamoto, R., H. A. Yanagisawa, et al. (2006). "A novel subunit of axonemal dynein conserved among lower and higher eukaryotes." FEBS Lett **580**(27): 6357-6360.

Yang, P., D. R. Diener, et al. (2006). "Radial spoke proteins of Chlamydomonas flagella." J Cell Sci **119**(Pt 6): 1165-1174.

Zhou, Q., L. Gheiratmand, et al. (2010). "A comparative proteomic analysis reveals a new bi-lobe protein required for bi-lobe duplication and cell division in Trypanosoma brucei." PLoS One **5**(3): e9660.

Appendix

Appendix A. Oligonucleotides used in this work

Target	Primer type	Sequence
Chapter 3		
PFC14	5' UTR intergration target	ATATATCTCGAGACGTCTTTTGTATTTTACGGAGG
		ATATATGGATCCTCTGCTTTTCTTTCTCTGTTTCG
	ORF intergration/RNAi target	ATATATGCGGCCGCTCTAGAATGGAGAAAACACAACCGT
		ATATATACTAGTCTCGAGACTCTTTCACAAGAGCCC
PFC15	5' UTR intergration target	ATATATCTCGAGCCTCTCTTCACTTTTCATTGTTACT
		ATATATGGATCCTGTTGAACCCCGTAAGAAC
	ORF intergration/RNAi target	ATATATGCGGCCGCTCTAGAATGGCAAGTTCTACAGCA
		ATATATACTAGTCTCGAGACATCTCTGGGTTCTCCT
PFC1	5' UTR intergration target	ATATATCTCGAGAGGTGAACAGACCGAATC
		ATATATGGATCCGGTTGCGGAAGATAATTACTTC
	ORF intergration/RNAi target	ATATATGCGGCCGCTCTAGAATGACGACGATGCAGAG
		ATATATACTAGTCTCGAGAAGGTGCGAAGGCTG
PFC5	5' UTR intergration target	ATATATCTCGAGAACATTCGTAGTGATTCTCTACG
		ATATATGGATCCTGATAAAGTTTTATCGCTGACCTTT
	ORF intergration/RNAi target	ATATATGCGGCCGCTCTAGAGCTGAGCAGAGAAACA
		ATATATACTAGTCTCGAGACATCTCTCAATATATAATCGTCG
PFC3	5' UTR intergration target	ATATATCTCGAGTGAAAGGGAATTCGGCTCTA
		ATATATGGATCCTTAACAAGCGCGGCAAA
	ORF intergration/RNAi target	ATATATGCGGCCGCTCTAGAATGTCGGCCACTTATCC
		ATATATACTAGTCTCGAGATGCGCACTCCTCTAC
PAR1	5' UTR intergration target	TACTCTAGAATGATCGAGGTGCAACTTAAC
		TACCTCGAGCCCTCGTCACCTCTTG
	ORF intergration/RNAi target	TACCTCGAGTCCATTACGTGTGTGAACTG
		TACGGATCCTGTATGTTTGTTCTTCGGTTCC
Chapter 4		
FCP1	Mr Gene insert for endogenous tagging	AAGCTTTCTTGTCTGACAGCTGCTGGAGGCACTTATTACCGCATGCTGTCAATGGATGCCAC TCTGTTGGGGATGTTTTATGAATGGATAAGATACGAACAACAAGCTCGAGTTTTCATAATCC GCATGCGGCATCCGTCGACGAAGCGCAGGCGTATCCCAATCACGATGAGGAAAGCAATGTT TCTCTCTCATGTGATTCGTCGCACAACACTAGTGGATCCTCTTGTCTGACAGCTGCTGGAGGC ACTTATTACCGCATGCTGTCAATGGATGCCACTCTGTTGGGGATGTTTTATGAATGGATAAG ATACGAACAACAAGAAAGTTGGCAATGCTTATGAGCGTGCATGCACATATGGAAGTGTGAC TGAGGCATACTGTCATATACATCACTGCTTCTGTGTTGTGTAGTCCATGTATGTCAACGACTT TAGTTGTGTTTTCCGTAAAGATGTTGTGCCTTGTGCATAAGTGACTAATTATGGCTTCCAGTT GGTCTCATTTTCTCCGTGTCATTTCATGCATAGTATCAACTTTTGTTGCTATCTTTCCTTACCAT TTTGTAGACGAAACATCATTCCAAGATTTCCACATCCAAGAGAGAGTTGAGCCAAGAATTC
FCP1 RNAi	ORF RNAi target	ATATATtctagaCCTATTGGCGTTGTTGGTCT
		ATATATtctagaCATTCGCCTCTGTGCAGTTA
PFAZ RNAi	ORF RNAi target	ATATATTCTAGAGGACAGCGGTGTCTTCTCTC
		ATATATTCTAGACAGCCTCCTTTGTGTGTTCA
PFAZ ORF	ORF intergration target	ATATATCTCGAGGTAGCCGTCCTCATCGTGTT
		ATATATACTAGTCTGCTCGACCCTTTCTTTGTT
PFAZ UTR	3'UTR intergration target	ATATATGGATCCAAGCTTATTTCCTAGACTATCACACAAACATGC
		ATATATAAGCTTCGATGCCAACAACAACAAAA
	3'UTR full length	ATATATGAATTCCTATGAGGTCCTTCCGTCCA
SAP-P RNAi	ORF RNAi target	ATATATTCTAGAAAGGATGAGGCGGAAAGTG
		ATATATTCTAGAAGCACCCCACATTATTGACG
SAP-B RNAi	ORF RNAi target	ATATATTCTAGACATTAAGGAGTGACCGGAAA
		ATATATTCTAGACTTCTTCCGCTTTTTGCTTT
SAP-P OX	ORF Full length	ATATATTCTAGAAGCACCACTGCACTGTCTTC
		AGCGTAATAGGATCCTATTTGTCG
SAP-B OX	ORF Full length	ATATATTCTAGAAGCACCACTGCACTGTCTTC
		ATATATGGATCCTCAGTAGTTGGCTTCACGAGC
SAP-P Tag	ORF intergration target	ATATATCTCGAGTTGAAGGGTTAAAGCGTTTGTT
		ATATATACTAGTTTTGTCGGCCTCCCG
	3'UTR intergration target	ATATATAAGCTTGATCGTATTACGCTCCATGTTCA
		ATATATCTCGAGCGCCGTGGTTATCGTAAACT
	3'UTR full length	ATATATGCATGCTCGGCCTAAGAGATCGAATG
SAP-B Tag	ORF intergration target	ATATATCTCGAGAGCTGAAGGATGCGAAAGTC
		ATATATACTAGTGTAGTTGGCTTCACGAGCAC
	3'UTR intergration target	ATATATAAGCTTGGTACGCCCGCTCACAC
		ATATATCTCGAGCTTCGAGTGCCTTCCTTGAC

	3'UTR full length	ATATATGCATGCAACGGAACCTTTTTCTTTTTCA
Chapter 5		
CMRP	ORF intergration/RNAi target	ATATATctcgagATGATATACTCTGGTGAGATAGAAAATG
		ATATATggatccGCCATGAACCTTGTCATCAA
	5' UTR intergration target	ATATATactagtGATGTATGCGACAAGCCTGA
		ATATATctcgagTCTGTTATCGGATGGAAAGAAG
BILBO1	ORF intergration/RNAi target	ATATATactagtctcgagGCGTTTCTCGTACAAGTAGCAG
		ATATATggatccCACCCATTTGTTGAGCTCCT
	ORF Full length	ATATATggatccTTAATCTCGCGGATAGGACC
	5' UTR intergration target	ATATATactagtATAACTGCTCCGTGGGAATG
		ATATATctcgagACTAATATAAATAAGCAATAATTTT

Appendix B. Plasmid vectors, 1 of 3. p2T7-177 (Wickstead, Ersfeld et al. 2002).

Image sourced from http://www.billwickstead.net/vectors.shtml

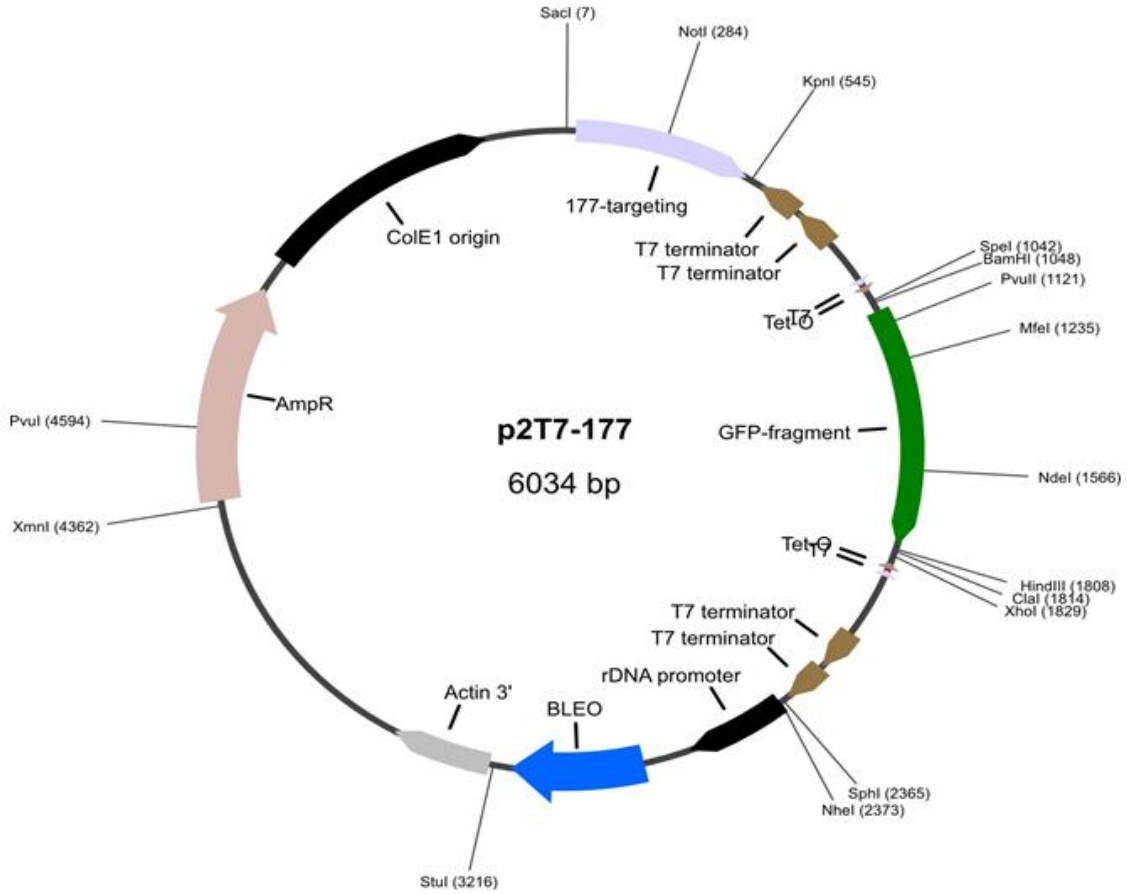

p2T7-177 vector for inheritable inducible RNAi against target mRNA. Target sequence replaces the GFP ORF and is expressed from two opposing T7 RNA polymerase promoters under control of the Tet operator. Linearisation with NotI allows integration into the mini-chromosome 177 repeats.

Appendix B. Plasmid vectors, 2 of 3. pEnT6B-Y (Kelly, Reed et al. 2007).

Image sourced from http://www.billwickstead.net/vectors.shtml

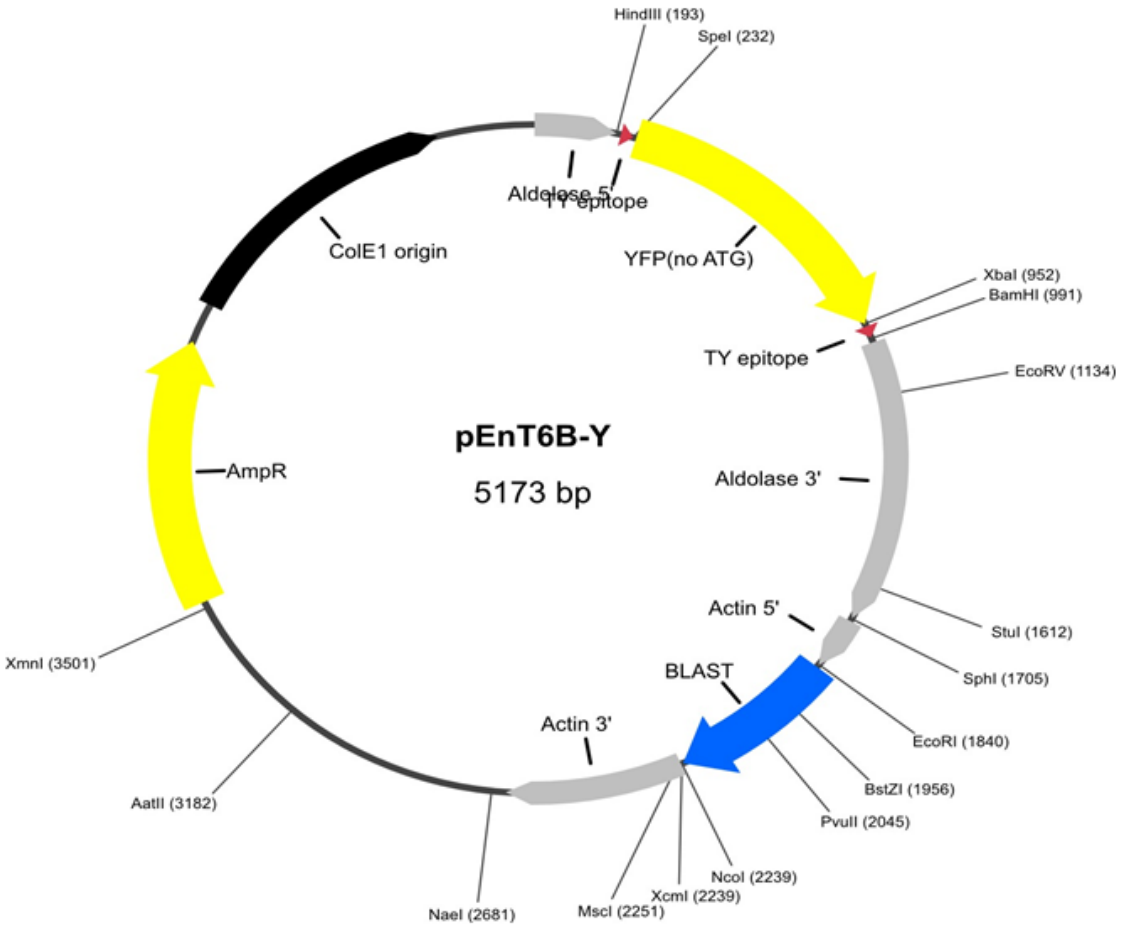

pEnT6B-Y vector for the expression of chimeric proteins with N or C terminal YFP and/or Ty epitope tags from endogenous loci. For N terminal tagging 150bp of ORF starting at or immediately after the start codon and 150bp of 5' UTR immediately upstream of the start codon are inserted between the XbaI and BamHI sites (to include YFP) or between the SpeI and BamHI sites (to exclude YFP) and separated by a unique site. For C terminal tagging 150 bp of 3' UTR immediately downstream of the stop codon and 150bp of ORF up to but not including the stop codon are inserted between the Hind III and SpeI sites (to include YFP) or the HindIII and XbaI sites (to exclude YFP) and separated by a unique site. The full length 3' UTR can be introduced between the BamHI and SphI sites if necessary. Linaerisation at the unique site introduced between the ORF and UTR inserts allows the integration of the construct into one of the endogenous alleles of the gene of interest.

Appendix B. Plasmid vectors, 3 of 3. pDex577-g (Kelly, Reed et al. 2007).

Image sourced from http://www.billwickstead.net/vectors.shtml

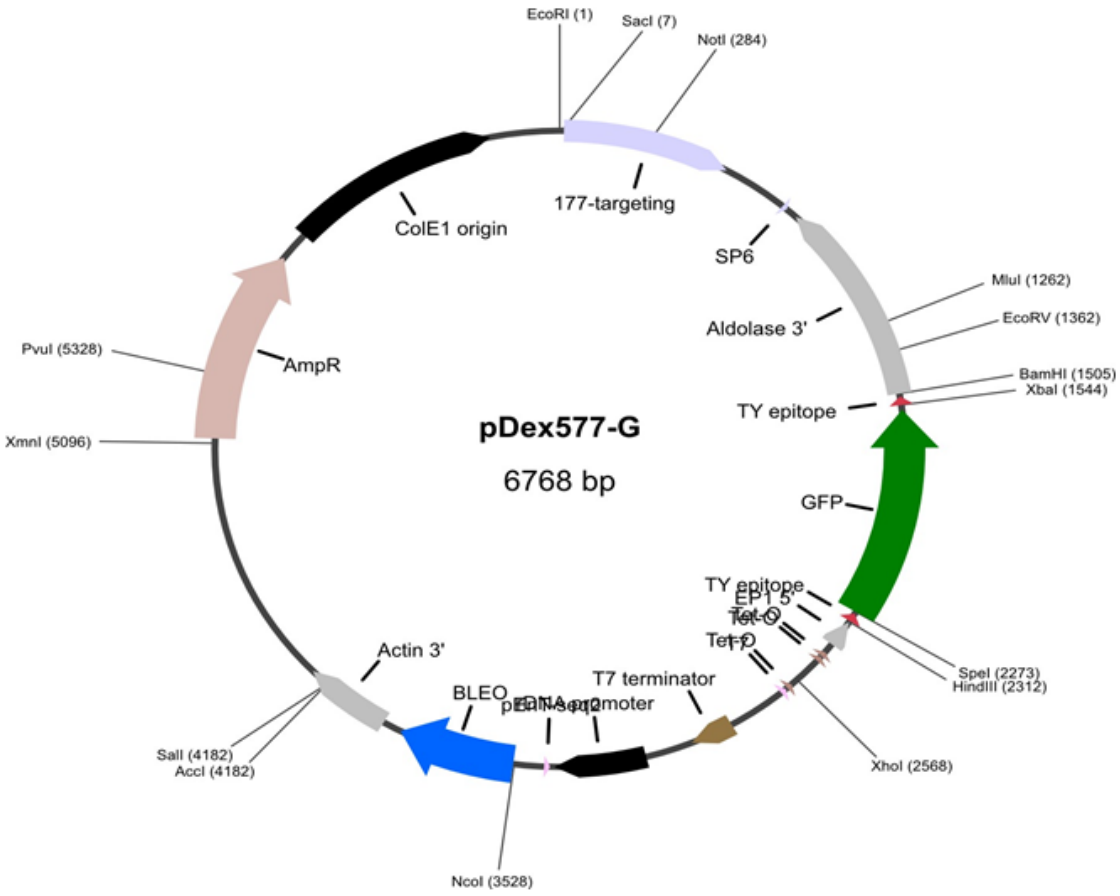

pDex577-G vector for inducible and inheritable ectopic expression of proteins of interest. Transcription is driven from a T7 RNA-polymerase promoter under control of a Tet operator. For an N terminal tag full length ORF is inserted between the XhoI and BamHI sites (to include GFP) or the SpeI and BamHI sites (to exclude GFP). For a C terminal tag full length ORF is inserted between the HindIII and SpeI sites (to include GFP) or the HindIII and XbaI sites (to exclude GFP). Inserting full length ORF between the HindIII and BamHI sites allows inducible expression of untagged protein. The vector is linearised at the NotI site for integration into the mini-chromosome 177 repeats. The inclusion of the aldolase 3'UTR means that for most proteins induction will lead to overexpression.

Appendix C. 1 of 3. ImageJ macro used to identify FPCs and measure fluorescence intensity.

This macro requires a reference image (in this case I used total BILBO1 as detected by BB2 using a fluorophore 594 conjugated secondary antibody) and a measurement image (here, this was GFP::BILBO1 native fluorescence). A maxima finding/dynamic thresholding protocol is used to define collar boundaries in the reference image and then measures the fluorescence intensity within this boundary in the measurement image. Each structure measured is give a unique identifier and an image is generated that marks each structure with this identifier. A manual step is then required whereby the user reviews the structures detected and assigns them to pre-determined groups (e.g. 1K1N, 2K1N, 2K2N in this case) using a numerical code. Once this is complete measurements and assignments are collated by the macro and output as a tab-delimited text file.

```
macro 'collar_counter [c]'
{

draw = 2; check = 1; measure = 2; ref = 1; map = 3;
name = newArray(nImages);

for (image = 0; image < nImages; image++) {selectImage(image+1); name[image] = getTitle();}

Dialog.create("Select Images");
Dialog.addChoice("Select reference image ", name);
Dialog.addNumber("Enter slice to draw on ", 7);
Dialog.addNumber("Enter reference slice ",2);
Dialog.addChoice("Select Measurement image ", name);
Dialog.addNumber("Enter threshold slice ", 2);
Dialog.addNumber("Enter measurement slice ", 1);
Dialog.addNumber("Enter maximum particle size in pixels ", 75);
Dialog.addNumber("Enter threshold modifier ", 0.5);
Dialog.addNumber("Enter minimum signal multiplier above background ", 2);
Dialog.addNumber("Enter noise level for Maxima finding ", 10);
Dialog.addNumber("Enter Maxima factor ", 0);
Dialog.show;

ref_image = Dialog.getChoice();
draw_slice = Dialog.getNumber();
ref_slice = Dialog.getNumber();
measure_image = Dialog.getChoice();
threshold_slice = Dialog.getNumber();
measure_slice = Dialog.getNumber();
particle_size = Dialog.getNumber();
threshold_modifier = Dialog.getNumber();
signal_multiplier = Dialog.getNumber();
noise = Dialog.getNumber();
maxima_factor = Dialog.getNumber();


selectWindow(ref_image);
setSlice(ref_slice);
run("Duplicate...", ref_image);
temp = getTitle();
run("16-bit");
options = "noise="+noise+" output=[Point Selection]";
run("Find Maxima...", options);
getSelectionCoordinates(x, y);
options = "noise="+noise+" output=[Segmented Particles]"
run("Find Maxima...", options);
segment = getTitle();
selectWindow(temp); close();
selectWindow(segment);
run("16-bit");
changeValues(1,255,pow(2,16));
run("Invert");
selectWindow(measure_image);
setSlice(threshold_slice);
run("Duplicate...", measure_image);
ref_slice = getTitle();
imageCalculator("Subtract", ref_slice, segment);
selectWindow(segment); close();
```

Appendix C. 2 of 3. ImageJ macro used to identify FPCs and measure fluorescence intensity.

```
selectWindow(measure_image);

directory = getInfo("image.directory");
tempArray=split(getTitle(), '.');
base_name = tempArray[0];
measurements = File.open(directory + base_name + "_collars.txt");

setSlice(measure_slice);
run("Duplicate...", measure_image);
selectWindow(measure_image); close();
run("Images to Stack", "name=measure title=[]");


selectWindow(ref_image);
setSlice(draw_slice);
run("Duplicate...", ref_image);
selectWindow(ref_image);
setSlice(draw_slice);
run("Duplicate...", ref_image);
selectWindow(ref_image); close();
run("Images to Stack", "name=draw title=[]");



selectWindow("measure");
setSlice(measure);
getRawStatistics(nPixels, mean, background, max, std, histogram);
setSlice(ref);
getRawStatistics(nPixels, mean, ref_background, max, std, histogram);



setFont("Serif", 12, "bold");

print(measurements, "Image, Collar, Type, Int, #P, Mean, Maxima, x, y");

setColor(255,255,255);
selectWindow("draw");
setSlice(check);

for (a=0; a<x.length; a++) {drawLine(x[a], y[a], x[a], y[a]);}

for (a=0; a<x.length; a++)
        {
        selectWindow("measure");
        setSlice(ref);
        maxima_value = getPixel(x[a], y[a]);
        v = 0; pixels = 0;
        for (x_co = -maxima_factor; x_co <= maxima_factor; x_co++)
                {
                for (y_co = -maxima_factor; y_co <= maxima_factor; y_co++)
                        {
                        v = v + getPixel(x[a] + x_co, y[a] + y_co); pixels++;
                        }
                }
        v = v/pixels;
        threshold_min = (threshold_modifier*(v - background)) + background;
        setThreshold(threshold_min,4095);
        doWand(x[a], y[a]);
        getSelectionCoordinates(xCoordinates, yCoordinates);
        getSelectionBounds(m,n,o,p);
        resetThreshold();
        getRawStatistics(nPixels, mean, min, ref_max, std, histogram);


        if (nPixels < particle_size && ref_max > ref_background*signal_multiplier)
                {
                setSlice(measure);
                getRawStatistics(nPixels, mean, min, max, std, histogram);
                intensity = (nPixels*mean)-(nPixels*background);
                makeSelection("polygon", xCoordinates, yCoordinates);
                setColor(0); fill();
                setBatchMode(false);
```

Appendix C. 3 of 3. ImageJ macro used to identify FPCs and measure fluorescence intensity.

```
selectWindow("draw");
               makeRectangle(m-75,n-75,o+150,p+150);
               run("To Selection");
               makeSelection("polygon", xCoordinates, yCoordinates);
               setSlice(check);
               setColor(255,0,0);
               drawLine(x[a], y[a], x[a], y[a]);
               Dialog.create ("Type of collar");
               Dialog.addNumber("Enter type for collar " + a + ": ", 0);
               Dialog.show;
               assignment = Dialog.getNumber;
               setBatchMode(true);
               print (measurements, base_name + ", " + a + ", " + assignment + ", " +
intensity + ", " + nPixels + ", " + mean + ", " + maxima_value + ", " + x[a] + ", " + y[a]);
               setColor(0,0,255);
               drawLine(x[a], y[a], x[a], y[a]);
               drawString(assignment, m-3,n-3);
               setColor(255,255,255);
               setSlice(draw);
               drawString(a + ": " + assignment,m - 3,n - 3);
               for (line_draw = 0; line_draw < xCoordinates.length - 1; line_draw++)
                       {
                       drawLine(xCoordinates[line_draw],              yCoordinates[line_draw],
xCoordinates[line_draw+1], yCoordinates[line_draw+1]);
                       }
               drawLine(xCoordinates[xCoordinates.length-1], yCoordinates[xCoordinates.length-
1], xCoordinates[0], yCoordinates[0]);
               }
       }
selectWindow("draw");
saveAs("Tiff", directory + base_name + "_collars.tif");
close(); close();
print (measurements, "Measurement image: " + measure_image);
print (measurements, "Measurement slice: " + measure_slice);
print (measurements, "Reference slice: " + ref_slice);
print (measurements, "Display image: " + ref_image + ", slice " + draw_slice);
print (measurements, "Max particle size: " + particle_size);
print (measurements, "Threshold modifier: " + threshold_modifier);
print (measurements, "Min signal above background: " + signal_multiplier);
print (measurements, "Maxima finder noise setting: " + noise);
print (measurements, "Maxima size factor: " + maxima_factor);
print (measurements, "Measurement image background: " + background);
print (measurements, "Reference image background: " + ref_background);
File.close(measurements);
Dialog.create("Finished");
Dialog.addMessage("Done");
Dialog.show();
}
```

Appendix D. Publications

OPEN ACCESS Freely available online

PLoS one

A Protein-Protein Interaction Map of the *Trypanosoma brucei* Paraflagellar Rod

Sylvain Lacomble[ϑ], **Neil Portman**[ϑ], **Keith Gull***

Sir William Dunn School of Pathology and Oxford Centre for Integrative Systems Biology, University of Oxford, Oxford, United Kingdom

Abstract

We have conducted a protein interaction study of components within a specific sub-compartment of a eukaryotic flagellum. The trypanosome flagellum contains a para-crystalline extra-axonemal structure termed the paraflagellar rod (PFR) with around forty identified components. We have used a Gateway cloning approach coupled with yeast two-hybrid, RNAi and 2D DiGE to define a protein-protein interaction network taking place in this structure. We define two clusters of interactions; the first being characterised by two proteins with a shared domain which is not sufficient for maintaining the interaction. The other cohort is populated by eight proteins, a number of which possess a PFR domain and sub-populations of this network exhibit dependency relationships. Finally, we provide clues as to the structural organisation of the PFR at the molecular level. This multi-strand approach shows that protein interactome data can be generated for insoluble protein complexes.

Citation: Lacomble S, Portman N, Gull K (2009) A Protein-Protein Interaction Map of the *Trypanosoma brucei* Paraflagellar Rod. PLoS ONE 4(11): e7685. doi:10.1371/journal.pone.0007685

Editor: Adam Yuan, Temasek Life Sciences Laboratory, Singapore

Received September 2, 2009; **Accepted** October 12, 2009; **Published** November 3, 2009

Funding: This work was supported by the Wellcome Trust, Human Frontier Science Program, the EP Abraham Trust, the Engineering and Physical Sciences Research Council (EPSRC) and the Biotechnology and Biological Sciences Research Council (BBSRC). SL was supported by a Henry Goodger Scholarship. KG is a Wellcome Trust Principal Research Fellow. The funders had no role in study design, data collection and analysis, decision to publish, or preparation of the manuscript.

Competing Interests: The authors have declared that no competing interests exist.

* E-mail: keith.gull@path.ox.ac.uk

ϑ These authors contributed equally to this work.

Introduction

Trypanosomatid protozoan parasites are the causative agents of a number of diseases responsible for the death of thousands of people in developing countries. There is currently little hope for a vaccine and existing treatment regimes are associated with high toxicity. All trypanosomes produce a single flagellum which is involved in numerous aspects of parasite biology including motility, cytokinesis, environment sensing, attachment to the host [1,2,3,4,5,6] and in the case of the African trypanosome *Trypanosoma brucei*, correct generation and function of the flagellum is essential for the survival of the mammalian bloodstream stage [7]. The flagellum incorporates the canonical 9+2 microtubular eukaryotic axoneme and, as with the flagella of many species, has several additional lineage specific features. One of these additional features is an extra-axonemal para-crystalline structure termed the paraflagellar rod (PFR). The PFR of *T. brucei* has a complex subdomain organisation which includes proximal, intermediate, and distal domains as well as links to specific doublets of the axoneme and the flagellum attachment zone (FAZ) [8,9]. In addition to its role in motility [10,11], the PFR serves as a platform for metabolic and signaling enzymes [2,12,13] and is essential for the survival of the mammalian infective form of the parasite in the host bloodstream [14].

The eukaryotic flagellum is a widely conserved organelle and was a feature of the ancestor of all eukaryotes. The flagellum is implicated in an ever growing spectrum of human genetic disease [15] and is an attribute of many pathogenic organisms. It has been the subject of a number of recent proteomic characterisations in several model organisms and this analysis of components has also been extended to substructures of the axoneme such as the radial spokes and basal bodies [16,17]. Our group has recently produced a *T. brucei* flagellar proteome [7] as well as a PFR proteome generated using comparative proteomics that consists of 30 high confidence proteins including 20 that were previously annotated in the genome as hypothetical [18]. Although these studies have improved our knowledge of the protein composition of the flagellum, the contribution of many of these newly identified components to structure and function remains to be determined.

A variety of functional genomics tools that have the potential to complement these large-scale proteomic assays of the flagellum are available. Yeast two-hybrid analyses have been extensively used to systematically investigate interactions of proteins in many model organisms [19,20,21,22] at genome scale. Although local studies of flagellar functions have used the yeast two-hybrid approach to interrogate specific protein-protein interactions [23,24,25,26], the utility of this technique for high throughput investigation has yet to be exploited for this organelle. A systematic interrogation of protein interactions in the flagellum is likely to provide valuable insight into its molecular architecture and functions. Another very powerful tool for the analysis of protein function in *T. brucei* is the ability to inducibly ablate protein expression by RNAi [27]. This has been done for individual proteins involved in a variety of cell processes as well as systematically as part of the Trypanofan project [28]. We have recently demonstrated that combining inducible RNAi with comparative proteomics techniques is a very powerful approach for the interrogation of dependent cohorts and sub-cohorts within complex

protein structures [18]. We were able to identify an inter-dependent subset of proteins within the PFR cohort and propose a role for calcium signalling in the regulation of PFR adenylate kinases [18]. There is also evidence for either direct or indirect interactions between the major PFR components and calmodulin [13], strengthening the hypothesis for a major role for calcium in PFR function. We aim to provide evidence of interactions within the flagellum by a systematic yeast two-hybrid screen and to employ the above biochemical analyses to further elucidate the nature of the interactions.

Our PFR proteome forms a discreet subset of proteins within the flagellum and here we have used this as a training set for interrogating protein interactions and dependencies within the insoluble structural fraction of the flagellum. We have generated an open reading frame (ORF) library of 28 PFR proteins which is fully compatible with Gateway® cloning technology. We have used this library to perform a yeast two-hybrid screen and have identified novel protein-protein interactions within the PFR cohort. We have created a Gateway® compatible inducible RNAi vector based on p2T7-177 [29]–p2T7-177-GTW - and have successfully used this to ablate the expression of a number of PFR proteins. We have used this new vector in conjunction with biochemical and proteomics techniques to interrogate the nature of the interactions detected in the yeast two-hybrid screen and have identified new dependency networks and clues to the hierarchical nature of these interactions.

Methods

Cell Culture

Procyclic form *Trypanosoma brucei brucei* were cultured at 28°C in SDM 79 medium supplemented with 10% v/v foetal calf serum (Gibco) [30]. Cells were diluted as necessary to maintain the culture in log-phase and RNAi induction was achieved by the addition of doxycyclin to the culture medium to a final concentration of 1 μg ml^{-1}.

Vector Construction

The nucleotide sequence 5′-CTAGTGGGGACAACTTTGTACAAAAAAGTTGGCtcttgaggttccaggcttctcgagCCCAACTTTCTTGTACAAAGTTGTCCCCTTCGA-3′, containing AttB1, AttB2 and restriction enzyme recognition sites for XbaI, BamHI, HindIII and XhoI was inserted into p2T7-177 between the restriction sites for XbaI and ClaI such that the sites were destroyed. A BP reaction (Invitrogen) between this plasmid and pDNR223 was performed to obtain p2T7-177-GTW.

ORFeome Construction

Open reading frames were amplified from *T. brucei* (strain 927) genomic DNA by PCR using primers containing AttB1 and AttB2 recognition sequences (Table S1) positioned relative to the ORF as previously described [31]. Purified ORF fragments were transferred to pDNR223 using BP clonase (Invitrogen) and from there to p2T7-177 GTW, pAD and pDB using LR clonase (Invitrogen). pDNR223, pAD and pDB were kind gifts of Prof Marc Vidal, Dana Farber Cancer Institute, Harvard University.

Transfection. 10–15 μg of purified linearised plasmid DNA was used to transfect 2.5 10^7 of logarithmically growing 29:13 procyclic form *T. brucei* [32] by electroporation (3×100 μs pulses of 1700 V at interval of 200 ms). Transfected cells were selected by the addition of 5 μg ml^{-1} Phleomycin to the growth medium.

Preparation of Flagella, Western Blotting and DiGE Analysis

Cell fractionation, Western blotting and DiGE analyses were conducted as previously described [18].

Immunofluorescence

Cells were settled onto glass slides and extracted by the addition of 1% Nonidet P-40 in PEME (100 mM PIPES, pH 6.9, 2 mM EGTA, 1 mM $MgSO_4$, 0.1 mM EDTA). Extracted cells were fixed in methanol at −20°C and then labeled with BB2 [33] (α-Ty epitope). Labeling was visualized with 488 fluor-conjugated α-mouse IgG1 (Invitrogen). The slides were mounted in Vectashield mounting medium with 4′, 6′ - diamino-2-phenylindole (Vector Laboratories Inc) and examined on a Leica DM5500B.

Transmission Electron Microscopy

For thin-section electron microscopy cells were fixed in culture by addition to the growth medium of glutaraldehyde to a final concentration of 2.5% (w/v). Cells were collected by centrifugation and fixed again in 4% (w/v) formaldehyde, 2% (w/v) glutaraldehyde in 100 mM sodium phosphate buffer, pH 7.0 before post-fixation with 1% (w/v) osmium tetroxide in 100 mM sodium phosphate buffer. After several washes, cells were en bloc stained with 1% (w/v) aqueous uranyl acetate before dehydration and embedding in epoxy resin. Sections were stained with aqueous uranyl acetate and Renyold's lead citrate, and viewed in an FEI Tecnai-F12 electron microscope operating at 80 kV.

Yeast Two-Hybrid Assay

Yeast two-hybrid plasmids (pDB-ORF and pAD-ORF) were transformed in yeast cells (MaV103 (MATa) and MaV203 (MATα) respectively) and selected on medium lacking the leucine or tryptophan amino acid respectively. Auto-activation of each transformed MaV103 strain was tested on four selective media [34]. For the beta-galactosidase assay, patches of cells were plated on a nitrocellulose membrane placed onto a YPD plate and incubated overnight. Cells present on the nitrocellulose membrane were frozen in liquid nitrogen for 10 seconds and placed on Whatman paper filters pre-incubated with Z-buffer (8.52 g/L Na2HPO4, 5.5 g/L NaH2PO4, 0.75 g/L KCl and 0.12 g/L MgSO4) containing 0.18% (v/v) of 2-mercapto-ethanol and 0.07% of bromo-4-chloro-3-indolyl B–D galacto-sidase (X-gal). Membranes were incubated at 37°C and photographed after 1 h, 4 h and 24 h. Pairs of interactions were examined by individually mating each MaV103-DB-ORF with MaV203-AD-ORF in 96 well plates containing 100 μL/well of YPD. Multi-well plates were incubated overnight at 30°C with shaking and then plated on selective medium lacking both leucine and tryptophan. After the generation of diploid cells, patches representing single potential interaction pairs were examined using the four yeast two-hybrid assays as previously described [34].

Results

A Yeast Two Hybrid Screen Identifies Eight Novel Interactions

We screened a number of PFR proteins identified in our comparative proteomics analysis [18] for interactions using a yeast two-hybrid assay. We successfully amplified 28 open reading frames by PCR and subsequently cloned them into the Gateway® compatible library vector pDNR223 using the BP clonase. This 'ORFeome' serves as a foundation for subsequent functional genomic analyses and we employed the Gateway® technology to transfer these open reading frames into the yeast two-hybrid plasmids pAD (prey) and pDB (bait).

To identify protein-protein interactions in the PFR, we designed a matrix yeast two-hybrid assay by mating strains containing each bait to strains containing each prey and subsequently testing all

700 resulting pair-wise combinations (after removing auto-activators which are discussed later). Interactions were visualised using the one colorimetric and three auxotrophic assays described previously [34]. Resulting interactions were ranked according to the number of assays in which they were observed; 4 interactions were detected in all four assays, 3 interactions were detected in three assays, one interaction in two assays and two interactions in one assay. The interactions of PFC3-PFR5 and PFC4-PFC16 reciprocate in both bait and prey configurations and both PFC3 and PFC6 interact with themselves. All other interactions were seen in only one configuration (Figure S1). In total, 8 non-redundant interactions were detected in the yeast two-hybrid screen (Figure 1) and these can be divided into two clusters: PAR1-PFC3-PFR5-PFC20-PFC6-PFR6 and PFC4-PFC16. In the first of these clusters, PFC3, PFC6 and PFC20 all interact with PFR5 while PFC3 also interacts with PAR1.

Importantly, each of the bait constructs has been tested for self-activation in the four yeast two-hybrid assays (Figure S2). PFC2, PFC11 and PFC20 appear to be strong self-activators (in all four assays) preventing any further investigation of these in the bait configuration. PFC3 and PFR5 are weak auto-activators only in the colorimetric beta-galactosidase assay allowing the interactions of these proteins to be screened using the other three assays.

A Gateway® Compatible RNAi Vector Facilitates a Functional Genomics Analysis

The availability of our PFR ORFeome in a Gateway® compatible format provides the opportunity to perform relatively high-throughput studies of PFR component function using genomics tools such as RNA interference. To facilitate this analysis, we modified the p2T7-177 inducible RNAi vector [29] to make it Gateway® compatible. We inserted the Gateway® cassette containing the *ccdB* toxic gene and the chloramphenicol resistance gene flanked by two attR recognition sequences necessary for LR recombination between the two tetracycline operators of p2T7-177 (Figure 2A). We named this plasmid p2T7-177-GTW and assessed its suitability by using it to generate a *T. brucei* procyclic form cell line (*snl4*) in which inducible RNAi is targeted against PFR2. We compared the phenotype of *snl4* with the previously described *snl2* PFR2 knock down mutant [35]. After RNAi induction, the level of PFR2 protein is reduced as revealed by Western blotting with the anti-PFR2 antibody L8C4 (Figure 2B). Defective motility is clearly apparent and cells are completely paralysed. At the structural level, EM analysis shows that the PFR structure is greatly reduced (Figure 2C) as seen in *snl2* [35,36] demonstrating the utility of p2T7-177-GTW for future RNAi studies.

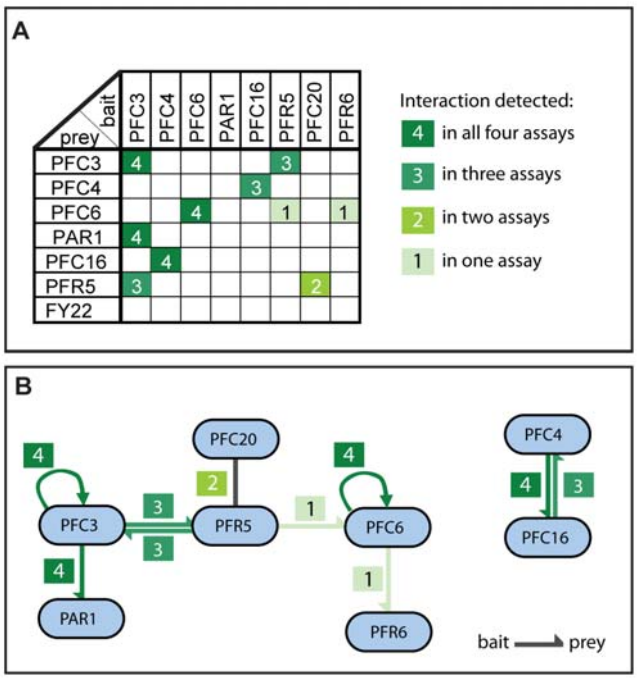

Figure 1. A yeast two-hybrid interaction map for the PFR. A. Summary table of all yeast two-hybrid interactions. For each pair, the number of assays in which an interaction was observed is shown. B. Cartoon representation of the yeast two-hybrid interactions described in A. The number of assays in which an interaction was detected is shown.
doi:10.1371/journal.pone.0007685.g001

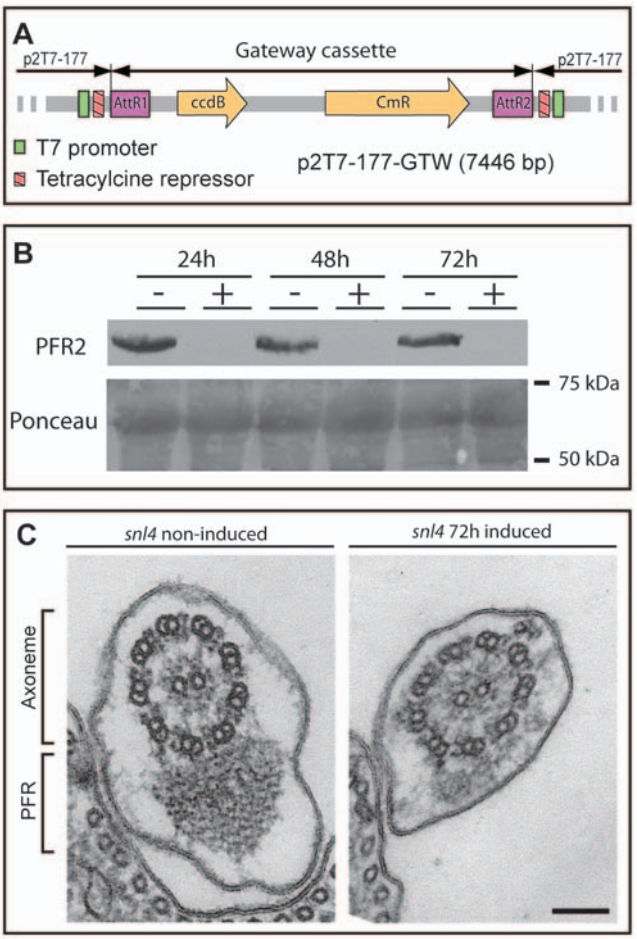

Figure 2. A Gateway® compatible vector for RNAi analysis in *T. brucei*. A. p2T7-177-GTW. The Gateway® cassette containing the chloramphenicol resistance gene and the toxic *ccdB* gene was inserted into the inducible expression site of the p2T7-177 plasmid. B. Western blotting analysis of whole cell lysates of *snl4* (procyclic form *T. brucei* containing p2T7-177-GTW-PFR2) over an RNAi induction time course. PFR2 protein (visualised with L8C4 antibody) is undetectable after 24 hours of RNAi induction. Ponceau stained membrane is shown as a loading control. C. Transmission electron micrographs of non-induced and 72 hour induced *snl4* flagellar cross-sections reveal the absence of a large part of the PFR structure. Bar 100 nm.
doi:10.1371/journal.pone.0007685.g002

Biochemical Analysis Provides Insight into the Nature of the PFC4-PFC16 Interaction

The interaction observed between PFC4 and PFC16 is particularly intriguing as we have previously shown that these otherwise dissimilar proteins share a small motif of 21 amino acids [18]. In order to interrogate whether this motif was responsible for this interaction, we constructed additional yeast two-hybrid vectors containing the domain of PFC4 and PFC16 alone in each bait/prey configuration and assayed the interactions of these with each of the full length open reading frames. No interaction was detected by any of the four yeast two-hybrid assays suggesting that this motif alone is not sufficient to maintain this protein interaction (data not shown).

We then asked whether ablation of one component had an effect on the other. We generated a cell line with a Ty epitope tagged copy of PFC4 [18] at one of the endogenous alleles and inducible RNAi (via p2T7-177-GTW) against PFC16. Whole cells lysates of non-induced, 24, 48 and 72 hours RNAi induced samples were compared by Western blotting using BB2 antibody which recognises the epitope tag. As expected, in the non-induced sample, a single band with apparent molecular weight consistent with the predicted molecular weight of Ty-PFC4 protein was observed. Interestingly, a second band with higher mobility in the gel was observed in samples made 24 hours after RNAi induction. This second band persisted until at least 72 hours after induction (Figure 3A). We performed a reciprocal analysis generating a cell line with Ty epitope tagged PFC16 in a PFC4 inducible RNAi background. Again, Western blotting of non-induced whole cell lysate with BB2 antibody revealed a single band consistent with the predicted molecular weight of Ty-PFC16 protein. Intriguingly, as before, a second band was observed after 24 h of RNAi induction that persisted until at least 72 h after RNAi induction (Figure 3B). Importantly, the RNAi induced bands in the two cell lines are of different apparent molecular weight and are therefore likely to be modified forms of the Ty epitope tagged protein in question and not an artefact of the RNAi. Western blotting of detergent and salt dissections of non-induced and induced Ty-PFC4/PFC16 RNAi cells revealed that both Ty-PFC4 bands are present in the same cell fractions (Figure 3C) suggesting that the localisation of this modified version of the protein is not altered.

In order to determine possible post-translational modifications of PFC4 and PFC16, we analysed the protein sequences using NetPhos [37] which suggests that PFC4 and PFC16 contain thirteen and eleven possible phosphorylation sites respectively. Further analysis using Phobius [38] Glycosylation predictor [39] and Myristoylator [40] predicts no glycosylation or myristoylation sites in either protein (Fig 3D).

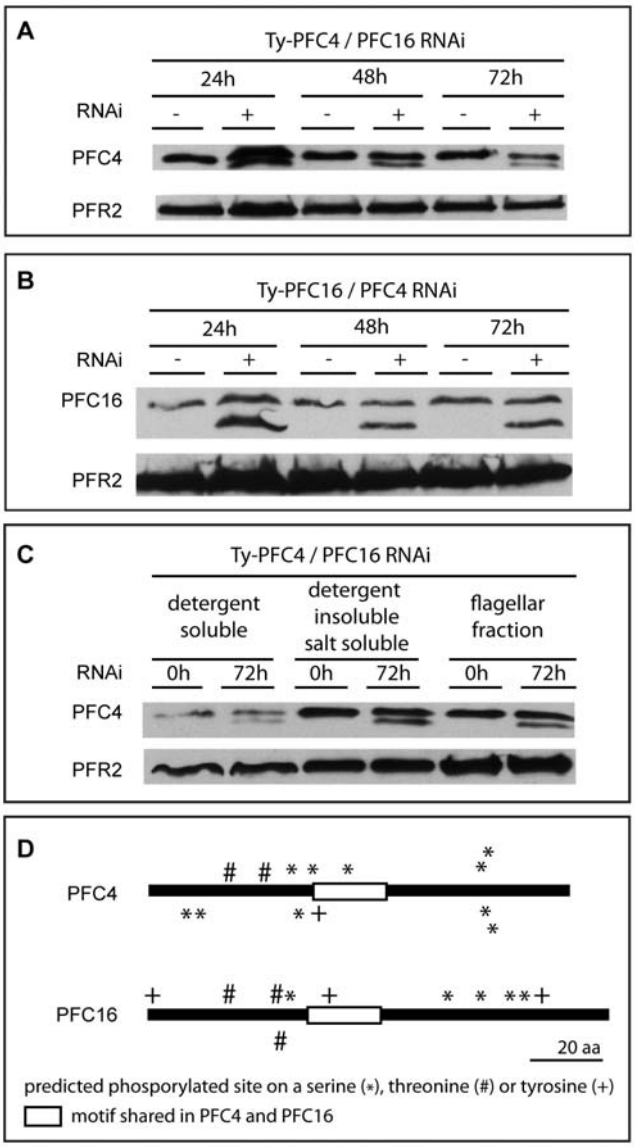

Figure 3. Analysis of PFC4 and PFC16 after induction of RNAi. A. Ty-PFC4 after RNAi ablation of PFC16. B. Ty-PFC16 after RNAi ablation of PFC4. In both cases a second band with higher mobility in the gel appears as soon as 24 hours after RNAi induction. C. Western blotting analysis of various cell fractions showing Ty-PFC4 after RNAi ablation of PFC16. Both bands are present in all cell fractions. Ty epitope tagged PFR proteins were detected using BB2 antibody. Loading control was performed using L8C4. D. Cartoon representation of predicted post-translational modification sites and conserved motifs for both PFC4 and PFC16.
doi:10.1371/journal.pone.0007685.g003

Proteomic Analysis Reveals Dependencies Supporting the Identified Interactions

We have recently demonstrated the power of combining RNAi ablation of key proteins with comparative proteomics techniques to identify dependent sub-groups of proteins within the larger complex of the PFR [18]. This methodology can be used to detect changes in protein composition as a result of RNAi directed against specific components. We tested interactions detected in our yeast two-hybrid screen (PFC3/PAR1) using a combination of inducible RNAi, purification of flagella and 2D-DiGE analysis. Resulting spot patterns were matched using Decyder software to a reference 2D gel map of PFR proteins within the context of purified flagella. Samples prepared 72 hours after RNAi induction against PFC3 showed a number of spots with a twofold or greater decrease in volume when compared to non-induced samples (consistent with criteria applied previously– [18]) (Figure 4A). As expected a group of five spots of approximately 80 kDa that correspond to PFC3 showed two- to four-fold reduction in volume (3.8, 3.7, 3.1, 2.8 and 2.3-fold reductions). Interestingly the volume of a spot of approximately 65 kDa that corresponds to PAR1 also showed a 2.1-fold decrease. This result shows that PAR1 is not stably incorporated into the structure of the flagellum in the absence of PFC3 protein and supports the interaction of these two proteins observed in our yeast two-hybrid screen. Greater than twofold reductions in spot volumes following PFC3 RNAi were also observed for three other spots.

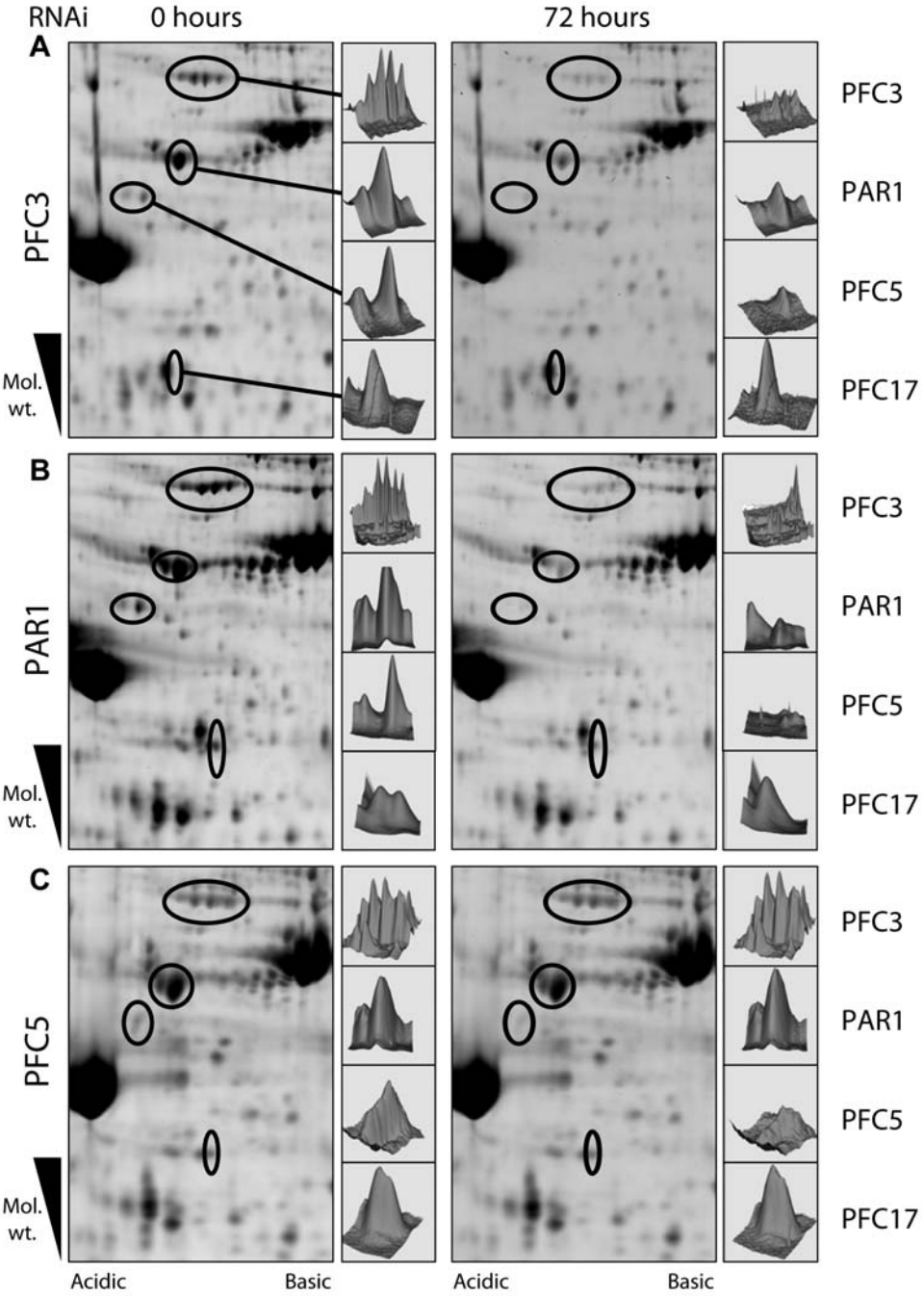

Figure 4. Two-dimensional DiGE analysis of PFC3, PAR1 and PFC5 non-induced and RNAi induced flagella. The gels were analyzed using Decyder software (GE Healthcare), which was used to generate three-dimensional representations of the spots that show a change in volume after induction. Reductions in volume were seen for spots corresponding to PFC3, PAR1, PFC5 and PFC17 in both PFC3 and PAR1 RNAi induced environments. Reduction in volume was seen only for spot corresponding to PFC5 following RNAi ablation of PFC5.
doi:10.1371/journal.pone.0007685.g004

These correspond to PFC5 (two spots–2.1-fold and 2.7-fold reductions in volume) and PFC17 (one spot–2.1-fold reduction in volume). PFC3 or PAR1 interactions with either PFC5 or PFC17 were not observed by yeast two-hybrid analysis. Reciprocal experiments showed that RNAi induction for 72 hours against PAR1 phenocopies the PFC3 result with spot volume reductions for PAR1 (3.7-fold reduction), PFC3 (3.1, 4.9, 4.5, 3.2 and 2.2-fold reductions), PFC5 (2.1 and 2.7-fold reductions) and PFC17 (2.1-fold reduction) (Figure 4B). RNAi against PFC5, however, only resulted in a reduction in volume of the two spots corresponding to PFC5 itself (1.5 and 2.0 -fold reductions) (Figure 4C). Taken together these data suggest a hierarchical dependency sub-network whereby PAR1 and PFC3 are both necessary for the incorporation of all four proteins into the PFR. RNAi/DiGE analyses were also carried out on the potential hub interactor, PFR5 but no protein composition phenotype, other than ablation of the RNAi target protein, were observed (data not shown).

Ablation of the PFC3/PAR1 Complex Does Not Affect Structural Morphology of the PFR

Using immunofluorescence light microscopy of detergent extracted cells, we analysed cell lines containing a Ty epitope tagged copy of PFC3 at one of the endogenous alleles (18) and inducible RNAi against PFC3, PAR1 or PFC5 with the BB2 antibody. Comparison of cells 72 hours after RNAi induction with non-induced controls showed no gross morphological changes (Figure 5). In addition, consistent with our previous results, PFC3 signal was absent in the majority of cells following PFC3 RNAi and was greatly reduced following PAR1 RNAi. Furthermore, RNAi against PFC5 did not affect PFC3 localisation. In order to determine if loss of the PFC3/PAR1 complex has any effect on the structure of the PFR, we analysed PFC3 and PAR1 RNAi mutants 72 hours after RNAi induction by thin section electron microscopy. To enable us to determine efficacy of the RNAi induction, we used cell lines containing an allele of the RNAi target tagged with the Ty epitope at the endogenous locus. Interestingly, despite the loss of two relatively high abundance proteins from the PFR (Figure 4), no observable changes could be detected in the PFR structure (Figure 6A). Western blotting analysis of samples taken from the cultures prior to fixation confirmed that the RNAi induction was successful as target proteins were ablated (Figure 6B).

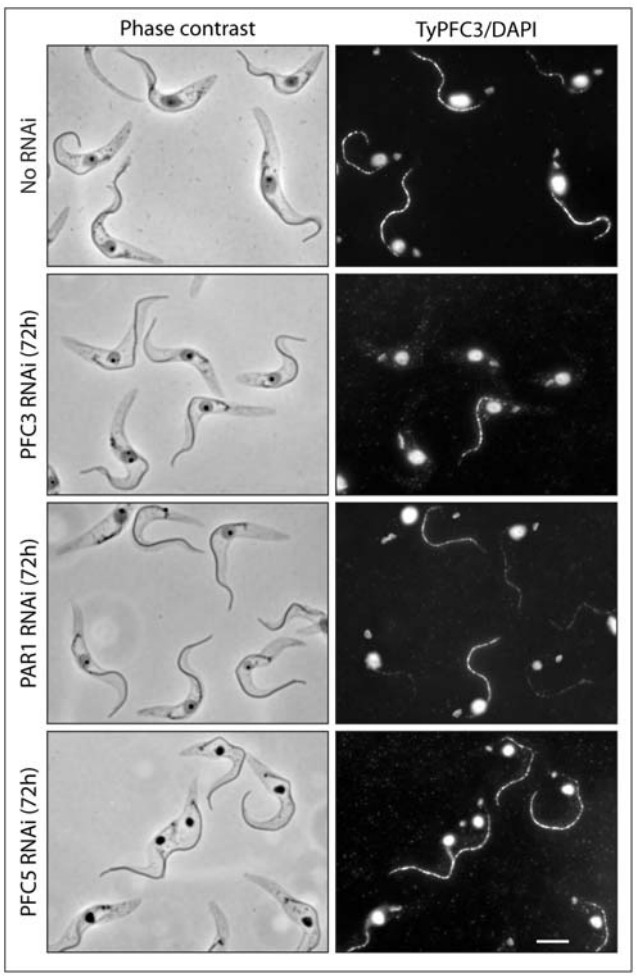

Figure 5. Immunofluorescence light microscopy of detergent extracted cells. BB2 antibody was used to detect Ty-PFC3 (flagellar signal) in PFC3, PAR1 and PFC5 RNAi environments (72 hours induction). Without RNAi induction, Ty-PFC3 is present in all flagella. After RNAi against PFC3 or PAR1, the majority of flagella no longer stain for Ty-PFC3 (it is likely that flagella that do stain represent those present prior to RNAi induction). After RNAi against PFC5, all flagella retain Ty-PFC3. DNA is visualised with DAPI. Bar–5 μm.
doi:10.1371/journal.pone.0007685.g005

Discussion

Studies in *T. brucei* benefit from the availability of a completed and well annotated genome [41] as well as a wealth of functional genomics tools. This organism is an excellent model for the study of many eukaryotic cell processes, such as flagellar function, as well as being an important parasite in its own right. The almost total lack of introns in the genome and the poly-cistronic method of transcription employed by trypanosomatids greatly facilitate the prediction of open reading frames and thus aid in proteomic and

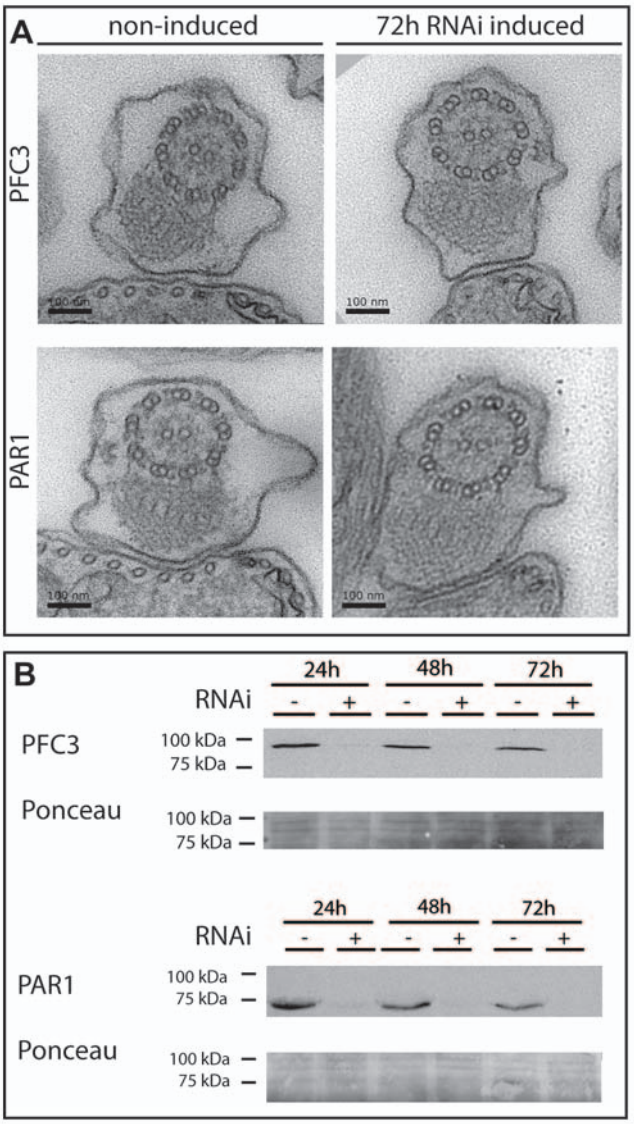

Figure 6. Analysis of PFC3 and PAR1 after induction of RNAi. A. Thin-section electron microscopy of whole cells reveals no detectable structural change in the PFR organisation after RNAi ablation of either PFC3 or PAR1. B. Western blotting analysis shows ablation of both PFC3 and PAR1 protein levels by 24 hours after induction of RNAi. Ty epitope tagged PFR proteins were detected using BB2 antibody. Ponceau stained membranes show loading of protein samples.
doi:10.1371/journal.pone.0007685.g006

functional genomics studies such as mass spectrometry, RNAi, overexpression and epitope tagging.

Historically, large scale forward genetic analyses have met with limited success in *T. brucei* [42,43], and hence the need for systematic phenotype analysis remains paramount. To this end we have exploited cutting edge high-throughput Gateway® cloning strategies to produce an ORFeome library of PFR components. This ORFeome constitutes a platform for functional genomics studies to investigate protein interactions, sub-cellular localisation and mutant analyses.

We have developed a new vector utilising the well characterised RNAi reverse genetics techniques available for *T. brucei* that is fully compatible with the Gateway® technology. We have demonstrated the utility of this vector by ablating five distinct PFR proteins including PFR2 and in this last case have reproduced a phenotype consistent with the well characterised *snl2* mutant cell line. Taken together, these tools constitute a first step towards a high throughput functional genomics system in *T. brucei* that we have used here in conjunction with yeast two-hybrid and proteomics techniques to generate a protein-protein interaction network for the paraflagellar rod.

We have identified eight novel protein-protein interactions within the PFR using a yeast two hybrid screen of 28 PFR components. Our subsequent reverse genetics analysis of the protein set provided supporting evidence for a number of these interactions and also identified several novel protein dependencies not detected in our initial screen. It is perhaps surprising that, given the central role of PFR1 and PFR2 in the PFR, no interactions were detected between these two proteins and any of the others in this study. Yeast two-hybrid analyses typically suffer from a high frequency of false negative results and this may be a particular problem when dealing with very insoluble proteins such as PFR components. There is also the distinct possibility that many interactions within the PFR do not occur on a one-to-one basis. It may be that PFR1 and PFR2 must be part of a complex in order to interact with other PFR proteins or that less abundant components interact with PFR1 or PFR2 only as cohorts. Another possibility is that a chaperone-assisted folding process that is not present in yeast is required for some PFR component interactions. Finally, there is also the very likely possibility that we have not yet identified all of the PFR components and may be missing key mediators between PFR1/2 and the other PFR proteins. All of the interactions and dependencies that we identified fall into two clusters. The smaller cluster involves two proteins that share a motif, and the larger cluster involves eight proteins (one fifth of all identified PFR proteins) of which several contain a PFR domain.

The smaller cluster consists of PFC4 and PFC16 which show consistent interactions with each other in all yeast two-hybrid assays in both bait and prey configurations. We previously showed that PFC4 and PFC16 share a 21 amino acid motif [18], although this domain is not sufficient for maintaining the yeast two-hybrid interaction. RNAi/epitope tagging analyses reveal an intriguing relationship between these two proteins in that absence of one results in an additional higher mobility band for the other by Western blotting. We cannot currently exclude a role for degradation in this process; however the direct interaction of these two proteins suggests that the additional bands are the result of differential post-translational modifications although we have so far been unable to determine the nature of these modifications.

The larger cluster has two main hub interacting proteins, PFC3 and PFR5 which interact directly with each other. PFR5 interacts with PFC20 and possibly also with PFC6, although the evidence for this second interaction is weaker than that observed for other interactions in this screen. PFC6 interacts with itself and may also interact with PFR6, although again, the evidence for this latter interaction is relatively weak. It is interesting to note that PFC6 may interact with two proteins (PFR5, PFR6) that contain a PFR domain as well as interacting with itself. Similarly, the hub protein PFC3 interacts with two PFR domain containing proteins (PAR1, PFR5) as well as interacting with itself. We went on to investigate a number of these interactions by RNAi/DiGE analysis which has the power to provide context to the yeast two-hybrid data. While yeast two-hybrid analysis showed an interaction between PFC3 and PAR1, RNAi/DiGE provided an insight into the nature of this interaction in that PFC3 and PAR1 are mutually dependent on each other for correct assembly into the PFR structure. RNAi/DiGE analyses also reveal dependency relationships not detected in the yeast two-hybrid screen with incorporation of both PFC5 and PFC17 being dependent upon the presence of PFC3/PAR1. RNAi ablation of PFC5 does not affect the assembly of PFC3, PAR1 or PFC17 which suggests a hierarchical directionality to this dependency network.

One surprising, and likely significant result from our analysis is that a successful ablation by RNAi of the PFC3/PAR1 network results in no gross changes in the morphology of the PFR polymeric structure. This may represent evidence that the three major zones of the PFR and their distinct morphologies are heavily reliant for their formation on only a relatively few structural proteins, perhaps PFR1 and PFR2 (the only proteins that have been shown to localise to the PFR whose ablation results in a failure of PFR assembly). A picture then emerges of these few structural proteins being responsible for the major PFR lattice structure onto which is built a cohort of numerous other proteins with domain architectures suggesting a role in metabolism, signalling and regulation [2,13,18]. Taken together this supports the role of the PFR as an extra-axonemal structure critically involved in trypanosome sensory, motility and signalling cell biology [2,10,11,13,18]. It seems unlikely that abundant proteins such as PFC3 and PAR1, that are important enough to be conserved in the genomes of every sequenced trypanosomatid, lack a function. In these terms we will have to await the development of more sensitive phenotype tests before the function of these network proteins emerges.

In this study, we have developed a number of genomics tools for *T. brucei* and have used these to undertake the first large protein-protein interaction study of the PFR. Using a combination of technologies, we have identified eight novel protein-protein interactions and five protein dependencies. By combining the information presented in this study with the interactions and dependencies previously identified, we can summarise the current state of our knowledge of the PFR protein network (Fig. 7) to provide a framework for the continuing effort to elucidate the functions of this iconic structure. The position of PFR2 in the scheme represents the fact that many of the proteins included in this study were identified due to their dependence on PFR2, either directly or indirectly, for incorporation into the PFR. It is likely that PFR1 will occupy a similar position in such a network although there are currently no data available on protein components of the PFR that specifically depend on the presence of PFR1. A number of studies in recent years have provided insight into the PFR as a platform for regulatory and metabolic functions. This study supports the notion of a dynamic structure with a complex hierarchy of interacting and inter-dependent components [12,13,18].

Supporting Information

Figure S1 Yeast 2-Hybrid screen. A. Summary table describing the interactions detected in the PFR screen with the associated

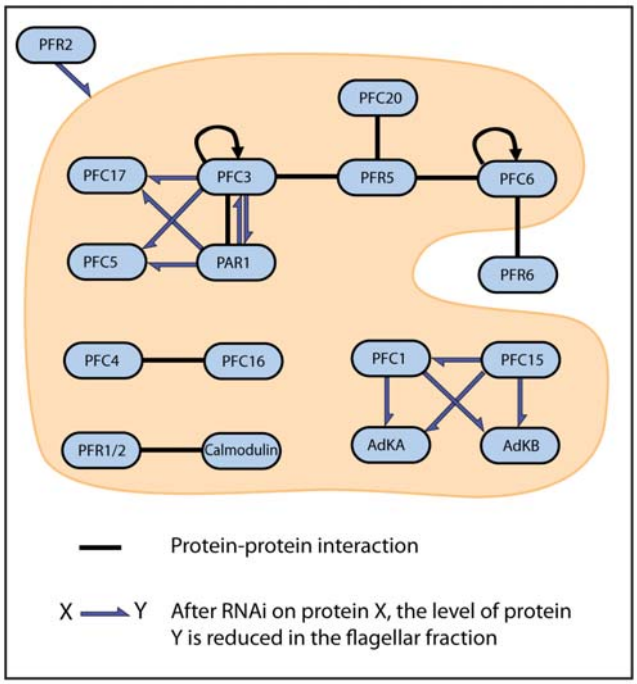

Figure 7. Summary of protein-protein interactions and dependencies of PFR components. Interactions drawn from this study and available literature [13,18]; black bars represent interactions observed by yeast two-hybrid or affinity pulldown. Gray arrows represent dependencies detected by combined RNAi/comparative proteomics techniques.
doi:10.1371/journal.pone.0007685.g007

protein-protein interaction network. B. The preys PFC1, PFR2 and PFC3 have been tested again all baits. The prey PFC3 interacts with both PFC3 and PFR5 baits in 4 and 3 assays respectively. C. PFC4 prey interacts with PFC16 baits in 3 assays and PFC6 prey interacts with itself (4 assays), with PFR5 and PFR6 (both in one assay).
Found at: doi:10.1371/journal.pone.0007685.s001 (0.29 MB PDF)

Figure S2 Auto-activation assay of PFR baits. A. Cartoon illustrating that some ORFs fused with the Gal4 DNA binding domain have the ability to activate the transcription of the reporter genes.This behaviour has to be tested to decrease the false positive rate. B. The diagram shows the position of each DB-ORF for this assay. C. Readout of the four autoactivation assays (b-galactosidase assay, auxotrophic media lacking histidine and complemented with 20 and 60 mM 3AT and media lacking the uracil amino acid. PFC11, PFC2, PFC20 are strong auto-activators in all assays. PFC3 and PFR5 are weak auto-activators.
Found at: doi:10.1371/journal.pone.0007685.s002 (0.06 MB PDF)

Table S1 PCR primers used to generate the ORFeome. AttB1 and AttB2 recognition sequences are shown in lower case.
Found at: doi:10.1371/journal.pone.0007685.s003 (0.01 MB PDF)

Acknowledgments

We thank Prof Marc Vidal (Dana Farber Cancer Institute, Harvard University) for the generous gift of yeast strains and yeast two-hybrid plasmids. We also thank Dr Ana G. Rondon for technical advice regarding the yeast two-hybrid experiment.

Author Contributions

Conceived and designed the experiments: SL NP. Performed the experiments: SL NP. Analyzed the data: SL NP KG. Contributed reagents/materials/analysis tools: SL NP KG. Wrote the paper: SL NP KG.

References

1. Oberholzer M, Bregy P, Marti G, Minca M, Peier M, et al. (2007) Trypanosomes and mammalian sperm: one of a kind? Trends Parasitol 23: 71–77.
2. Oberholzer M, Marti G, Baresic M, Kunz S, Hemphill A, et al. (2007) The Trypanosoma brucei cAMP phosphodiesterases TbrPDEB1 and TbrPDEB2: flagellar enzymes that are essential for parasite virulence. FASEB J 21: 720–731.
3. Ogbadoyi EO, Robinson DR, Gull K (2003) A high-order trans-membrane structural linkage is responsible for mitochondrial genome positioning and segregation by flagellar basal bodies in trypanosomes. Mol Biol Cell 14: 1769–1779.
4. Robinson DR, Gull K (1991) Basal body movements as a mechanism for mitochondrial genome segregation in the trypanosome cell cycle. Nature 352: 731–733.
5. Beattie P, Gull K (1997) Cytoskeletal architecture and components involved in the attachment of Trypanosoma congolense epimastigotes. Parasitology 115 (Pt 1): 47–55.
6. Vickerman K (1973) The mode of attachment of Trypanosoma vivax in the proboscis of the tsetse fly Glossina fuscipes: an ultrastructural study of the epimastigote stage of the trypanosome. J Protozool 20: 394–404.
7. Broadhead R, Dawe HR, Farr H, Griffiths S, Hart SR, et al. (2006) Flagellar motility is required for the viability of the bloodstream trypanosome. Nature 440: 224–227.
8. Bastin P, Matthews KR, Gull K (1996) The paraflagellar rod of kinetoplastida: solved and unsolved questions. Parasitol Today 12: 302–307.
9. Maga JA, LeBowitz JH (1999) Unravelling the kinetoplastid paraflagellar rod. Trends Cell Biol 9: 409–413.
10. Santrich C, Moore L, Sherwin T, Bastin P, Brokaw C, et al. (1997) A motility function for the paraflagellar rod of Leishmania parasites revealed by PFR-2 gene knockouts. Mol Biochem Parasitol 90: 95–109.
11. Bastin P, Sherwin T, Gull K (1998) Paraflagellar rod is vital for trypanosome motility. Nature 391: 548.
12. Pullen TJ, Ginger ML, Gaskell SJ, Gull K (2004) Protein targeting of an unusual, evolutionarily conserved adenylate kinase to a eukaryotic flagellum. Mol Biol Cell 15: 3257–3265.
13. Ridgley E, Webster P, Patton C, Ruben L (2000) Calmodulin-binding properties of the paraflagellar rod complex from Trypanosoma brucei. Mol Biochem Parasitol 109: 195–201.
14. Griffiths S, Portman N, Taylor PR, Gordon S, Ginger ML, et al. (2007) RNA interference mutant induction in vivo demonstrates the essential nature of trypanosome flagellar function during mammalian infection. Eukaryot Cell 6: 1248–1250.
15. Gerdes JM, Davis EE, Katsanis N (2009) The vertebrate primary cilium in development, homeostasis, and disease. Cell 137: 32–45.
16. Yang P, Diener DR, Yang C, Kohno T, Pazour GJ, et al. (2006) Radial spoke proteins of Chlamydomonas flagella. J Cell Sci 119: 1165–1174.
17. Kilburn CL, Pearson CG, Romijn EP, Meehl JB, Giddings TH, Jr. (2007) New Tetrahymena basal body protein components identify basal body domain structure. J Cell Biol 178: 905–912.
18. Portman N, Lacomble S, Thomas B, McKean PG, Gull K (2009) Combining RNA interference mutants and comparative proteomics to identify protein components and dependences in a eukaryotic flagellum. J Biol Chem 284: 5610–5619.
19. Rual JF, Venkatesan K, Hao T, Hirozane-Kishikawa T, Dricot A, et al. (2005) Towards a proteome-scale map of the human protein-protein interaction network. Nature 437: 1173–1178.
20. Li S, Armstrong CM, Bertin N, Ge H, Milstein S, et al. (2004) A map of the interactome network of the metazoan C. elegans. Science 303: 540–543.
21. LaCount DJ, Vignali M, Chettier R, Phansalkar A, Bell R, et al. (2005) A protein interaction network of the malaria parasite Plasmodium falciparum. Nature 438: 103–107.
22. Uetz P, Giot L, Cagney G, Mansfield TA, Judson RS, et al. (2000) A comprehensive analysis of protein-protein interactions in Saccharomyces cerevisiae. Nature 403: 623–627.
23. Ahmed NT, Gao C, Lucker BF, Cole DG, Mitchell DR (2008) ODA16 aids axonemal outer row dynein assembly through an interaction with the intraflagellar transport machinery. J Cell Biol 183: 313–322.
24. Tam LW, Wilson NF, Lefebvre PA (2007) A CDK-related kinase regulates the length and assembly of flagella in Chlamydomonas. J Cell Biol 176: 819–829.

25. Lucker BF, Behal RH, Qin H, Siron LC, Taggart WD, et al. (2005) Characterization of the intraflagellar transport complex B core: direct interaction of the IFT81 and IFT74/72 subunits. J Biol Chem 280: 27688–27696.
26. Zhang Z, Jones BH, Tang W, Moss SB, Wei Z, et al. (2005) Dissecting the axoneme interactome: the mammalian orthologue of Chlamydomonas PF6 interacts with sperm-associated antigen 6, the mammalian orthologue of Chlamydomonas PF16. Mol Cell Proteomics 4: 914–923.
27. Motyka SA, Englund PT (2004) RNA interference for analysis of gene function in trypanosomatids. Curr Opin Microbiol 7: 362–368.
28. Subramaniam C, Veazey P, Redmond S, Hayes-Sinclair J, Chambers E, et al. (2006) Chromosome-wide analysis of gene function by RNA interference in the african trypanosome. Eukaryot Cell 5: 1539–1549.
29. Wickstead B, Ersfeld K, Gull K (2002) Targeting of a tetracycline-inducible expression system to the transcriptionally silent minichromosomes of Trypanosoma brucei. Mol Biochem Parasitol 125: 211–216.
30. Brun R, Jenni L (1977) A new semi-defined medium for Trypanosoma brucei sspp. Acta Trop 34: 21–33.
31. Rual JF, Hirozane-Kishikawa T, Hao T, Bertin N, Li S, et al. (2004) Human ORFeome version 1.1: a platform for reverse proteomics. Genome Res 14: 2128–2135.
32. Wirtz E, Leal S, Ochatt C, Cross GA (1999) A tightly regulated inducible expression system for conditional gene knock-outs and dominant-negative genetics in Trypanosoma brucei. Mol Biochem Parasitol 99: 89–101.
33. Bastin P, Bagherzadeh Z, Matthews KR, Gull K (1996) A novel epitope tag system to study protein targeting and organelle biogenesis in Trypanosoma brucei. Mol Biochem Parasitol 77: 235–239.
34. Walhout AJ, Vidal M (2001) High-throughput yeast two-hybrid assays for large-scale protein interaction mapping. Methods 24: 297–306.
35. Bastin P, Ellis K, Kohl L, Gull K (2000) Flagellum ontogeny in trypanosomes studied via an inherited and regulated RNA interference system. J Cell Sci 113 (Pt 18): 3321–3328.
36. Bastin P, Pullen TJ, Sherwin T, Gull K (1999) Protein transport and flagellum assembly dynamics revealed by analysis of the paralysed trypanosome mutant snl-1. J Cell Sci 112 (Pt 21): 3769–3777.
37. Blom N, Gammeltoft S, Brunak S (1999) Sequence and structure-based prediction of eukaryotic protein phosphorylation sites. J Mol Biol 294: 1351–1362.
38. Kall L, Krogh A, Sonnhammer EL (2004) A combined transmembrane topology and signal peptide prediction method. J Mol Biol 338: 1027–1036.
39. Hamby SE, Hirst JD (2008) Prediction of glycosylation sites using random forests. BMC Bioinformatics 9: 500.
40. Bologna G, Yvon C, Duvaud S, Veuthey AL (2004) N-Terminal myristoylation predictions by ensembles of neural networks. Proteomics 4: 1626–1632.
41. Berriman M, Ghedin E, Hertz-Fowler C, Blandin G, Renauld H, et al. (2005) The genome of the African trypanosome Trypanosoma brucei. Science 309: 416–422.
42. Monnerat S, Clucas C, Brown E, Mottram JC, Hammarton TC (2009) Searching for novel cell cycle regulators in Trypanosoma brucei with an RNA interference screen. BMC Res Notes 2: 46.
43. Morris JC, Wang Z, Drew ME, Englund PT (2002) Glycolysis modulates trypanosome glycoprotein expression as revealed by an RNAi library. EMBO J 21: 4429–4438.